Titre: Title:	Rheological study and rheo-microscopy of semi-flexible fiber suspensions
Auteur: Author:	Mahdi Keshtkar
Date:	2009
Type:	Mémoire ou thèse / Dissertation or Thesis
Référence: Citation:	Keshtkar, M. (2009). Rheological study and rheo-microscopy of semi-flexible fiber suspensions [Thèse de doctorat, École Polytechnique de Montréal]. PolyPublie. https://publications.polymtl.ca/8459/

URL de PolyPublie: PolyPublie URL:	https://publications.polymtl.ca/8459/
Directeurs de recherche: Advisors:	
Programme: Program:	Non spécifié

UNIVERSITÉ DE MONTRÉAL

RHEOLOGICAL STUDY AND RHEO-MICROSCOPY OF SEMI-FLEXIBLE FIBER SUSPENSIONS

MAHDI KESHTKAR
DÉPARTMENT DE GÉNIE CHIMIQUE
ÉCOLE POLYTECHNIQUE DE MONTRÉAL

THÈSE PRÉSENTÉE EN VUE DE L'OBTENTION
DE DIPLÔME DE PHILOSOPHIAE DOCTOR
(GÉNIE CHIMIQUE)
JUIN 2009

Your file Votre référence
ISBN: 978-0-494-53799-2
Our file Notre référence
ISBN: 978-0-494-53799-2

UNIVERSITÉ DE MONTRÉAL

ÉCOLE POLYTECHNIQUE DE MONTRÉAL

Cette thèse intitulée :

RHEOLOGICAL STUDY AND RHEO-MICROSCOPY OF SEMI-FLEXIBLE FIBER SUSPENSIONS

présentée par: KESHTKAR Mahdi

en vue de l'obtention de diplôme de : Philosophiae Doctor

a été dûment acceptée par le jury d'examen constitué de :

M. PATIENCE Gregory-S., Ph. D., président

Mme HEUZEY Marie-Claude, Ph. D., membre et directrice de recherche

M. CARREAU Pierre, Ph. D., membre et codirecteur de recherche

M. AJJI Abdellah, Ph. D., membre

M. TUCKER III Charles L., Ph. D., membre

To CANADA; for giving me the chance to experience the concept of liberty!

ACKNOWLEDGEMENTS

I wish to thank all those who helped me in the completion of this study and made the way of research smooth for me.

First of all, I would like to convey my gratitude to my supervisors, Professor Marie-Claude Heuzey and Professor Pierre J. Carreau, who provided me with fundamental advises. They always supported me very well in my research with availability, patience and encouragement. I am very grateful for the things that I learnt from them; not only the scientific matters, but also lots of knowledge which are very helpful in all aspects of my life. It had been a true privilege to learn from such competent and sincere supervisors.

I owe special gratitude to the staff of CREPEC who made the working place a fascinating area. I would like to thank Mrs. Diane Héroux for her great kindness and dedication in all the administrative jobs. My especial thanks are due to Ms. Melina Hamdine for her sympathy, support, availability and many things that I have learnt from her. I would like to thank Mr. Jacques Beausoleil for his availability and technical assistance.

I also gratefully thank Professor Jose Perez Gonzales, Professor Lourdes de Vargas, Benjamín and Francisco for providing the experimental setup for the rheo-microscopy in Mexico and their kindness during my stay in Mexico.

I like to extent my thanks to the entire technical and administrative staff of the Chemical Engineering Department in Ecole Polytechnique de Montreal.

I would like to acknowledge financial support from the Natural Sciences and Engineering Research Council of Canada (NSERC-CIAM program).

I would also like to send a heartfelt acknowledgment to my friends who made all these years vey joyful with interesting, intellectual and creative ideas. Shant, Hassan, Hesam, Hesamodin, Amir Hossein, Yalda, Christophe, Julien, Fatemeh, Samaneh, Emma, Bahador, Babak, Roozbeh, Farrokh, Amin, Pasha, Aysan ,...

Finally I could not have accomplished this without all the supports of my family. They are the driving force behind all of my successes. To them I tribute a fervent thanks.

RÉSUMÉ

Le mouvement de suspensions de particules est un sujet fort intéressant pour les scientifiques et les ingénieurs grâce à leurs applications diverses dans les industries pharmaceutique, pétrochimique, de forage, des pâtes et papiers, des matériaux composites et les processus en biologie. Les matériaux thermoplastiques renforcés avec des fibres courtes sont largement utilisés dans les industries manufacturières. Ils sont particulièrement importants car ils peuvent être mis en forme par des équipements de transformation des plastiques conventionnels tels que l'extrusion ou le moulage par injection.

Les propriétés mécaniques d'un produit fini dépendent fortement de ses caractéristiques microstructurales : la quantité de fibres dans le composite, le rapport de forme de la fibre (longueur sur diamètre), et l'orientation des fibres. Contrairement aux composites avec fibres structurelles continues, les fibres courtes ne sont pas nécessairement distribuées de façon optimale. L'orientation des fibres est influencée par la fraction volumique du renfort, le rapport de forme, les propriétés intrinsèques des fibres et de la matrice, et les conditions du procédé. Lors de la mise en forme, les fibres bougent, tournent, peuvent se casser et se plier car elles subissent différentes pressions et contributions de l'écoulement qui peuvent changer l'état de leur l'orientation. Une des propriétés majeures qui peut influencer l'orientation des fibres est la capacité des fibres à se courber : ce qu'on appelle la flexibilité de la fibre. La flexibilité de la fibre varie avec les propriétés intrinsèques de la fibre, son rapport de forme et les forces appliquées.

Afin d'avoir une compréhension approfondie du mouvement des fibres et de l'optimisation du procédé pour obtenir les propriétés requises, la connaissance de la rhéologie des matériaux renforcés en fibres courtes est essentielle. Généralement la rhéologie des suspensions de fibres est très complexe dû à plusieurs facteurs : les interactions fibres-fibres, fibres-paroi, fibres-matrice et les phénomènes de rupture et de migration des fibres. Malgré ces nombreuses difficultés, un grand nombre d'expériences et recherches théoriques ont été dévolues à l'analyse et à la prédiction du comportement rhéologique des suspensions de fibres. Néanmoins, parmi ces recherches il y a très peu d'investigations qui se sont concentrées sur le rôle de la flexibilité des fibres. La littérature récente ne dénombre pas de données expérimentales fiables sur les effets de la flexibilité et sur la rhéologie et la microstructure de ces suspensions. Pour combler ce vide, dans ce travail une étude exhaustive des effets de flexibilité des fibres sur les propriétés rhéologiques est présentée, par l'entremise de l'utilisation de systèmes modèles bien contrôlés. Les microstructures des suspensions sont aussi examinées par des expériences en rhéo-microscopie. La rigidité effective qui caractérise l'importance relative de la rigidité des fibres par rapport aux forces hydrodynamiques qui agissent sur elles a été utilisée comme critère de flexibilité de la fibre. En se basant sur ce paramètre, la rigidité intrinsèque de la fibre et son rapport de forme deviennent des paramètres dominants dans l'investigation des effets de flexibilité. Afin d'examiner les effets du rapport de forme et de la rigidité des fibres, des suspensions de fibres variées ont été préparées pour investiguer les effets de divers paramètres reliés à la flexibilité (rigidité, rapport de forme) aussi bien que le rôle des interactions dans les régimes dilué et semi-

concentré dans une matrice newtonienne, une huile de silicone. Il a été observé que la viscosité et la première différence de contraintes normales augmentaient toutes deux pour une flexibilité plus grande. Ces augmentations étaient plus prononcées pour le régime semi-concentré. L'augmentation des propriétés rhéologiques a été attribuée aux interactions entre fibres, plus nombreuses lorsque des fibres flexibles sont utilisées. Par des expériences de démarrage en cisaillement simple dans le sens horaire, les contraintes de cisaillement et de forces normales ont montré un pic attribué à l'orientation des fibres sous écoulement. L'importance de ce pic augmente avec la flexibilité de la fibre. Pour un écoulement similaire dans le sens anti-horaire, un spic « retardé » a été observé, et en augmentant la flexibilité de la fibre la déformation à laquelle le pic est observé diminue. Étant donné que le pic observé lors de l'écoulement inverse est attribué au culbutage des fibres, les résultats en transitoire suggèrent que les fibres flexibles sont moins orientées lors de l'écoulement précédent que les fibres rigides.

L'évolution des microstructures des diverses suspensions à été investiguée à différentes vitesses de déformation en utilisant un microscope InfiniVar® à réglage continu placé sous la plaque inférieure d'un rhéomètre. Les composantes du tenseur d'orientation d'ordre deux ont été calculées à différents temps en utilisant les images obtenus lors des expériences de visualisation. Les expériences de visualisation du mouvement des fibres ont montré que l'orientation est dépendante du taux de cisaillement et de la force appliquée. La rhéo-microscopie des diverses suspensions a démontré que celles préparées avec des fibres flexibles étaient moins orientées dans la direction de

l'écoulement, comparé aux fibres rigides – et ce particulièrement à des taux de cisaillement plus faibles. Cela a été attribué à leur forme légèrement courbée contrairement à la forme rectiligne des fibres rigides. Un modèle de type GENERIC (« General Equation for Non-equilibrium Reversible-Irreversible Coupling ») a été utilisé afin de décrire les phénomènes observés. Les paramètres de ce modèle ont été obtenus par lissage des données de contraintes en démarrage de cisaillement simple à un seul taux de cisaillement. En utilisant ces paramètres intégrés, la capacité de ce modèle à prédire les premières différences de contraintes normales et les propriétés rhéologiques à d'autres taux de cisaillement a été examinée. De plus, l'orientation des fibres prévue par le modèle a été confrontée avec les résultats de rhéo-microscopie. Le modèle prévoit qualitativement l'orientation de fibres avec flexibilités variées. Cependant, plus d'effort doit être dévolu au développement d'un modèle qui saura décrire quantitativement le comportement complexe rhéologique des suspensions de fibres concentrées et semi-concentrées à des taux de cisaillement divers, ce qui est très difficile à accomplir présentement.

Finalement, le dernier point abordé dans cette étude concerne l'effet de la flexibilité des fibres sur le comportement rhéologique de suspensions dans une matrice visoélastique (un polyéthylène basse densité (PEBD) fondu) sous cisaillement simple et oscillatoire avec grandes et petites déformations.

Le cisaillement oscillatoire sous grandes déformations (« LAOS ») a été utilisé pour essayer de comprendre la relation qui existe entre les contraintes et l'orientation des

fibres. Les suspensions de PEBD fondu contenant des fibres avec des flexibilités différentes ont été utilisées pour cette dernière étude. Pour tous les composites, la contrainte a diminué avec le temps dans les expériences de LAOS. Ce comportement était plus prononcé dans le cas des fibres rigides. La diminution des contraintes a été expliquée en terme de différents niveaux d'orientation et de flexibilité des fibres. L'énergie dissipée par cycle de LAOS a aussi été évaluée pour chaque composite. Ces calculs ont démontré que plus d'énergie est dissipée lorsque la flexibilité des fibres augmente. De plus, l'énergie dissipée a diminué avec le temps et cela a été interprété par une réduction de contacts entre fibres en fonction du temps. Ce phénomène a été plus prononcé dans le cas des fibres rigides. Les observations ont aussi indiqué que les contacts entre fibres ont diminué plus rapidement pour ces suspensions. La première différence de contrainte normale a montré une réponse périodique non-sinusoïdale. En plus de la seconde harmonique observée pour le PEBD par l'analyse par transformée de Fourrier rapide (« FFT »), la présence d'une première harmonique correspondant à la fréquence appliquée a été observée pour les suspensions. Cela a résulté en des courbes de Lissajou asymétriques pour la contrainte normale des suspensions. Cette asymétrie a aussi été plus prononcée dans le cas des fibres rigides. Ces résultats sont expliqués en termes des effets de mémoire liés au temps et déclenchés par l'orientation des fibres.

ABSTRACT

The flow of particle suspensions are of great interest for scientists and engineers because of their wide applications such as in biological processes, pharmaceutical processes, oil industries and drilling , pulp and paper industries, composite manufacturing and etc.

Thermoplastic materials reinforced with chopped fibers are used increasingly in the manufacturing industries. They are particularly important since they can be shaped in conventional plastics processing equipment such as extruders and injection molding machines. The mechanical properties of the final products are highly dependant on the microstructural characteristics of the suspensions such as fiber volume fraction in the composite, fiber aspect ratio (the ratio of fiber length to fiber diameter), and the orientation state of the fibers.

In opposition to structural continuous fiber composites, chopped fibers are not necessarily distributed in an optimal way. The orientation of these materials is influenced by fiber volume fraction, fiber aspect ratio and intrinsic properties and processing conditions. During processing, fibers move, rotate, break or bend because of different stresses and changes in their orientation state. One of the properties that may influence fiber orientation is the ability of fibers to be bended and characterized as fiber flexibility. Fiber flexibility varies with the intrinsic properties of the fiber and its aspect ratio, and is coupled to the strength of the flow field.

The knowledge of the rheology of fiber reinforced materials is essential to have a through understanding of their flow and optimizing processes to achieve the desired products.

In general the rheology of fiber suspensions is quite complex due to several factors like fiber-fiber, fiber-wall, fiber-matrix interactions and phenomena such as fiber breakage and migration. Despite these numerous difficulties, a large number of experimental and theoretical investigations have been devoted to the analysis and prediction of the rheological behavior of fiber suspensions. However, among these studies there are very few investigations that focus on the role of fiber flexibility and the current literature lacks the reliable experimental data on the effect of fiber flexibility on rheology and microstructure of fiber suspensions. Thus, in this work we perform a comprehensive study of the effect of fiber flexibility and associated parameters on rheological properties, using well-controlled systems. We also visualize suspensions microstructure using rheo-microscopy and finally use available models in the literature to understand the observed phenomena in rheometry and rheo-microscopy experiments. The effective stiffness, which characterizes the relative importance of fiber stiffness to hydrodynamic forces acting on the fibers, has been used as a criterion for fiber flexibility. Based on this parameter, the fiber intrinsic stiffness and aspect ratio are ruling parameters involved in probing flexibility effects.

To investigate the effect of fiber aspect ratio and fiber stiffness, various fiber suspensions were prepared to examine the effect of flexibility parameters (stiffness, aspect ratio) as well as the role of interactions in the semi-dilute and semi-concentrated regimes with a high viscosity silicone oil as the matrix, which has a Newtonian behavior. Both viscosity and first normal stress differences increased with larger fiber flexibility, and the increases were more pronounced in the semi-concentrated regime.

The enhancement of the rheological properties was attributed to additional fiber-fiber interactions when using more flexible fibers. By conducting stress growth experiments in the forward and reverse flow directions, shear stress and normal force overshoots were observed in the forward flow and attributed to fiber orientation under flow. Both the overshoot magnitude and width augmented with increasing fiber flexibility. Under flow reversal a delayed overshoot was detected and as fiber flexibility increased the strain at which the overshoot started got smaller. Since the reverse overshoot has been attributed to fiber tumbling, our transient results suggest that flexible fibers were less oriented in the previous forward flow than rigid fibers.

The evolution of the suspensions microstructure was monitored at different shear rates using a continuously-focusable InfiniVar® microscope placed under the lower plate of a rheometer. The components of the second-order orientation tensor at different times were calculated using the images obtained from the visualization experiments. The flow visualization experiments showed that fiber orientation is dependent on the shear rate and the amount of applied strain. Rheo-microscopy of the various suspensions showed that suspensions prepared with more flexible fibers were oriented less in the flow direction as compared to rigid fibers, especially at low shear rates. This was attributed to their slightly curved shape as opposed to the straight shape of the rigid fibers. A GENERIC-type model (General Equation for Non-equilibrium Reversible-Irreversible Coupling) was used to describe the phenomena observed. The model parameters were obtained by fitting the stress growth viscosity data at a single shear rate. Using these fitted parameters, the ability of the model to predict first normal stress difference and

rheological properties at other shear rates was examined. In addition, the fiber orientation as predicted by the model was confronted with the rheo-microscopy results. The model predicts qualitatively well fiber orientation for fibers of various flexibilities. However, more efforts have to be devoted to the development of a model that would describe quantitatively the complex rheological behavior of semi-concentrated and concentrated suspensions of flexible fibers at various shear rates, which is not an easy task to undertake.

The last point tackled in this work was concerned with the effect of fiber flexibility on the rheological behavior of fiber suspensions in a viscoelastic matrix (molten LDPE) under simple shear flow, and small and large amplitude oscillatory shear. Large amplitude oscillatory shear (LAOS) was used to help understanding the relationship between stress growth observations and fiber orientation. Molten LDPE suspensions containing fibers with different flexibilities were used in this study. For all composites the stress signal decreased with time in the LAOS experiments, and this behavior was more pronounced in the case of the more rigid fibers. The stress decrease was explained in terms of different levels of fiber orientation and fiber flexibility. The energy dissipated per LAOS cycle was evaluated for each composite, and these calculations showed that more energy was dissipated as fiber flexibility increased. In addition, the dissipated energy decreased with time and this was interpreted as a reduction of fiber contacts as a function of time. This phenomenon was more pronounced in the case of the more rigid fibers and the observations indicated that fiber contacts reduced faster for these suspensions. The first normal stress difference showed a non sinusoidal periodic

response, and fast Fourier transform (FFT) analysis indicated the presence of a first harmonic corresponding to the applied frequency for the fiber-filled systems, in addition to the second harmonic observed for the neat LDPE. It resulted in asymmetric strain-normal force Lissajou curves, with this asymmetry being more pronounced in the case of the more rigid fibers. These results were explained in terms of time-dependent memory effects induced by fiber orientation.

CONDENSÉ EN FRANÇAIS

Au cours des dernières décennies, le mouvement des particules en suspension a été le sujet d'un grand intérêt pour la recherche parmi les scientifiques et les ingénieurs grâce à leurs nombreuses applications dans plusieurs domaines tels que dans les industries pharmaceutique, pétrochimique, de forage, des pâtes et papiers, des matérieux composites et les processus en biologie.

Les matériaux renforcés sont utilisés dans une variété d'applications structurales qui demandent un large ratio force-poids. Ces derniers remplacent avantageusement leurs homologues tels que métaux, bois et céramiques. Les polymères composites sont obtenus en ajoutant un renfort solide à une matrice polymérique. Les fibres de verre, le carbone, le Kevlar®, le nylon, l'alcool polyvinylique (PVA) et les fibres naturelles qui sont généralement des fibres de cellulose sont les renforts les plus courants. Ces fibres peuvent être utilisées sous forme de filaments continus, étoffes tissées ou fibres coupées. Ces renforts ajoutent de la force et de la rigidité à la matrice polymérique. Bien que les propriétés mécaniques des composites à fibres courtes soient inférieures à celles des composites à fibres continues, l'utilisation d'équipements conventionnels tels que l'extrudeuse ou la machine à injection popularisent l'usage des composites renforcés de fibres courtes.

Les composites à renfort de particules ou de fibres courtes sont manufacturés par des processus variés : la compression, le moulage par injection et l'extrusion. Pendant la transformation des composites renforcés de fibres courtes, les fibres subiront des rotations, des translations, elles se plieront et se casseront. Les propriétés du produit fini sont fortement liées aux caractéristiques microstructurales et à l'orientation des fibres. La structure est affectée par certains attributs tels que les propriétés intrinsèques et les interactions entre fibres, les propriétés du fluide et les contraintes imposées.

L'analyse et la compréhension de la relation qui existe entre ces caractéristiques, la structure de la suspension et les propriétés macroscopiques aident à mieux faire la conception et l'optimisation du processus de mise en forme et des produits. Malgré le fait qu'il y ait eu plusieurs propositions de modèles (mécaniques et numériques) et des expérimentations avancées concernant les suspensions de fibres, il reste plusieurs questions sans réponses. Ces questions sont toujours d'actualité car la communauté scientifique porte beaucoup d'intérêt à la microstructure des suspensions incluant celles des nanocomposites (impliquant les nano-patricules, les micro-fibres, les nano-fibres et les nanotubes de carbone). Un des facteurs importants qui peut impacter l'orientation des fibres et les propriétés rhéologiques est la flexibilité de la fibre. Cette flexibilité peut varier avec les propriétés de la fibre et la force de l'écoulement. Certains travaux théoriques ont essayé de démontrer le comportement de ces suspensions, par contre il y a un manque chronique de données expérimentales fiables concernant la rhéologie et le mouvement de suspension de fibres flexibles.

L'objectif de cette thèse est d'élucider les effets de la flexibilité des fibres sur les suspensions , de même que les paramètres associés sur les propriétés rhéologiques et les microstructures des suspensions. Afin de caractériser les effets de la flexibilité des fibres sur la rhéologie et les microstructures, à la fois des études expérimentales et de la modélisation sont utilisés dans ce travail. Pour investiguer le rôle de la flexibilité de la fibre sur le comportement rhéologique des suspensions, la flexibilité doit être d'abord définie. Comme ci-haut mentionné dans l'introduction, la flexibilité de la fibre dépend de la rigidité intrinsèque, ldu rapport de forme et de la contrainte que les fibres subissent. La rigidité effective caractérise l'importance relative de la rigidité des fibres et les forces hydrodynamiques. L'inverse de cette rigidité effective peut être utilisée comme un critère de flexibilité : lorsque la rigidité effective est faible, la flexibilité est élevée. En conséquence, la rigidité intrinsèque de la fibre et le rapport de forme sont des paramètres clés dans l'investigation des effets de flexibilité. Ainsi, différentes fibres (de polyarylate (ou Vectran®), d'alcool polyvinylique (PVA) et de nylon), ayant des modules d'Young variés, ont été choisies pour cette investigation.

Dans la première partie de ce projet, le comportement rhéologique de suspensions modèles basée sur une huile de silicone, donc un fluide newtonien, et de fibres avec des flexibilités différentes a été investigué sous écoulement en cisaillement stationnaire et transitoire. Différentes suspensions de fibres ont été préparées afin d'examiner les effets des paramètres de la flexibilité (la rigidité et le rapport de forme) et aussi le rôle des

interactions dans des conditions de régime semi-dilué et semi-concentré. Il a été constaté que la viscosité et la première différence de contraintes normales augmentent avec la flexibilité. Ces augmentations étaient aussi plus prononcées dans le régime semi-concentré. L'augmentation des propriétés rhéologiques a été attribuée aux fortes interactions fibre-fibre lorsque des fibres flexibles sont utilisées. Les expériences en SAOS (« small amplitude oscillatory shear »), ou cisaillement oscillatoire à faible amplitude, ont démontré que suite à un précisaillement à faible taux de cisaillement, lorsque la flexibilité et le rapport de forme de la fibre augmentent, la viscosité complexe de la suspension et le module élastique augmentent aussi. Le comportement des suspensions dépend de l'histoire mécanique car en effectuant le précisaillement à un taux de cisaillement plus élevé, les propriétés linéaires viscoélastique dépendent alors seulement du rapport de forme des fibres, indépendamment du module d'Young.

Des expériences de démarrage en cisaillement simple ont été faites dans des conditions d'écoulement dans le sens horaire et anti-horaire. Des pics pour la contrainte de cisaillement et la force normale ont été observés lors du mouvement en sens horaire; ces pics ont été attribués à l'orientation des fibres sous écoulement. Avec la flexibilité, la hauteur et largeur des pics augmentent aussi. Dnas le sens anti-horaire, un pic retardé a été observé. Avec l'augmentation de la flexibilité de fibre, la déformation à laquelle le pic de retour commence diminue. Étant donné que dans le sens anti-horaire le pic est attribué au basculement des fibres, les résultats transitoires ont suggéré que les fibres

flexibles étaient moins orientées sous écoulement lors du test précédent dans le sens horaire que les fibres rigides.

L'énergie requise pour l'orientation des fibres dans l'écoulement dans le sens horaire, et aussi l'énergie requise pour basculer les fibres dans la direction inverse ont été évaluées. Ce calcul a été fait à partir de l'aire sous la courbe de la contrainte en fonction de la déformation. Les résultats ont démontré que les valeurs de l'énergie requise pour l'orientation et le culbutage des fibres augmentent avec le taux de cisaillement. De plus, pour toutes les suspensions, l'énergie requise pour le culbutage des fibres est plus grande que l'énergie nécessaire pour l'orientation initiale des fibres dans la direction de l'écoulement. Également, en augmentant la flexibilité des fibres, l'énergie requise pour l'orientation et le culbutage des fibres augmente aussi Cette énergie dissipée est consommée afin de surmonter la force de friction statique aux points de contacts entre les fibres, et aussi vaincre les forces de flexion et d'étirements des fibres. Dans le cas des fibres flexibles, l'énergie considérable requise indique les fortes interactions qui existent entre elles, et la présence d'une structure similaire à celle d'un réseau percolé.

L'évolution de la microstructure des suspensions a été observée à divers taux de cisaillement en utilisant un microscope InfiniVar® à réglage continu placé sous la plaque inférieure d'un rhéomètre. La plaque en métal inférieure du rhéomètre Paar Physica UDS 200 a été remplacée par une plaque en verre pour les expéreinces de visualisation. Le microscope a été jumelé à une caméra couleur CCD (Lumenera) et les

données ont été obtenues en utilisant le logiciel StreamPix III® (NorPix). Des échantillons de suspensions ont été déformées sous écoulement à des taux de cisaillements différents jusqu'à l'obtention d'un régime permanent, et des séquences d'images ont été obtenues à une vitesse de 4 images par seconde. Pour chaque suspension et chaque taux de cisaillement, l'expérience a été répétée à 3 reprises. Ainsi 600 à 750 fibres ont été observées. Les images ont été utilisées pour calculer l'orientation du tenseur d'orientation de second ordre. Afin d'évaluer les composants de ce tenseur d'orientation, les calculs étaient basés sur l'hypothèse que la majorité des fibres, après avoir été comprimées entre les plaques parallèles lors de l'installation de l'échantillon, étaient en grande majorité dans le plan $r\theta$ et avaient donc une orientation planaire. Les expériences de visualisation ont démontré que l'orientation des fibres est dépendante du taux de cisaillement et de la déformation appliquée. La rhéo-microscopie des différentes suspensions a aussi démontré que les suspensions préparées avec des fibres plus flexibles étaient moins orientées dans la direction de l'écoulement que les fibres rigides, en accord avec les résultats précédents. Ainsi à un taux de cisaillement de 1 s^{-1} le taux d'évolution de l'orientation était plus rapide pour les fibres rigides.

Un modèle mésoscopique dans le cadre de GENERIC (« General Equation for Non-Equilibrium Reversible-Irreversible Coupling ») a été utilisé afin de prédire le comportement rhéologique des suspensions de fibres semi-flexibles et de leurs microstructures. Le modèle prend en compte les interactions entre fibres et aussi la nature semi-flexible de ces fibres. L'avantage d'utiliser la méso-hydrodynamique est la

garantie que les équations du modèle respectent la thermodynamique. Également, l'approche méso-hydrodynamique nous aide à comprendre les phénomènes en apportant une manière simple de lier la physique microscopique au comportement macroscopique observé. Nous avons comparé les prédictions du modèle GENERIC de Rajabian *et al.* (2005) avec les données rhéologiques obtenues dans les expériences de démarrage en cisaillement simple. Le fait que nous ayons utilisé une matrice newtonienne pour cette étude a avantageusement réduit le nombre de paramètres phénoménologiques ajustables du modèle de 8 à 3. La capacité de ce modèle à prédire l'orientation des fibres sous écoulement en cisaillement a aussi été examinée en comparant avec l'étude de visualisation. Les prédictions du modèle s'accordent qualitativement avec les données rhéologiques et la visualisation. Toutefois, plus d'effort doit être dévolu pour le développement d'un modèle qui décrira quantitativement le comportement complexe rhéologique des suspensions de fibre flexibles concentrées ou semi-concentrées, et ce à divers taux de cisailement.

Finalement, les effets de flexibilité sur le comportement rhéologique de suspensions de fibres dans une matrice viscoélastique (polyéthylène bassse densité (PEBD) fondu) ont été étudiés en cisaillement simple et oscillatoire à petite et grande déformation (SAOS et LAOS). Le cisaillement oscillatoire à large amplitude de déformation (LAOS) a aidé à la compréhension de la relation entre l'augmentation de la contrainte et l'orientation des fibres. Le torque brut et le signal de la force normale ont été obtenus à partir d'un rhéomètre à déformation imposée et l'utilisation d'une carte ADC (« Analog-to-Digital

Converter ») afin de garantir des résultats plus précis. Pour tout les composites, le signal de la contrainte a diminué avec le temps dans les expériences de LAOS. Ce comportement était aussi plus prononcé dans le cas des fibres plus rigides. La diminution de la contrainte a été expliquée par l'orientation plus efficace de ces dernières. L'énergie dissipée par cycle de LAOS a été évaluée pour chaque composite, et l'étude a démontré que pour les fibres avec plus de flexibilité. plus d'énergie était dissipée. De plus, l'énergie dissipée diminuait avec le temps, et cela a été interprété par une réduction dynamique des contacts entre les fibres. Ce phénomène transitoire a été plus prononcé dans le cas des fibres rigides, et les observations ont indiqué que la réduction des contacts entre ces fibres était plus importante. La première différence de contrainte normale a démontré une réponse non-sinusoidale et périodique en LAOS. L'analyse par transformée de Fournier (FFT) rapide a montré, pour les composaites, la présence d'une première harmonique correspondant à la fréquence appliquée, aussi bien qu'une deuxième harmonique aussi observée pour le PEBD sans fibres. Ces harmoniques ont résulté en des courbes de Lissajou asymétriques pour la force normale en fonction de la déformation des suspensions. Cette asymétrie a aussi été plus prononcée dans le cas des fibres rigides. Ces résultats ont été expliqués en termes d'effets de mémoire lié au temps et par l'orientation plus importante de ces fibres.

Table of Contents

List of Tables

List of Figures

ABREVIATIONS

Greek Symbols

γ	Strain
γ_R	Amplitude of strain in oscillatory shear flow
$\dot{\gamma}$	Shear rate
$\lvert\dot{\gamma}\rvert$	Second invariant of rate of deformation tensor
$\Delta\rho$	Mass density difference
δ	Phase angle
δ_1	First fundamental shift angle
η	Shear viscosity
η_m	Matrix viscosity
η_r	Relative viscosity
η^*	Complex viscosity
θ_{max}	Maximum angular deformation
Λ	Mobility tensor
Λ_{ff}	Mobility parameter
λ	Fiber shape factor
$\boldsymbol{\sigma}$	Stress tensor
ϕ_f	Fiber concentration
ϕ^*	Critical concentration
Φ	Free energy
Ξ	Dissipation potential
Ψ_1	First normal stress difference coefficient
$\boldsymbol{\Psi}(\mathbf{P})$	Distribution function
ω	frequency
$\boldsymbol{\omega}$	Vorticity tensor

Roman Symbols

a_2	2nd order orientation tensor
a_4	4th order orientation tensor
B_{ff}	Fiber-fiber interaction coefficient
C_I	Coefficient of interaction
D	Fiber diameter
D_r	Coefficient of rotational diffusion
E_b	Bending modulus of a rod
E_Y	Young's modulus

E	Energy per unit volume
E_σ	Dissipated energy
F	Normal force
g	Gravity constant
G'	Storage modulus
G''	Loss modulus
h	Average distance between fibers
K	Carter (1967) model constant
k_B	Boltzmann's constant
K_{flex}	Flexibility parameter
L	Length of fiber
n	Number density of fibers
N_1	First normal stress difference
N_2	Second normal stress difference
$\mathbf{P}$	Vector representing a single fiber orientation
w_{obs}	Observability correction function
Pe	Peclet number
r	Fiber aspect ratio
r_e	Equivalent aspect ratio
S	Entropy
S^{eff}	Effective stiffness
S_{order}	Entropy due to orientational ordering
S_{inter}	Entropy due to fiber-fiber interactions
T	Temperature
T	Torque
t_s	Sedimentation time
v_f	Volume of a single fiber

CHAPTER 1 - Introduction and Thesis Objective

In the past few decades, the flow of particle suspensions has generated considerable interest for research among engineers and scientists because of their numerous applications, both in engineering and scientific disciplines.

The reinforced materials are being used in a variety of structural applications requiring a high strength to weight ratio and are gradually replacing their metallic, wooden, ceramic and other counterparts. Polymeric composites are obtained by adding solid reinforcement to a polymeric matrix. Fibrous reinforcements consist of glass, carbon, Kevlar®, nylon, vinylon (PVA), and natural fibers which are mainly cellulose fibers. These fibers may be used in the form of continuous bundles or fibers, woven fabrics or chopped fibers. These materials add stiffness and strength to the polymeric matrix that can easily be processed.

Although the mechanical properties of short fiber reinforced materials are inferior to those of continuous fiber composites, the use of conventional processing equipments such as extruders and injection molding machines to produce short fiber-filled composites has made them quite popular.

Short-fiber filled composites are manufactured by various processes such as compression, injection molding or by extrusion. During the processing of fiber-reinforced composites; fibers will translate, rotate, bend and break. The mechanical properties of the final product are highly dependant on microstructural characteristics and orientation of fibers. The structure is affected by such features as fiber properties,

interactions, suspending fluid properties, and the flow field imposed. Understanding the relationships among these features, the suspension structure and the macroscopic properties can therefore aid in the design and optimization of processes and products.

Despite the fact that the proposal of various models and experiments involving fiber suspensions has been performed intensively in the past, numerous questions have still remained open.

One important factor that could impact orientation of fibers and rheological properties is fiber flexibility. The flexibility of the fiber may vary with the properties of the fiber, the strength of the flow field and furthermore its aspect ratio. Some theoretical works have tried to model the behavior of this kind of suspensions, but there is a lack of reliable experimental data in the literature on the rheology and flow of flexible fiber suspensions. The main objective of this thesis is to elucidate the effect of fiber flexibility and its associated parameters on the rheological properties and microstructure of various suspensions. To this end experimental and modeling studies are used to tackle the problem. Experimental studies in rheometry and flow visualization are performed using well-controlled model systems, and the modeling of the effects of fiber flexibility on the rheology and microstructure of these suspensions is performed.

In this context, the thesis is presented as follows:

In Chapter 2 the main findings about the rheology of fiber suspensions in the literature is reviewed. In particular, this chapter focuses on determining the impact of different parameters influencing the rheology of fiber suspensions, as described in the literature. This section is followed by a literature survey of various visualization techniques, and

finally different approaches for modeling the rheological and orientation of fiber suspensions are described in this chapter.

Chapter 3 summarizes the main findings of the three articles that represent the core of this thesis and that are subsequently presented in individual chapters.

Chapter 4 (Article 1) reports an experimental study on the rheology of model suspensions that is performed to elucidate the relationships between fiber concentration, fiber aspect ratio, flexibility and their effects on rheological properties.

Chapter 5 (Article 2) deals with an experimental and theoretical analysis of the effect of fiber flexibility on the rheological properties and microstructure of semi-flexible fiber suspensions in a Newtonian matrix.

In Chapter 6 (Article 3), the effect of fiber flexibility on the rheological properties of a fiber-filled viscoelastic material in simple shear flow and small and large amplitude oscillatory shear is analyzed.

Finally, a general discussion is presented in Chapter 7, while conclusions and recommendations are stated in Chapter 8.

CHAPTER 2 - Literature Review

It is of interest to understand the role of concentration and aspect ratio and their relation to the degree of interparticle interaction (fiber-fiber) as well as orientation distribution and interaction with the suspending medium. Before reviewing the rheology, it is important to have a basic understanding of fiber suspensions.

For this reason, first fiber suspensions are classified according to their concentration and length. Then the criteria for Brownian motion and particle sedimentation are discussed. This is followed by a review of the experimental work on the rheology of fiber suspensions in simple shear flow and small and large amplitude oscillatory shearing, and a literature survey concerning the characterization of fiber orientation. Finally different models and approaches to predict fiber motion are examined.

2.1 Concentration Regimes

Short fiber composites are reinforced with a fiber length small compared to the dimensions of the part. They may be considered as uniform cylinders suspensions characterized by their concentration, ϕ and their aspect ratio (r=L/D) where L is fiber length and D its diameter. The volume fraction of particles may also be presented by number density n (number of particles per unit volume):

$$n = \frac{\phi}{v_f} \tag{2-1}$$

where v_f is the volume of a single fiber.

The behavior of fiber suspensions is highly dependent on the concentration and aspect ratio of the fibers within the suspension. For this reason, three concentration regimes based on the degree of particle interaction and fiber excluded volume are introduced, as *dilute*, *semidilute*, and *concentrated.* (Tucker & Advani, 1994):

Dilute Regime. The *dilute* regime is described as one having a sufficiently low concentration of fibers in which a fiber is free to rotate without interference from contact with other fibers. Furthermore, it is assumed that there is no hydrodynamic interaction. Theoretically, this occurs when the average distance between the center of mass of two rods is more than length of the fibers. Therefore, a perfectly disperse suspension must obey the constraint $n << 1/L^3$ or $\phi << 1/r^2$ to be considered as *dilute.*

Semidilute Regime. The *semi-dilute* regime is such that hydrodynamic interaction, as a result of the relatively close proximity between fibers, is the predominant phenomena and some physical contact between fibers is present. Interaction between fibers is achieved when $n > 1/L^3$, but when the mean spacing between fibers, h, is on the order of the diameter of the fiber, physical contact between rods becomes an increasingly significant phenomena; therefore, the upper limit is subject to the constraint $h >> D$ (Doi & Kuzuu, 1980). The mean spacing between fibers is a function of the orientation state of the rods within the suspension.

For a random orientation state, the mean spacing is estimated as $h \approx 1/nL^2$, and for a suspension whose fibers are completely aligned, the mean spacing is of the order $h \approx 1/\sqrt{nL}$ (Doi & Edwards, 1978). This leads to two upper limits: $n << 1/(L^2 D)$ for

random orientation and $n << 1/(LD^2)$ for aligned orientation. So a suspension is considered as semi-dilute if (Eberle et al., 2008):

$$1/L^3 << n << 1/L^2D \quad \text{or} \quad 1/r^2 << \phi << 1/r \quad \text{for random alignment} \tag{2-2}$$

$$1/L^3 << n << 1/\sqrt{nL} \quad \text{or} \quad 1/r^2 << \phi << \pi/4 \quad \text{for alignment fibers} \tag{2-3}$$

Concentrated Regime. The *concentrated* regime is where $n \geq 1/L^2D$ or $\phi \geq 1/r$. In this range, the dynamic properties of the rods can be severely affected by fiber-fiber interactions and can lead to solidlike behavior (Doi & Kuzuu, 1980). Above some critical concentration ϕ^*, rodlike particles will preferentially align and become nematic. Doi and Edwards (1978) estimated the critical concentration to be $\phi^* \approx 4/r$, and Flory (1956) estimated $\phi^* \approx 12.5/r$. Because of this some authors classify the suspensions with concentrations lower than critical concentration as *semi-concentrated* regime (Petrich et al., 2000).

Figure 2.1 summarizes the definition of the concentration regimes.

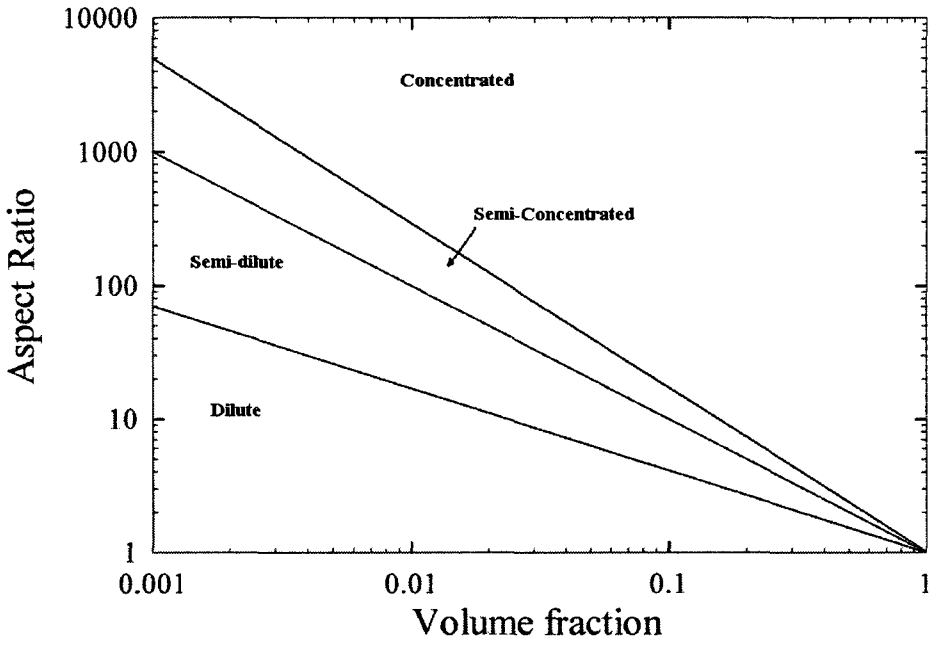

Figure 2.1 : Representation of concentration regimes (Tucker and Advani, 1994).

2.2 Sedimentation Time

Because of the difference in densities of particles and suspending medium, the fibers suspended in a fluid with viscosity of η_m are subject to sedimentation. Chaouche and Koch (2001) calculated the time required for a fiber oriented parallel to the vertical direction through a distance equivalent to its length by:

$$t_s = 8\eta_m L / \Delta\rho g D^2 \ln(2r - 0.72) \tag{2-4}$$

This characteristic time should be taken into account in experiments.

2.3 Brownian Motion

Brownian motion refers to the randomly movement of the particles. The relative effect of Brownian motion on the orientation of the fibers within the suspension can be determined by considering the ratio of the experimental shear rate, $\dot{\gamma}$, to the rotational diffusion constant, D_r, also known as the Péclet number, Pé = $\dot{\gamma}$ / D_r. For a fiber:

$$Pe = \eta_m \dot{\gamma} \pi L^3 / 3k_B T \ln r \tag{2-5}$$

in which η_m is the matrix viscosity, L is the fiber length, k_B is Boltzmann's constant, and T is the absolute temperature. If Pe is larger than 10^8, the fibers can be considered as non-Brownian (Chaouche and Koch, 2001).

2.4 Rheological Behavior of Fiber Suspensions

Fiber suspensions exhibit non-Newtonian behavior and are classified as complex fluids. Rheological properties are strongly dependent on concentration, aspect ratio and orientation of fibers. The fiber-fiber interactions and fiber-matrix are of great importance. Many investigations in this field have been carried out and their results are summarized below.

2.4.1 Steady State Viscosity

In steady state the presence of fibers increases the viscous and elastic components of suspension.

Whether in Newtonian or non-Newtonian medium, the presence of fibers increases the shear viscosity, especially at low shear rates (Kataoka & Kitano, 1981a, b; Nicodemo & Nicolais, 1974). The relative viscosity ($\eta_r = \eta/\eta_m$ with η and η_m, respectively, the viscosity of the suspension and the matrix) is a linear function of volume fraction of fiber suspensions ranging from dilute regime to semi-dilute regime (Bibbo *et al.* 1985; Kataoka & Kitano, 1981a; Sepehr *et al.* 2004a) and becomes quadratic for more concentrated systems (Djalili-Moghaddam & Toll, 2005). The increase is more pronounced for the longer fibers (Djalili-Moghaddam & Toll, 2005; Ganani & Powell, 1986; Huq & Azaiez, 2005) while a decrease is found for higher shear rates (Goto *et al.* 1986; Kataoka & Kitano, 1981a, b; Petrich *et al.* 2000; Chaouche and Koch 2001). Using a falling ball viscometer, Milliken *et al.* (1989) determined the relative viscosity of a suspension of fibers randomly oriented in a Newtonian fluid. They showed that η_r varies linearly for low concentrations (ϕ_f <12.5%) and η_r increased to a cubic relation for higher concentrations (12.5% <ϕ_f <23.15%). Using the same technique and same composite, Mondy *et al.* (1990) showed that for the same concentration (ϕ_f = 0.05), $\eta_r = 1.52$ for particles aligned while $\eta_r = 2.37$ for isotropic fiber orientation. This experiment demonstrates that viscosity of suspensions depend on fiber orientation. In simple shear, an isotropic fiber orientation generates a more viscous dissipation than the case of fibers aligned in the flow direction.

Ganani and Powel (1985) reviewed most the literature in the field of fiber suspensions in a Newtonian matrix. They found that the viscosity is dependent on the fiber fraction and

their aspect ratio. They also found that the dependence of a suspension viscosity on shear rate is more pronounced as the fiber aspect ratio increases. For suspensions of fibers in Newtonian matrix in non-dilute regimes, a slight shear thinning behavior is observed by many scientists (Kataoka & Kitano, 1981a; Goto *et al.* 1986a; Petrich *et al.* 2000; Sepehr *et al.* 2004a). The shear thinning behavior was explained by the destruction of a fiber network by increasing shear rate (Zirnsak *et al.*, 1994). The formation of a structure at low shear rates was attributed by Chaouche and Koch (2000) to inter-particle adhesive forces. Soszynksi and Kerekes (1988 a,b) studied flocs formation using nylon fibers of aspect ratios from 65 to 189 suspended in aqueous sugar solutions. They suggested that flocs formation is due to mechanical contacts and coherence of the fibers due to interlocking by the elastic bending of the fibers. In the mechanism proposed, called "elastic fiber interlocking", fibers become locked to form a network because of their elasticity.

The results by Czarnecki and White (1980) on glass fiber filled polystyrene indicated that the point of start of shear-thinning decreased as the fiber volume fraction increased. Crowson et al. (1980 a,b) reported that the Newtonian plateau which appears in viscoelastic materials (zero shear viscosity) tended to disappear when the fiber content increased especially with large aspect ratio fibers. The same behavior was reported by several authors (Laun, 1984; Greene & Wilkes, 1995; Kitano et al., 1984b; Mobuchon et al., 2005; Mutel & Kamal, 1984; Ramazani et al., 2001). In power law region viscosity of composite become close to neat matrix and at high shear rates the effect of

fibers are very low. (Czarnecki & White, 1980; Kitano & Kataoka, 1980, 1981b; Mutel & Kamal, 1984; Ramazani et al. 2001; Huq & Azaiez, 2005).

Composites with long fibers show yield stresses (Thomasset et al., 2005). However Laun (1984) found similar results and reported that concentrated short fiber suspensions were highly shear dependent and may present an unbounded value of the viscosity at low shear rates which suggests a yield stress.

2.4.2 Steady-State Normal Forces

Similar to the phenomena that are observed for the steady shear viscosity, the first normal stress difference of the suspensions is found to increase as the fiber volume fraction and aspect ratio increase (Chan et al., 1978; Goto et al. 1986; Mobuchon et al., 2005; Zirnsak et al., 1994; Nicodemo and Nicolais, 1974 ; Czarnecki and White, 1980; Sepehr et al., 2004a,b). In addition, N_2 is often neglected (Weissenberg hypothesis) since $N_2 \approx$ -10% N_1 (Bird et al. 1987). This result is confirmed for suspensions in a Newtonian fluid (Petrich *et al.* 2000; Sepehr et al. 2004b) and in a polymer melt (Chan et al., 1978).

The suspensions of fibers based on a Newtonian fluid exhibit a first normal stresses difference (Goto et al. 1986b; Kitano and Kataoka, 1981a; Petrich et al. 2000, Sepehr et al. 2004), while for the Newtonian matrix, $N_1 = 0$. This behavior is attributed to fiber-fiber interactions (Petrich et al., 2000; Sepehr et al., 2004b; Zirnsak et al., 1994).

In contrast to Brownian fiber suspensions and other fluids that undergo molecular relaxation and where N_1 is proportional to $\dot{\gamma}^2$, rigid fiber suspensions with contacts

show primary normal stress differences linearly proportional to shear rate (Sudararajakumar and Koch, 1997; Petrich et al., 2000)

Carter (1967) proposed the following correlation for the first normal stress difference as a function of shear rate, fiber content and fiber aspect ratio:

$$N_1 = K\eta_m\dot{\gamma}\frac{\phi\, r^{1.5}}{\ln 2r - 1.8} \tag{2-6}$$

This equation is based on the assumption that collisions between fibers are the major cause for nonzero normal stresses in steady flow. In this equation K is a constant that must be determined experimentally. Different authors have calculated K (Carter, 1967; Kitano and Kataoke 1981a; Goto *et al.,* 1986a; Zirnask *et al.,* 1994; Petrich *et al.,* 2000 and Sepehr *et al.,* 2004a) and it ranged from 0.04 to 0.32.

The presence of fibers in molten polymers increases the first difference of normal stresses of polymers (Chan et al. 1978; Kataoka & Kitano, 1981b; Mobuchon et al., 2005; Mutel & Kamal, 1984). Dependency on the shear rate of fiber-reinforced polymers is very close to that of neat polymer (i.e. N_1 is proportional to $\dot{\gamma}^2$ &, according to the theory of Lodge (1964).

2.4.3 Transient Shear Flow

The rheological behavior of fiber filled systems is sensitive to the distribution of fibers and their orientation, especially for concentrated suspensions (Laun, 1984; Milliken et al., 1989; Mondy et al., 1990; Ausias et al., 1992; Souloumiac and Vincent, 1998 ; Mobuchon et al., 2005; Sepehr et al., 2004 a, b).

When a fiber suspension is sheared, fibers with initially isotropic orientations evolve to reach a steady state when fibers become aligned in the flow direction. The change of fiber orientation during shear flow is reflected by the appearance of a peak viscosity which depends on the volume fraction and aspect ratio of fibers. For a neat matrix or polymers reinforced by glass beads there is no pronounced overshoot (Laun 1984; Sepehr et al. 2004b). Similarly, a second stress growth experiment in the same direction shows no viscosity overshoot since fibers are already oriented in flow direction by first experiment (Mutel & Kamal, 1987; Sepehr et al. 2004a; Sepehr et al., 2004a).

If after a stress growth experiment another experiment takes place in reverse direction a delayed overshoot is observed. This has been attributed to the tumbling of some fibers and called a "reverse overshoot" (Barbosa et al., 1994; Ramazani et al., 2001; Sepehr et al. 2004a; Sepehr et al., 2004b).

Laun (1984) found that a change of fiber orientation during shear flow gave rise to a pronounced overshoot of the normal stress before reaching a steady value. Sepehr et al. (2004a,b) measured the first normal stress difference in forward and reverse flow in stress growth and creep experiments using parallel plate rheometers and observed a huge peak in N_1. The peak in normal stress differences is much higher than the viscosity overshoot. By inversion the direction of flow N_1 exhibit negative values and then presents a positive peak before reaching steady state. The negative values of N_1 were attributed to a crystalline structure of the fiber suspensions under flow.

2.4.4 Dynamic Rheological Properties of Fiber Suspensions

In order to obtain information about the microstructure of suspensions, oscillatory shear flow experiments are commonly used by investigators, and more generally small amplitude oscillatory shear (SAOS). However several contradictions between published results can be observed.

From dynamic measurements of glass fiber in polypropylene, Mutel and Kamal (1986) found that at a frequency of 10 rad/s, these properties strongly dependent on strain, although pure resin dynamic properties showed strain-independent behavior over a broad strain range. This was not strange since, fiber orientation, which influenced rheological properties, was strongly affected by strain and actually at high strains the structure is changed and fibers tend to be aligned in flow direction.

Bibbo (1987) found dynamic viscosity depended strongly on fiber orientation for suspensions of nylon fibers in a Newtonian suspending medium. To study dynamic rheological properties, Greene and Wilkes (1995) used short and long glass fibers in polycarbonate, polypropylene and nylon-66. They found that storage and loss modulus and dynamic viscosity increased with fiber volume fraction. They also found that fibers increased the viscous and elastic nature of the fiber-filled composite at low frequencies and to a lesser extent at higher frequencies. The fibers increase the elastic component more than the viscous component at low frequencies and less at higher frequencies. Kitano *et al.* (1984) showed that polyethylene-based suspensions of vinylon fibers, which are more flexible than glass fibers, exhibited a stronger dependence of rheological properties on the fiber volume fraction as compared to glass fiber suspensions. They also

obtained the same results as Greene and Wilkes (1995) about the effect of fibers on tan (δ) – ratio of *G'/G"*- at different frequencies. In contradiction with these findings, Mobuchon *et al.* (2005) showed that the suspensions elasticity were the same as the matrix for glass fibers suspended in polypropylene, and hence tan (δ) was independent of fiber concentration and orientation. This behavior has also been confirmed by several investigators (Laun, 1984; Zirnsak *et al.,* 1994; Sepehr *et al.,* 2004a; Ferec *et al.,* 2008).

Gou *et al.* (2005) studied dynamic properties for the glass fiber suspension in linear low density polyethylene (LLDPE) using parallel plate rheometer. The authors found pronounced influence of fiber loading on storage modulus, loss modulus and dynamic viscosity. All these properties increased with fiber loading.

Regarding the effect of fiber aspect ratio on dynamic properties, Kotsilkova (1992) compared the dynamic rheological properties of pure silicone oil and suspensions containing glass fibers and glass beads. It was found that the storage and loss moduli and the complex viscosity were very sensitive to the aspect ratio. For the whole frequency range, these properties were larger for glass fiber than glass bead suspensions. Pre-shearing of the suspensions decreased these values. Based on the different behaviors of fiber and bead suspensions the author suggested that the structure, formed by entangled long fibers, was much larger in comparison with the structure associated with interactions between small particles.

Also, Guo *et al.* (2005) studied the dynamic properties of glass fiber suspensions with two different aspect ratios in a linear low density polyethylene (LLDPE). The authors reported that the storage and loss moduli increased with the fiber aspect ratio.

Investigating the effects of time, frequency and strain amplitude, Kim and Song (1997) concluded that the orientation of fibers decreased the complex viscosity η^*, and as the strain amplitude increased more fibers aligned with the flow direction. Finally, by modelling the nonlinear behavior of dilute suspensions of fibers in an Oldroyd-B fluid, Harlen and Koch (1997) indicated that fibers oriented in the flow direction during a cycle of oscillation. Petrich *et al.* (2000) also confirmed these findings through experiments on cellulose acetate propionate filaments and carbon fibers suspended in a Boger fluid.

Laun (1986) proposed an empirical relationship between the dynamic properties and the first normal stress difference coefficient, ψ_1:

$$\psi_1(\dot{\gamma}) = 2\frac{G'}{\omega^2}\left[1+\left(\frac{G'}{G''}\right)^2\right]^{0.7} \tag{2-7}$$

The alternative form is:

$$\psi_1(\dot{\gamma}) = 2\eta''(\sec\delta)^{1.4}\omega \tag{2-8}$$

The validity of this rule for suspensions of glass fiber in polypropylene was investigated by Mobuchon et al. (2005). They found this rule is applicable except at very low shear rates, which is due to domination of fiber-fiber interactions at low shear rates in concentrated regimes.

Large amplitude oscillatory shear (LAOS) (Dealy and Wisbbrun, 1990) provides a useful method to investigate complex fluids that exhibit microstructures that depend on the deformation history. The concept of large amplitude oscillatory shear (LAOS) in experimental studies was first applied years ago by Philippoff (1966), and Tee & Dealy (1975) to explore the nonlinear response of polymer solutions.

Fourier Transform (FT) rheology is the most common method for quantifying LAOS experiments (Wilhelm, 2002). For high deformation rates, if the material subjected to a shear deformation in which the shear strain is

$$\gamma(t) = \gamma_R \sin \omega t \tag{2-9}$$

where γ_R is the shear strain amplitude and ω is the angular frequency; the shear stress can be represented as a Fourier series of odd harmonics:

$$\sigma(t) = \sum_{m=1,odd}^{\infty} \sigma_m \sin(m\omega t + \delta_m) \tag{2-10}$$

where $\sigma_m(\omega,\gamma_0)$ and $\delta_m(\omega,\gamma_0)$ are the amplitudes and phase contents of harmonics respectively, and depend on both strain amplitude and frequency. Only odd harmonics are included in this representation because the stress response is assumed to be of odd symmetry with respect to directionality of shear strain or shear rate, i.e., the material response is unchanged if the coordinate system is reversed (Bird *et al.* 1987).

A Fourier-transformation of the time dependant torque is able to show in a very sensitive way the components of the higher harmonics at odd multiples of the applied frequency (Wilhelm, 2002).

Ericsson *et al.* (1997) investigated the dynamic properties of a glass fiber-filled polypropylene using a sliding plate rheometer. They showed that the loops of the shear stress vs. shear rate, or Lissajous curves, became skewed for an applied strain of 0.1, indicating the presence of higher harmonics. Mutel *et al.* (1986) characterized the behavior of a 10 wt % fiber filled polypropylene under oscillatory shear flow using parallel plates in rotational flow. Even if at low deformation the loss and storage moduli exhibited strong strain dependence, they found that the stress response presented no higher harmonics. By increasing the fiber concentration up to 40 wt %, Mutel (1989) observed a slight third harmonic for strain amplitude of 2.1. It is also possible to measure the normal stress differences for large amplitude oscillatory shear flow, as done by Endo and Nagasawa (1970) for concentrated polystyrene solutions in chlorinated diphenyl. They showed that the normal stress differences oscillated at twice the applied frequency, as predicted by the theory on elastic liquids (Lodge, 1964).

Ferec *et al.* (2008) measured the shear stress and primary normal stress difference responses to large amplitude sinusoidal strain input for suspensions of glass fibers in polybutene (Newtonian matrix) and polypropylene (viscoelastic matrix). They observed that the responses were very sensitive to fiber orientation. For suspensions of the Newtonian matrix the stress amplitude grew with time, but for the non-Newtonian matrix the stress amplitude decreased. Also the stress responses for all suspensions were harmonic, whereas the normal force responses were non-harmonic.

2.5 Fiber Orientation

The orientation distribution of short fibers in, for example, injection molded products requires a three-dimensional description and is correspondingly more complicated and difficult to determine. Changes in fiber orientation occur during the processing of short fiber composite materials. The changes are related to the geometrical properties of the fibers, the rheological properties of the matrix and the change in shape of the material which is produced by the processing operation. In these operations, the suspension undergoes both extensional flow and shear flow. During the extensional flow, the fibers could be oriented perpendicular to the elongation direction or rotate toward the direction of extension. In simple shear flow as shown in **Figure 2.2**, the rotation of the particle which is caused by the flow occurs. The rotation of fibers is called tumbling motion with a preferred residence time in the principal direction of flow. But for a population of fibers due to different interaction, the fibers motion is more complicated.

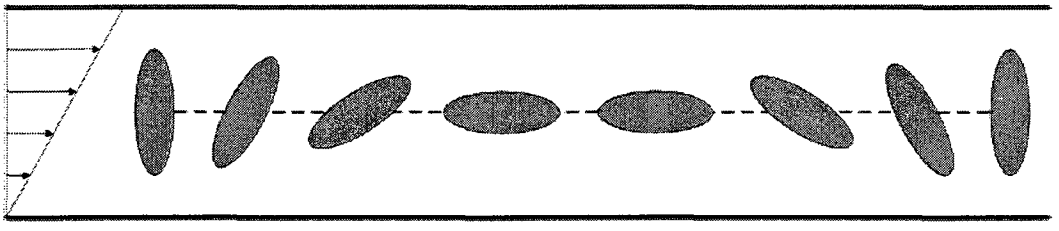

Figure 2.2 : Tumbling motion of a single particle in shear flow

Before one can predict the orientation of fibers in flow, one should be able to characterize and describe the orientation state of fibers. To represent the orientation state, one could use the orientation tensor description which has been successfully used

to describe the orientation state of short fibers (Advani and Tucker 1987; Tucker and Advani, 1990).

Orientation of each rigid or semi-flexible fiber can be characterized by a unit vector **P** placed in the average direction of its length as shown in **Figure 2.3**. The orientation of carbon nanotubes with completely curved shape has also been presented using this method by Fan and Advani (2005). In some composites, flexible fibers predominate and their descriptions require more details (Yamamoto and Matsouka, 1993; Yamamoto and Matsouka, 1996; Joung et al., 2001; Ross and Klingenberg, 1997; Schmid et al., 2000; Switzer and Klingenberg, 2003). This researchers have used direct particle level simulation techniques to calculate the position and orientation history of a system of particles in a fluid by numerically solving Nerwton's equations of motion (conservation of linear and angular momentum) for each particle in the system. Curvature and bending of fibers is modeled as linked spheres (Yamamoto and Matsuoka, 1993; Yamamoto and Matsuoka, 1996), rigid prolate spheroids connected end-to-end (Ross and Klingenberg, 1997), circular cylinders with hemispherical end-caps (Schmid et al., 2000; Switzer and Klingenberg, 2003). But here we are talking about rigid or semi-flexible fibers with limited amount of bending.

The components of $\boldsymbol{P}$ can be related to angles θ and φ:

$$P = \begin{cases} p_1 = \sin\theta\cos\varphi \\ p_2 = \sin\theta\sin\varphi \\ p_3 = \cos\theta \end{cases} \tag{2-11}$$

However, as there will be many fibers, it will be important to use a description that will embody many different directions. The most basic description is the probability distribution function $\Psi(\theta,\varphi)$. The probability distribution gives us a measure of the state of fiber orientation at a small element of suspension. Thus one can define $\Psi(\theta,\varphi)\sin\theta d\theta d\varphi$ which describe the probability of a fiber being orientated between the specific angles θ and $\theta+d\theta$ and angles φ and $\varphi+d\varphi$ (Figure 2.3). Here, $\sin\theta d\theta d\varphi$ is the increment in area on the surface of the unit sphere.

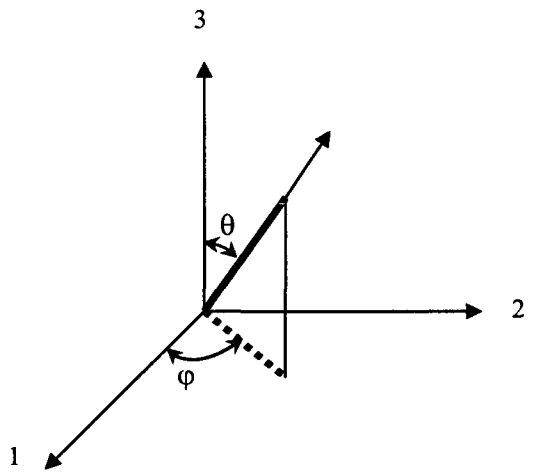

Figure 2.3 : Orientation of a single fiber in space

The distribution function must satisfy two conditions. First, one end of the fiber is the same as the other end. Thus, Ψ must be periodic:

$$\psi(\theta,\varphi)=\psi(\pi-\theta,\varphi+\pi) \tag{2-12}$$

The second condition arises from the physical fact that all fibers have some orientation, so the integral of the distribution function over all directions can be normalized:

$$\int_{\theta=0}^{\pi}\int_{\varphi=0}^{2\pi}\psi(\theta,\varphi)\sin\theta d\theta d\varphi = \oint\psi(P)dP = 1 \tag{2-13}$$

However, a more compact description of the state of fiber orientation in a composite is obtained by the second moments of the probability distribution function. These moments are called orientation tensors (Advani & Tucker, 1987). The dyadic products of unit vector P, weighted by the distribution function are integrated over all possible directions to form the orientation tensors of the second and fourth order, respectively:

$$a_2 = \langle PP \rangle = \int_P PP\psi dP \tag{2-14}$$

$$a_4 = \langle PPPP \rangle = \int_P PPPP\psi dP \tag{2-15}$$

Since the distribution function is even, the orientation tensors of odd order are all zero. Also, the higher is the order tensor, the better the description of the orientation of the fibers.

From the normalization condition (equation 2-13) it can be shown that:

$$tra_2 = a_{ii} = 1 \tag{2-16}$$

and;

$$a_{ijkk} = a_{ij} \tag{2-17}$$

As a result, only five and fifteen components are sufficient to determine a_2 and a_4, respectively.

2.6 Calculation of Orientation Tensors

A number of different methods for measurement of fiber orientation distribution exist, although most techniques have the similarity that they involve the inspection of the fiber cross-sections on a carefully prepared image. Consider the fiber presented in **Figure 2.3**. The components of the second-order orientation tensor, a_2, which provides a concise description of the orientation state of N fibers can be expressed as below,

$$a_{ij} = \frac{1}{N}\sum_{k=1}^{N} a_{ij}^{k} = \frac{1}{N}\left(\sum_{k=1}^{N} P_i^k P_j^k\right) \tag{2-18}$$

where as described before $P_i^k P_j^k$ is a dyadic product of the kth fiber's vector components.

For any fiber, the probability of its intersection with a section plane decreases with the decreasing its angle with section plane and reduced fiber length, leading to progressive undercounting of fibers as their angle with section plane decreases (Tucker and Advani, 1994). To correct for this bias, a weighting function, w_{obs}, which is referred to as the observability-correction function, must be applied to the sectional distribution data. Alternative forms of this function were presented by Zhu et al., (1997); Bay and Tucker, (1992); and Möginger and Eyerer, (1991) and are presented in Table 2.1.

Table 2.1 : Alternative forms of observability-correction function	
Zhu et al. (1997)	$w_{obs} = (r\cos\theta + \sin\theta)^{-1}$
Bay and Tucker (1992)	$w_{obs} = \begin{cases} (r\cos\theta)^{-1} & for\ \theta \le \theta_C = \cos^{-1}(1/r) \\ 1 & for\ \theta \ge \theta_C \end{cases}$
Moginger and Eyerer (1991)	$w_{obs} = \left\{ r^2\cos^4 + \left[\left(\frac{r+\delta}{1+\delta} \right)^2 + \left(\frac{r(1+\delta)}{1+\delta} \right)^2 \right] \sin^2\theta\cos^2\theta + \sin^4\theta \right\}^{-0.5}$ where δ is found by solving $r = \frac{\delta(1=2\delta+\delta^2)}{\frac{\pi}{4v_f} - 1 - 2\delta - \delta^2}$ and v_f is fiber volume fraction

where $r = L/D$ is the fiber aspect ratio.

In order to derive an unbiased estimate of the orientation tensor, the tensor components of each fiber must be weighted by observability-correction function, w_{obs}^k. This results in the following equation for the weighted orientation tensor,

$$a_{ij} = \frac{\sum_{k=1}^{N} w_{obs}^k a_{ij}^k}{\sum_{k=1}^{N} w_{obs}^k} \qquad (2\text{-}19)$$

If most of the fibers, be parallel to plane 1-2 (flow and vorticity plane). In this case the fiber orientation can be redefined as illustrated in **Figure 2.4**. Hence, $w_{obs}^k = 1$ (Bay and Tucker, 1992) and the components of the second-order orientation tensor can be calculated as:

$$a_{ij} = \frac{\sum_{k=1}^{N} P_i P_j}{N} \tag{2-20}$$

where N is the total number of fibers.

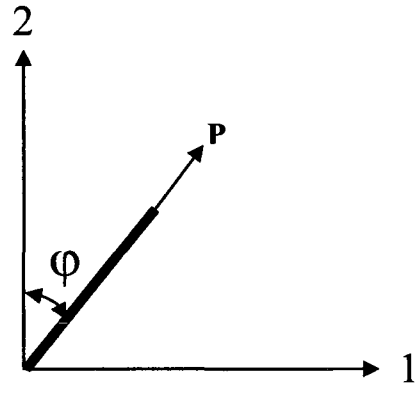

Figure 2.4 : Unit vector P describing the orientation state of a fiber in 1-2 plane.

2.7 Graphical Representation of Orientation Tensors

One can use the components of the orientation tensor in two or three dimensions to draw an ellipse or ellipsoid to describe orientation state graphically. The method to present two dimensional orientation tensors as ellipses is described in this section. From the image analysis of fibers, a vector with the average direction of each fiber can be associated. Using method described in previous section (2-6), the components of a_{ij} can be calculated. Next, the principal values of the second order orientation tensor can be calculated by diagonalizing it from a_2 to a_2 * using following equation;

$$a_2^* = Q \times a_2 \times Q^T = \begin{bmatrix} \cos(\theta) & \sin(\theta) \\ -\sin(\theta) & \cos(\theta) \end{bmatrix} \begin{bmatrix} a_{11} & a_{12} \\ a_{21} & a_{22} \end{bmatrix} \begin{bmatrix} \cos(\theta) & -\sin(\theta) \\ \sin(\theta) & \cos(\theta) \end{bmatrix} = \begin{bmatrix} a_{11}^* & 0 \\ 0 & a_{22}^* \end{bmatrix} \quad (2\text{-}21)$$

The diagonal components of a_2^*, a_{11}^* and a_{22}^* will be the length of major and minor axes of the ellipse. Therefore, in the ellipse, the major axis represents the preferred orientation of fibers. The value of the major and minor axes of the ellipse represents the degree of orientation in that direction (Advani and TuckerIII 1990).

Thus an elongated ellipse will signify higher degree of alignment in the direction of the major axis, whereas a circle will signify no particular preference of orientation as shown in some examples in **Figure 2.5**. From the ellipse, one can gauge the preferred fiber orientation direction and the magnitude of this alignment.

2.8 Dynamics of Orientation of Fibers

After describing various methods of representation of orientation, in this section the mathematical models developed to describe the dynamics of orientation is presented.

2.8.1 Motion of a single fiber

The pioneering work of Jeffery (1922) to describe the motion of a single fiber is the basis of most of the models for dynamics of orientation of fibers in suspensions. A comprehensive discussion of suspensions of rigid, neutrally buoyant and axisymmetric particles is given by Brenner (1974).

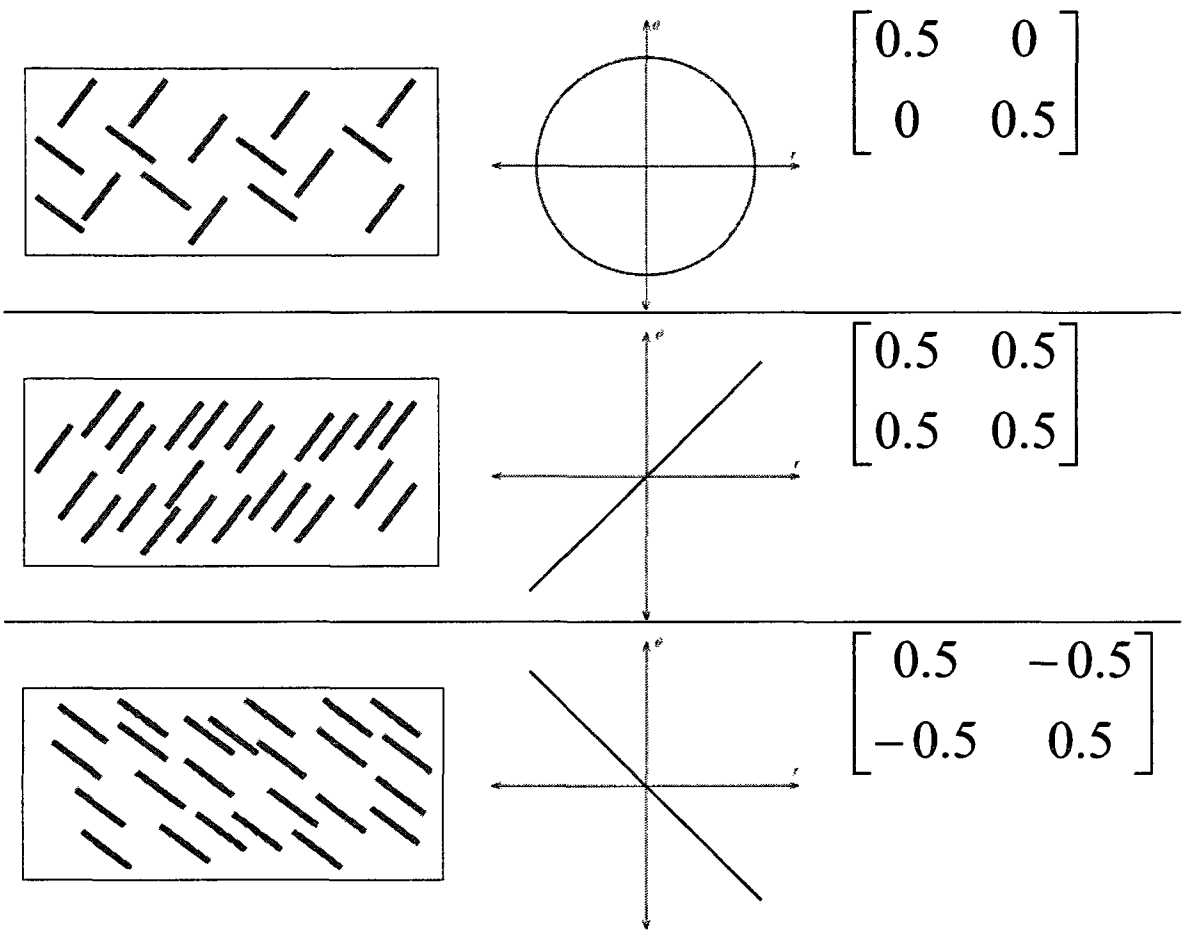

Figure 2.5 : Illustration of second order orientation tensor and use of an ellipse to graphically represent the orientation state in a planar region.

A review on this subject also can be found in Petrie (1999). The work of Jeffery (1922) deals specifically with particles possessing fore-and-aft symmetry suspended in a Newtonian liquid in a flow with a homogeneous velocity gradient. The motion was referred to as Jeffery orbit. In the absence of inertia and external forces, the equation of Jeffery is formulated as followed:

$$\frac{DP}{Dt} = \dot{P} = -\frac{1}{2}\omega.P + \frac{1}{2}\lambda\left(\dot{\gamma}.P - \dot{\gamma} : PPP\right) \tag{2-22}$$

λ is the shape factor of particle and for fibers it is expressed by:

$$\lambda = \frac{r^2 - 1}{r^2 + 1} \tag{2-23}$$

$\dot{\gamma}$ corresponds to rate of deformation tensor and ω to the vorticity tensor.

One important prediction concerning the motion of a fiber in a simple shearing flow is the rotation of the particle which is caused by the flow (Figure 2.2).

The fiber spends most of the time aligned with flow. As it rotates away from the plane, the fiber flips rapidly until it becomes nearly aligned again. The period of the rotation is:

$$T = \frac{2\pi}{\dot{\gamma}}\left(r + \frac{1}{r}\right) \tag{2-24}$$

Jeffery hypothesized particle as a prolate spheroid, which is an idealization of a rigid fiber, to obtain his results. However, in reality, many fibers have rod-like shapes that are best described as cylindrical. After experimental investigation on measuring the period of rotation by several authors using different particles (Bretherton, 1962; Burgers, 1938; Cox, 1971; Trevlyan and Mason, 1951; Mason and Manley, 1957; Nawab and Mason, 1958) an equivalent aspect ratio, r_e, was introduced (also called effective aspect ratio). This effective aspect ratio, r_e, can be inserted to Jeffery equations instead of r.

Trevlyan and Mason (1951), Mason and Manley (1957) and Nawab and Mason (1958) estimated r_e experimentally by measurement of the period of rotation of cylindrical rods. They found that r_e decreased from $0.7r$ to $0.53r$ as the aspect ratio, r, increased from 20.4 to 115.3. Forgacs and Mason (1959) concluded that imposed shear can bend

fibers with low modulus and decrease the effective aspect ratio and shorten the period of rotation; so they introduced an effective aspect ratio by following formula:

$$r_e = 1.24r / \sqrt{\ln r} \tag{2-25}$$

Elongated particles are not perfectly rigid and can deform during flow. The straining motion in the flow field can produce sufficiently large axial forces to cause the fiber to buckle during rotation. Forgacs and Mason (1959) found the critical stress required to buckle a fiber to be

$$\left(\dot{\gamma}\ \eta_0\right)_{crit} \cong \frac{E_b(\ln 2r - 1.75)}{2r^4} \tag{2-26}$$

In which the bending modulus of the rod is $E_b \approx 2E_Y$, where E_Y is the Young's modulus of the fiber is.

A flexible fiber in a flowing fluid can assume a variety of shapes as it rotates. Arlov et al. (1958) and Forgacs and Mason (1959) performed experiments on different types of flexible fibers to examine fiber motion. Dilute suspensions of fibers were observed between rotating concentric cylinders. Stiff fibers tended to rotate with periodic closed orbits as predicted by Jeffery. The effective flexibility of fibers was varied by adjusting the fluid viscosity, the shear rate, and by using fibers of different aspect ratios. As the fluid viscosity and shear rate increase, the viscous forces acting on a fiber increase to cause it to appear more flexible. Longer fibers exhibit lower critical stresses necessary for buckling [see Eq. (2-26)], and thus are effectively more flexible.

As the fibers become flexible, they exhibite more complex rotations classified as *flexible* orbits. Arlov et al. (1958) qualitatively classified the dynamics of flexible fibers into five modes: *"flexible spin"*, *"flexible spin-rotation"* and some other configurations when the fiber is extremely flexible, such as *"springy rotations"*, *"snake turn"* and *"S-turns"*. Examples of the various conformations of flexible fibers observed are summarized in **Figure 2.6**.

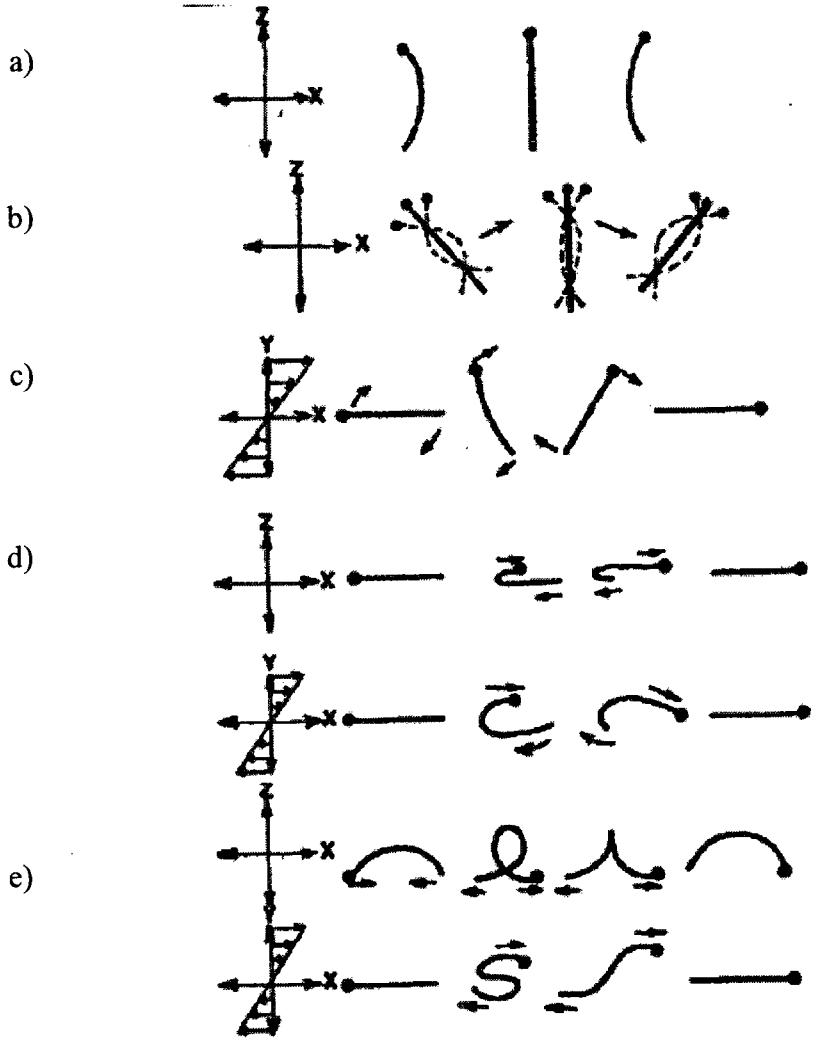

Figure 2.6 : Typical rotational orbits of flexible fibers. The black dots denote the same end of a fiber throughout each type of rotation. a) flexible orbit, b) flexible spin rotation, c) springy rotation, d) snake turn e) S-turns (Arlove et al. 1958)

The equation of Jeffery (1922) describes well the motion of a particle for dilute suspensions because fiber moves freely without being subjected to mechanical and hydrodynamic interactions in particular. In the industrial world, the suspensions are concentrated so that the fibers can no longer be considered separately. However for such systems, the theory of Jeffery (1922) predicts qualitatively the dynamics of orientation, but the level of alignment is different, without exhibiting periodic rotations. These effects are mainly attributed to interactions between the fibers; hence Folgar and Tucker (1984) modified Jeffery's theory to include a phenomenological term that prevented full alignment of fiber orientation, called the Folgar-Tucker model. From a phenomenological concept, the diffusion term was introduced as $D_r \nabla \ln \psi = C_I |\dot{\gamma}| \nabla \ln \psi$. D_r and C_I are the coefficients of rotational diffusion and interaction, while $|\dot{\gamma}|$ is the second invariant of the rate of deformation tensor and ∇ is gradient operator. Finally the equation of motion is given by:

$$\frac{DP}{Dt} = \dot{P} = -\frac{1}{2}\omega.P + \frac{1}{2}\lambda\left(\dot{\gamma}.P - \dot{\gamma} : PPP\right) - D_r.\nabla \ln \psi \tag{2-27}$$

.

2.8.2 Evolution of the orientation tensor

The time evolution of the distribution function of orientation satisfies equation of continuity in the sense that a particle which leaves an orientation should reappear in another. Therefore, a balance of flows leads to (Bird et al., 1987b):

$$\frac{D\psi}{Dt} = -\nabla.\left(\dot{P}\psi\right) \tag{2-28}$$

By combination of equations (2-28) with (2-14) and (2-15), Advani and Tucker (1987) derived the evolution of the second order orientation tensor a_2, expressed as follows:

$$\frac{Da_2}{Dt} = \dot{a}_2 = -\frac{1}{2}(\omega.a_2 - a_2.\omega) + \frac{1}{2}\lambda(\dot{\gamma}.a_2 + a_2.\dot{\gamma} - 2a_4 : \dot{\gamma}) + 2D_r(\mathrm{I} - 3a_2) \tag{2-29}$$

where **I** is the unit tensor.

Folgar and Tucker (1984) suggested a phenomenological model for D_r, which is expressed as $D_r = C_I|\dot{\gamma}|$, where an interaction coefficient, C_I, is an phenomenological parameter that must be determined by comparing predictions with experiments. Sepehr et al. (2004b) and Ferec (2008) has brought a complete literature review about this coefficient.

Model predictions of the rheological stress growth functions using the Folgar-Tucker model compared to experimental results suggest that the rate of fiber orientation is much slower than theory predicts (Sepehr et al. 2004b). This was attributed to fiber-fiber contact reducing the rate of fiber orientation. As a result Sepehr et al.(2004a) introduced a "slip" parameter to the F-T model, effectively reducing the rate of fiber reorientation.

$$\gamma_s = \alpha\gamma \tag{2-30}$$

where the slip coefficient, α , is some value between 0-1. The addition of the slip parameter to the equations governing fiber motion results in a loss of model objectivity. However, the physical aspects of the model are still valid in the case of simple shear flow.

Ferec et al. (2009) developed a model that in addition to orientation tensors, interaction tensors were introduced and a new equation of change for the second-order orientation

tensor was derived, and an additional extra stress term was developed to take into account the contribution induced by the interacting forces. (For details see Ferec et al., 2009)

2.8.3 Evolution of orientation tensor in thermodynamic approach

Following a thermodynamic approach based on Hamiltonian structure (Grmela, 1986; Grmela and Carreau, 1987), Authors (Gosh 1993, Gosh *et al.* 1995) proposed an alternative to describe the evolution of orientation tensor. The time evolution of microstructure tensor can be written as:

$$\dot{a}_2 = -\frac{1}{2}(\omega.a_2 - a_2.\omega) + \frac{1}{2}(\dot{\gamma}.a_2 + a_2.\dot{\gamma}) - \Lambda.a_2.\frac{\partial \Phi}{\partial a_2} \tag{2-31}$$

The equation consists of a convective part and a dissipative part. Where Λ is the mobility tensor and Φ is the free energy of system. The derivative of the thermodynamic potential is expressed by:

$$\frac{\partial \Phi}{\partial a_2} = \frac{k_B T}{2}\left[\beta I - S_B a_2^{-1} - L^2 S_L a_2^{-1}.a_2^{-1} + 2\frac{S_0}{L^2}\left(I - \frac{a_2}{L^2}\right)\right] \tag{2-32}$$

with k_B the Boltzmann constant and T the absolute temperature. β is a multiplier of Lagrange which makes it possible to take account that fibers preserve their initial lengths through the flow. S_B takes account the dissipative contribution of Boltzmann due to orientational ordering. S_L is a coefficient which balances the contribution of semi-flexibility of fibers and finally S_0 introduced by Onsager (1949) and measures the volume excluded by fibers.

In their paper, Ghosh et al. (1995) introduced an isotropic mobility tensor by the following expression:

$$\Lambda = \Lambda_0 \frac{\left(1-\frac{n^2}{n_0^2}\right)}{\left[1-a\ tr\left(\frac{a_2.a_2}{L^4}\right)\right]^2} I \tag{2-33}$$

where Λ_0 is mobility constant, n_0 the maximum concentration of fibers and a is a parameter for correction of orientation ($0 \le a \le 1$).

Rajabian et al. (2005) developed a mesoscopic model in the framework of GENERIC (General Equation for Non-equilibrium Reversible-Irreversible Coupling), which guarantees the compatibility of dynamics of suspensions with thermodynamics. The model takes into account the fiber-fiber interactions and also the semi-flexible nature of the fibers. The time evolution of second order orientation tensor is expressed as:

$$\frac{da_2}{dt} = \dot{a}_2 = -\frac{1}{2}(\omega.a_2 - a_2.\omega) + \frac{1}{2}\lambda(\dot{\gamma}.a_2 + a_2.\dot{\gamma} - 2a_4 : \dot{\gamma}) - \frac{\partial \Xi}{\partial \Phi_{a_2}} \tag{2-34}$$

where Ξ is dissipation potential and Φ_{a_2} is the free energy derivative with respect to the second order orientation tensor. The free energy is given by:

$$\Phi(u,\ a_2) = E(u) - k_B T S(a_2) \tag{2-35}$$

where E is the overall kinetic energy, S the entropy of system and $\boldsymbol{u}$ is the overall momentum. The overall kinetic energy is given by:

$$E(\boldsymbol{u}) = \int dr \frac{u_i u_j}{2\rho} \tag{2-36}$$

The entropy is a function of orientation of fibers, a_2, and is expressed in two terms:

$$S = S_{order} + S_{inter} \tag{2-37}$$

S_{order} is the entropy due to the orientational ordering and S_{inter} due to the fiber-fiber interactions. The orientational order entropy is due to presence of fibers and two type of fibers are distinguished: rigid and semi-flexible fibers. For rigid fibers the entropy is analogous to well known Grmela-Carreau (1987) entropy for polymeric chains and is given by:

$$S_{order}^{rig} = \frac{1}{2} n_f \ln \det \frac{a_2}{L^2} \tag{2-38}$$

where n_f is the number density of fibers. For semi-flexible fibers the orientational order entropy is given by:

$$S_{order}^{flex} = -n_f L^2 K_{flex} tra_2^{-1} \tag{2-39}$$

The entropy for orientational ordering for fibers with limited flexibility is follows from the expression derived by Khokhlov and Semenev (1985) in kinetic theory. By K_{flex}, $(0 < K_{flex} < 1)$, a macroscopic or phenomenological parameter characterizing the flexibility is denoted. To be able to consider fibers of varied flexibility, orientational ordering entropy is given by:

$$S_{order}^{fib} = n_f K_{flex} L^2 tr\boldsymbol{a}_2^{-1} + n_f (1 - K_{flex}) \frac{1}{2} \ln \det \frac{\boldsymbol{a}_2}{L^2} \tag{2-40}$$

The entropy due to the topological fiber–fiber interactions is obtained from Onsager's theory (1949) as follows:

$$S_{inter} = -B_{ff} l^{-4} n_f^2 \left((tra)^2 - traa \right) \tag{2-41}$$

By B_{ff} a phenomenological parameter proportional to the fiber-fiber interactions is denoted. B_{ff} has to be determined from the experimental data of fiber orientation tensors components or optionally from the measured viscosity and first normal stress difference for the suspensions. (Rajabian *et al.*, 2005; Rajabian *et al.*, 2008)

Altogether, using equation 2-35, the free energy is expressed as:

$$\Phi(u,\ a) = \int dr \frac{u_i u_j}{2\rho} - k_B T[(1-K_{flex})\frac{1}{2} n_f \ln \det \frac{a_2}{L^2} - K_{flex} L^2 n_f tra^{-1} - B_{ff} L^{-4} n_f^2 \left((tra_2)^2 - tra_2 a_2\right)] \tag{2-42}$$

and The free energy derivative ϕ_a is obtained from the following expression:

$$\phi_{a_2} = \frac{\partial \phi}{\partial a_{i2}} = -\frac{k_B T}{2}\left[n_f (1-K_{flex}) a_2^{-1} + n_f K_{flex} a_2^{-1} a_2^{-1} I - 2 n_f B_{ff} (I - a_2)\right] \tag{2-43}$$

In the absence of dissipation phenomena only the advective parts appears in the time evolution equation and the total free energy remains unchanged with the flow. Neglecting the dissipation terms indeed simplifies equation 2-34 to the original Jeffery's model, initially developed for a single fiber's motion in a viscous flow. Rajabian et al. (2005) used the modified form of the dissipation potential proposed as by Edwards *et al.* (2003), which depends on the free energy derivative with respect to the second order orientation tensor, ϕ_a, as follows:

$$\Xi = \Lambda_{ff}\left(\frac{\partial v_s}{\partial x_r}\frac{\partial v_r}{\partial x_s}\right)^{1/2}\left(\phi_{a_2} - \frac{1}{3} tr\phi_a I\right) a_2 \left(\phi_{a_2} - \frac{1}{3} tr\phi_a I\right) \tag{2-44}$$

where Λ_{ff} is a fiber mobility parameter that has to be determined from rheological data or orientation tensor components.

This approach is suitable for studying the microscopic phenomena easily using phenomenological parameters. For example most of the work in the area of rheology of flexible fibers is related to direct simulation techniques in which one calculates the position, orientation history and shape of fibers due to bending and twisting in a fluid as described previously (Wang *et al.,* 2006; Yamamoto and Matsuoka, 1993; Yamamoto and Matsuoka, 1996; Ross and Klingenberg 1997; Schmid *et al.,* 2000; Joung *et al.,* 2001; Switzer and Klingenberg, 2003). Such approaches require detailed initial physics that must be provided into the simulation tool, but in return detailed information about the motion of the particles and the behavior of the suspension is obtained. The disadvantage of this approach is the limited number of fibers that can be considered and the complexity of the calculations, including the numerical solution of the governing equations.

But meso-hydrodynamics approach contributes to the understanding of the phenomena observed by providing a simple way to link the microscopic physics involved to the macroscopic behavior observed (Rajabian *et al.,* 2005). In addition, another advantage of the mesocopic modeling approach is that the solution of the governing equations is relatively simple compared to particle level simulations. So, relatively simple mesoscopic models can be incorporated into larger computer programs to calculate complex flows of suspensions.

2.9 Closure Approximations

In equations giving the evolution of second order orientation tensor a_2, it is necessary to know the 4th order orientation tensor a_4. Generally the orientation tensor a_2 is used to represent the state of orientation, while the tensor a_4 remains unknown. However the evolution of a_4 involves 6th order orientation tensor a_6 (Advani & Tucker, 1987) and this pattern repeats itself for higher order tensors. This problem is avoided by using the closure approximations which allow evaluating a tensor of order (2i +2) by a tensor of order (2i). Up to date, many closure approximations have been developed and used in the numerical simulation. In this section, a brief review of closure approximations is presented followed by the details of orthotropic closure approximation which was used in our simulations.

Advani and Tucker (1987, 1990) proposed a hybrid closure approximation, which combines linear and quadratic forms of closure approximations.

$$a_{ijkl}^{Hyb} = (1-f)a_{ijkl}^{Lin} + f a_{ijkl}^{Qua} \tag{2-45}$$

where $f = 1 - 27\det(a_2)$ and a_{ijkl}^{Lin} and a_{ijkl}^{Qua} are linear and quadratic closure approximations respectively defined as:

$$\begin{aligned} a_{ijkl}^{Lin} = & -\frac{1}{35}\left(\delta_{ij}\delta_{kl} + \delta_{ik}\delta_{jl} + \delta_{il}\delta_{jk}\right) \\ & + \frac{1}{7}\left(a_{ij}\delta_{kl} + a_{ik}\delta_{jl} + a_{il}\delta_{jk} + a_{kl}\delta_{ij} + a_{jl}\delta_{ik} + a_{jk}\delta_{il}\right) \end{aligned} \tag{2-46}$$

$$a_{ijkl}^{Qua} = a_{ij} a_{kl} \tag{2-47}$$

Advani and Tucker (1990) showed that linear closure approximation works well when the fibers remain nearly random, but introduces an artificial instability into the equations for highly aligned suspensions. The quadratic closure approximation performs well for highly aligned states, but introduces steady-state errors for more random states. The hybrid closure performs well over the entire range of orientation states from random to aligned one.

A natural closure approximation was later proposed by Verley and Dupret (1994). It is a polynomial function of the second-order orientation tensor, which agrees with the analytic solutions of the orientation distribution function when assuming no fiber-fiber interactions. Cintra and Tucker (1995) proposed an orthotropic fitted closure approximation in which three independent terms of the fourth-order orientation tensor were selected by assuming orthotropy. They reported that orthotropic fitted closure approximation was more accurate than any earlier closure approximation, and slightly more accurate than Verley and Dupret's (1994) natural closure. Chuang and Kwon (2002) proposed an invariant-based optimal fitting (IBOF) closure approximation. It adopted the most general expression of a full symmetric fourth order tensor using a symmetric second order tensor and an identity tensor. IBOF is a hybrid of the natural and the orthotropic fitted approximations. They stated that IBOF required less computational time.

2.9.1 Orthotropic Fitted Closure Approximation

Cintra and Tucker (1995) originally developed orthotropic closure approximations. In the formulation of the orthotropic closure, the principal axes of a_4 are the same as those of a_2. When a_4 is expressed in its principal axes, some of its components are constrained to zero, while the remaining components are functions of the eigenvalues of a_2. a_2 having a trace of one; hence, only two of the eigenvalues, λ_1 and λ_2, are independent with $\lambda_1 \geq \lambda_2$ and the summation of eigenvalues is equal to 1.

According to the orthotropic properties of a_4, there are six non-zero principal components of a_4. Cintra and Tucker (1995) suggested to use a contracted notation and each pair of indices in a_{ijkl} is is replaced by a single index that ranges from 1 to 6: $A_{mn} \Leftrightarrow a_{ijkl}$, where *m* is related to *ij* and *n* is related to *kl* according to Table 2-2.

Table 2.2 : Relationship between indices in contracted and tensor notation

m or *n*	*ij* or *kl*
1	11
2	22
3	33
4	23 or 32
5	31 or 13
6	12 or 21

With full symmetry and normalization conditions, only three of the six principal values of a_{ijkl} are independent (A^*_{11}, A^*_{22} and A^*_{33})

The components have to be written in terms of the eigenvalues of a_2 :

$$\begin{cases} A_{11}^{*} = f_{11}(\lambda_1, \lambda_2) \\ A_{22}^{*} = f_{22}(\lambda_1, \lambda_2) \\ A_{33}^{*} = f_{33}(\lambda_1, \lambda_2) \end{cases} \tag{2-47}$$

Wetzel and Tucker (1999) proposed the following polynomial equation to calculate the components:

$$\begin{aligned} A_{mm}^{*} = {} & C_m^1 + C_m^2\lambda_1 + C_m^3\lambda_2 + C_m^4\lambda_1\lambda_2 + C_m^5{\lambda_1}^2 + C_m^6{\lambda_2}^2 \\ & + C_m^7{\lambda_1}^2\lambda_2 + C_m^8\lambda_1{\lambda_2}^2 + C_m^9{\lambda_1}^3 + C_m^{10}{\lambda_2}^3 + C_m^{11}{\lambda_1}^2{\lambda_2}^2 \\ & + C_m^{12}{\lambda_1}^3\lambda_2 + C_m^{13}\lambda_1{\lambda_2}^3 + C_m^{14}{\lambda_1}^4 + C_m^{15}{\lambda_2}^4 \end{aligned} \tag{2-48}$$

Here, m ranges from 1 to 3. The final task is to get C_m^k parameters. Cintra and Tucker (1995) suggest values for C_m^k to form the closure approximations ORF and ORL (obtained by quadratic polynomial interpolation). These relationships provide significant improvements compared with basic approximations such as quadratic closure approximation but generate non-physical oscillations, especially for low coefficients of interaction C_I (phenomenological parameter in equation 2-29) in simple shear flow.

Verweyst (1998) and Wetzel (1999) introduced another version of orthotopic fitted closure approximations, ORT, that differs from ORF or ORL and in that analytical solutions corresponding to $C_I = 0$ and $\lambda = (r^2+1)/(r^2-1) = 1$ are adopted, similar to the procedure used for the Natural closure approximation proposed by Verleye and Dupret (1994).

2.10 Constitutive Equations for Fiber Suspensions

To model a process correctly, it is important to have the general constitutive equation, which represents the behavior of material for different flow conditions (e.g. shear flow, elongational flow or combination of both) and for transient flow. It is also important to take account of the effects of orientation of fibers and different interactions associated with fibers and matrix.

Lipscomb et al. (1988) developed the constitutive equation as follows:

$$\sigma = -PI + \eta_m \dot{\gamma} + \eta_m \phi_f \left[\mu_1 \dot{\gamma} + \mu_2 \dot{\gamma} : a_4 + \mu_3 (\dot{\gamma}.a_2 + a_2.\dot{\gamma}) + 2\mu_4 a_2 D_r \right]$$

μ_1, μ_2, μ_3 and μ_4 are four shape factors that depend on the geometry and aspect-ratio of the fibers. Different expressions of the parameters μ_1, μ_2, μ_3 and μ_4 had been proposed in the literature .

For most practical applications, suspensions are either in the semi-dilute or concentrated regions however most of the models are based on the assumption of a dilute regime, in which direct interactions between the fibers can be neglected. Among the few studies that attempted to model semi-concentrated fiber suspensions was the work of Dinh and Armstrong (1984). The constitutive equation proposed by these authors gave the stress in terms of an integral over a function of the Cauchy strain tensor and the orientation vector for a fiber. An expression was also obtained for the evolution of the fiber orientation. The development was restricted to homogeneous flows. It was found that in start-up of shear or elongational flow the orientation of the fibers and the measurable rheological properties both depended only on the total applied strain. A well constitutive

equation for concentrated regime is not fully developed yet and it is still a challenging issue for researchers.

Ferec et al. (2009) extended Dinh and Armstrong (1984) model. It takes into account fiber-fiber interactions with linear lubrication forces and an additional extra stress term was developed to take into account the contribution induced by the interacting forces. (See Ferec *et al.* 2009 for details)

2.11 Conclusion

Despite the fact that experimental works and proposing models involving fiber suspensions has been done intensely in the past. Numerous questions are still open. These questions are full of actuality because the intrest that scientific community addresses to nano or nano-micro structure suspensions, carbon nanotubes or green composites. One of these questions is about flexibility. As fiber intrinsic stiffness decreases or they become longer, they may be bent under flow. There is scarce data in literature regarding this issue and the role of fiber flexibility on rheological properties and microstructure of suspensions is an open area for research.

CHAPTER 3 - Summary of the Articles

Chapters 4 to 6 present the main scientific findings of this work and represent the core of the thesis. Each of these chapters consists of an article that has been submitted to a peer-reviewed journal (the article in Chapter 4 has already been published). The following is a brief description of each chapter:

- Chapter 4 provides a systematic experimental study of the influence of fiber flexibility on the rheological properties of various suspensions of non-Brownian fibers. To accomplish this, experiments on 3 types of fibers with different elastic moduli and two different aspect ratios are considered. The aspect ratio was varied by choosing fibers of different length but the same diameter. The article focuses mainly on the experimental aspect, however a qualitative comparison with existing models for semi-flexible fiber suspensions is achieved. Different rheological measurements have been performed to elucidate the connections between fiber concentration, aspect ratio and flexibility and the resulting rheological properties.
- In Chapter 5 a study of the time evolution of the orientation of fibers under shear flow is presented. The fiber orientation is determined experimentally under different shear rates using traditional rheometry and rheo-microscopy. A GENERIC-type model (General Equation for Non-equilibrium Reversible-Irreversible Coupling) is used as an attempt to describe the phenomena observed.

Finally Chapter 6 investigates the effect of fiber flexibility on the rheological behavior of a molten fiber-filled LDPE under simple shear, small and large amplitude oscillatory shear flows.

CHAPTER 4 - Rheological Behavior of Fiber-Filled Model Suspensions: Effect of Fiber Flexibility*[1]

M. Keshtkar, M.C. Heuzey, P.J. Carreau

Center for Applied Research on Polymers and Composites (CREPEC), Chemical Engineering Department, Ecole Polytechnique, PO Box 6079, Stn Centre- Ville, Montreal, QC H3C 3A7, Canada

Abstract

The rheological behavior of model suspensions consisting of a Newtonian silicone oil and fibers of different flexibilities have been investigated in steady and transient shear flows. Various fiber suspensions have been prepared to examine the effect of flexibility parameters (stiffness, aspect ratio) as well as the role of interactions in the semi-dilute and semi-concentrated regimes. The viscous and elastic properties of the fiber suspensions are shown to be strongly enhanced by fiber flexibility. With increasing flexibility the suspensions also exhibit enhanced shear-thining and the shear rate for the onset of shear-thinning decreases. In start-up flow, and especially at low shear rate, the suspensions show large stress overshoots, and under reversal flow delayed overshoots. The magnitude of overshoot increases as flexibility increases. This last effect has been attributed to less orientation of the flexible fibers in the flow direction during forward flow. Finally the effects are more pronounced in the semi-concentrated regime, and this is attributed to enhanced fiber-fiber interactions.

---

* This article is accepted in Journal of Rheology.

4.1 Introduction

Reinforced materials are used in a variety of structural applications that require a high strength to weight ratio and are highly competitive to metallic materials. Polymeric composites are obtained by adding solid reinforcements to a polymeric matrix. Fibrous reinforcements such as glass, carbon, Kevlar, nylon, vinylon (PVA) and natural fibers add stiffness and strength to the polymeric matrix and are widely used in the composite industry. These fibers may be used in the form of continuous bundles of fibers, woven fabrics or chopped fibers. Using chopped fibers as reinforcement is of great interest since conventional processing equipments such as extruders and injection molding machines can be used to produce parts.

During the processing of fiber-reinforced thermoplastics, the material undergoes severe shear and extensional flow deformations, which cause translation, rotation, bending and breaking of the fibers. These phenomena influence the mechanical properties of the final parts that are highly dependent on the microstructural characteristics and fiber orientation. The composite structure is affected by the flow field, fiber and suspending fluid properties and all possible interactions between fiber and matrix and within fibers. For example, one important factor is fiber flexibility. The flexibility varies with the intrinsic properties of the fiber and its aspect ratio [Wang *et al.* (2006)], and is coupled to the strength of the flow field. Understanding the relationships between the suspensions structure and these features can be highly useful in designing and optimizing processing conditions [Switzer and Klingenberg (2003)].

In general the rheology of fiber suspensions is quite complex due to several factors like fiber-fiber, fiber-wall, fiber-matrix interactions and phenomena such as fiber breakage and migration. Despite these numerous difficulties, a large number of experimental and theoretical investigations have been devoted to the analysis and prediction of the rheological behavior of fiber suspensions. However, among these studies there are very few investigations that focus on the role of fiber flexibility. Arlov *et al.* (1958) were among the first authors to investigate the role of fiber flexibility and classified the dynamics of flexible fibers into different modes: "flexible spin", "flexible spin-rotation", "springy rotations", "snake turn" and "S-turns". Following them, Forgacs and Mason (1959) investigated the role of fiber flexibility on the rotation period of fibers in the dilute regime and compared the behavior with the Jeffery (1922) model predictions. Using a Couette geometry they observed that as the stiffness decreased or aspect ratio increased the fibers tended to bend and not follow the orbits predicted by the Jeffery model. The fibers went instead through what has been called "flexible orbits". They also found that the critical stress to bend the fibers was

$$\left(\dot{\gamma}\ \eta_m\right)_{crit} \cong \frac{E_b(\ln 2r - 1.75)}{2r^4} \qquad (4\text{-}1)$$

where η_m is the viscosity of the suspending fluid (matrix) and E_b the bending modulus of the rod, $E_b \approx 2E_Y$, with E_Y the Young modulus of the fibers, and r is the apparent aspect ratio , which is the ratio of length to diameter of fibers.

The results of Forgacs and Mason (1959) indicated that axial forces imposed by shear flow can bend the fibers of low modulus or high aspect ratio and decrease the apparent

aspect ratio and shorten the period of rotation. These results stress the important role of fiber flexibility on the dynamics and orientation of fibers.

Another experimental work concerning the role of fiber flexibility is the study of Kitano *et al.* (1984a,b). They showed that polyethylene-based suspensions of vinylon fibers, which are more flexible than glass fibers, exhibited a stronger dependence of rheological properties on the fiber volume fraction as compared to glass fibers. However, the sizes for the glass and vinylon fibers were not the same; therefore it is difficult to elucidate the role of fiber flexibility from their work. Goto *et al.* (1986) also investigated the behavior of various suspensions based on glass, carbon, vinylon and nylon fibers in glycerin as a Newtonian suspending medium and in a hydroxyethyl cellulose (HEC) solution as a viscoelastic suspending fluid. The viscous and elastic properties of their suspensions were strongly affected by fiber flexibility, but as they used fibers with different aspect ratios depending on the type, it remains impossible to distinguish between the effects of number density and fiber flexibility. For example, the suspension containing 0.5% nylon fiber volume in a 2% HEC solution exhibited larger shear stresses in the range of shear rates of 0.1 to 100 s^{-1} as compared to glass fiber suspensions. On the other hand, carbon fibers - which are more rigid than glass - also showed larger stresses in the same range of deformation rate. Once more, these results are not well conclusive on the role of fiber flexibility.

One of the systematic experimental studies regarding the effect of fiber flexibility is the work of Soszynksi and Kerekes (1988 a,b) who studied flocs formation using nylon fibers of aspect ratios from 65 to 189 suspended in aqueous sugar solutions. They

suggested that flocs formation is due to mechanical contacts and coherence of the fibers due to interlocking by the elastic bending of the fibers. In the mechanism proposed, called "elastic fiber interlocking", fibers become locked to form a network because of their elasticity.

Regarding the effect of fiber aspect ratio on dynamic properties, Kotsilkova (1992) compared the dynamic rheological properties of pure silicone oil and suspensions containing glass fibers and glass beads. It was found that the storage and loss moduli and the complex viscosity were very sensitive to the aspect ratio. For the whole frequency range, these properties were larger for glass fiber than glass bead suspensions. Pre-shearing of the suspensions decreased these values. Based on the different behaviors of fiber and bead suspensions the author suggested that the structure, formed by entangled long fibers, was much larger in comparison with the structure associated with interactions between small particles.

Also, Guo *et al.* (2005) studied the dynamic properties of glass fiber suspensions with two different aspect ratios in a linear low density polyethylene (LLDPE). The authors reported that the storage and loss moduli increased with the fiber aspect ratio.

Beside experimental investigations, many authors have worked on the predictions of rheological properties of suspensions of flexible and semi-flexible fibers. Most of the work in this area is related to direct simulation techniques in which one calculates the position, orientation history and shape of fibers due to bending and twisting in a fluid by numerically solving the equations of motion for each particle in the suspension [Yamamoto and Matsouka (1993, 1996); Ross and Klingenberg (1997); Schmid *et al.*

(2000); Joung *et al.* (2001); Switzer and Klingenberg (2003); Wang *et al.* (2006)]. Such approaches require detailed initial physics that must be provided into the simulation tool, in return detailed information about the motion of particles and behavior of the suspension is obtained. The disadvantage of this approach is the limited number of fibers generally considered and the complexity of the calculations, including the numerical solution of the governing equations. The results lead to different conclusions about the effect of fiber flexibility on the rheological behavior of suspensions. For example, Joung *et al.* (2001) carried out a direct simulation of flexible fibers in a Newtonian medium and modeled the fibers as chains of beads joined with connectors. Their simulation results accounted for long and short range hydrodynamic interactions and predicted that as the fiber flexibility increased the suspension viscosity was enhanced. On the other hand, Switzer and Klingenberg (2003) applied particle level simulations and modeled fibers as linked, rigid spherocylinders connected by ball and socket joints. They considered interactions between the fibers with short-range repulsive forces and inter-fiber static friction, but hydrodynamic interactions were neglected in concentrated fiber suspensions. The simulation results showed that the suspensions viscosity decreased as the fiber flexibility increased.

In another approach, a mesoscopic model was developed by Rajabian *et al.* (2005) for predicting the rheological behavior of semi-flexible fiber suspensions. The semi-flexible nature of the fibers was considered in the choice of the entropy function. These theoretical efforts have not undergone sufficient assessments by comparison with

experimental data, largely due to the lack of reliable experimental data on the effect of fiber flexibility in the current literature.

In this work we perform a comprehensive study of the effect of fiber flexibility and associated parameters on rheological properties, using well-controlled systems. We also discuss the results in the light of the predictions from different models.

4.2 Experimental

4.2.1 Fibers and concentration regimes

In order to investigate the role of fiber flexibility on the rheological behavior of fiber suspensions, a criterion for flexibility needs to be defined. As previously mentioned in the introduction, the fibers effective flexibility depends on the intrinsic fiber stiffness, aspect ratio and the stress imposed on the fibers. We use the following criterion for the effective stiffness, as proposed by Switzer and Klingenberg (2003):

$$S^{eff} = E_\gamma \pi D^4 / 64\eta_m \dot{\gamma} L^4 \qquad (4\text{-}2)$$

in which L and D are the length and diameter of fiber, respectively. The effective stiffness characterizes the relative importance of the fiber stiffness and hydrodynamic forces. As $S^{eff} \to 0$, the fibers behave like completely flexible threads, whereas for $S^{eff} \to \infty$, the fibers become rigid and retain their equilibrium shape under flow [Switzer and Klingenberg (2003)]. The inverse of the effective stiffness can be used as a criterion for flexibility: the lower the effective stiffness, the higher the flexibility. Therefore, the fiber intrinsic stiffness and aspect ratio are ruling parameters involved in probing flexibility effects. Based on this, various fibers (polyarylate (Vectran®), vinylon

(PVA) and nylon fibers with two different aspect ratios have been chosen for this investigation. Fiber characteristics and the critical stress to bend the fibers, calculated by equation 4-1, are listed in Table 4-1. Hence, in this study three different intrinsic stiffness and two different aspect ratio values are considered, which provide a good range of properties.

As our main objective is to investigate fiber flexibility, the question is how to prepare suspensions with different aspect ratios and distinguish between the effects of fiber density, aspect ratio and flexibility. We use for that the average distance between fibers, *h*. Doi and Edwards (1978 a,b) have defined various concentration regimes based on the average distance between fibers. If the particles are randomly oriented, *h* can be estimated by [Dinh and Armstrong (1984)]:

$$\frac{h}{D} = \frac{\pi}{4\phi r} \equiv \frac{1}{nL^2 D} \tag{4-3}$$

in which ϕ is the volume fraction of fibers. A suspension is considered semi-dilute if:

$$\left(\frac{L}{D}\right)^{-2} < \phi_v < \left(\frac{L}{D}\right)^{-1} \quad \text{or} \quad nL^3 >> 1 \quad but \quad nL^2 D < 1 \tag{4-4}$$

In this regime the average distance between the fibers varies from the fiber length to the fiber diameter, hence the rotation of a fiber may imply contact with other fibers. In this case the fibers mostly interact through long range hydrodynamic interactions. On the other hand, a suspension is in the semi-concentrated regime if:

$$\phi_v > \left(\frac{L}{D}\right)^{-1} \quad \text{or} \quad nL^2 D > 1 \tag{4-5}$$

In this case the average distance between the fibers is less than the fiber diameter and additional non-hydrodynamic interactions become important, while every fiber interacts with other fibers in the form of a network. For this work the samples were prepared in the semi-dilute and semi-concentrated regimes based on a constant h/D or $r\phi$ in each concentration regime. The h/D values were adjusted to ≈ 1.37 and ≈ 0.34 for the semi-dilute and semi-concentrated regimes, respectively. Another issue that has been considered for preparing the samples with high aspect ratio was to ensure that the chosen concentration would not lead to experimental problems such as samples coming out of the rheometer parallel disk geometry or wall effects. We have tested various fiber concentrations in the semi-concentrated regime to find the suitable content that would give reproducible results. The nomenclature and properties of the suspensions in the semi-dilute and semi-concentrated regimes are presented in Table 4.2.

4.2.2 Suspending fluid and suspension preparation

A high viscosity silicone oil, polydimethylsiloxane (Clearco Products) with a density of $0.974\ \text{g/cm}^3$ and a nominal viscosity of 103 ± 2 Pa.s at 20°C has been selected as the suspending medium. The steady-state viscosity, η, and complex viscosity η^* of the silicone oil have been measured, and both were equal and independent of the shear rate or frequency in the experimental range investigated. The behavior is therefore Newtonian and this was also confirmed by the absence of significant normal stress differences.

The suspensions were prepared by hand mixing using a spatula. The sedimentation times of the fibers in the silicone oil matrix were calculated using the following equation from Chaouche and Koch (2001):

$$t_s = 8\eta_m L / \Delta\rho g D^2 \ln(2r - 0.72) \quad (4\text{-}6)$$

The values for the various fibers are reported in Table 4-1, and all the rheological experiments were carried out in times shorter than the sedimentation times of the suspensions.

Since different fiber types were used, it was crucial to look at the compatibility between fibers and the silicone oil. The interactions between the suspending fluid and the particles can play a major role on the rheological behavior of the suspensions [Mary *et al.* (2006)]. The degree of wetting is described by the contact angle, the angle at which the liquid-vapor interface meets the solid-liquid interface. A contact angle of 90° or greater generally characterizes a surface as non-wettable, and one less than 90° as wettable [Neumann and Good (1979)]. The contact angle between the silicone oil and various films prepared using nylon, PVA and polyarylateVectran was measured using a goniometer (Model 100-00 of Ramé-Hart, Netcong, NJ, USA). The measured contact angles between the polymer films and the silicone oil were 26 ± 2°, 19 ± 2° and 29 ± 2° for nylon, PVA and polyarylateVectran, respectively. These results suggest that all fibers are well wetted by the silicone oil and that the wetability is not significantly different to affect the different rheological responses reported for the various suspensions.

4.2.3 Rheometry

The rheological properties of the fiber suspensions were investigated using a strain controlled rheometer (ARES, TA Instruments). All experiments were carried out at 20 °C using a Peltier device. A parallel disk geometry with 50 mm diameter was used for all experiments. The samples were progressively squeezed between the parallel disks and it is assumed that this squeezing oriented the fibers in the plane of the parallel disks (planar random orientation). The ratio of gap to fiber diameter was therefore large enough to avoid wall effects. The same technique has been applied by Tommasset *et al.* (2004) for suspensions of long glass fibers in polypropylene. The gap has to be set to a value larger than the length of the fibers to avoid any wall effects and not influence the rheological measurements. For low aspect ratio fibers a gap- to- fiber length of 3:1 was used, which has been suggested to prevent wall effects.[Sepehr *et al.* 2004] For high aspect ratio and the highest concentration, and applying squeezing method, the effect of gap size on steady and transient rheological properties under shear flow was examined and it was determined that keeping the gap- to- fiber length as 2.5:2 will reduce wall effects with giving reproducable rheological properties. The torque, T, and normal force, F, can be measured as functions of the shear rate at the rim, $\dot{\gamma}_R$ using a force rebalance transducer. These raw data were used to calculate the viscosity and first normal stress difference assuming that the second normal stress difference was negligible (Weissenberg's hypothesis) [Carreau *et al.* (1997)]:

$$\eta(\dot{\gamma}_R) = \frac{T}{2\pi R^3 \dot{\gamma}_R}\left(3 + \frac{d\ln T}{d\ln \dot{\gamma}_R}\right) \tag{4-7}$$

$$N_1 = -(\sigma_{11} - \sigma_{22}) = \frac{2F}{\pi R^2}\left(1 + \frac{1}{2}\frac{d\ln F}{d\ln \dot{\gamma}_R}\right) \tag{4-8}$$

For small amplitude oscillatory shearing experiments, if the suspensions are not pre-sheared the reproducibility of the results is poor and the suspensions show nonlinearity at very low strain amplitude. We applied pre-shearing to samples at low ($\dot{\gamma} = 0.1\ s^{-1}$) and high ($\dot{\gamma} = 5\ s^{-1}$) rates to see the effect of the flow history on the linear viscoelastic properties of the suspensions. The pre-shearing was performed up to a strain of 1000 to make sure that steady state was reached and that fiber orientation was achieved. After applying pre-shearing the maximum error associated with the dynamic measurements was 8%, which is an acceptable value for filled systems.

4.3 Results and discussion

4.3.1 Steady state shear viscosity

The literature on fiber suspensions indicates that adding fibers to either Newtonian or non-Newtonian fluids will increase both the shear viscosity and the first normal stress differences of the suspensions [Nawab and Mason (1958); Ziegel (1970); Nicodemo and Nicolais (1974); Tanaka and White (1980); Kitako and Kataoka, (1980), (1981), (1984); Folgar (1983); Ganani and Powell (1985, 1986); Petrich *et al.* (2000); Sepeher *et al.* (2004); Gou *et al.* (2005); Mobuchon *et al.* (2005)]. Figure 4.1 compares the steady-state viscosity as a function of shear rate (ranging from 0.01 to 10 s^{-1}) for the various fiber

suspensions in silicone oil. Each curve represents an average of three sets of data for which sufficient time was allowed to reach steady state. Unfilled and filled symbols show the viscosity for the semi-dilute and semi-concentrated suspensions, respectively. We observe that for a specific fiber type with a certain aspect ratio the viscosity increases as the volume fraction increases. There are large error bars for the viscosity of the suspensions in the semi-dilute regime at low shear rates. This could be caused by heterogeneity in the case of the more dilute suspensions. The suspensions in the semi-concentrated regime show a pronounced shear-thinning behavior and the suspension viscosity increases with fiber flexibility. Overall, our results are in agreement with the findings of Petrich *et al.* (2000). They compared the steady shear viscosity of glass fiber suspensions in different ranges of nL^2D (0-3.5) at a shear rate of 0.5 s^{-1}. Their results showed that for aspect ratios of 50 and 72 at the same $r\phi$, the viscosity of glass fiber suspensions was independent of the aspect ratio. Our results show that in the semi-dilute regime the viscosity of the polyarylate (Vectran®) fiber suspensions, which are the most rigid fiber in terms of the Young modulus, is independent of the aspect ratio in agreement with the findings of Petrich *et al.* (2000). However, as the fiber flexibility increases (PVA and nylon fiber suspensions), the fibers with the higher aspect ratio result in larger viscosity. Petrich *et al.* (2000) showed that the microstructure and rheological properties of their semi-dilute fiber suspensions were in good agreement with theoretical results based on hydrodynamic interactions [Rahnama *et al.* (1995)]. Considering these, we can conclude that in the semi-dilute regime, where fibers interact

mostly through long range hydrodynamic interactions, fibers with high aspect ratio and low stiffness are more influenced by the flow.

In the semi-concentrated regime the effect of fiber flexibility on the rheological behavior can be observed again for both the low and high aspect ratios. As fiber flexibility increases the viscosity increases considerably, especially for the fibers with a high aspect ratio. The results also show that with a certain fiber type and at constant nL^2D (in our case $nL^2D \approx 2.9$), the viscosity becomes independent of the aspect ratio at high shear rates. At low shear rates, the suspensions with high aspect ratio fibers show quite a large viscosity. This can be explained by additional fiber-fiber contacts in the semi-concentrated regime, and also to the formation of a network at low shear rates. As fiber flexibility and fiber length increases there are indeed more contacts between fibers and the network structure is enhanced. Kerekes and Schell (1995) have studied the effect of fiber size on floc formation in paper pulps and showed that increasing the fiber length led to a decrease in uniformity of the suspensions due to an increasing degree of fiber contacts and floc size. In addition, the results of Petrich *et al.* (2000) demonstrated that the hydrodynamic model of Rahnama *et al.* (1995) underestimated the viscosity of semi-concentrated fiber suspensions. However, these were well described by the simulation results of Sundararajakumar and Koch (1997) based on fiber-fiber mechanical contacts. Hence, it is believed that the dominant mechanism in the semi-concentrated regime is fiber-fiber interactions [Sudararajakuar and Koch (1997), Petrich and Koch (1998), Sepehr *et al.* (2004)].

Djalili-Moghadam and Toll (2006) also discussed the formation of a structure at low shear rates, attributed by Chaouche and Koch (2000) to inter-particle adhesive forces. The measurement of adhesive forces is a difficult task, and therefore it is challenging to determine their importance. We, however, believe that the adhesive force effects are similar for the different fibers it is previously shown all fibers are well wetted by silicone. On the other hand, Soszynksi and Kerekes (1988) interpret floc formation by the "elastic fiber interlocking" described earlier, which fibers become locked and form a network because of their elasticity. Nevertheless, whatever is the mechanism of floc formation these structures can be destroyed as the shear rate increases, which will lead to a shear-thinning behavior and a decreasing viscosity.

Another reason that may cause the difference in rheological behavior of fibers with different flexibilities is the non-straight equilibrium shape of the more flexible fibers. Switzer and Klingenberg (2003), who have used particle level simulations, showed that relatively small deviations from a perfectly straight shape could result in large increases of the suspensions viscosity. As shown in Table 4-1, as the fiber aspect ratio increases or the fiber stiffness decreases, the critical stress needed for fiber bending decreases and the probability of finding curved fiber shapes increases. Also, Ganini and Powell (1986) found that the dependence of a suspension viscosity on shear rate is more pronounced as the fiber aspect ratio increases. Based on the results presented in Figure 4.1 and from the discussion above, we can conclude that as fiber flexibility increases a stronger structure may be formed, which could be due to the non-straight-shape of the more flexible fibers, resulting in more inter-particle interactions. At a given $r\phi$, the shear-thinning effect

becomes more pronounced as the fiber aspect ratio and flexibility increase, but as the shear rate or stress increases the break-up of the flow-induced flocculated structure is easier, leading to a more pronounced shear-thinning behavior.

Figure 4.2 reports the shear viscosity of the various suspensions versus $1/S^{eff}$ for different shear rates. In the semi-dilute regime, the effect of flexibility on the suspension viscosity at different shear rates is not significant. However, for the semi-concentrated suspensions the dependence of the suspension viscosity on fiber flexibility is quite significant and more pronounced at low shear rates as shown by Switzer and Klingenberg (2003) using a direct simulation of flexible fiber suspensions. But in contradiction with our experimental data and those of Goto *et al.* (1986), their results predict that increasing the fiber flexibility (or decreasing E_Y) would lead to lower values of the steady shear viscosity. They explained this by the fact that rigid fibers have a straight shape while flexible fibers may have permanent deformed shape, and highlighted the importance that those differences between equilibrium shapes must be considered in the simulation work in order to predict correctly the rheological behavior.

Rajabian et al. (2005) studied the effect of fiber flexibility using a mesoscopic model by introducing a fiber flexibility parameter in the free energy term. Their simulation results showed that at a given shear rate the steady state values of the viscosity and first normal stress differences increased, as fiber flexibility increased. These increases depend on fiber content and aspect ratio, where at higher aspect ratio and fiber content the effect of fiber flexibility on the rheological behavior is more significant, which is in agreement with our experimental findings.

4.3.2 Normal forces

In suspensions where fibers undergo hydrodynamic and Coulombic solid-body interactions, normal stress differences are exhibited. The secondary normal forces are much less than the primary normal forces and can be neglected [Petrich *et al.* (2000), Sepehr *et al.* (2004)]. In contrast to Brownian fiber suspensions and other fluids that undergo molecular relaxation and where N_1 is proportional to $\dot{\gamma}^2$, rigid fiber suspensions with contacts show primary normal stress differences linearly proportional to shear rate [Sudararajakumar and Koch (1997), Petrich *et al.* (2000)]. Figure 4.3 presents the first normal stress difference (N_1) data scaled by $\eta\dot{\gamma}$ in the semi-dilute and semi-concentrated regimes. In both regimes the addition of fibers results in significant normal forces under shear flow, and as the fiber content increases, the first normal force increases. In the semi-dilute regime the variation of $N_1/\eta\dot{\gamma}$ with $\dot{\gamma}$ is low as N_1 shows a linear dependence with shear rate. For the low aspect ratio fibers, $N_1/\eta\dot{\gamma}$ is nearly independent of the fiber stiffness but for the high aspect ratio this value depends on the fiber flexibility and increases as the fiber flexibility increases. The values of $N_1/\eta\dot{\gamma}$ in the semi-dilute regime are in good agreement with the results of Petrich et al. (2000) for glass fibers with an aspect ratio of 50 suspended in polybutene.

Carter (1967) proposed the following correlation for the first normal stress difference as a function of shear rate, fiber content and fiber aspect ratio:

$$N_1 = K\eta_m\dot{\gamma}\frac{\phi\, r^{1.5}}{\ln 2r - 1.8} \tag{4-9}$$

This equation is based on the assumption that collisions between fibers are the major cause for nonzero normal stresses in steady flow. In this equation K is a constant that must be determined experimentally. Different authors have calculated K [Carter (1967), Kitano and Kataoke (1981), Goto *et al.* (1986), Zirnask *et al.* (1994); Petrich *et al.* (2000) and Sepehr *et al.* (2004)] and it ranged from 0.04 to 0.32. Figure 3 shows that only the normal stress data in the semi-dilute regime follow the linear dependence with shear rate as predicted by Equation 4-9. The K value for both low and high aspect ratio fibers is 0.1 ± 0.01 in the semi-dilute regime, which is in the range of the values reported in the literature (0.04-0.32).

For the semi-concentrated regime Figure 4.3 shows that $N_1 / \eta\dot{\gamma}$ increases drastically with the fiber aspect ratio, which is in agreement with the simulation findings of Sundararajakumar and Koch (1997). The $N_1 / \eta\dot{\gamma}$ data in this regime is no longer constant as predicted by Equation 4-9, but N_1 can be correlated by a power-law expression as proposed by Goto *et al.* (1986):

$$N_1 = m\dot{\gamma}^n \tag{4-10}$$

Using carbon, nylon, vinylon and glass fibers suspended in glycerin, Goto *et al.* (1986) calculated n to be less than unity. For suspensions prepared using nylon fibers in glycerin (the most flexible fibers in the work of Goto *et al.* (1986)), n had the lowest value. Our data in the semi-concentrated regime are in good agreement with the findings of Goto *et al.* (1986)): m increases with fiber flexibility, but n ranges from 0.44 (NM-140C, most flexible fibers) to 0.82 (VM-35C, most rigid fibers). In addition, for NM-140C the power-law behavior is observed only at lower shear rates. Overall as the

flexibility increases n decreases, which means a stronger shear-thinning behavior, in agreement with the results for the steady state shear viscosity.

Figure 4.4 shows the effect of fiber flexibility on first normal stress difference scaled by $\eta\dot{\gamma}$ at different shear rates. The enhancement of the first normal stress difference with increasing fiber flexibility is more pronounced at lower shear rates. Since the presence of normal stresses for fiber suspended in a Newtonian fluid is due to fiber-fiber interactions [Petrich *et al.* (2000), Sepehr *et al.* (2004)], we can conclude that in the case of more flexible fiber suspensions, the role of fiber-fiber interactions is more important. This is in agreement with our findings on the viscosity and the theoretical results of Rajabian *et al.* (2005).

4.3.3 Linear Viscoelastic Properties

Complex viscosities in oscillatory experiments for concentrated suspensions performed after pre-shearing are shown in Fig. 4.5a. After applying the low pre-shear rate ($\dot{\gamma} = 0.1\ s^{-1}$) there are prominent differences in the behavior of these suspensions. For both the low and high aspect ratio fiber suspensions, the complex viscosity gets larger as fiber flexibility increases. But in the case of the high pre-shear rate ($\dot{\gamma} = 5\ s^{-1}$) (results not shown for conciseness), the complex viscosity does not depend on the fiber stiffness but only on the aspect ratio. For the suspensions with the high aspect ratio, the complex viscosity is much larger at low frequencies. For all the suspensions whether sheared at low or high shear rates, at high frequency, the complex viscosity tends to go to a

Newtonian plateau for frequencies above 10 rad/s, which is in agreement with the results of Petrich *et al.* (2000) and the data presented and reviewed by Ganani and Powell (1985). We also observed that suspensions pre-sheared at high shear rate show a lower complex viscosity as compared to those pre-sheared at low rate. This again supports the idea of the formation of network-like structures at low shear rates, with a stronger network formed as fiber flexibility increases.

The storage modulus of suspensions pre-sheared at low shear rate ($\dot{\gamma} = 0.1\ s^{-1}$) is presented in Fig. 4.5b. *G'* increases as fiber flexibility increases. From low to high aspect ratio fibers the increase in *G'* is huge at low frequencies. Also for high aspect ratio fibers, the storage modulus increases as fiber stiffness decreases. Also similarly to the behavior of the complex viscosity, after performing pre-shearing at high rate, the storage modulus only depended on the aspect ratio and increased with increasing fiber aspect ratio but the behavior was independent of the fiber stiffness (results not shown).

The dependence of dynamic properties on aspect ratio is in agreement with findings of Kotsilkova (1992) who found that the storage and loss moduli and the complex viscosity of glass fibers and glass beads suspended in silicone oil were very sensitive to the aspect ratio. Based on the different behaviors of fiber and bead suspensions, the author suggested that a more pronounced structure was formed by entangled fibers as particle aspect ratio increases. Also, Guo *et al.* (2005) showed that both the storage and loss moduli for glass fiber suspensions in a linear low density polyethylene (LLDPE) increased with the aspect ratio, which is in agreement with our results.

4.3.4 Transient flow experiments

Stress growth experiments have been conducted in the semi-concentrated regime for the most rigid and most flexible fibers in terms of the Young modulus (polyarylate and nylon), and for fibers with two different aspect ratios. The stress growth behavior of the two extreme (most and least flexible) suspensions is presented in Figure 4.6. The first stress growth for an applied shear rate of 1 s^{-1} in the clockwise (CW) direction is followed by a second test at the same shear rate and in the same direction, and finally by a third test in the counter clockwise (CCW) direction, without any delay between the tests. The strain shown in all figures is calculated at the edge of the concentric disks, i.e. $\gamma = \theta R / H$, where θ is the angular displacement of the rotating disk. The absolute value of the strain has been used and the strain is considered zero at the beginning of each test. During the first test all the suspensions exhibit large overshoots. Since the matrix is Newtonian and its transient behavior is extremely fast without any overshoot (not shown in Figure 4.6), the observed overshoot in the stress growth test is due to the presence of the fibers [Sepehr *et al.* 2004]. As loading the samples in the rheometer and subsequent squeezing and trimming is user-dependent, the results of the first stress growth experiments can vary each time the test is repeated, therefore a large error bar is seen. For that reason, Sepehr *et al.* (2004) have used this first CW test as a pre-conditioning. For the second test in the same direction (CW), the viscosity rapidly reaches a steady state value similar to the one in the first test. The absence of an overshoot in the second CW test has been attributed to the previous orientation of the fibers in the first one [Laun (1984); Ausias *et al.* (1992); Sepehr *et al.* (2004)]. Following these two transient tests,

the experiment in the CCW direction is immediately performed. A delayed overshoot can be observed in Figure 6 for both fiber types, and this has been attributed to the tumbling of some fibers and called a "reverse overshoot" [Sepehr *et al.* (2004)].

The normalized stress growth function in the first CW, second CW and CCW tests for the various suspensions prepared with different fiber flexibilities and for the unfilled silicone oil are presented for an applied shear rate of 1 s^{-1} in Figure 4.7. Figure 4.7a shows the effect of flexibility on the transient behavior in the first CW stress growth. It is seen that the response of the silicone oil is fast and rapidly reaches a steady state value, which is the usual characteristic of a Newtonian fluid. Adding fibers results in a significant overshoot and slightly delayed the response time before reaching steady state. It can be seen that the magnitude of the overshoot gets larger as the fiber aspect ratio is increased. This is due to the fact that for fibers of an initially random orientation the suspension viscosity scales with nL^3, whereas for aligned fibers in the flow direction it scales with nL^2D [Leal and Hinch (1971)]. For the low aspect ratio fiber suspensions, the fiber stiffness does not influence the peak magnitude and the strain at which the suspensions reach steady state. However, for the higher aspect ratio, and as the fiber Young modulus decreases, the amplitude of the peak increases and the suspension reaches steady state at larger strain. This is an indication that the orientation of the fibers in the flow direction is not as important as fiber flexibility increases due to more interactions with other fibers, and as compared to the rigid fiber suspensions. These results are in agreement with the model predictions of Rajabian *et al.* (2005) who have

shown that both overshoot magnitude and time for reaching steady state increased as fiber flexibility increased.

Figure 4.7b presents the effect of fiber flexibility on the results for flow reversal experiments In reverse stress growth experiments the suspensions exhibit first a plateau and then show a large delayed overshot at a deformation of about 35. As the fiber flexibility increases, the deformation at which the first transition plateau ends and the overshoot starts is seen to decrease. Also, by increasing fiber flexibility and aspect ratio, the magnitude of the stress overshoot increases. Sepehr *et al.* (2004) explained the overshoot in the reverse direction by a tilting over of the fibers in the new flow direction, forming a new aligned fiber structure. Our results suggest that this tilting over occurs at lower deformation for the more flexible fiber suspensions.

The corresponding transient results for the normal stress differences are presented in Figure 4.8. In the first CW stress growth experiments, the low aspect ratio suspensions first reach a plateau and then a large overshoot is observed at a strain of about 30 and eventually reach a steady state value, identical to the first plateau. For these low aspect ratio suspensions, the transient behavior of the first normal stress difference is not influenced by fiber stiffness. For the large aspect ratio fiber suspensions, the first plateau cannot be observed and the suspensions rapidly start to show overshoots. As fiber flexibility increases the width and magnitude of the overshoot increase, in agreement with the predictions of the model of Rajabian *et al.* (2005). For the second CW tests, the overshoot almost vanishes for low aspect and rigid fibers, but as flexibility and aspect ratio increase there is again a small overshoot, probably due to the presence of fibers not

well oriented in the flow direction in the case of the more flexible fibers. For the 3rd CCW flow experiments all suspensions first exhibit negative normal stress values, the effect being more pronounced as flexibility increases. Then, the normal stress differences increase and reach a positive steady state value identical to that obtained in the 1st CW experiment. The same behavior has been observed by Sepehr *et al.* (2004) for suspensions of glass fibers in polybutene and attributed to a crystalline structure of the fiber suspensions under flow.

The energy per unit volume for orienting the fibers in the 1st CW flow and also the energy required to tumble the fibers in the 3rd CCW test can be calculated from the area under the overshoots:

$$E = \int \sigma d\gamma = \dot{\gamma} \int \eta d\gamma \qquad (4\text{-}11)$$

The calculated values for two different shear rates (0.1 and 1 s^{-1}) are presented in Figure 4.9. The results show that both energy values for orientation and tumbling of the fibers increase with shear rate, which is in agreement with the findings of Sepehr *et al.* (2004). For all suspensions in this work the energy required for tumbling the fibers is more than the energy required for initially orienting the fibers in the flow direction. Also, as fiber flexibility increases the amount of energy required for orientation and tumbling of fibers gets larger. The energy is consumed in order to overcome static friction forces at contact points between fibers and to overcome the drag forces and bending of fibers. The larger energy required in the case of flexible fibers is indicative of the stronger interactions between them and the presence of a network-like structure.

4.4 Conclusion

The rheological behavior of various fiber suspensions with different fiber flexibilities has been investigated in steady and transient shear and SAOS flows using a parallel disk geometry. The effective stiffness, which characterizes the relative importance of fiber stiffness to hydrodynamic forces acting on the fibers, has been used as a criterion for fiber flexibility. Precautions have been taken to avoid wall effects.

Both viscosity and first normal stress differences increase with larger flexibility, and the increases are more pronounced in the semi-concentrated regime. The enhancement of the rheological properties has been attributed to additional fiber-fiber interactions when using more flexible fibers.

The SAOS experiments showed that as fiber aspect ratio and stiffness increased, suspension's complex viscosity and storage modulus increased after pre-shearing at low shear rates. The behavior has been attributed to formation of a network like structure after low pre-shearing and as fiber flexibility increased, the structure was stronger. The behavior of suspensions depended on flow history and by pre-shearing at higher shear rates the linear viscoelastic properties depended on only aspect ratio of fibers and were independent of fibers stiffness.

Stress growth experiments have been carried out in the forward and reverse flow directions, and shear stress and normal force overshoots have been observed in the forward flow and attributed to fiber orientation under flow. Both the overshoot magnitude and width augment with increasing fiber flexibility. Under flow reversal a delayed overshoot has been detected and as fiber flexibility increases the strain at which

the overshoot starts gets smaller. Since the reverse overshoot has been attributed to fiber tumbling, our transient results suggest that flexible fibers are less oriented in the previous forward flow than rigid fibers.

4.5 Acknowledgements

The authors would like to acknowledge financial support from the Natural Sciences and Engineering Research Council of Canada (NSERC-CIAM program). We wish to thank Dr. Thomas Griebel (from SwissFlock Inc.) for providing nylon fibers and Dr. Takashi Takayama (from Kuraray Co.,Ltd.) for providing Vectran® and PVA (Kuralon®) fibers.

4.6 References

Arlov, A. P., Forgacs, O. L., and Mason, S. G. "Particle motions in sheared suspensions 4. General behavior of wood pulp fibers," *Sven. Papperstidn.* ***61***, 61 (1958)

Ausias, G., Agassant, J. F., Vincent, M., Lafleur, P. G., Lavoie, P. A., and Carreau, P. J. "Rheology of short glass fiber reinforced polypropylene," *J Rheol* ***36***(4), 525-542 (1992)

Bibbo, M. A., "Rheology of semi-concentrated fiber suspensions," Ph.D.Thesis, Massachusett Institute of Technology, (1987)

Carreau, DeKee, and Chhabra. *Rheology of polymeric systems* (NewYork: Hanser/Gardner 1997).

Carter, L. F. (1967). *A study of the rheology of suspensions of rod-shaped particles in a Navier–Stokes liquid.* University of Michigan, Ann Arbor, MI.

Chaouche, M., and Koch, D. L. "Rheology of non-Brownian rigid fiber suspensions with adhesive contacts," *J Rheol* ***45***(2), 369-382 (2001)

Dinh, S. M., and Armstrong, R. C. "Rheological equation of state for semiconcentrated fiber suspensions," *J Rheol* ***28***(3), 207-227 (1984)

Djalili-Moghaddam, M., and Toll, S. "Fibre suspension rheology: effect of concentration, aspect ratio and fibre size," *Rheolgica Acta* ***45***, 315-320 (2006)

Doi, M., and Edwards, S. F. "Dynamics of rod-like macromolecules in concentrated solution I," *Journal of the Chemical Society. Faraday transactions II* ***74***, 560-570 (1987a)

Doi, M., and Edwards, S. F. "Dynamics of rod-like macromolecules in concentrated solution II," *Journal of chemical society. Faraday Society II* ***74***, 918-932 (1978b)

Folgar, F. (1983). *Fiber orientation distribution in concentrated suspensions: a predictive model.* University of Illinois at Urbana-Champaign, USA.

Forgacs, O. L., and Mason, S. G. "Particle motions in sheared suspensions IX. Spin and deformation of threadlike particles," *J. Colloid Interface Sci.* ***14***, 457 (1959)

Ganani, E., and Powell, R. L. " Rheological properties of rodlike particles in a Newtonian and a Non-Newtonian fluid," *J Rheol* ***30***(5), 995-1013 (1985)

Ganani, E., and Powell, R. L. "Suspensions of rodlike particles: Literature review and data correlations," *J Compos Mater* ***19***(3), 194-215 (1985)

Goto, S., Nagazono, H., and Kato, H. "The flow behavior of fiber suspensions in Newtonian fluids and polymer solutions. I: Mechanical properties," *Rheolgica Acta* ***25***, 119-129 (1986)

Guo, R., Azaiez, J., and Bellehumeur, C. "Rheology of fiber filled polymer melts: Role of fiber-fiber interactions and polymer-fiber coupling," *Polym Eng Sci* ***45***(3), 385-399 (2005)

Jeffery, G. B. "The motion of ellipsoidal particles immersed in a viscous fluid," *Proceedings of the Royal Society of London* ***102***, 161-179 (1922)

Joung, C. G., Phan-Thien, N., and Fan, X. J. "Direct simulations of flexible fibers," *J. Non-Newton. Fluid Mech.* ***99***(1), 1-36 (2001)

Kitano, T., and Kataoka, T. "The rheology of suspensions of vinylon fibers in polymer liquids. II. Suspensions in polymer solutions," *Rheologica Acta* ***20***(4), 403-415 (1981)

Kitano, T., Kataoka, T., and Nagatsuka, Y. "Dynamic flow properties of vinylon and glass fiber reinforced polyethylene melts," *Rheologica Acta* ***23***(4), 408-416 (1984a)

Kitano, T., Kataoka, T., and Nagatsuka, Y. "Shear flow rheological properties of vinylon and glass fibers reinforced polyethylene melts," *Rheologica Acta* ***23***, 20-30 (1984b)

Kerekes, R. J., and Schell, C. J. "Effects of fiber length and coarseness on pulp flocculation," *Tappi J.* ***78***, 133-139 (1995)

Kotsilkova, R. "Dynamic Rheological Properties Of Glass Fiber Suspensions," Theoretical and Applied Rheology, edited by Moldenaers, P., Keunings, R., *Proc. XIth Int. Congr. On Rheology*, Brussels, Belgium, 856-858(1992)

Laun, H. M. "Orientation effects and rheology of short glass fiber-reinforced thermoplastics," *J Rheol* ***30***(3), 459-501 (1986)

Mary, B., Dubois, C., Carreau, P. J. and Brousseau, P. "Rheological properties of suspensions of polyethylene-coated aluminum nanoparticles." *Rheolgica Acta* **45**, 561 573 (2006).

Mobuchon, C., Carreau, P. J., Heuzey, M.-C., Sepehr, M., and Ausias, G. "Shear and extensional properties of short glass fiber reinforced polypropylene," *Polym Compos* ***26***(3), 247-264 (2005)

Nawab, M. A., and Mason, S. G. "The viscosity of dilute suspensions of threalike particles," *J. Non-Newton. Fluid Mech.* ***62***, 1248-1253 (1985)

Neumann A. W., Good, R. J. In: Good, R. J., Stromberg, R., *Surface and ColloidScienc, Vol II.* (New-York: Plenum 1979)

Nicodemo, L., and Nicolais, L. "Viscosity of concentrated fiber suspensions," *Chem. Eng. Journal* ***8***, 155-156 (1974)

Petrich, M. P., and Koch, D. L. "Interactions between contacting fibers," *Phys Fluids* ***10***(8), 2111 (1998)

Petrich, M. P., Koch, D. L., and Cohen, C. "Experimental determination of the stress-microstructure relationship in semi-concentrated fiber suspensions," *J. Non-Newton. Fluid Mech.* ***95***(2-3), 101-133 (2000)

Rahnama, M., Koch, D. L., and Shaqfeh, E. S. G. "Effect of hydrodynamic interactions on the orientation distribution in a fiber suspension subject to simple shear flow," *Phys Fluids 7*(3), 487 (1995)

Rajabian, M., Dubois, C., and Grmela, M. "Suspensions of semiflexible fibers in polymeric fluids: Rheology and Thermodynamics," *Rheologica Acta* ***44***, 521-535 (2005)

Ross, R. F., and Klingenberg, D. J. "Dynamic simulation of flexible fibers composed of linked rigid bodies," *J Chem Phys* ***106***(7), 2949 (1997)

Schmid, C. F., Switzer, L. H., and Klingenberg, D. J. "Simulations of fiber flocculation: effects of fiber properties and interfiber friction," *J Rheol* ***44***(4), 781-809 (2000)

Sepehr, M., Ausias, G., and Carreau, P. J. "Rheological properties of short fiber filled polypropylene in transient shear flow," *J. Non-Newton. Fluid Mech.* ***123***(1), 19-32 (2004)

Sepehr, M., Carreau, P. J., Moan, M., and Ausias, G. "Rheological properties of short fiber model suspensions," *J Rheol* ***48***(5), 1023-1048 (2004)

Soszynski, R. M., and Kerekes, R. J. " Elastic interlocking of nylon fibers suspended in liquid. Part 1. Nature of cohesion among fibers," *Nord. Pulp Pap. Res. J.* ***3***, 172-179 (1988a)

Soszynski, R. M., and Kerekes, R. J. " Elastic interlocking of nylon fibers suspended in liquid. Part 2. Process of interlocking," *Nord. Pulp Pap. Res. J.* ***3***, 180-184 (1988b)

Sundararajakumar, R. R., and Koch, D. L. "Structure and properties of sheared fiber suspensions with mechanical contacts," *J. Non-Newton. Fluid Mech.* ***73***(3), 205-239 (1997)

Switzer III, L. H., and Klingenberg, D. J. "Rheology of sheared flexible fiber suspensions via fiber-level simulations," *J Rheol* ***47***(3), 759-778 (2003)

Tanaka, H., and White, J. L. "Experimental investigations of shear and elongational flow properties of polystyrene melts reinforced with calcium carbonate, titanium dioxide, and carbon black," *Polym Eng Sci* ***20***(14), 949-956 (1980)

Thomasset, J., Carreau, P. J., Sanschagrin, B., and Ausias, G. "Rheological properties of long glass fiber filled polypropylene," *J. Non-Newton. Fluid Mech.* ***125***(1), 25-34 (2005)

Wang, G., Yu, W., and Zhou, C. "Optimization of the rod chain model to simulate the motions of a long flexible fiber in simple shear flows," *Eur J Mech B Fluids* ***25***(3), 337-347 (2006)

Yamamoto, S., and Matsuoka, T. "Method for dynamic simulation of rigid and flexible fibers in a flow field," *J Chem Phys* ***98***(1), 644 (1993)

Yamamoto, S., and Matsuoka, T. "Dynamic simulation of microstructure and rheology of fiber suspensions," *Polym Eng Sci* ***36***(19), 2396-2403 (1996)

Ziegel, K. D. "The viscosity of suspensions of large nonspherical particle in polymer fluids," *J. Colloid Interface Sci.* ***34***(2), 185-196 (1970)

Zirnsak, M. A., Hur, D. U., and Boger, D. V. "Normal stresses in fibre suspensions," *J. Non-Newton. Fluid Mech.* ***54***, 153-193 (1994)

Table 4.1 : Characteristics and nomenclature of the fibers used in this study

Fiber nomenclature	**Fiber**	**Young's Modulus (GPa)**	**Diameter (μm)**	**Aspect Ratio**	**Critical Stress (Pa)**	t_s **(h)**
N36, N140	Nylon	2.0	14	36 140	2×10^3 14	~ 84 ~ 250
P36, P140	PVA	26	14	36 140	2.9×10^3 180	~ 42 ~ 130
V35, V140	Polyarylate (Vectran®)	76	18	35 140	9×10^3 500	~ 24 ~ 75

Table 4.2 : Suspensions characteristics: semi-dilute regime (nL2D ≈ 0.73, h/D ≈ 1.37) and semi-concentrated regime (nL2D ≈ 2.9, h/D ≈ 0.34)

Code	Fiber Type	Aspect Ratio	Vol. %
VM-35SD VM-35SC	Vectran	35.0	1.6 6.5
PM-36SD PM-36SC	PVA	36.0	1.6 6.5
NM-36SD NM-36SC	Nylon	36.0	1.6 6.5
VM-140SD VM-140SC	Vectran	140	0.40 6.5
PM-140SD PM-140SC	PVA	140	0.40 6.5
NM-140SD NM-140SC	Nylon	140	0.40 6.5

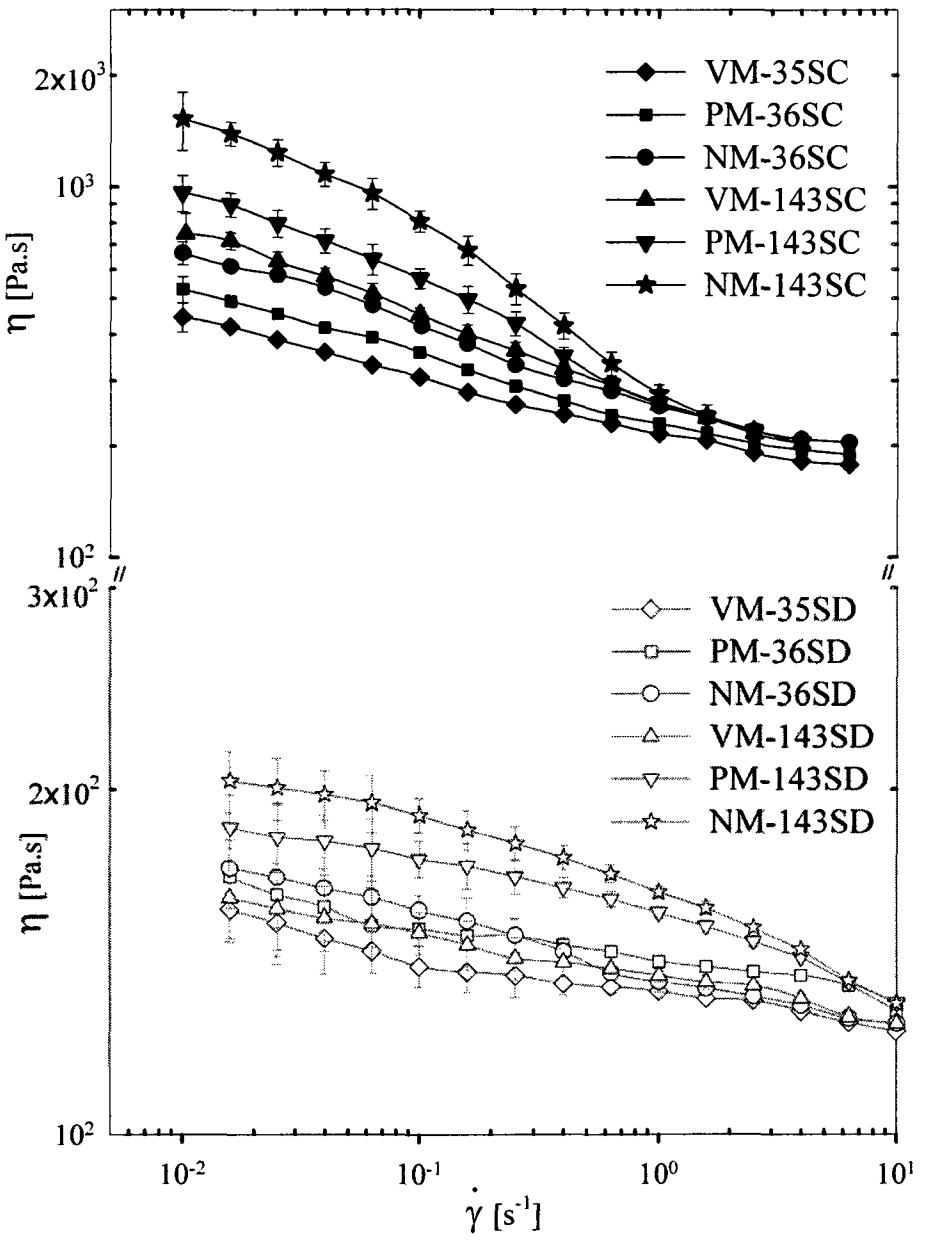

Figure 4.1 : Steady shear viscosity of fiber suspensions in the semi-dilute (open symbols) and semi-concentrated (filled symbols) regimes.

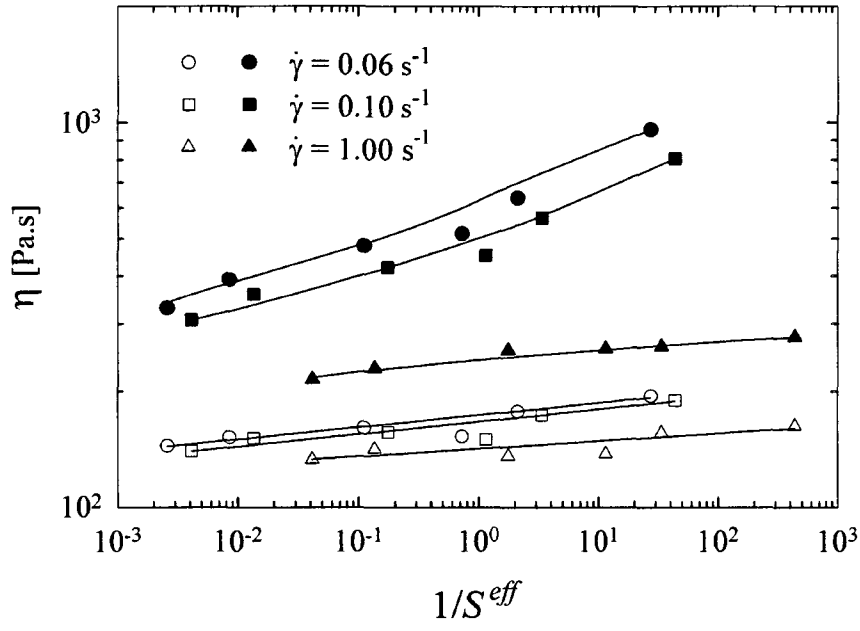

Figure 4.2 : Effect of fiber flexibility on suspensions viscosity at different shear rates in the semi-dilute (open symbols) and semi-concentrated (filled symbols) regimes.

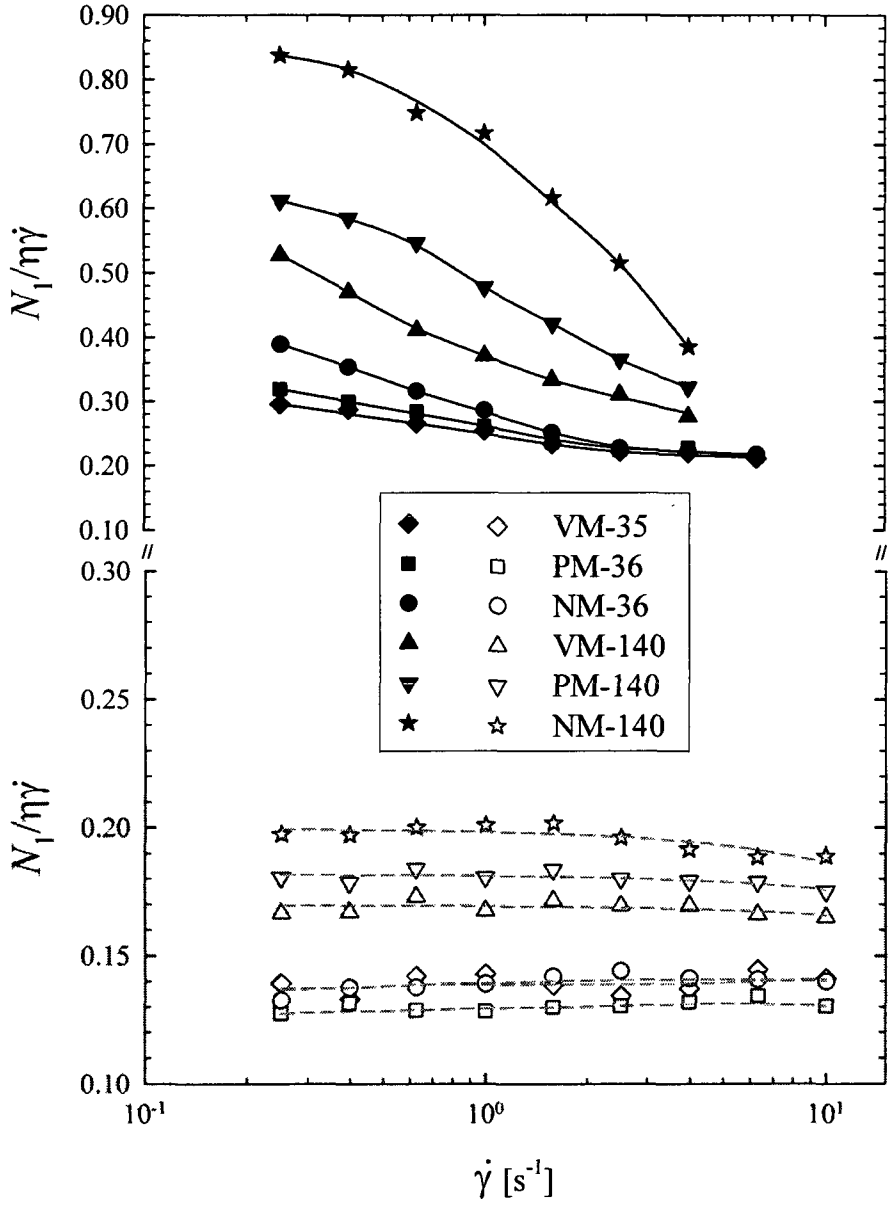

Figure 4.3 : First normal stress difference scaled by ($\eta\dot{\gamma}$) in the semi-dilute (open symbols) and semi-concentrated (filled symbols) regimes.

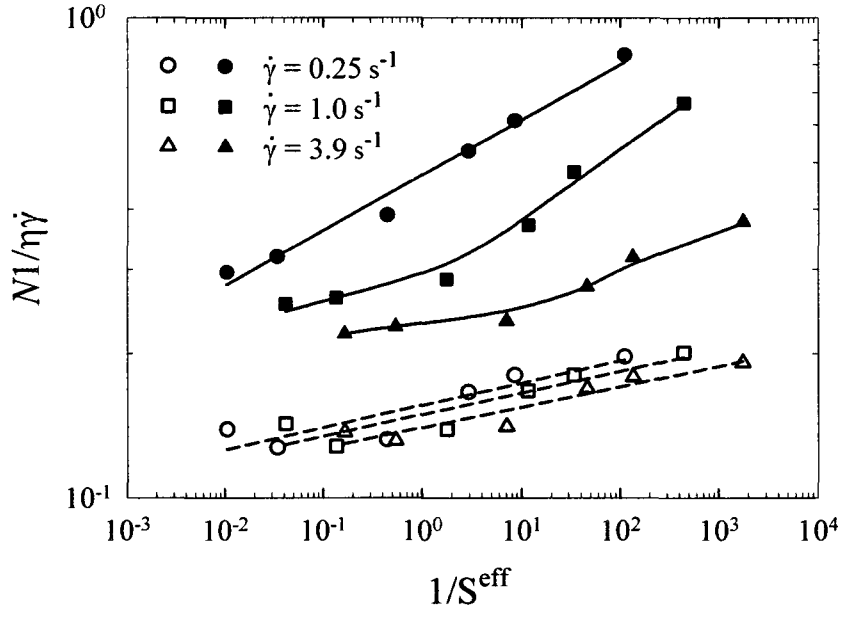

Figure 4.4 : Effect of fiber flexibility on first normal stress difference of suspensions scaled by $(\eta\dot{\gamma})$ in the semi-concentrated (open symbols) and concentrated (filled symbols) regimes.

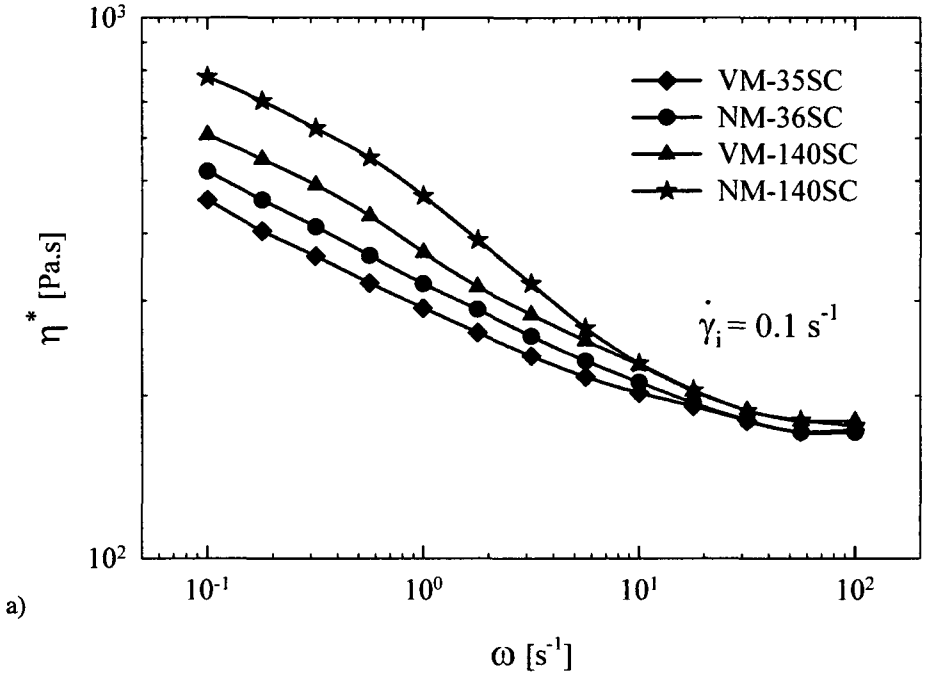

a)

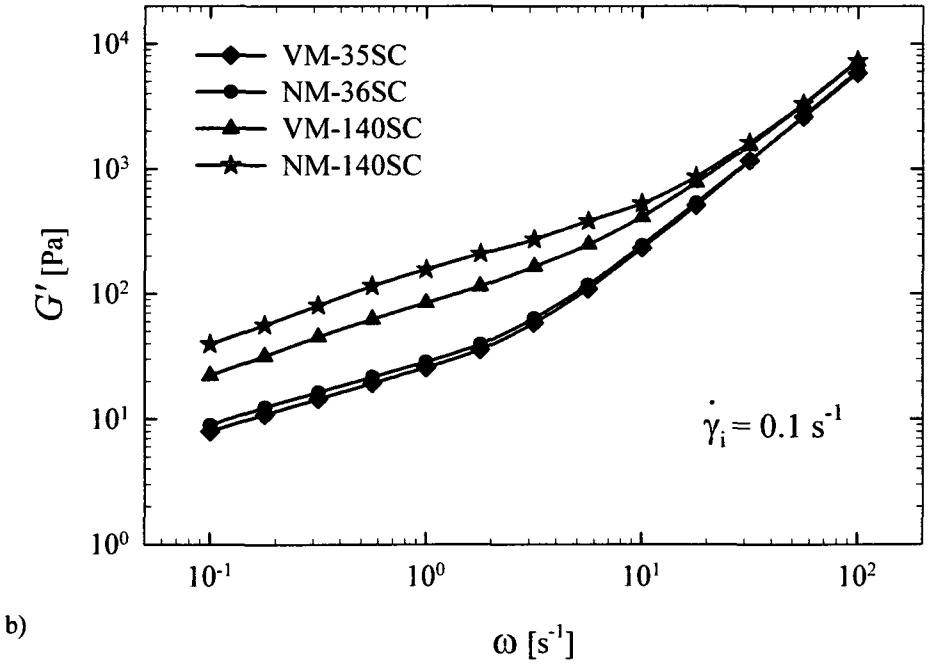

b)

Figure 4.5 : Linear viscoelastic properties of suspensions after pre-shearing at $\dot{\gamma} = 0.1 s^{-1}$: a) Complex viscosity, b) Storage modulus

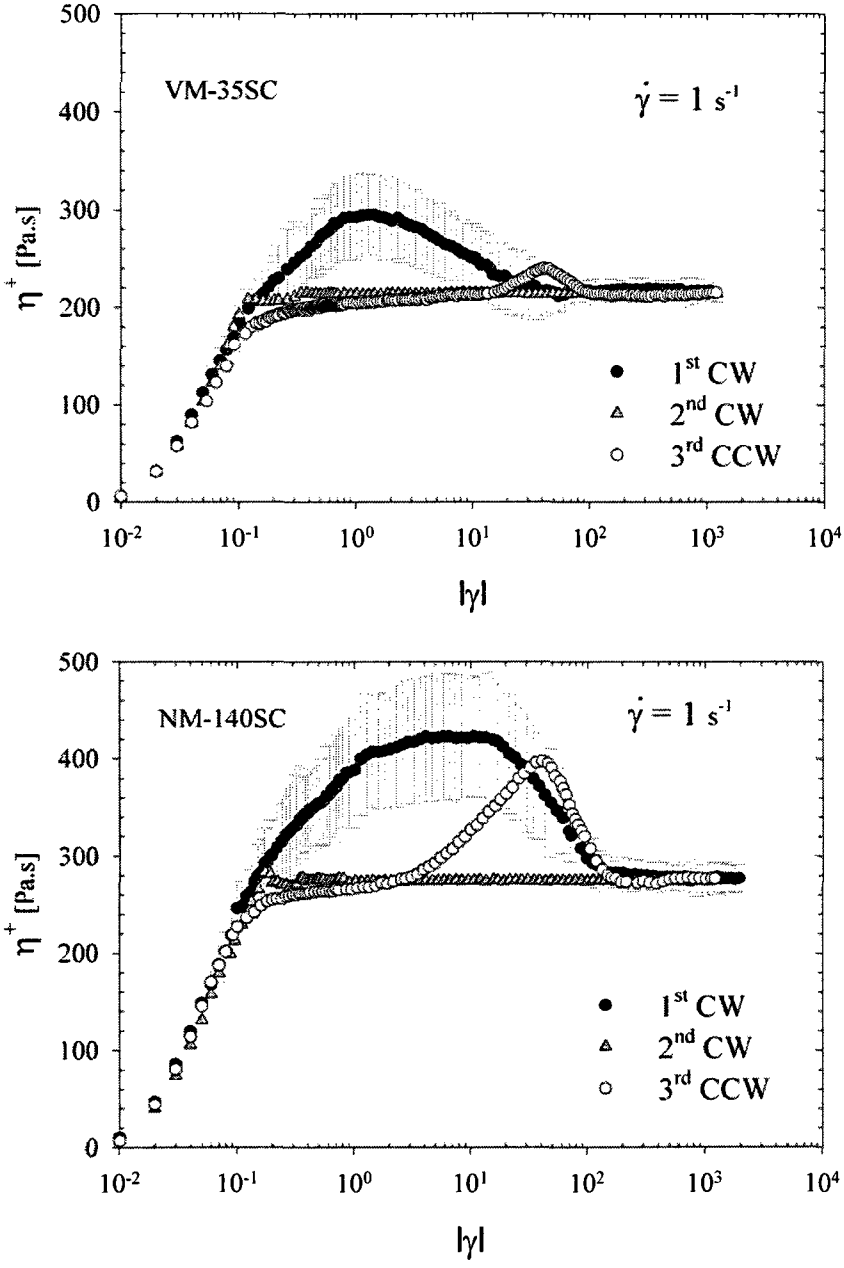

Figure 4.6 : Stress growth behavior of suspensions prepared with the a) most rigid (VM-36SC) and b) most flexible (NM-140SC) fibers, in 1st forward, 2nd forward and 3rd reverse flow directions.

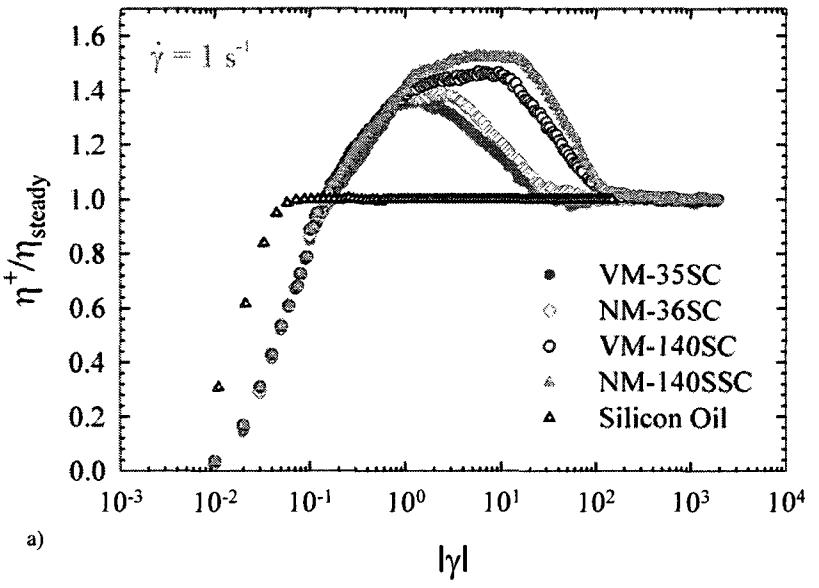

a)

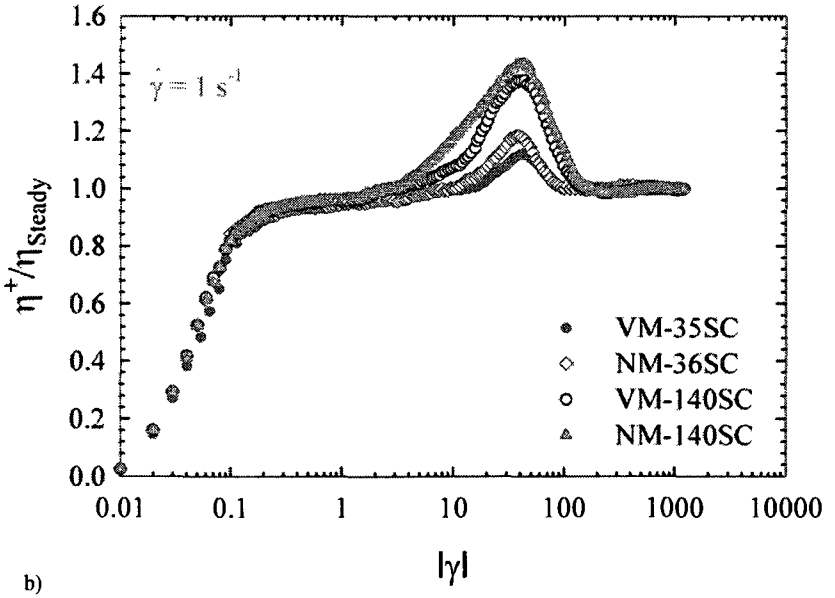

b)

Figure 4.7 : Effect of fiber flexibility on the normalized stress growth function of different suspensions in a) 1st CW and b) 3rd CCW flow directions (shear rate = $1s^{-1}$).

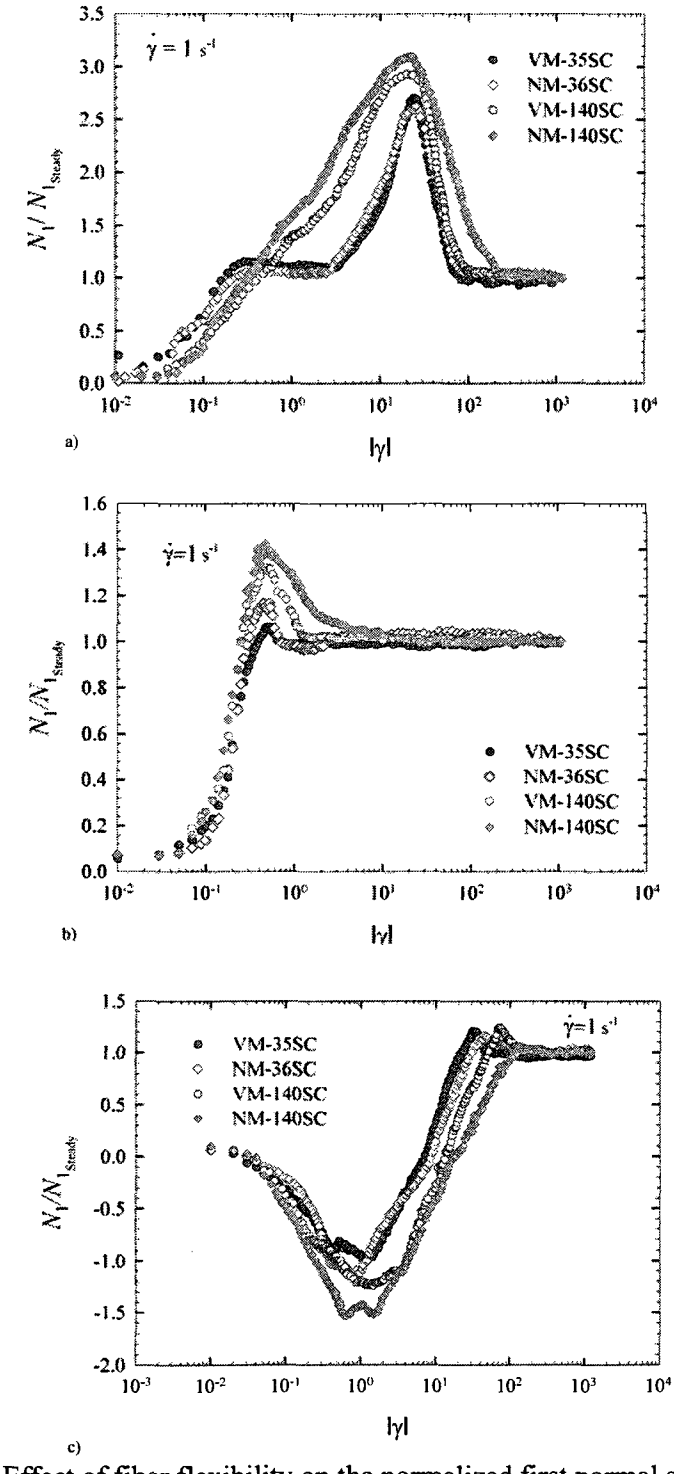

Figure 4.8 : Effect of fiber flexibility on the normalized first normal stress difference of different suspensions in stress growth experiments: a) 1st CW, b) 2nd CW and c) 3rd CCW flow directions (shear rate = 1s^{-1}).

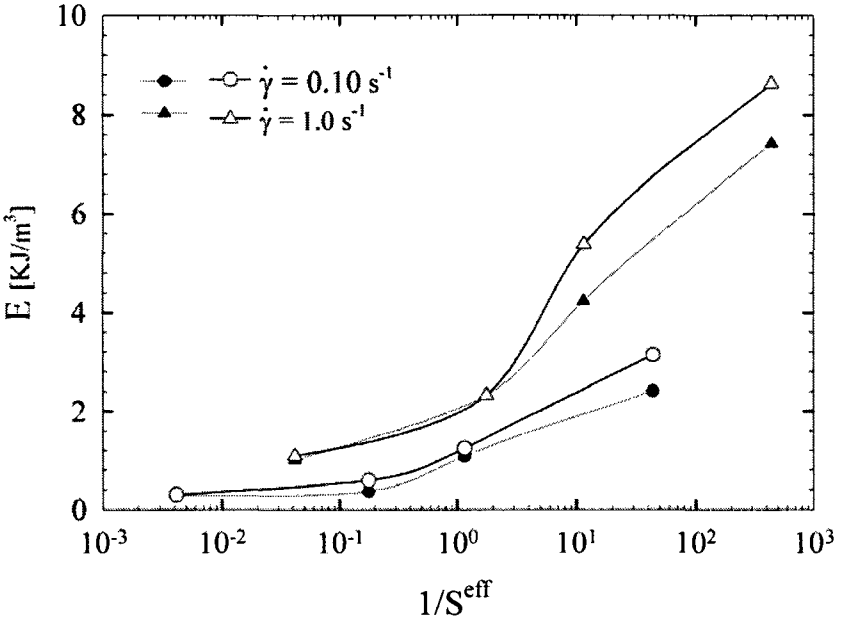

Figure 4.9 : Energy required for orienting (filled symbols) and tumbling (open symbols) fibers at shear rates of $0.1s^{-1}$ and $1s^{-1}$.

CHAPTER 5 - Rheological Properties and Microstructural Evolution of Semi-Flexible Fiber Suspensions under Shear Flow*[2]

M. Keshtkar, M-C. Heuzey*, P.J. Carreau, M. Rajabian, C. Dubois

Center for Applied Research on Polymers and Composites (CREPEC), Chemical Engineering Department, Ecole Polytechnique, PO Box 6079, Stn Centre-Ville, Montreal, QC H3C 3A7, Canada

* Author to whom correspondence should be addressed; email: marie-claude.heuzey@polymtl.ca

Abstract

The rheological behavior of model suspensions consisting of a Newtonian silicone oil and fibers with different flexibilities has been studied in transient shear flow. The viscous and elastic properties of the fiber suspensions were shown to increase markedly with fiber flexibility. The suspensions exhibited a viscosity overshoot in stress growth experiments, and the magnitude and width of the overshoot became larger as the fiber flexibility increased. The evolution of the suspensions microstructure has been monitored at different shear rates. The components of the second-order orientation tensor at different times were calculated using the images obtained from the visualization experiments. The flow visualization experiments showed that fiber

* This article was submitted to Journal of Rheology.

orientation is dependent on the shear rate and the amount of applied strain. Finally, a mesoscopic model in the framework of GENERIC (General Equation for Non-equilibrium Reversible-Irreversible Coupling) has been used to predict the rheological behavior of semi-flexible fiber suspensions as well as their microstructure. The model takes into account fiber-fiber interactions and also the semi-flexible nature of the fibers. The predictions of the model are in good agreement with the rheological and visualization data.

Key words: fiber suspension, flexibility, orientation, generic model

5.1 Introduction

Reinforced materials have gained popularity in a variety of applications ranging from everyday use goods to advanced engineering and structural materials. Polymeric composites are obtained by adding solid reinforcements to a polymeric matrix. Fibrous reinforcements such as glass, carbon, Kevlar, nylon, vinylon (PVA) and natural fibers add stiffness and strength to the polymeric matrix and are widely used in the composite industry. Using short fibers as reinforcement is of great interest since conventional processing equipments like extruders and injection molding machines can be used to produce these composite parts.

The mechanical properties of fiber-reinforced polymers are highly dependent on fiber orientation. During the processing of fiber-reinforced thermoplastics, the material undergoes severe shear and extensional flow deformations, which cause translation, rotation, bending and breaking of the fibers. These phenomena influence the mechanical properties of the final parts that are highly dependent on the microstructural characteristics and fiber orientation. The composite structure is affected by the flow field, fiber and suspending fluid properties and all possible interactions between the fibers and the matrix and within fibers. A key factor is fiber flexibility, which varies with the intrinsic properties of the fiber and its aspect ratio [Wang *et al.* (2006)], and is coupled to the strength of the flow field. The understanding of the relation between the suspension structure and rheological properties will help control the orientation of the

fibers during processing and enable one to design and manufacture composite materials with optimal properties.

The simulation of fiber suspensions has been the subject of many publications over the past three decades, but only a few of these investigations have looked at the flexibility of fibers. Most of the work in this area is related to direct simulation techniques in which one calculates the position, orientation history and shape of fibers due to bending and twisting in a fluid. This is done by numerically solving the equations of motion for each particle in the suspension [Wang *et al.* (2006); Yamamoto and Matsuoka (1993, 1996); Ross and Klingenberg (1997); Schmid *et al.* (2000); Joung *et al.* (2001); Switzer and Klingenberg (2003)]. Such approaches require detailed initial physics that must be provided into the simulation tool, but in return detailed information about the motion of the particles and the behavior of the suspension is obtained. The disadvantage of this approach is the limited number of fibers that can be considered and the complexity of the calculations, including the numerical solution of the governing equations. The results have led to contradictory conclusions about the effect of fiber flexibility on the rheological behavior of suspensions. For example, Joung *et al.* (2001) modeled flexible fibers in a Newtonian fluid as chains of beads joined with connectors. Their simulation results accounted for long and short range hydrodynamic interactions and predicted that the suspension viscosity was increased as the fiber flexibility increased. On the other hand, Switzer and Klingenberg (2003) modeled fibers as linked, rigid spherocylinders connected by ball and socket joints. They considered interactions between the fibers with short-range repulsive forces and inter-fiber static friction, but hydrodynamic

interactions were neglected in concentrated fiber suspensions. The simulation results showed that the suspensions viscosity decreased as the fiber flexibility increased, in contradiction with the simulation results of Joung *et al.* (2001).

In another approach, a mesoscopic model was developed by Rajabian *et al.* (2005) for predicting the rheological behavior of semi-flexible fiber suspensions. The fiber suspension is regarded as a fluid characterized by the classical hydrodynamic fields and by some additional microstructure variables. The time evolution of the hydrodynamic fields is linked to the time evolution of the extra fields characterizing the microstructure. The framework for the time evolution equations is provided by GENERIC (see [Grmela and Oettinger (1997); Oettinger and Grmela (1997)]).

The advantage of the meso-hydrodynamics is the guarantee of the intrinsic compatibility of the governing equations with thermodynamics. Also the meso-hydrodynamics approach contributes to the understanding of the phenomena observed by providing a simple way to link the microscopic physics involved to the macroscopic behavior observed [Rajabian *et al.* (2005)]. In addition, another advantage of the mesocopic modeling approach is that the solution of the governing equations is relatively simple compared to particle level simulations. So, relatively simple mesoscopic models can be incorporated into larger computer programs to calculate complex flows of suspensions.

Rajabian *et al.* (2005, 2008) considered the semi-flexible nature of the fibers in the choice of the entropy function. Their simulation results showed that by increasing fiber flexibility both viscosity and first normal stress difference were increased. These

theoretical efforts have not undergone sufficient assessments, largely due to the lack of reliable experimental data on the effect of fiber flexibility in the current literature.

In this paper we first look at the effect of fiber flexibility on the rheological behavior and orientation of fibers suspended in a Newtonian fluid under simple shear flow, using conventional rheometry and rheo-microscopy. Then we fit the mesoscopic model of Rajabian *et al.* (2005) to the rheological data. The fact that the matrix is Newtonian reduces the number of adjustable phenomenological parameters from 8 to 3. The ability of the model to predict the orientation of the fibers under shear flow is also examined.

5.2 GENERIC model

5.2.1 Model definition

We consider suspensions of symmetrical prolate spheroids having large aspect ratios L/D >>1, uniformly dispersed in a Newtonian fluid. The suspensions are assumed to be incompressible and isothermal. Figure 5.1a depicts the orientation of a single fiber in the Cartesian coordinate system with a unit vector $\boldsymbol{P}$ representing its spatial alignment. A group of fibers is represented by a configuration distribution function $\psi(\boldsymbol{P})$. The probability distribution gives us a measure of the state of fiber orientation at a small element of suspension. Thus one can define $\psi(\boldsymbol{P})d\boldsymbol{P}$ which describe the probability of a fiber being orientated between the specific angles α and $\alpha + d\alpha$ and angles φ and $\varphi + d\varphi$. The distribution function should also satisfy the normalization conditions defined as:

$$\int \psi(\mathrm{P}) d\mathrm{P} = 1 \tag{5-1}$$

The state variable used in this work is a symmetric second order tensor, hereafter called the second-order orientation tensor $\boldsymbol{a}$, which its components are expressed by:

$$\boldsymbol{a}_{ij} = \int \boldsymbol{P}_i \boldsymbol{P}_j \psi(\boldsymbol{P}) d\boldsymbol{P} \tag{5-2}$$

The orientation tensor represents a compact description of the fibers at any point and any time. Since the fiber length is assumed to be constant, trace of $\boldsymbol{a}$ is:

$$\boldsymbol{a}_{ii} = 1 \tag{5-3}$$

The overall free energy of a suspension of fibers in a viscous fluid can be expressed by the momentum field and the orientation tensor $\boldsymbol{a}$, [Rajabian *et al.* 2005, 2008]:

$$\phi(\mathrm{u}, \boldsymbol{a}) = \int \mathrm{dr} \frac{\mathrm{u_j u_j}}{2\rho} - \frac{\mathrm{k_B T}}{2} \left[(1 - \mathrm{K_{flex}}) \mathrm{n_f} \ln \boldsymbol{a} - \mathrm{K_{flex}} \mathrm{n_f} \mathrm{tr} \boldsymbol{a}^{-1} - 2\mathrm{B_{ff}} \left((\mathrm{tr}\boldsymbol{a})^2 - \mathrm{tr}\boldsymbol{a}\boldsymbol{a} \right) \right] \tag{5-4}$$

We note that the first term on the right hand side of Equation 5-4 is the total kinetic energy, and the terms inside the bracket are due to entropy from orientational ordering of the rigid fibers, and entropy functional of fibers with limited flexibility. In this equation $u(r)$ is the overall momentum field and r is the position vector. The flexibility of the fibers is taken into account by the expression proposed first by Khokhlov and Semenov (1985), which was transformed into the orientation tensor formulation (Rajabian *et al.* 2005, 2008). K_{flex} is a macroscopic or phenomenological parameter accounting for the semi-flexibility effects of fibers in the free energy functional, and it varies between 0 for rigid and 1 for semi-flexible fibers. Finally, the last term in Equation 5-4 denotes the

entropy functional due to the presence of fiber-fiber interactions. B_{ff} denotes a phenomenological parameter proportional to fiber-fiber excluded volume.

The standard equation for the time evolution of the second-order orientation tensor has been derived in details in Rajabian *et al.* (2005, 2008) and is the sum of reversible and dissipation terms as follows:

$$\frac{d\boldsymbol{a}_{ij}}{dt} = -\frac{1}{2}\boldsymbol{a}_{jk}\omega_{ik} - \frac{1}{2}\boldsymbol{a}_{ik}\omega_{jk} - \frac{1}{2}\lambda\left(-\boldsymbol{a}_{ikl}\dot{\gamma}_{jk} - \boldsymbol{a}_{jlk}\dot{\gamma}_{ik} + \boldsymbol{a}_{ilkj}\dot{\gamma}_{lk} + \boldsymbol{a}_{jlki}\dot{\gamma}_{lk}\right) - \frac{\partial\Xi}{\partial\phi_{\boldsymbol{a}_{ij}}} \tag{5-5}$$

where ω_{ij} and $\dot{\gamma}_{ij}$ represent the vorticity and rate of deformation tensors, respectively, defined as a functions of the velocity gradient tensor:

$$\omega_{ij} = \frac{\partial v_j}{\partial x_i} - \frac{\partial v_i}{\partial x_j} \tag{5-6}$$

$$\omega_{ij} = \frac{\partial v_j}{\partial x_i} + \frac{\partial v_i}{\partial x_j} \tag{5-7}$$

and λ is a material constant that depends on the fiber aspect ratio:

$$\lambda = \frac{(L/D)^2 - 1}{(L/D)^2 + 1} \tag{5-8}$$

The last term on the right hand side of Equation 5-5 denotes the dissipation part, which represents all terms relating to irreversible phenomena arising in the governing equation by means of a dissipation potential Ξ. The fourth-order orientation tensor $\boldsymbol{a}_{ijkl}$ defined as:

$$\boldsymbol{a}_{ijkl} = \int \boldsymbol{P}_i\boldsymbol{P}_j\boldsymbol{P}_k\boldsymbol{P}_l\psi(\boldsymbol{P})d\boldsymbol{P} \tag{5-9}$$

is to be expressed from the second-order orientation tensor. The procedure to estimate the fourth order as well as higher order orientation tensors from the second order orientation tensor known as closure approximation has been subject of various investigations in the past. Cintra and Tucker (1995) were the first to introduce a class of closure approximation called orthotropic closure ORF based on calculations of eigenvalues and eigenvectors of the orientation tensor which was later modified by Wervyst (1998) to improve its accuracy. Since the orthotropic closure is found to provide precise results in various types of flow fields, we opted to use the modified form of ORF closure for this investigation

The dissipation potential represents all irreversible terms in the governing equation making the free energy reach its minimum under flow conditions. In the absence of dissipation phenomena only the advective parts appears in the time evolution equation and the total free energy remains unchanged with the flow. Neglecting the dissipation terms indeed simplifies Equation 5 to the original Jeffery's model, initially developed for a single fiber's motion in a viscous flow. We use the modified form of the dissipation potential proposed as by Edwards *et al.* (2003), which depends on the free energy derivative with respect to the second order orientation tensor, ϕ_a, as follows:

$$\Xi = \Lambda_{ff}\left(\frac{\partial v_s}{\partial x_r}\frac{\partial v_r}{\partial x_s}\right)^{1/2}\left(\phi_{a_{jk}} - \frac{1}{3}tr\phi_a\delta_{ik}\right)a_{kl}\left(\phi_{a_{li}} - \frac{1}{3}tr\phi_a\delta_{li}\right) \tag{5-10}$$

where Λ_{ff} is a fiber mobility parameter that has to be determined from rheological data or orientation tensor components. The free energy derivative ϕ_a is obtained from the following expression:

$$\phi_{a_{ij}} = \frac{\partial \phi}{\partial a_{ij}} = -\frac{k_B T}{2}\left[n_f(1-K_{flex})a_{ij}^{-1} + n_f K_{flex} a_{ij}^{-1} a_{kl}^{-1}\delta_{kl} - 2n_f B_{ff}(\delta_{ij} - a_{ij})\right] \tag{5-11}$$

The extra stress tensor of the suspension is the sum of contributions from the the Newtonian matrix as well as the fibers according to the following expression:

$$\tau_{ij} = -\eta_m \dot{\gamma}_{ij} + \frac{1}{2}\lambda\left(\phi_{a_{lk}} a_{lijk} + \phi_{a_{lk}} a_{kijl} - 2\phi_{a_{mi}} a_{mljl}\phi_{a_{lk}} a_{ljik} + \phi_{a_{mi}} a_{mljl} - 2\phi_{a_{mj}} a_{mlil}\right)$$
$$-\frac{1}{2}\frac{\dot{\gamma}_{ij}}{(\partial_k \phi_{ul}\partial_l \phi_{uk})^{1/2}}\Lambda_{ff}\left(\phi_{a_{lm}} - \frac{1}{3}tr\phi_a \delta_{lm}\right)a_{mp}\left(\phi_{a_{lp}} - \frac{1}{3}tr\phi_a \delta_{lp}\right) \tag{5-12}$$

The first term on the right-hand side is the contribution from the suspending fluid, and the remaining terms are due to the presence of the particles; it takes into account the stress due to advection of the fibers, followed by the terms accounting for the irreversible phenomena appearing in the free energy through entropy.

The time evolution of the second-order orientation tensor (Equation 5-5) can be solved numerically for imposed flow conditions. In the most general case, a set of six highly coupled non-linear differential equations for the components of the orientation tensor are to be solved. A numerical code in Mathematica (a commercial software from Wolfram Research) was developed to compute the components of the orientation tensor a_{ij} and the extra stress tensor.

5.2.2 Model Calculations for Simple shear flow

The rate of strain and vorticity tensors in simple shear flow are given by:

$$\dot{\gamma}(t)=\dot{\gamma}_0\begin{pmatrix}0&1&0\\1&0&0\\0&0&0\end{pmatrix};\qquad \omega(t)=\dot{\gamma}_0\begin{pmatrix}0&-1&0\\1&0&0\\0&0&0\end{pmatrix} \tag{5-13}$$

where $\dot{\gamma}_0$ is the magnitude of the shear rate.

For concentric disk geometry, the shear rate is given $\dot{\gamma}=r\ \theta/H$ where r is the radial position, H is the gap between the two disks and θ is the angular velocity of one disk. The viscosity and first normal stress difference can be obtained using the following expression [Carreau et al. (1997)]:

$$\sigma_{z\theta}=\eta_m(\dot{\gamma}_R)\dot{\gamma}_R=\frac{T}{2\pi R^3}\left[3+\frac{d\ln\left(\frac{T}{2\pi R^3}\right)}{d\ln\dot{\gamma}_R}\right] \tag{5-14}$$

$$N_1=-(\sigma_{11}-\sigma_{22})=\frac{2F}{\pi R^2}\left(1+\frac{1}{2}\frac{d\ln F}{d\ln\dot{\gamma}_R}\right) \tag{5-15}$$

The torque T and the normal force F_z are expressed, respectively, by:

$$T=2\pi\int_0^R\sigma_{z\theta}(r)r^2dr \tag{5-16}$$

$$F=\pi\int_0^R\left[N_1(r)-N_2(r)\right]rdr \tag{5-17}$$

where $\sigma_{z\theta}(r)$ is the shear stress, and $N_1(r)$ and $N_2(r)$ are, respectively, the primary and secondary normal stress differences evaluated at the radial position r. Based on the Weissenberg hypothesis, N_2 is assumed to be negligible. To compare the experimental results for the shear stress $\sigma_{z\theta}$ and the primary normal stress differences N_1 with the model predictions, these quantities have to be evaluated in a similar manner. For the

model predictions, macroscopic quantities were calculated from the shear stress component $\sigma_{z\theta}(r)$, the $\theta\theta$-component $\sigma_{\theta\theta}(r)$ and the zz-component $\sigma_{zz}(r)$ of the total stress tensor, combining expressions (5-14) and (5-15) with Eqs. (5-16) and (5-17), to provide the simulated stress $\sigma_{z\theta}^{sim}$ and primary normal stress difference N_1^{sim}.

The derivatives in Eqs. (5-14) and (5-15) were obtained by plotting $\ln T$ versus $\ln \dot{\gamma}_R$ and $\ln F$ versus $\ln \dot{\gamma}_R$, respectively and used both for model and experimental data .

5.3 Experimental

5.3.1 Materials and suspension preparation

A high viscosity silicone oil, polydimethylsiloxane (Clearco Products) with a density of 0.974 g/cm^3 and a nominal viscosity of 103 ± 2 Pa.s at 20 °C has been selected as the suspending medium. The steady-state viscosity, η, and complex viscosity, η^*, of the silicone oil have been measured, and both were equal and independent of the shear rate or frequency used in the experimental range investigated. The behavior is therefore Newtonian and this was also confirmed by the absence of significant normal stress differences.

In order to investigate the role of fiber flexibility on the rheological behavior of fiber suspensions, a criterion for flexibility needed to be defined. We used the following criterion for the effective stiffness, as proposed by Switzer and Klingenberg (2003):

$$S^{eff} = E_Y \pi D^4 / 64 \eta_m \dot{\gamma} L^4 \qquad (5\text{-}18)$$

in which, L and D are the fiber length and fiber diameter, respectively, and E_Y is the fiber Young modulus and η_m is the matrix viscosity. The effective stiffness characterizes the relative importance of the fiber stiffness and hydrodynamic forces. As $S^{eff} \to 0$, the fibers behave like completely flexible threads, whereas for $S^{eff} \to \infty$, the fibers become rigid and retain their equilibrium shape under flow [Switzer and Klingenberg (2003)]. Based on these criteria, various fibers (polyarylate (Vectran®), vinylon (PVA) and nylon fibers) with different Young modulus were chosen for this investigation. Fiber key characteristics are listed in Table 5-1.

Chopped fibers were used as received from the suppliers, and their length values based on the manual measurement of 400 fibers using optical microscopy and image analysis are reported in Table 5-1. The quantities L_n and L_w, number and weight average fiber lengths, respectively, can be defined as:

$$L_n = \frac{\sum_i n_i L_i}{\sum_i n_i} \tag{5-19}$$

$$L_w = \frac{\sum_i n_i L_i^2}{\sum_i n_i L_i} \tag{5-20}$$

For all fibers used the ratio L_w / L_n is close to 1, therefore they are nearly monodisperse. Suspensions were prepared at three different volume concentrations ($\phi_f = 0.01, 0.03, 0.04$). It can be implied from the criteria: $\phi_f << 1/r^2$ for dilute suspensions, $1/r^2 << \phi_f << 1/r$ for semi-concentrated suspensions, and $\phi_f > 1/r$ for concentrated suspensions [Tucker III and Advani (1994)], that suspensions with

$\phi_f = 0.01$ corresponded to semi-dilute and $\phi_f = 0.03$ and $\phi_f = 0.04$ correspond to semi-concentrated suspensions. The suspensions formulated with nylon, PVA and Vectran fibers are referred later on as NS, PS and VS, respectively.

The suspensions were prepared by hand mixing using a spatula. The sedimentation times of the fibers in the silicone oil matrix were calculated using the following equation from Chaouche and Koch (2001):

$$t_s = 8\eta_m L / \Delta\rho g D^2 \ln(2r - 0.72) \tag{5-21}$$

The sedimentation times for the various samples are presented in Table 5-1, and all the rheological experiments were carried out in times shorter than the reported values.

Since different fiber types are used, it is crucial to look at the compatibility between fibers and silicone oil. The interactions between the suspending fluid and the particles can play a major role on the rheological behavior of the suspensions [Mary *et al.* (2006)]. The degree of wetting is described by the contact angle, the angle at which the liquid-vapor interface meets the solid-liquid interface. If the wetting is favorable the contact angle is low, and the fluid spreads to cover a large area of the surface. On the other hand if the wetting is unfavorable, the fluid forms a compact droplet on the surface. A contact angle of 90° or greater generally characterizes a surface as non-wettable, and one less than 90° as wettable [Neumann and Good (1979)]. The contact angle between silicone oil and various films prepared using nylon, PVA and Vectran was measured using a goniometer (Model 100-00 of Ramé-Hart, Netcong, NJ, USA). The measured contact angles between the polymer films and the silicone oil were 26 ± 2°, 19 ± 2° and 29 ± 2° for nylon, PVA and Vectran, respectively. These results suggest

that all fibers were wetted well by the silicone oil and that the wettability does not vary enough to affect the rheological properties.

The Peclet number, the ratio of hydrodynamic forces to Brownian forces, can be estimated by [Chaouche and Koch (2001)]:

$$Pe = \eta_m \dot{\gamma} \pi L^3 / 3k_B T \ln r \tag{5-22}$$

in which k_B is Boltzmann's constant, and T is the absolute temperature. The Pe calculated at the lowest shear rate (0.1 s^{-1}) was 5.9×10^{11}. Since this Pe is larger than 10^8, the fibers can be considered as non-Brownian [Chaouche and Koch (2001)].

5.3.2 Rheological measurements

The rheological properties of the fiber suspensions were investigated using a parallel plate flow geometry and a stress-controlled rheometer (MCR 501, Paar Physica). All experiments were carried out at 20 °C. The gap between the parallel plates was set to 2 mm, hence a ratio gap to fiber length of 2:1 and gap to fiber diameter of 80-100, therefore large enough to avoid any wall effects. In addition, during loading the sample was progressively squeezed to orient the fibers in the plane of the plates (planar random). The same technique has been applied by Thommasset *et al.* (2005) for suspensions of long glass fibers in polypropylene. Also Bibbo (1987) showed that if the gap-to-fiber-length ratio is higher than 2, boundary effects are not significant, and this condition was achieved in our experiments.

By measuring the torque, T, and the normal force, F, as functions of the shear rate at the rim, $\dot{\gamma}_R$, the viscosity and first normal stress difference were calculated using Equations (5-14) and (5-15).

5.3.3 Visualization (rheo-microscopy) experiments

Visualization experiments were performed to characterize the fiber orientation. To this end another rheometer was used, the Paar Physica UDS 200 with parallel plate geometry (diameter = 50 mm). The lower metal plate was replaced by a glass plate and the temperature in the room was controlled at 20 °C by an air conditioner. The visualization was carried out using a continuously-focusable InfiniVar® microscope placed under the lower plate of the rheometer. The microscope was coupled to a color CCD camera (Lumenera) and the data acquired using the software StreamPix III® (NorPix). All the measurements were performed at the same light intensity, and the maximum depth of observation above the lower plate was measured to be 60 μm. The visualization window illuminate an area of (2393 μm × 1914 μm) in the radial position r/R = (21-23)/25. Fresh samples were loaded in the shearing cell as described previously and the gap was adjusted to 2 mm. Samples were deformed at various shear rates ($\dot{\gamma}|_{r=23}$ = 0.1, 0.5, 1, 2 and 4 s^{-1}) until steady state and sequences of images were collected at a rate of 4 images per second. A typical micrograph obtained from the visualization experiments is shown in Figure 2. In every single micrograph around 200-250 fibers were observable, and the visualization tests were repeated at least 3 times at each shear rate to collect as many

images for every suspension, hence around 600 to 750 fibers were visualized for the calculations of the second-order orientation tensor. This is well above the minimum 200 fibers suggested by Tucker and Advani (1994). In the case of semi-flexible fibers the angle with the flow direction changes along the fiber length, as illustrated in Figure 2. An end-to-end vector was used in this case to calculate the second-order orientation tensor.

As mentioned previously, the components of the orientation tensor were calculated using 3 images obtained from 3 different experiments, and overall more than 600 fibers were marked for these calculations. The standard deviation for the orientation tensor components was also evaluated from the measurements and was 12% at low strain and 5% at high strain and towards steady state.

5.3.4 Calculation of the orientation tensor components

The orientation of a single fiber can be described using a unit vector $\boldsymbol{P}$ along the fiber axis as shown in Fig. 1a. However, it is more convenient to describe the orientation state of a fiber population using the second-order orientation tensor, $\boldsymbol{a}$, as already explained in the section on modeling. Since the trace of $\boldsymbol{a}$ is always equal to 1, for a completely random orientation state $a_{ii} = 1/3$. In the limit where all the fibers are perfectly aligned with the flow direction (for example the θ direction) the only non-zero component is $a_{\theta\theta} = 1$. Since the images obtained from our visualization experiments are not suitable for evaluating the 3D components of the vector $\boldsymbol{P}$ (see Figure 5-2), our calculations have

been based on the hypothesis that most of the fibers, after sample squeezing between the parallel plates, were in the $r\theta$ plane. In this case we redefine the fiber orientation as illustrated in Fig. 5.1b. Hence, the components of the second-order orientation tensor can be calculated as:

$$a_{ij} = \frac{\sum_{k=1}^{N} P_i P_j}{N} \tag{5-23}$$

where N is the total number of fibers. Rheological measurements in stress-growth experiments suggest that fibers reorient themselves from their initial orientation state to align with the flow direction [Sepehr *et al.* (2004a, 2004b); Keshtkar *et al.* (2009)]. On the other hand Eberhardt *et al.* (2001) have measured the orientation of glass fibers in a polyarylamide in terms of the diagonal components of the second-order orientation tensor of an injection molded component, and they showed that only about 3% of the fibers were oriented in the gradient direction, (i.e. a_{zz} = 0.03). These results suggest that neglecting the orientation of the fibers in the gradient direction would be acceptable after a certain amount of strain, within experimental errors (5 to 12 %). Also Thomasset *et al.* (2005) and Ferec *et al.* (2008) assumed that the glass fibers in polypropylene were nearly oriented parallel to the plate (isotropic orientation in the shear plane) after squeezing the samples between the parallel plates, and that the component of the orientation tensor in the out-of-plane direction was only 10%. Using this assumption their model calculations were in good agreement with the experimental data. In summary, by neglecting the orientation tensor component in the out-of-plane direction, our data will contain acceptable errors that will be reduced as the strain is increased.

5.4 Steady State Flow Results

5.4.1 Steady state shear viscosity

Figure 5.3 compares the steady-state viscosity as a function of shear rate (ranging from 0.1 to 7 s^{-1}) for various fiber suspensions in silicone oil. Each curve represents an average of three sets of data for which sufficient time was allowed to reach steady state. It is observed that the addition of fibers to silicone oil (Newtonian viscosity ≈ 103 Pa.s) increased the viscosity and that for a specific fiber type the viscosity increased with volume fraction, as expected. For suspensions in the semi-dilute regime ($\phi_f = 0.01$), the viscosity was almost independent of fiber flexibility and no shear-thinning behavior was observed. On the other hand, increasing fiber content up to the semi-concentrated regime ($\phi_f = 0.03$ and $\phi_f = 0.04$) resulted in a shear-thinning behavior largely more pronounced at the highest concentration. In addition, the suspension viscosity increased with fiber flexibility and this enhancement was also more pronounced at high concentration and low shear rates.

Ganini and Powell (1985a, 1985b) reviewed most of the literature in the area of glass fibers suspended in Newtonian fluids and reported that the dependence of a suspension viscosity on shear rate was more pronounced as the fiber aspect ratio increased. Their literature investigation showed that for an aspect ratio of 35–45 a very weak shear-thinning at low shear rates was observed, followed by a Newtonian plateau for shear rates above 10 s^{-1}; but a strong shear-thinning behavior over a range of 0.1-100 s^{-1} for

aspect ratios larger than 100 was observed. Kitano and Kataoka (1981), who measured the shear viscosity of suspensions of vinylon fibers with r = 45 in a silicone oil found a significant shear-thinning in the 0.01 to 1 s^{-1} range, but the viscosity was constant above 1 s^{-1}. These are consistent with the shear-thinning behavior observed in our work.

It is believed that the dominant mechanism that affects the rheological properties in the semi-concentrated and concentrated regimes is fiber-fiber interactions [Sundararajakumar and Koch (1997); Petrich and Koch (1998); Sepehr et al. (2004a)]. Hence, the increase in the suspension viscosity in the case of the more flexible fibers could somehow be related to enhanced fiber-fiber interactions. At low shear rates network-like structures may be formed because of inter-particle adhesive forces [Chaouche and Koch (2001); Djalili Moghadam and Toll (2006)]. As the shear rate increases these structures may be destroyed, which can lead to a shear-thinning behavior and a decreasing viscosity. Our results indicate that as fiber flexibility increased a stronger structure may be formed, most probably due to the bending of the more flexible fibers, resulting in more inter-particle interactions and a larger viscosity.

5.4.2 Normal stress

In suspensions where fibers undergo hydrodynamic and Coulombic solid-body interactions, normal stress differences are exhibited. The secondary normal forces are much less than the primary normal forces and can be neglected [Petrich *et al.* (2000); Sepehr *et al.* (2004a)]. Carter (1967) proposed the following correlation for the first normal stress difference as a function of shear rate, fiber content and fiber aspect ratio:

$$N_1 = K\eta_m\dot{\gamma}\frac{\phi\, r^{1.5}}{\ln 2r - 1.8} \tag{5-24}$$

where K is a constant that must be determined experimentally. In contrast to Brownian fiber suspensions and other fluids that undergo molecular relaxation and where N_1 is proportional to $\dot{\gamma}^2$, rigid fiber suspensions with contacts show primary normal stress differences that are linearly proportional to shear rate [Sundararajakumar and Koch (1997), Petrich *et al.* (2000)]. Figure 5.4 presents the first normal stress difference (N_1) data scaled by $\eta\dot{\gamma}$ in the semi-dilute ($\phi_f = 0.01$) and semi-concentrated ($\phi_f = 0.03$) regimes. In both regimes the addition of fibers resulted in significant normal forces under shear flow, and these values increased with fiber content. In the semi-dilute regime the dimensionless value was independent of shear rate, in agreement with the model of Carter (1967) and also with the results of Petrich *et al.* (2000) for glass fibers with an aspect ratio of 50 suspended in polybutene. The K value of Carter model [Carter (1967)] was calculated to be 0.09 ± 0.01 in our experiments for the semi-dilute regime. Different authors have calculated K [Sepehr *et al.* (2004a); Keshtkar *et al.* (2009); Kitano and Kataoka (1981); Petrich *et al.* (2000); Carter (1967); Goto *et al.* (1986); Zirnsak *et al.* (1994)] and it ranged from 0.04 to 0.32 and our results are in good agreement with literature.

The N_1 data in the semi-concentrated regime is no longer linear with the shear rate as predicted by Equation 5-24, but N_1 can be correlated by a power-law expression as proposed by Goto *et al.* (1986):

$$N_1 = m\dot{\gamma}^n \tag{5-25}$$

Using carbon, nylon, vinylon and glass fiber suspensions in glycerin, Goto *et al.* (1986) calculated n to be less than unity. For suspensions prepared using nylon fibers in glycerin (the most flexible fibers in the work of [Goto *et al.* (1986)]), n had the lowest value and m had the highest value. Our data are in agreement with the findings of Goto *et al.* (1986), i.e. m is shown to increase with fiber flexibility. The exponent n has been evaluated in this regime to be 0.79, 0.74 and 0.64 for Vectran, PVA and nylon fiber suspensions, respectively. Overall, as flexibility increases n decreases, which means a stronger shear-thinning behavior, in agreement with observations for the steady state shear viscosity (Fig. 5.3). The enhancement of the first normal stress difference with increasing fiber flexibility is more pronounced at lower shear rates. Since the presence of normal stresses for fiber suspended in a Newtonian fluid is due to fiber-fiber interactions [Sepehr *et al.* (2004a), Petrich *et al.* (2000)], we can conclude that in the case of the more flexible fiber suspensions, the role of fiber-fiber interactions is predominant.

On the modeling side, Rajabian *et al.* (2005) and Switzer and Klingenberger (2003) showed that the first normal stress difference increases with fiber flexibility, in agreement with our experimental findings.

5.4.3 Fiber orientation

As discussed in the previous sections, the suspensions in the semi-concentrated regime showed a marked shear-thinning behavior, although the suspending medium was Newtonian. The shear-thinning behavior was also more pronounced as the fiber

flexibility increased. In order to investigate how the shear-thinning behavior could possibly be related to the orientation state of the fibers under shear, orientation measurements as described previously were performed at various shear rates ($\dot{\gamma}|_{r=23}$ = 0.1, 0.5, 1 and 2 s^{-1}) for suspensions in the semi-concentrated regime ($\phi_f = 0.03$). Micrographs similar to that presented in Figure 5.2 were analyzed to calculate the components of the second-order orientation tensor. The component of the orientation tensor in the flow direction, $a_{\theta\theta}$, is presented in Figure 5-5 as a function of shear rate. It has been determined for the dimensionless radial position r/R = (21 to 23)/25. For all suspensions, $a_{\theta\theta}$ is seen to increase with shear rate towards a maximum value (of ≈ 0.8), indicative of a shear flow-induced fiber orientation. At low shear rates the orientation with the flow direction is more important for the most rigid fibers, indicating that the latter are more easily oriented by than flexible fibers. However, with increasing shear rate the difference in the orientation state between the rigid and the flexible fibers becomes negligible.

The lower fiber orientation of flexible fibers at low shear rates is in agreement with the findings of Soszynksi and Kerekes (1988a, 1988b) who have studied floc formation using nylon fibers of aspect ratios ranging from 65 to 189 and suspended in aqueous sugar solutions. They suggested that floc formation is due to mechanical contacts and coherence of the fibers, due to interlocking by the elastic bending of the fibers. In the mechanism proposed, called "elastic fiber interlocking", the fibers become locked and form a network because of their elasticity. The formation of these flocs may explain the

low fiber orientation at low shear rates. Also, Chaouche and Koch (2001) experiments suggested that there was a flow-induced flocculation of the fibers at low shear rate, and that these flocs were held together by adhesive forces. They supported this assertion by visualization experiments and showed that at low enough shear rates, fiber contacts dominated the suspensions behavior. In a particle-level simulation, Schmid *et al.* (2000) predicted flocculation of flexible fibers in shear flow using inter-fiber friction in the absence of attractive forces. The subsequent shear-thinning behavior predicted by their simulations at high shear rate was attributed to a reversal of the flocculation phenomenon under flow. Also Switzer and Klingenberg (2003) observed the formation of flexible fiber agglomerates in their simulation work. The formation of large scale structures was also seen to be more pronounced by increasing the permanent fiber deformation (slightly bended fibers) in their simulations. The formation of these structures resulted in enhanced rheological properties; however, the suspensions tended to display a viscosity independent of shear rate. These experimental observations and model predictions are consistent with our experimental data, which show that at low shear rate the fibers were less oriented in the flow direction, especially for the more flexible fibers, which were shown in our visualization to have slightly curved shapes. However, with increasing shear rate the orientation of the fibers of different flexibilities became similar.

5.5 Model Predictions for Transient Shear Flows

As presented in Section 5.2, the model used in this work takes into account the flexible nature of the fibers, inter-particle interactions and the mobility of fibers. In this section the effect of each parameter on the rheological behavior is studied and interpreted, while in Section 5.6 the model predictions are compared to the transient experiment results. For all the simulations the model parameters were as following: $\eta_m = 100$ Pa.s, $\phi_f = 0.03$, and L/D = 70, and all the simulations were performed for $\dot{\gamma} = 1s^{-1}$. The initial second-order orientation tensor was considered to be:

$$\boldsymbol{a} = \begin{pmatrix} 0.45 & 0 & 0 \\ 0 & 0.1 & 0 \\ 0 & 0 & 0.45 \end{pmatrix} \tag{5-26}$$

5.5.1 Effect of fiber mobility

The effect of the fiber mobility is represented by the fiber mobility coefficient in the model, Λ_{ff}, and its effect on transient rheological properties is presented in Figures 5-6a (viscosity) and 5-6b (first normal stress difference). For both the viscosity and the first normal stress difference overshoots were observed, and the magnitude of these overshoots increased with a decrease of Λ_{ff}. In addition the steady-state value of these rheological functions, along with the strain to reach steady-state, increased as Λ_{ff} decreased. The observed overshoots in the stress growth test are due to the presence of the fibers and attributed to the progressive alignment of the fibers in the flow direction [Sepehr et al. (2004a); Laun (1986); Ausias *et al.* (1992)]. The effect of the fiber

mobility coefficient was more pronounced for the first normal stress difference (Figure 5-6b).

The fiber mobility coefficient represents the ability for the fibers to move beside each other, and by decreasing this resistance (larger Λ_{ff}) the fibers can flow more easily and orient themselves with the flow direction. The fiber shape and the inter-fiber friction are two factors that may influence the mobility. Using particle level simulations, Switzer and Klingenberg (2003) showed that relatively small deviations in the shape from a perfectly straight form can result in large increases of the viscosity of suspensions. Also, they showed that the viscosity increased with inter-fiber friction. The inter-fiber friction impacted more considerably the viscosity of the suspensions of non-straight fibers than those of straight fibers. Their simulation results are consistent with the current model predictions.

5.5.2 Effects of fiber flexibility

The semi-flexible nature of the fibers is represented by the fiber flexibility parameter K_{flex} in our model. Its effect on the transient rheological properties is presented in Figures 5.7a (viscosity) and 5.7b (first normal stress difference). , the fiber flexibility parameter is introduced in Section 5.2 through an entropic term of the free energy function, and varies between zero (rigid fibers) and 1. It is shown in Figure 5.8 that by increasing the flexibility, both the steady-state value and the magnitude of the overshoots for the viscosity (5.7a) and first normal stress difference (5.7b) become larger. The predictions are in agreement with the simulation studies of Rajabian *et al.*

(2005). Since, as mentioned previously, the presence of the overshoot is due to fiber alignment in the flow direction, the predictions suggest that flexible fibers are more resistant to flow-induced orientation. Conversely, rigid fibers tend to be more easily oriented than flexible fibers, and as a consequence, the rheological properties of the flexible fibers are enhanced further. These results are in agreement with the experimental data presented in Section 5.3. They are also in agreement with the experimental findings of Goto *et al.* (1986) who showed that nylon fiber suspensions (flexible fibers, E_Y = 2 GPa) had larger viscosities than glass fiber suspensions (rigid fibers, E_Y = 75 GPa) at the same volume concentration (ϕ_f = 0.005) and aspect ratio (r = 300). The predictions also are consistent with the direct simulation results of Joung *et al.* (2001) for flexible fibers in a Newtonian suspending medium. However, in contrast Switzer and Kligenberg (2003) predicted using direct simulation that increasing the fiber flexibility (or decreasing E_Y) led to lower values of the steady shear viscosity. They explained this by the fact that rigid fibers have a straight shape while flexible fibers may have permanent deformed shape, and those differences between equilibrium shapes must be considered in the simulations in order to predict correctly the rheological behavior.

5.5.3 Effects of fiber-fiber interactions

The phenomenological parameter B_{ff} takes into account interactions between fibers and appears in the dissipative term of the second-order orientation tensor $\boldsymbol{a}$. As explained in the modeling section this parameter is proportional to the fiber excluded volume. The effect of this parameter on the transient rheological properties is presented in Figures

5.8a (viscosity) and 5.8b (first normal stress difference). Both the steady state values and the overshoot magnitudes in transient shear flow were significantly increased as the value of B_{ff} decreased, with a larger effect on the first normal stress difference (Figure 8b). A physical interpretation of this parameter stands in mechanical contacts between fibers. These contacts may occur in semi-concentrated suspensions, in which the average distance between fibers is of the order, or less, than the fiber length, and play a major role in the concentrated regime, in which the average distance between fibers is less than the fiber diameter. In these regimes the fiber-fiber mechanical contacts can result in the formation of flocks or aggregates that may increase the viscosity and first normal stress difference. As the fiber-fiber interaction parameter decreased, the probability of contacts between fibers increased. Rajabian *et al.* (2005) have used 0 and negative values for this parameter. Since this is an entropic term, the negative values are not acceptable. The physical meaning of a 0 value is that the whole body of fibers are completely in contact with each other and this case is physically impossible. Hence, only positive values of B_{ff} have a physical meaning.

The effect of fiber–fiber contacts on the stress has been investigated by Sundararajakumar and Koch (1997). They simulated the dynamic behavior of fibers interacting through fiber-fiber contacts and neglected hydrodynamic interactions. The contacts caused fibers to flip more frequently as the concentration increased and resulted in orientational changes, which led to a significant increase in the viscosity. The latter was further enhanced by the transmission of stress through fiber contacts [Petrich et al. (2000)]. Also Thommaset et al. (1997), using direct simulation for long fibers, showed

that as the number of contacts increased the orientation of fibers in the flow direction decreased, which result in enhanced rheological properties.

As mentioned earlier, it is believed that the presence of normal stresses for fibers suspended in a Newtonian fluid is due to fiber-fiber interactions [Sepehr *et al.* (2004a), Petrich *et al.* (2000)], and the model predictions presented here were in agreement with these assumptions since a decrease in the B_{ff} parameter (or increase in fiber-fiber interaction) resulted in larger normal forces (Figure 5.8b).

5.6 Comparison of Model Predictions with Transient Experimental Data

For this part of the work, the model parameters (i.e. mobility parameter, Λ_{ff}, fiber-fiber interaction parameter, B_{ff} and flexibility parameter, K_{flex}) were determined from the measured rheological properties of the suspensions and subsequently used to predict fiber orientation. The predictions were performed for suspensions containing 3% vol of fibers with different flexibilities (suspensions NS (with nylon fibers), PS (PVA fibers) and VS (Vectran fibers)). It was assumed that before applying the shear flow the fibers were nearly all in a planar random orientation (plane $r\theta$, with θ the flow direction and r the vorticity direction) and that only a small portion of the fibers were aligned in the z-direction (gradient or out-of-plane direction). This initial orientation was chosen because of the sample loading method, as explained earlier. A similar assumption has been used

by Ferec *et al.* (2008) for their computations of fiber orientation. The initial value of the second-order orientation tensor was therefore imposed as in Equation (5-26).

The stress growth experimental data for $\dot{\gamma}_R$ = 1 s^{-1}, along with model predictions are presented in Figure 5.9 and the model parameters are listed in Table 5-2.

It can be seen in Figure 5.9a that during the stress growth experiments, all the suspensions exhibited large viscosity overshoots. Since the matrix was Newtonian and its transient behavior extremely fast and without any overshoot, the observed overshoot in the stress growth tests is exclusively due to the presence of the fibers [Sepehr *et al.* (2004a)]. Also as the fiber Young modulus decreased, the amplitude of the peak increased and the suspension reached steady state at larger strain. The corresponding transient results for the normal stress differences are presented in Figure 5.9b. All suspensions exhibited large normal stress overshoots at a strain of about 30, while steady state was reached for strains between 75 to 90, depending on fiber flexibility.

The GENERIC model predictions were confronted with these experiments. The model predicted the transient viscosity quite well for the three suspensions (Figure 5.9a), but using the parameters fitted to the viscosity data to predict N_1 was not so successful, especially for the width of the overshoot and the strain at which N_1 reached steady state. However, the overall qualitative behavior and the trend for the various suspensions were right.

It is also important to examine the ability of the model to predict the rheological properties at various shear rates, using the same parameters fitted at a shear rate of 1 s^{-1}. The model predictions for different shear rates ($\dot{\gamma}$ = 0.5, 1 and 5 s^{-1}) are shown in

Figure 5.10 for the most flexible (NS) and the most rigid (VS) fiber suspensions for $\phi_f = 0.03$. It can be seen that at $\dot{\gamma}$ = 0.5 s^{-1}, the model with the previously fitted parameters (for a shear rate of 1 s^{-1}) overpredicts both the overshoot and the steady state value of the viscosity, and that it was more pronounced for the high value of K_{flex} (most flexible fibers). On the other hand, the model underpredicts the overshoots and steady state values at the larger shear rate ($\dot{\gamma}$ = 5 s^{-1}). Nevertheless, the model predicts qualitatively well the shear-thinning behavior of these suspensions.

Once the model parameters were fitted to the rheological data and validated, their physical significance was examined to explain the suspension behavior. First the fitted parameters showed that for decreasing fiber stiffness the flexibility parameter had to be increased, as expected (Table 5-2). Also as the fiber flexibility increased the parameter related to the excluded volume of the fibers, B_{ff}, showed a lower value, meaning more inter-fiber interactions. In addition, by decreasing the fiber stiffness the mobility parameter was decreased. This resulted in an enhancement of the overshoot magnitude and steady state values for both the viscosity and first normal stress difference. An increasing fiber-fiber interaction and a decreasing mobility parameter for the more flexible fibers may be due to the curved shape of the flexible fibers as compared to the straight shape of the rigid ones. Also decreasing the mobility parameter has caused the fibers to have more resistance to orientation and made themselves orient more slowly, which increased the strain at which the steady state was reached.

In the next step, the parameters obtained from fitting the stress growth experiments data were used to evaluate the model ability to predict the orientation of the fibers in the

transient state. The predictions of the second-order orientation tensor component $a_{\theta\theta}$ are confronted in Figure 5.11 with visualization experimental data at $\dot{\gamma}$ = 1 s^{-1}. For all suspensions, the experimental orientation tensor component was evaluated at strains of 0, 4, 12, 20, 60 and 100 using the methodology described in Section 3. Strain 0 relates to the initial fiber orientation of the suspensions at rest before application of the shear. we note from Figure 5.11 that $a_{\theta\theta}$ increased with shear. This shows that the fibers, with initial random orientation in the $r\theta$ planes reoriented to align with the flow direction (θ). The rate of fiber orientation was very fast at low strains but at increasing strain, the rate decreased considerably and orientation hardly increased. Also these experimental results show that by increasing the flexibility, $a_{\theta\theta}$ (which is representative of the orientation in the flow direction) decreased. Rigid fibers oriented themselves more rapidly in the flow direction and the degree of orientation was higher than for flexible fibers. The model predictions in Figure 5.11 are qualitatively in agreement with the experimental data, although for all the suspensions the model overpredicts the orientation of the fibers. These overpredictions are probably more important since we considered most of fibers to be strictly in the $r\theta$ plane.

The simulation results presented in this section show that the GENERIC model can qualitatively describe the transient rheological behavior of fiber suspensions in a Newtonian fluid. In this context the model contains only three adjustable parameters that all have a physical significance. Obviously more efforts have to be devoted to the development of a model that would describe quantitatively the complex rheological

behavior of semi-concentrated and concentrated suspensions of flexible fibers at various shear rates, but this is not an easy task to undertake.

5.7 Conclusions

The rheological properties of suspensions with fibers of various Young moduli and hence different flexibilities were investigated. Both the viscosity and first normal stress difference were enhanced by increasing fiber flexibility. The larger rheological properties of the flexible fibers were attributed to their slightly curved shape as opposed to the straight shape of the rigid fibers. Rheo-microscopy of the various suspensions showed that fibers orient in the flow direction and that the fiber orientation increased with shear rate and the amount of strain applied. A GENERIC-type model was used to describe the phenomena observed. The model parameters were obtained by fitting the stress growth viscosity data at a single shear rate. Using these fitted parameters, the ability of the model to predict first normal stress difference and rheological properties at other shear rates was examined. In addition, the fiber orientation as predicted by the model was confronted with the rheo-microscopy results. The model predicts qualitatively well fiber orientation for fibers of various flexibilities.

5.8 Acknowledgements

The authors would like to acknowledge financial support from the Natural Sciences and Engineering Research Council of Canada (NSERC-CIAM program). We also wish to

thank Dr. Thomas Griebel (from SwissFlock Inc.) for providing the nylon fibers, and Dr. Takashi Takayama (from Kuraray Co. Ltd) for providing the Vectran® and PVA (Kuralon®) fibers. We also gratefully thank Professor Jose Perez Gonzales, Professor Lourdes de Vargas and Benjamín M. Marín-Santibáñez for providing the experimental setup for the rheo-microscopy.

5.9 References

Advani S.G., C.L. Tucker, *The use of tensors to describe and predict fber orientation in shorti fber composites*, Journal of Rheology 31 (1987) 751-

Ausias, G., J.F. Agassant, M. Vincent, P.G. Lafleur, P.A. Lavoie and P.J. Carreau, *Rheology of short glass fiber reinforced polypropylene.* Journal of Rheology 36 (4) (1992) 525-542.

Bibbo, M. A., *Rheology of semi-concentrated fiber suspensions.* Ph.D.Thesis, Massachusett Institute of Technology, (1987)

Carreau, P.J., D. De Kee, and R.P. Chhabara, *Rheology of polymeric systems.* 1997, NewYork: Hanser/Gardner.

Carter, L.F., *A study of the rheology of suspensions of rod-shaped particles in a Navier–Stokes liquid.* 1967, University of Michigan: Ann Arbor, MI.

Chaouche, M. and D.L. Koch, *Rheology of non-Brownian rigid fiber suspensions with adhesive contacts.* Journal of Rheology 45 (2) (2001) 369-382.

Cintra J.S., C.TuckerIII, *Orthotropic closure approxomations for flowinduced fiber orientation.* Journal of Rheology 39 (1995) 1095-1122.

Djalili-Moghaddam, M. and S. Toll, *Fibre suspension rheology: effect of concentration, aspect ratio and fibre size.* Rheolgica Acta 45 (2006) 315-320.

Edwards, B.J., M. Dressler, M. Grmela and A. Ait-Kadi, *Rheological models with microstructural constrains.* Rheol Acta 42 (2003) 64.

Eberhardt, C., A. Clarke, M. Vincent, T. Giroud, S. Flouret, *Fiber-orientation in short glass fiber composites- II: a quantitative error estimate of the 2D image analysis technique.* Composite Science and Technology 61 (2001) 1961-1974.

Férec. J., Heuzey,M.C., G. Ausias, and P.J. Carreau, *Rheological behavior of fiber-filled polymers under large amplitude oscillatory shear flow.* Journal of Non-Newtonian Fluid Mechanics 151 (1-3) (2008) 89-100.

Ganani, E. and R.L. Powell, *Rheological properties of rodlike particles in a Newtonian and a Non-Newtonian fluid.* Journal of Rheology 30 (5) (1985a) 995-1013.

Ganani, E. and R.L. Powell, *Suspensions of rodlike particles: Literature review and data correlations.* Journal of Composite Materials 19 (3) (1985b) 194-215.

Goto, S., H. Nagazono, and H. Kato, *The Flow Behavior Of Fiber Suspensions In Newtonian Fluids And Polymer Solutions. I: Mechanical Properties.* Rheolgica Acta 25 (1986) 119-129.

Grmela, M., H.C. Oettinger, *Dynamics and thermodynamics of complex fluids I. Development of a GENERIC formulatism.* Phys Rev E 55 (1997) 6620.

Joung, C.G., N. Phan-Thien, and X.J. Fan, *Direct simulations of flexible fibers.* Journal of Non-Newtonian Fluid Mechanics 99 (1) (2001) 1-36.

Keshtkar, M., M.C. Heuzey and P.J. Carreau, *Rheological behavior of fiber-filled model suspensions: effect of fiber flexibility.* Journal of Rheology 53 (3) (2009).

Khokhlov AR, S. A. *On the theory of liquid crystalline ordering of polymer chains with limited flexibility.* J Stat Phys 38 (1985), 161

Kitano, T. and T. Kataoka, *The rheology of suspensions of vinylon fibers in polymer liquids. II. Suspensions in polymer solutions.* Rheologica Acta 20 (4) (1981) 403-415.

Laun, H.M., *Prediction of elastic strains of polymer melts in shear and elongation.* Journal of Rheology 30 (3) (1986) 459-501.

Mary, B., Dubois, C., P. J. Carreau, & P. Brousseau, *Rheological properties of suspensions of polyethylene-coated aluminum nanoparticles.* Rheolgica Acta 45 (2006) 561-573.

Neumann A. W., Good, R. J. In: Good, R. J., Stromberg, R., *Surface and ColloidScienc, Vol II.* (New-York: Plenum 1979)

Oettinger, H.C., M. Grmela, *Dynamics and thermodynamics of complex fluids II. Illustration of a GENERIC formulatism.* Phys Rev E 55 (1997) 6633.

Petrich, M.P. and D.L. Koch, *Interactions between contacting fibers.* Physics of Fluids 10 (8) (1998) 2111-2113.

Petrich, M.P., D.L. Koch, and C. Cohen, *Experimental determination of the stress-microstructure relationship in semi-concentrated fiber suspensions.* Journal of Non-Newtonian Fluid Mechanics 95 (2-3) (2000) 101-133.

Rajabian, M., C. Dubois, and M. Grmela, *Suspensions of Semiflexible Fibers in Polymeric Fluids: Rheology and Thermodynamics.* Rheologica Acta 44 (2005) 521-535.

Rajabian, M., Dubois, C., M. Grmela, & P.J. Carreau, *Effect of polymer-fiber interactions on rheology and flow behavior of semi-flexible fibers in polymeric liquids.* Rheolgica Acta 47 (2008) 701-717.

Ross, R.F. and D.J. Klingenberg, *Dynamic simulation of flexible fibers composed of linked rigid bodies.* Journal of Chemical Physics 106 (7) (1997) 29-49.

Schmid, C.F., L.H. Switzer, and D.J. Klingenberg, *Simulations of fiber flocculation: effects of fiber properties and interfiber friction.* Journal of Rheology 44 (4) (2000) 781-809.

Sepehr, M., P.J. Carreau, M. Moan, G. Ausias, *Rheological properties of short fiber model suspensions.* Journal of Rheology 48 (5) (2004a) 1023-1048.

Sepehr, M., G. Ausias, and P.J. Carreau, *Rheological properties of short fiber filled polypropylene in transient shear flow.* Journal of Non-Newtonian Fluid Mechanics 123 (1) (2004b) 19-32.

Soszynski, R.M., and R.J. Kerekes, *Elastic interlocking of nylon fibers suspended in liquid. Part 1. Nature of cohesion among fibers.* Nord. Pulp Pap. Res. J. 3 (1988a) 172-179.

Soszynski, R.M., and R.J. Kerekes, *Elastic interlocking of nylon fibers suspended in liquid. Part 2. Process of interlocking.* Nord. Pulp Pap. Res. J. 3 (1988b) 180-184.

Sundararajakumar, R.R. and D.L. Koch, *Structure and properties of sheared fiber suspensions with mechanical contacts.* Journal of Non-Newtonian Fluid Mechanics 73 (3) (1997) 205-239.

Switzer III, L.H. and D.J. Klingenberg, *Rheology of sheared flexible fiber suspensions via fiber-level simulations.* Journal of Rheology 47 (3) (2003) 759-778.

Thomasset, J., M. Grmela, P.J. Carreau, *Microstructure and rheology of polymer melts reinforced by long glass fibers: direct simulations.* Journal of Non-Newtonian Fluid Mechanics 73 (1997) 195-203.

Thomasset, J., P.J. Carreau, B. Sanschagrin, G. Ausias, *Rheological properties of long glass fiber filled polypropylene.* Journal of Non-Newtonian Fluid Mechanics 125 (1) (2005) 25-34.

Tucker III, C.L. and S.G. Advani, *Flow and rheology of polymer composites manufacturing.* (Edited by S.G. Advani) 147-202, Elsevier Science, New York (1994).

VerWeyst B, *Numerical solutions of flow induced fiber orientation in three-dimensionalgeometries* . PhD thesis, Department of Mechanical Engineering, University of Illinois at Urbana- Champaign, USA

Wang, G., W. Yu, and C. Zhou, *Optimization of the rod chain model to simulate the motions of a long flexible fiber in simple shear flows.* European Journal of Mechanics, B/Fluids 25 (3) (2006) 337-347.

Yamamoto, S. and T. Matsuoka, *Method for dynamic simulation of rigid and flexible fibers in a flow field.* Journal of Chemical Physics 98 (1) (1993) 644.

Yamamoto, S. and T. Matsuoka, *Dynamic simulation of microstructure and rheology of fiber suspensions.* Polymer Engineering and Science 36 (19) (1996) 2396-2403.

Zirnsak, M.A., D.U. Hur, and D.V. Boger, *Normal stresses in fibre suspensions.* Journal of Non-Newtonian Fluid Mechanics 54 (1994) 153-193.

Table 5.1 : Characteristics and nomenclature of the fibers used in this study

Fiber nomenclature	**Young's Modulus (GPa)**	**Density (kg/m^3)**	L_n **(mm)**	L_w **(mm)**	**Aspect Ratio**	$t_s(h)$
N	2.0	1140	0.96	0.98	70	144
P	26	1300	0.98	0.99	70	73
V	76	1410	1.25	1.27	70	43

Table 5.2 : Model Parameters for different suspensions

Parameter	**NS**	**PS**	**VS**
K_{flex}	0.49	0.36	0.28
Λ_{ff}	2.6×10^{-6}	7.9×10^{-6}	9.5×10^{-6}
B_{ff}	7.9	8.8	9.3

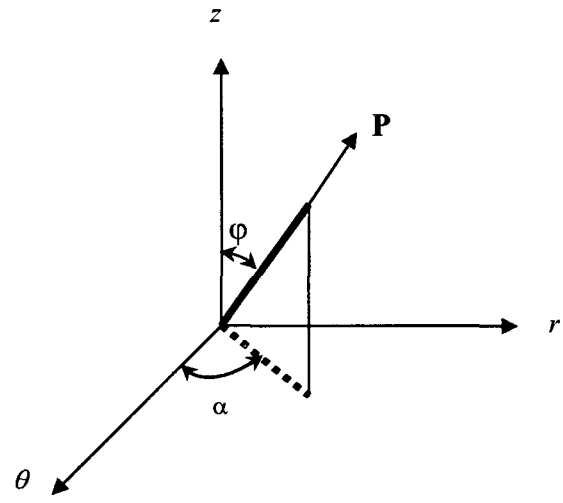

a)

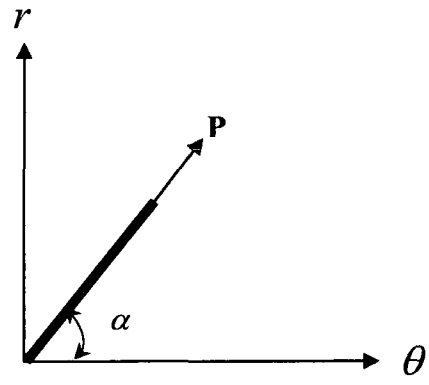

b)

Figure 5.1 : Unit vector **P** describing the orientation state of a fiber. (a) in cylindrical coordinates; (b) in $r\theta$ plane. (θ, z and r represent flow, gradient and vorticity directions, respectively)

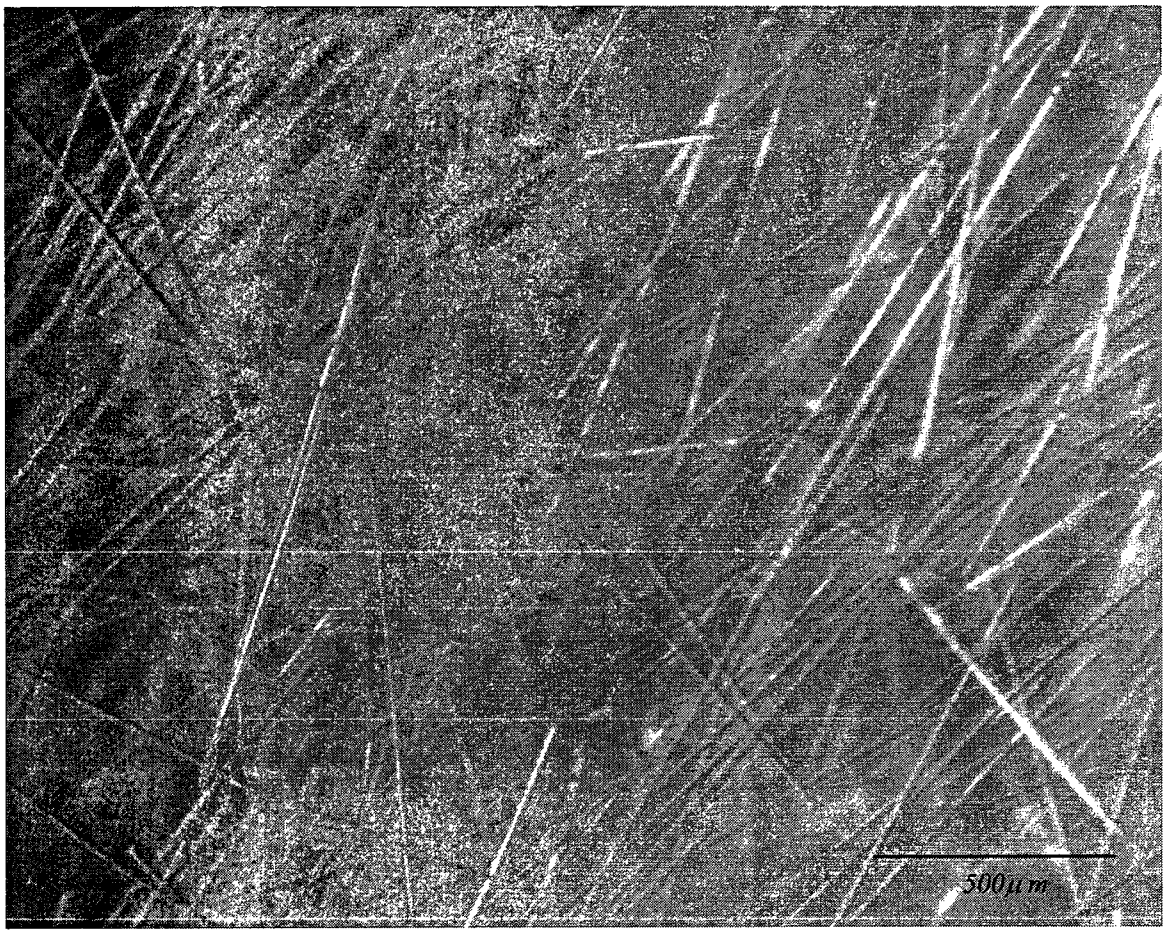

Figure 5.2 : Micrograph of a fiber suspension in visualization experiments

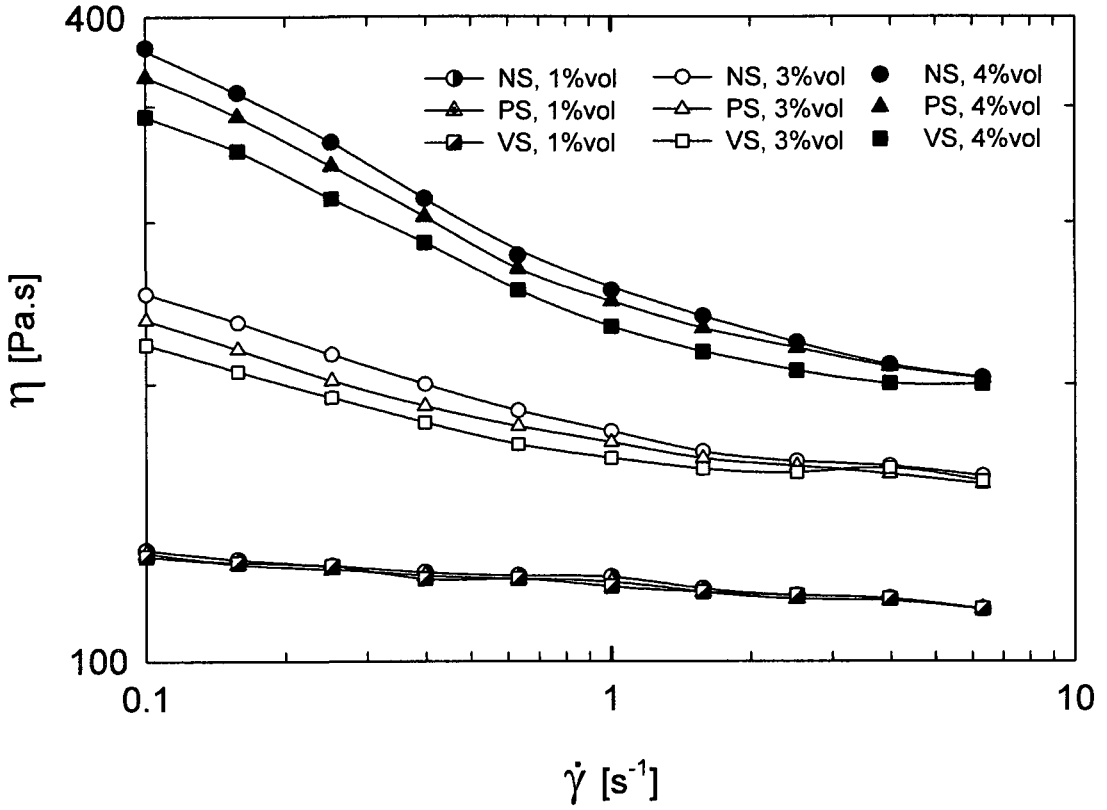

Figure 5.3 : Steady shear viscosity of fiber suspensions

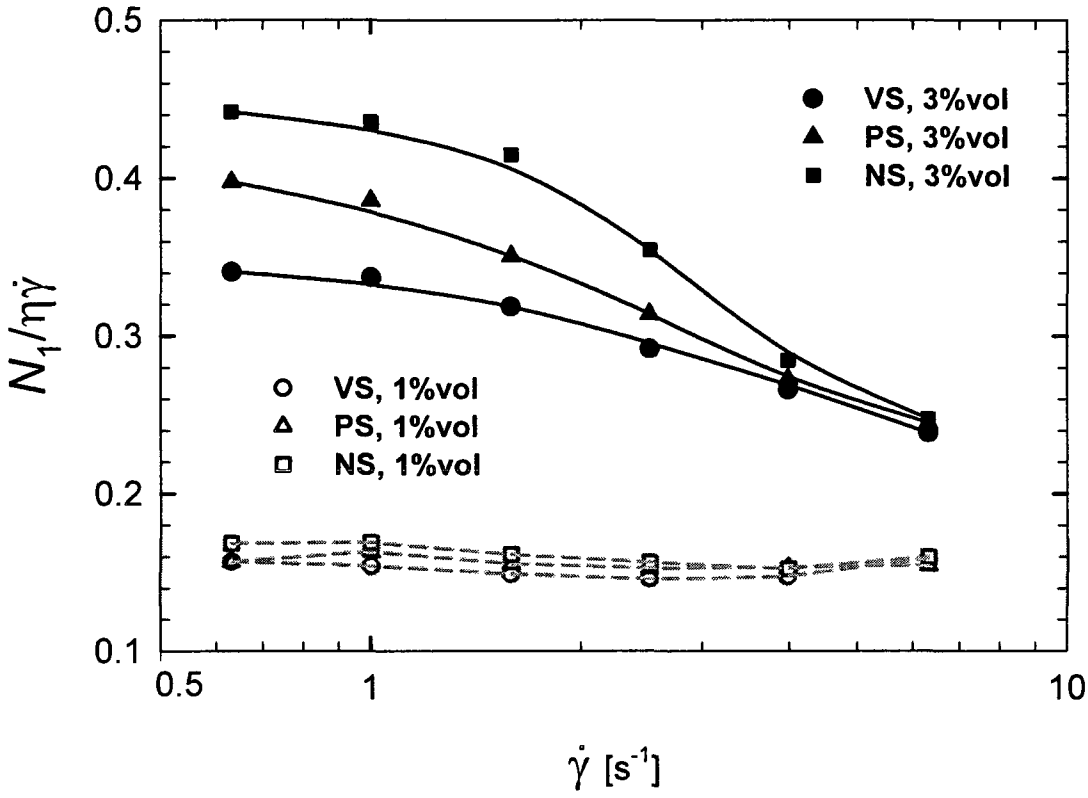

Figure 5.4 : First normal stress scaled by $\eta\dot{\gamma}$ in semi-dilute (open symbols) and semi-concentrated (filled symbols) regimes

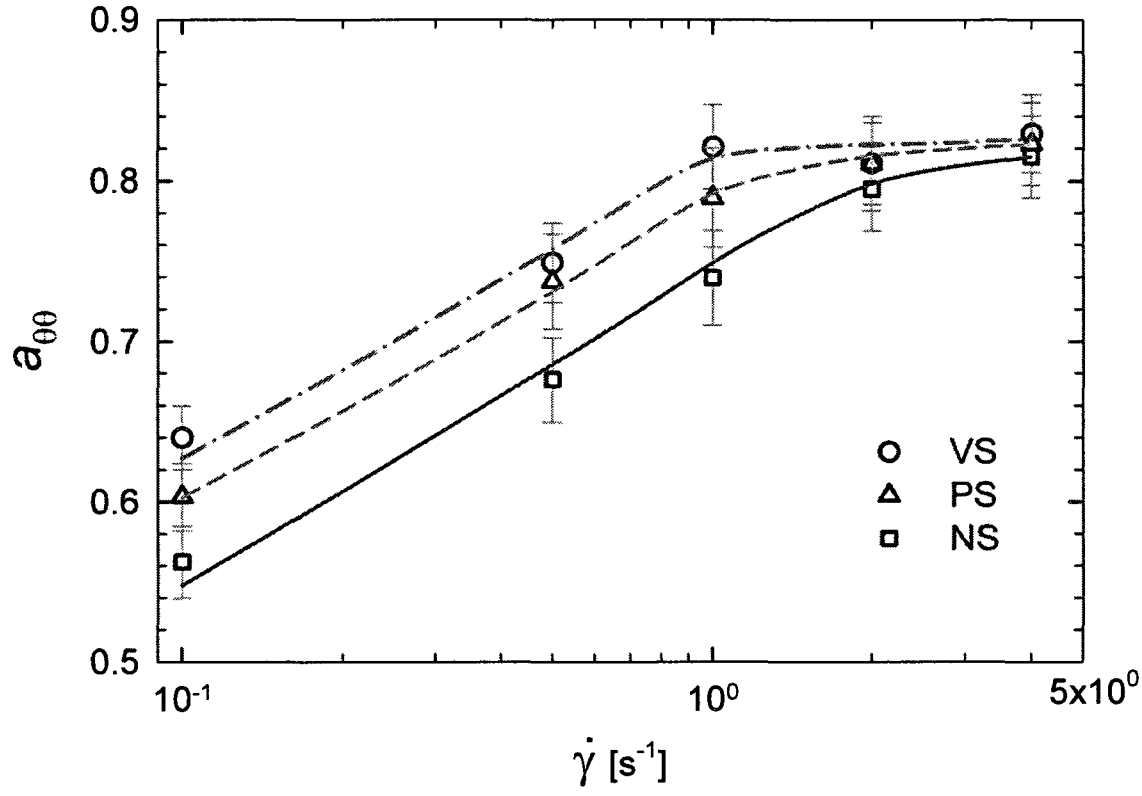

Figure 5.5 : Steady state fiber orientation in the flow direction $a_{\theta\theta}$ determined experimentally ; $\phi_f = 0.03$

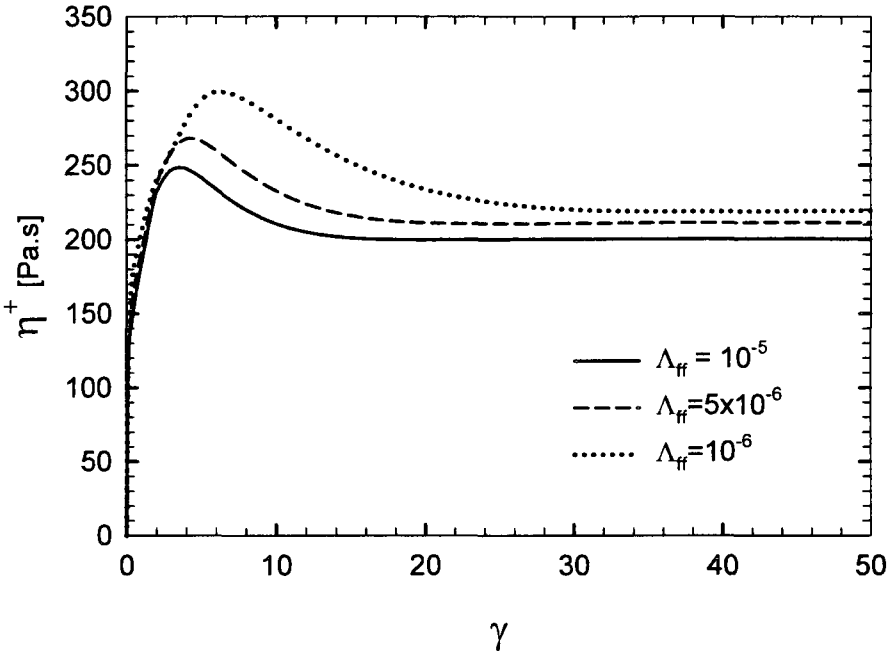

a)

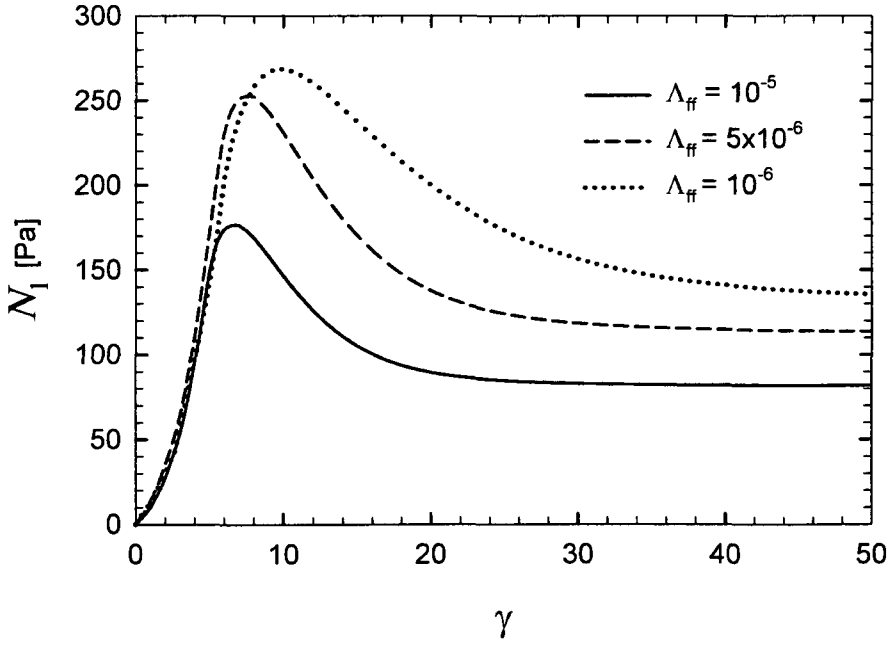

b)

Figure 5.6 : Effect of fiber mobility on the stress growth behavior of semi-flexible fiber composites, $\dot{\gamma} = 1s^{-1}$, $\phi_f = 0.03$, L/D=70, K_{flex}= 0.5 and B_{ff}= 5 (a) viscosity; (b) first normal stress difference

a)

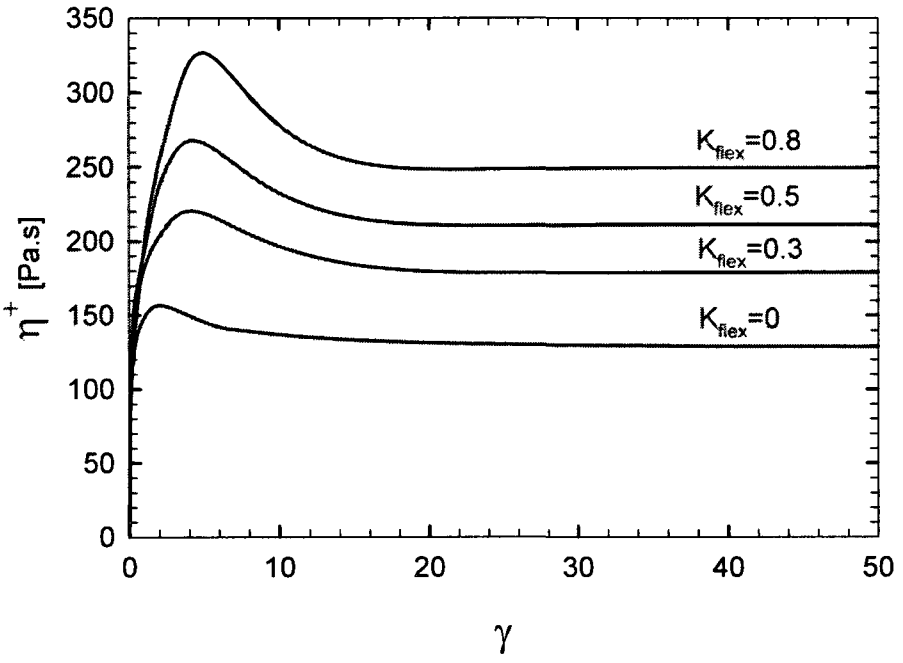

a)

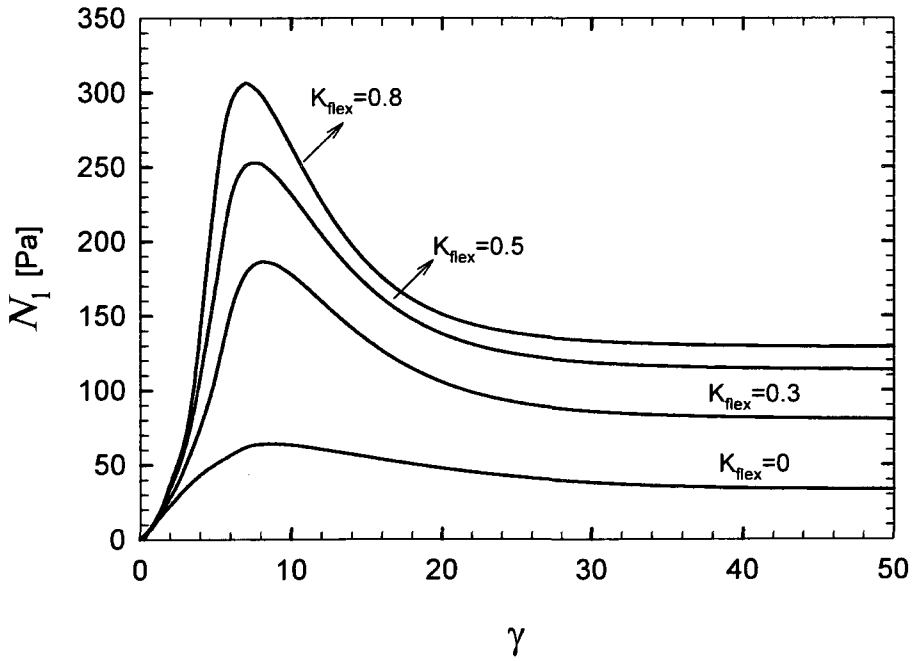

b)

Figure 5.7 : Effect of fiber flexibility on the stress growth behavior of semi-flexible fiber composites, $\dot{\gamma} = 1s^{-1}$, $\phi_f = 0.03$, L/D=70 , Λ_{ff}=5×10^{-6} and B_{ff}= 5 (a) viscosity; (b) first normal stress difference

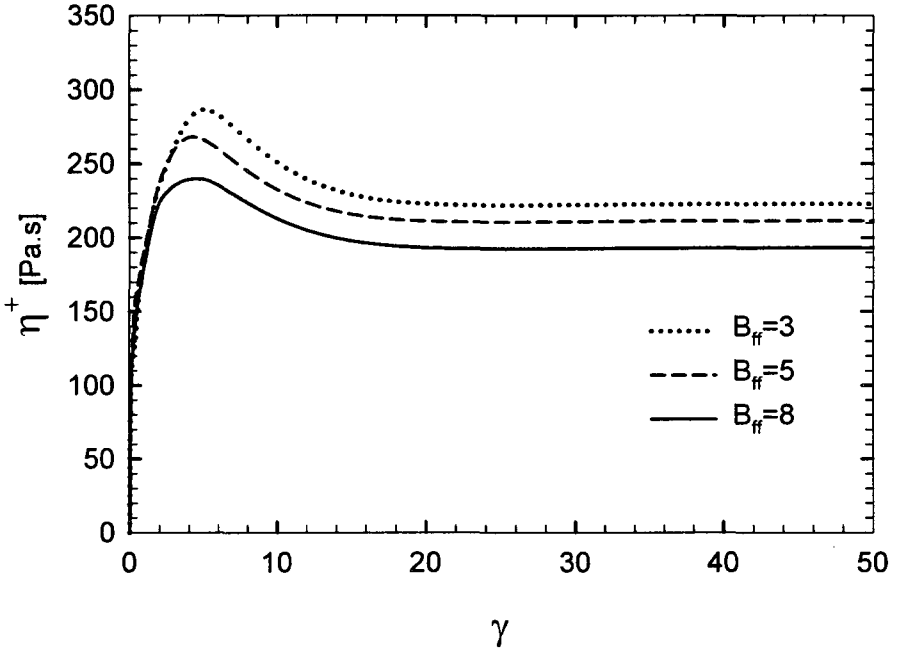

a)

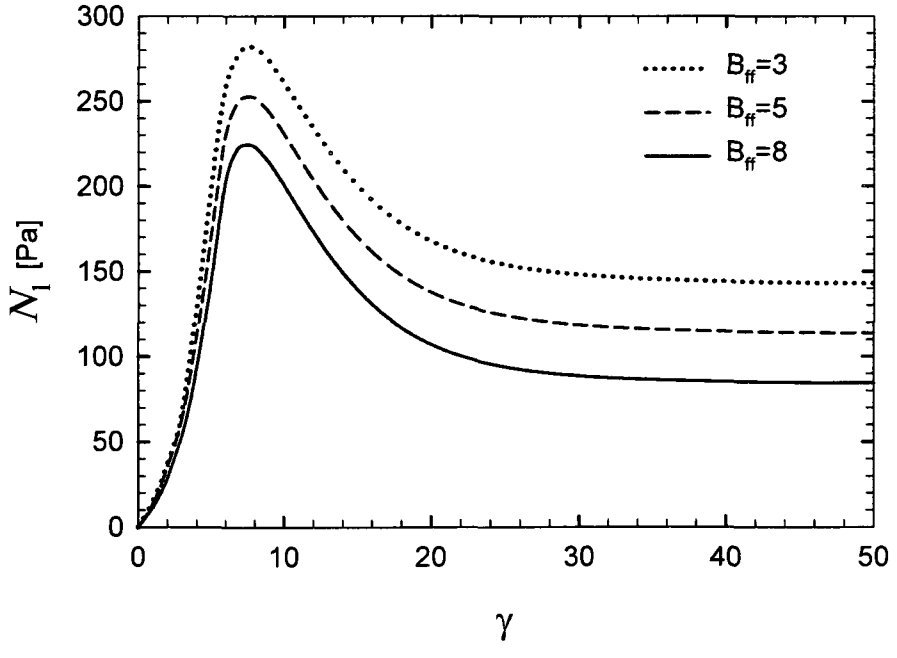

b)

Figure 5.8 : Effect of fiber-fiber interaction parameter on the stress growth behavior of semi-flexible fiber composites, $\dot{\gamma} = 1s^{-1}$, $\phi_f = 0.03$, L/D=70, Λ_{ff}=5×10^{-6} and K_{flex}= 0.5 (a) viscosity; (b) first normal stress difference

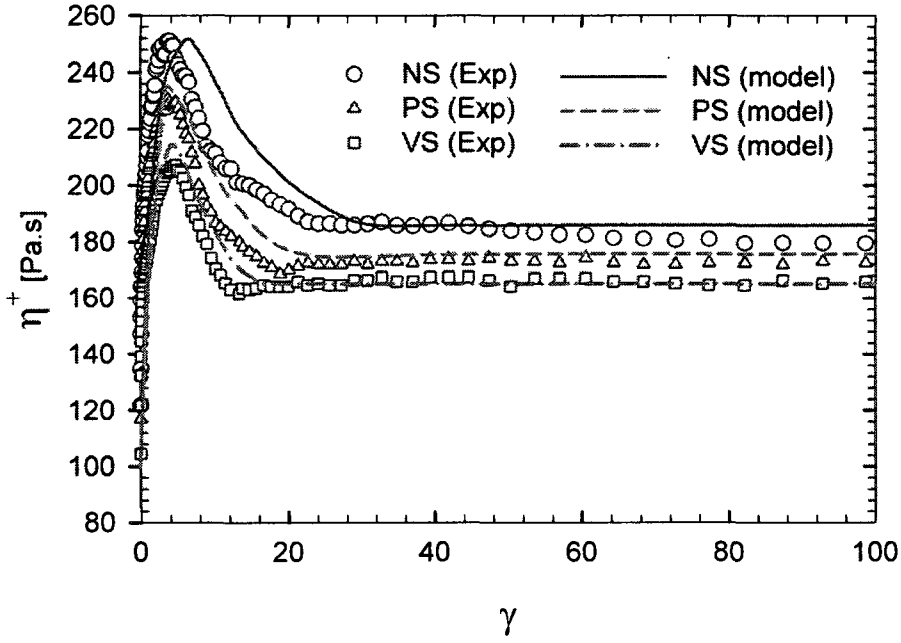

a)

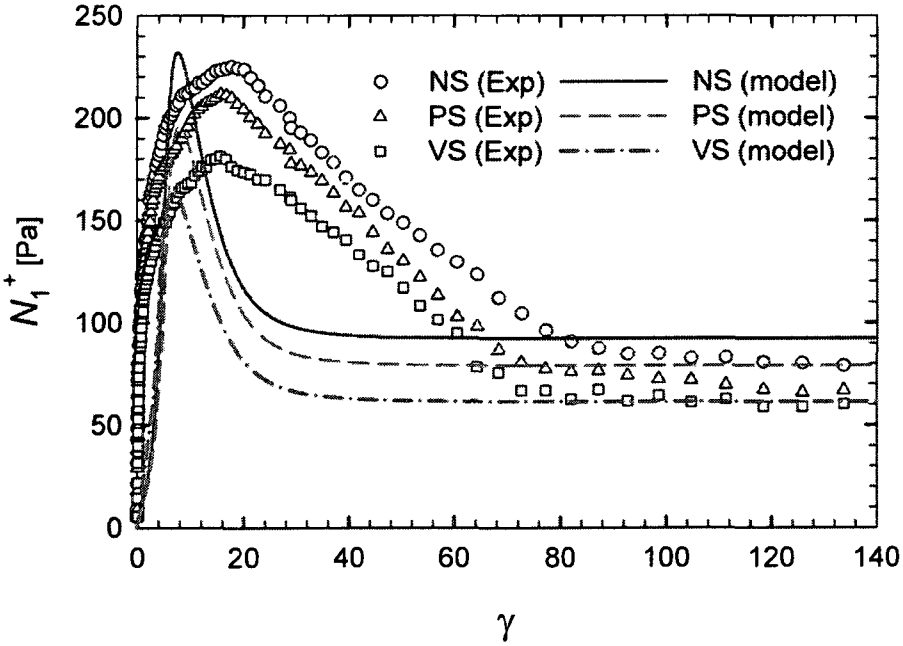

b)

Figure 5.9 : Experimental and predicted stress growth functions (a) viscosity; (b) N_1; $\dot{\gamma} = 1\ s^{-1}$ and $\phi_f = 0.03$. The lines represent the predictions of the GENERIC model (Parameters in Table 5-2)

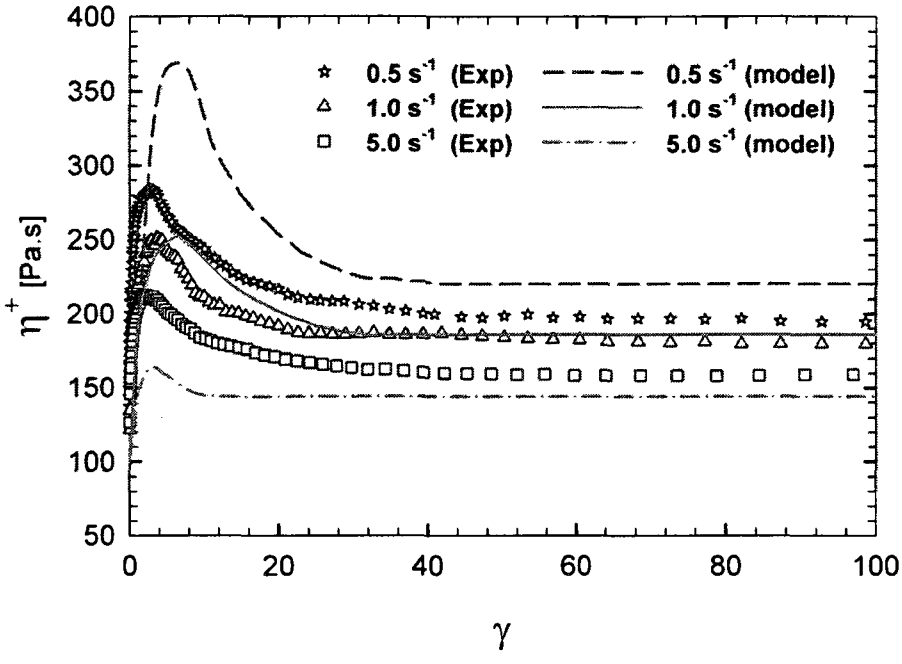

b)

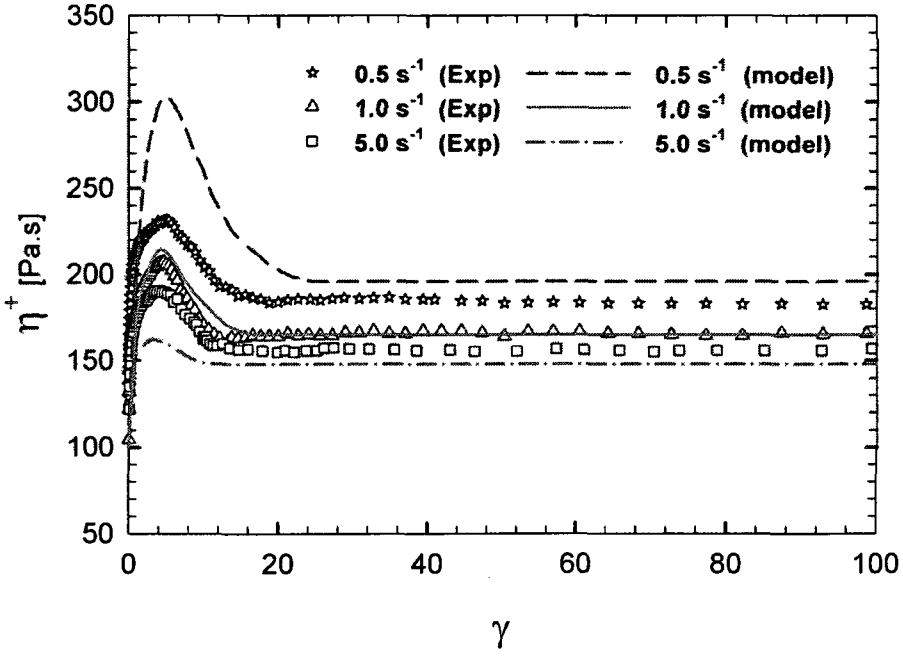

b)

Figure 5.10 : Experimental results and model predictions of the viscosity in stress growth at $\dot{\gamma}$ = 0.5 s^{-1}, 1 and 5 s^{-1}. (a) NS (most flexible), (b) VS (most rigid). $\phi_f = 0.03$ (Parameters in Table 5-2)

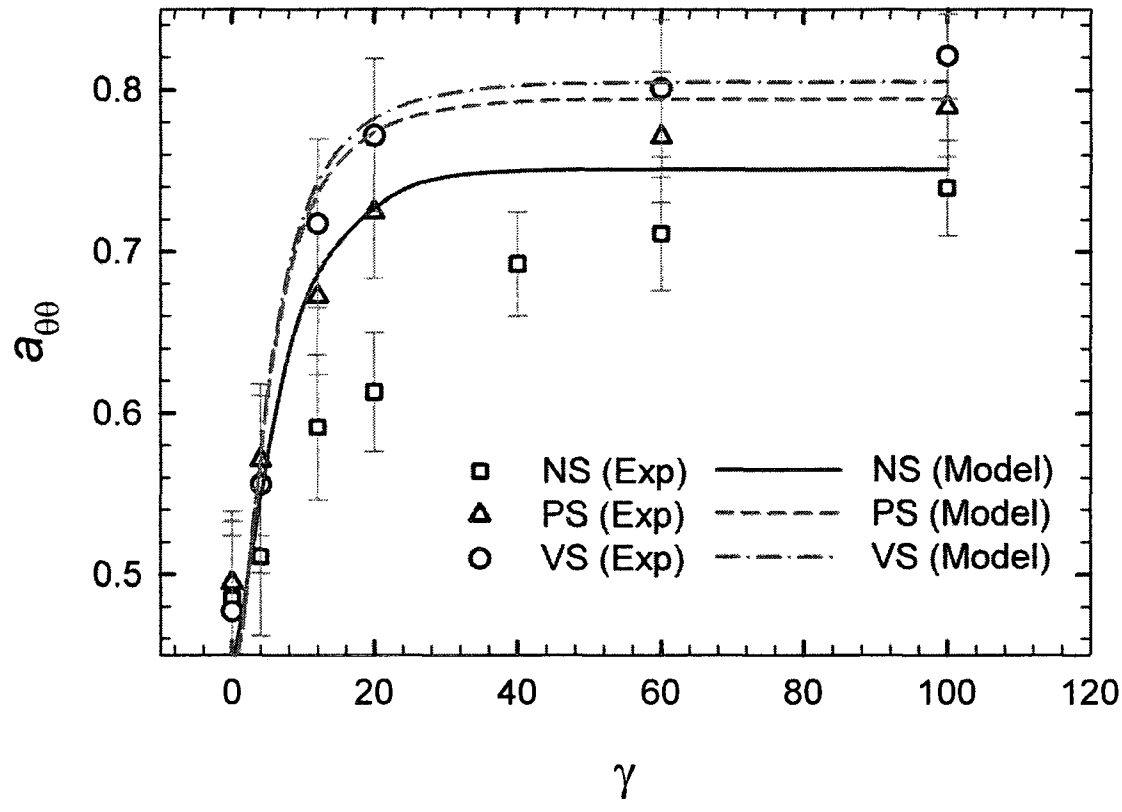

Figure 5.11 : Experimental and predicted fiber orientation represented through the $a_{\theta\theta}$ in stress growth at $\dot{\gamma} = 1\ s^{-1}$. The lines represent the GENERIC model predictions (Parameters in Table 5-2)

CHAPTER 6 - RHEOLOGY OF LDPE-BASED SEMI-FLEXIBLE FIBER SUSPENSIONS[3]

M. Keshtkar, M-C. Heuzey, P.J. Carreau

Center for Applied Research on Polymers and Composites (CREPEC),

Chemical Engineering Department, Ecole Polytechnique, PO Box 6079,

Stn Centre- Ville, Montreal, QC H3C 3A7, Canada

Abstract

Molten LDPE suspensions containing fibers of different flexibilities have been studied in simple shear flow and small (SAOS) and large amplitude oscillatory shearing (LAOS). The suspensions exhibited viscosity and normal stress overshoots in stress growth experiments, and the magnitude and width of the overshoots became larger as the fiber flexibility increased. LAOS was used to help understanding the relationship between stress growth and fiber orientation. For all composites the stress signal decreased with time in LAOS, and this behavior was more pronounced in the case of the more rigid fibers. The energy dissipated per LAOS cycle was evaluated for each composite, and these showed that more energy was dissipated as fiber flexibility increased. In addition, the dissipated energy decreased with time and this has been interpreted in terms of reduction of fiber contacts. The first normal stress difference showed a non-sinusoidal periodic response, and fast Fourier transform (FFT) analysis

[*] This paper has been submitted to Polymer Composites Journal

indicated the presence of a first harmonic corresponding to the applied frequency for the fiber-filled systems, in addition to the second harmonic observed for the neat LDPE. It resulted in asymmetrical strain-normal force Lissajou curves for the suspensions, with this asymmetry being more pronounced in the case of more rigid fibers.

Keywords: Rheology; LDPE; Shear flow; Fiber suspensions; Fiber flexibility; LAOS; Fiber orientation

6.1 Introduction

The mechanical properties of fiber reinforced composites are strongly dependent on microstructure and fiber orientation. The structure itself is highly affected by material characteristics such as fiber properties, component interactions, suspending fluid properties, but also on the imposed flow field. Understanding the relationships between rheology, suspension structure and macroscopic properties can be extremely useful in the design and optimization of processes and composite properties [1]. One aspect that may impact fiber orientation is fiber flexibility. The flexibility may vary with fiber properties such as stiffness and aspect ratio. The rheology of fiber-reinforced matrices is quite complex due to several factors like fiber-fiber, fiber-wall, fiber-matrix interactions and phenomena such as fiber breakage and migration, and many investigation have been conducted to understand the relations between rheology and the microstructure. However, among these studies very few have focused on the role of fiber flexibility.

Using a Couette geometry and fiber suspensions of various stiffness, aspect ratio, suspending fluid viscosity and applied shear rate, Forgacs and Mason [2] observed that as the stiffness decreased or aspect ratio increased – hence larger flexibility - the fibers tended to bend and not follow the orbits predicted by the Jeffery model. The fibers went instead through what has been called "flexible orbits". They also found that the critical stress to bend the fibers was:

$$\left(\dot{\gamma}\ \eta_m\right)_{crit} \cong \frac{E_b(\ln 2r - 1.75)}{2r^4} \tag{6-1}$$

where η_m is the viscosity of the suspending fluid (matrix) and E_b the bending modulus of the rod, $E_b \approx 2E_Y$, with E_Y the Young modulus of the fiber, and r is the apparent aspect ratio of the fibers, which is the ratio of fiber length to diameter.

The results of Forgacs and Mason [2] indicated that axial forces imposed by shear flow can bend fibers with low modulus or high aspect ratio, decrease the apparent aspect ratio and shorten the period of rotation. These results stress the important role of fiber flexibility on the dynamics and orientation of fiber suspensions. Recently, Keshtkar *et al.* [3] showed that by increasing fiber flexibility (reducing the fiber's Young modulus or increasing its aspect ratio) both viscosity and normal stress differences increased for suspensions of fibers in silicone oil, especially in the semi-concentrated regime.

In order to obtain information about the microstructure of suspensions, oscillatory shear flow experiments are commonly used by investigators, and more generally small amplitude oscillatory shear (SAOS). However, several contradictions between published results can be observed. From dynamic measurements of glass fibers in polypropylene, Mutel and Kamal [4] found that at a frequency of 10 rad/s the suspension properties strongly depended on strain, although the pure resin properties showed strain-independent behavior over a broad strain range. To study dynamic rheological properties, Greene and Wilkes [5] used short and long glass fibers in polycarbonate, polypropylene and nylon-66. They found that the storage and loss moduli and the complex viscosity increased with fiber volume fraction. They also observed that presence of fibers increased the viscous and elastic nature of the fiber-filled composite at low frequencies, and to a lesser extent at higher frequencies. The increase of the elastic

component was more important than the viscous one at low frequencies and less at high frequencies. Kitano *et al.* [6] showed that polyethylene-based suspensions of vinylon fibers, which are more flexible than glass fibers, exhibited a stronger dependence of rheological properties on the fiber volume fraction as compared to glass fiber suspensions. They also verified the results of Greene and Wilkes [5] about the effect of fibers on tan (δ) – ratio of *G'/G"*- at different frequencies. In contradiction with these findings, Mobuchon *et al.* [7] showed that the suspension elasticity was the same as the matrix for glass fibers suspended in polypropylene, and hence tan (δ) was independent of fiber concentration and orientation. This behavior has also been confirmed by several investigators [8-11]. Investigating the effects of time, frequency and strain amplitude, Kim and Song [12] concluded that the orientation of fibers decreased the complex viscosity η*, and as the strain amplitude increased more fibers aligned with the flow direction. Finally, by modelling the nonlinear behavior of dilute suspensions of fibers in an Oldroyd-B fluid, Harlen and Koch [13] indicated that fibers oriented in the flow direction during a cycle of oscillation.

Large amplitude oscillatory shear (LAOS) [14] provides a useful method to investigate complex fluids that exhibit microstructures that depend on the deformation history. Fourier Transform (FT) rheology is the most common method for quantifying LAOS experiments [15]. The stress response to a sinusoidal strain input can be represented as Fourier series of odd harmonics [16]. By applying a large deformation amplitude in oscillatory shear flow, the non-linear properties of polymers arise and the stress response is no longer harmonic [16, 17].

Ferec *et al.* [11] measured the shear stress and primary normal stress difference responses to large amplitude sinusoidal strain input for suspensions of glass fibers in polybutene (Newtonian matrix) and polypropylene (viscoelastic matrix). They observed that the responses were very sensitive to fiber orientation. For suspensions of the Newtonian matrix the stress amplitude grew with time, but for the non-Newtonian matrix the stress amplitude decreased. Also the stress responses for all suspensions were harmonic, whereas the normal force responses were non-harmonic.

The overall objective of this work is to investigate the effect of fiber flexibility on the rheological behavior of model fiber suspensions in a polymer melt under simple shear flow, SAOS and LAOS, to help understanding the relationship between fiber flexibility, suspensions microstructure, rheological properties and fiber orientation.

6.2 Experimental

6.2.1 Materials

Low density polyethylene (LDPE 1043N, Exxon) was used as the matrix. Fibers of polyaryl (Vectran®, $E_Y = 76$ GPa), polyvinyl alcohol (PVA, $E_Y = 26GPa$) and nylon ($E_Y = 2$GPa) were used to prepare the suspensions. An effective fiber flexibilty can be estimated from the following relationship: $1/S^{eff} = \dot{\gamma}\eta_m L^4 / E_Y I$ [1], in which $\dot{\gamma}$ is the shear rate, $I = \pi D^4 / 64$ the area moment of inertia, and L and D the fiber length and diameter, respectively. The effective stiffness, S^{eff}, characterizes the relative importance of fiber stiffness and hydrodynamic forces. As $S^{eff} \to 0$, the fibers behave like

completely flexible threads, whereas for $S^{eff} \to \infty$, the fibers become rigid and retain their equilibrium shape under flow [1]. In this work, fibers with different Young moduli were used. Since all experiments were performed at 150 °C, it is necessary to have information about the Young modulus of these fibers at this temperature. The Young moduli of nylon, PVA and Vectran fibers at 150 °C are reported in the literature and were found to be ~0.3, ~7.2-9 and 38 GPa, respectively [18-20]. For this values of Young modulos, the effive stiffness of fibers varies from 2.5×10^{-2} for the nylon fibers up to 2.0×10^{-4} for the vectran fibers at a shear rate of 0.1 s^{-1}. The nomenclature and properties of the various suspensions and the critical stress to bend the fibers at 150 °C, calculated from Equation 6.1, are listed in Table 6-1. Chopped fibers were used as received from the suppliers, and their length values, based on the manual measurement of 400 fibers using optical microscopy and image analysis, are reported in Table 6-1. The quantities L_n and L_w, number and weight average fiber lengths, respectively, can be defined as:

$$L_n = \frac{\sum_i n_i L_i}{\sum_i n_i} \tag{6-2}$$

$$L_w = \frac{\sum_i n_i L_i^2}{\sum_i n_i L_i} \tag{6-3}$$

The fibers were nearly monodisperse since the ratio L_w / L_n was close to 1, as reported in Table 1. The sedimentation times of the fibers in the molten LDPE were calculated using the following equation from Chaouche and Koch [21]:

$$t_s = 8\eta_m L / \Delta\rho g D^2 \ln(2r - 0.72) \quad (6\text{-}4)$$

The sedimentation times for the various samples are also reported in Table 6-1, and all the rheological experiments were carried out in times shorter than the reported values.

To prepare the samples required for rheometry, the LDPE was blended in an internal mixer (Brabender) with 1 wt % stabilizer (Irganox B225) in order to reduce thermal degradation and with 1 and 5 vol. % of fibers. The materials were mixed at 40 rpm at 150°C for 10 minutes under a nitrogen atmosphere. The neat LDPE also was processed at the same condition. Then disk shape samples were compression molded at 150°C. All samples were prepared following the same procedure. According to the definition of the fiber concentration regimes [22], suspensions containing 1 vol. % of fibers are in the semi-dilute regime, where, $1/r^2 << \phi_f << 1/r$, and those with 5 vol. % of fibers are in the concentrated regime, where $\phi_f > 1/r$.

6.2.2 Rheometry

The rheological measurements in simple shear and SAOS were carried out using an Anton Paar Physica rheometer (MCR 501), while the large amplitude oscillatory shear (LAOS) experiments were performed using a TA-Instruments ARES rheometer. In both cases the flow geometry used consisted of 25 mm diameter parallel plates. The strain-controlled rheometer used to perform the LAOS measurements allowed a maximum amplitude deformation of θ_{max} = 0.5 rad. For all experiments the gap, *H*, was set to 2 mm and this provided a maximum deformation of 3.13 ($\gamma_R = R\theta_{max} / H$). The ratio of

gap-to-fiber length was therefore 2:1. Bibbo [23] showed that if such a ratio is used, boundary effects are insignificant.

This ARES rheometer was equipped with a standard 2KFRTN1 force transducer, which can measure a maximum torque of 200 mN·m and a maximal normal force of 20 N (as specified by the manufacturer). The raw data, collected from the signal panel, were digitized using a 12-bit 16 channel USB-based Analog to Digital Converter (ADC) with a 100 ksamples/s rate (National Instruments DAQ-Pad 6020E). This ADC card was plugged into the ARES computer that contains a home-written LabView routine to acquire the raw data. Three channels were used to sample simultaneously the strain, the torque and the normal force. For all tests, the scan rate was fixed to 10 000 data per second and then averages for each 1 000 data were used to generate 10 average values per second. To reduce the mechanical and electronic noises, the rheometer was placed on a stable environmental table and the connections made with double shielded BNC cables. The torque, T, and normal force, F, could be measured as functions of the shear rate at the rim, $\dot{\gamma}_R$, using a force rebalanced transducer. These data were used to calculate the viscosity and first normal stress difference assuming that the second normal stress difference was negligible (Weissenberg's hypothesis) from the following expressions [24]:

$$\sigma_{z\theta} = \eta_m(\dot{\gamma}_R)\dot{\gamma}_R = \frac{T}{2\pi R^3}\left[3 + \frac{d\ln\left(\frac{T}{2\pi R^3}\right)}{d\ln\dot{\gamma}_R}\right] \tag{6-5}$$

$$N_1 = -(\sigma_{11} - \sigma_{22}) = \frac{2F}{\pi R^2}\left(1 + \frac{1}{2}\frac{d\ln F}{d\ln \dot{\gamma}_R}\right) \tag{6-6}$$

The derivatives in Eqs. (5) and (6) were obtained by plotting $\ln T / 2\pi R^3$ versus $\ln \dot{\gamma}_R$ and $\ln F$ versus $\ln \dot{\gamma}_R$, respectively, for the various suspensions. These expressions were developed for steady shear flow, while no analytical solution exits for large amplitude oscillatory shear flow. Hence Eqs. (5) and (6) were used as approximations in the case of LAOS [11].

For the LAOS experiments a series of precautions were taken. First we tested the system for a completely Newtonian fluid. High viscosity silicone oil, polydimethylsiloxane (Clearco Products) with a density of 0.974 g/mL and a nominal viscosity of 103 ± 2 Pa.s at 20 °C was selected for this experiment. The steady-state viscosity, η, and complex viscosity, η^*, of the silicone oil were measured, and both were equal and independent of the shear rate or frequency used in the experimental range investigated. The behavior was therefore Newtonian and it was also confirmed by the absence of significant normal stress differences. A LAOS test was performed at 20 °C under a strain deformation of 5 and a frequency of 0.05 Hz for 2400 s, and we examined the Lissajous curves ($\sigma_{z\theta}$ versus γ_R) at different cycles of oscillation. When the stress-strain loops are plotted an ellipse should be obtained if the signal response is harmonic. The Lissajou curve of the silicone oil was completely elliptical and independent of time, with a fundamental shift angle of 90° that represents a true Newtonian behavior.

The possible effect of viscous dissipation that can cause a temperature increase during the experiments, and result in sample degradation was verified for the LDPE matrix. A LAOS test was performed at 150 °C under a strain deformation of 3 and a frequency of 0.005 Hz for 1800 s, then followed by a rest time of 600 s, and again the same LAOS test was conducted. The Lissajous curves of $\sigma_{z\theta}$ and N_1 versus γ_R at the 5th cycle of oscillation for both LAOS tests were examined and they completely overlaid each other, showing no noticeable change in the shear stress or primary normal stress difference responses, therefore indicating that the effect of viscous dissipation in these tests was not important.

Finally the possible impact of fluid inertia was investigated. The complex Reynolds number Re^* is used to evaluate the fluid inertia in rotational shear flow [25]:

$$\mathrm{Re}^* = 2\pi\rho f H^2 / \eta_m^* \tag{6-7}$$

where ρ is the fluid density, f is the applied frequency and η_m^* the complex viscosity of the matrix. The largest calculated value of Re^* was for the LDPE-VEC suspension (Vectran fibers) and was about 3.4×10^{-9}, which is much lower than 1. Therefore, all the suspensions were considered as inertialess in this work.

6.3 RESULTS AND DISCUSSION

6.3.1 Steady state rheological behavior

Figure 6.1 compares the steady shear viscosity (Fig. 6.1a) and the first normal stress difference (Fig. 6.1b) as a function of shear rate for the various fiber suspensions in

LDPE (5 vol. %). In Fig. 6.1a it is observed that the addition of fibers to LDPE increases its viscosity. The viscosity behavior of the composites is similar to that of the matrix, but the increase is more important at low shear rates. For suspensions in the semi-dilute regime ($\phi_f = 0.01$), the viscosity is almost independent of fiber flexibility (not shown here). On the other hand, the suspensions viscosity increases with fiber flexibility in the concentrated regime and this increase is also more pronounced at low shear rates. The results are in good agreement with results of Mobuchon *et al.*, [7] who studied the rheological behavior of neat polypropylene and composites of polypropylene with 10 wt% (semi-dilute) and 30 wt% (concentrated) glass fibers. Djalili-Moghadam and Toll [26] have hypothesized that some kind of structures may be formed at low shear rate. Chaouche and Koch [21] suggested that these structures, especially in concentrated fiber suspensions, may result from inter-particle adhesive forces. On the other hand, Soszynksi and Kerekes [27,28] interpreted floc formation by the "elastic fiber interlocking" mechanism, in which fibers become locked and form a network due to their elasticity. Independently of the exact origin for floc formation, as the shear rate increases these structures can be destroyed and it leads to a shear-thinning behavior and decreasing viscosity. Our results suggest that as fiber flexibility increases a stronger network is formed at low shear rate, resulting in an enhanced viscosity. This may be due to fiber bending in the case of the flexible fibers, as opposed to straight rigid fibers. Switzer and Klingenberg [1], who have used particle level simulations, showed that relatively small deviations from a perfectly straight shape could result in large increases of the suspensions viscosity. As shown in Table 6-1, as the fiber stiffness decreases, the

critical stress needed for fiber bending decreases and the probability of finding curved fiber shapes increases in the case of the nylon fibers. Hence fiber bending can occur at very low shear rates and the bending could lead to enhanced properties.

Fig. (6.1b) shows that the addition of fibers results in a significant increase of the normal forces under shear flow. The normal forces also increase with fiber content. At low fiber concentration ($\phi_f = 0.01$) the normal forces are independent of fiber flexibility (not shown here) but at high fiber content ($\phi_f = 0.05$) and as the fiber Young modulus gets smaller, the first normal stress difference increases. The enhancement of normal stresses for fibers suspended in a viscoelastic fluid is believed to be due to fiber-fiber interactions [7,29]. As for viscosity results we can conclude that the role of fiber-fiber interactions is enhanced for the most flexible fibers.

Rajabian *et al.* [30], using a mesoscopic model, and Switzer and Klingenberger [1], using a particle level simulation, - two quite different approaches - showed that the first normal stress difference increased as fiber flexibility increased, in agreement with our experimental findings.

6.3.2 Linear viscoelastic properties

Figure 6.2 reports the complex viscosity as a function of deformation at different frequencies for composites with $\phi_f = 0.05$. The reinforced systems exhibit a nonlinear viscoelastic behavior down to very low strain amplitudes. At higher frequencies, the shear-thinning behavior is more pronounced and η^* is found to be a strong function of the deformation amplitude even at small strain. According to Hyun *et al.* [31] these suspensions are of type I (strain-thinning). This behavior is not unusual since fiber orientation, which influences rheological properties, is strongly affected by strain and high strain tends to align fibers in the flow direction [4]. Also the decrease of the complex viscosity is much faster in the nonlinear zone for the rigid fibers compared to the flexible fibers, and this means that the rigid fibers tend to be aligned in the flow direction more easily than flexible fibers.

For the small amplitude oscillatory frequency sweep tests, a strain amplitude of 0.05 was used for the neat LDPE and the composites of $\phi_f = 0.01$ whereas a lower strain amplitude of 0.005 was used for the composites with $\phi_f = 0.05$.

Figure 6.3 compares the complex viscosity, η^*, and the dynamic storage modulus, G', of the neat LDPE and the concentrated suspensions. The effect of pre-shearing on the linear viscoelastic properties is also shown in this figure. We note that the behavior of η^* (Fig. 6.3a) and G' (Fig. 6.3b) is typical of homogeneous polymer melts. The properties of the semi-dilute composites ($\phi_f = 0.01$) are very close to those of the neat polymer (not

shown here), but significant enhancements of both dynamic properties are observed for the concentrated fiber suspension ($\phi_f = 0.05$). The increases of η^* and G' are independent of frequency, except for the nylon fiber suspensions in the concentrated regime and without pre-shearing. Also in the semi-dilute regime the fiber flexibility does not influence the suspension dynamic properties, but in the concentrated regime, the suspensions prepared with nylon fibers (the most flexible) show a huge enhancement of the dynamic properties as compared to the suspensions of rigid fibers (Vectran fibers).

Stress-growth experiments suggest that fibers reorient themselves from their initial orientation state to align themselves in the flow direction [3, 8, 10, 29, and 32]. The suspensions were pre-sheared at $\dot{\gamma} = 0.1 s^{-1}$ until a steady state was reached, followed by a frequency sweep. As shown in Figures 6.3a &b both the complex viscosity and the storage modulus decrease upon the application of pre-shearing, but again the properties are enhanced with increasing fiber flexibility. The effect of pre-shearing on the dynamic properties is slightly more pronounced for the rigid fibers and this could be due to a more efficient orientation of the rigid fibers in the flow direction from pre-shearing, as compared to the flexible fibers.

Finally, the out-of-phase angle is shown in Figure 6.4. For rigid fibers the phase angle is independent of fiber content and pre-shearing. However, for nylon fibers and the non pre-sheared sample the phase angle is lower than that of the matrix, which means a larger elasticity, in agreement with the finding of Greene and Wilkes [5] for long glass fibers of length of 3 to 6mm, which could be bent or broken. After pre-shearing the phase angle becomes almost equal to the matrix phase angle at all frequencies. The

independency of the phase angle with fiber content indicates that the elasticity of the suspensions is that of the matrix, and that the characteristic elastic time of the composites, defined by [24]:

$$\lambda = \frac{G'}{G''\omega} \tag{6-8}$$

is independent of fiber content and is equal to that of the matrix, confirming the findings of Hashemi *et al.* [33] and Mobuchon *et al.* [7] for different composites.

6.3.3 Transient flow behavior

Figure 6.5 compares the stress growth behavior of the neat LDPE and suspensions with different fiber flexibilities in experiments carried out at 0.1 s^{-1} in the clockwise and counter-clockwise directions. We note in Figure 6.5a that the transient viscosity does not exhibit an overshoot for the unfilled LDPE, whereas a large overshoot is observed for the fiber-filled LDPE suspensions. The peak for the overshoot occurs at a strain between 1 and 3, in agreement with findings of Sepehr *et al.* [29] for suspensions of glass fibers in polypropylene at the same shear rate. Also as the fiber Young modulus decreases, the amplitude of the peak increases and the suspension reaches steady state at a larger strain. However, if we normalize the transient viscosity data with the steady state value, the reduced overshoot magnitude is the same for all suspensions (results not shown). These results are in agreement with the predictions of the model of Rajabian *et al.* [30].

Figure 6.5b presents the transient viscosity of the neat LDPE and the concentrated composites in reverse flow. In reverse stress growth experiments carried out

immediately after the initial forward flow, in contrast to pure LDPE, the suspensions exhibit first a plateau and then show a delayed overshoot. As the fiber flexibility increases, the deformation at which the first transition plateau ends and the overshoot starts is seen to decrease. Also, by increasing fiber flexibility, the magnitude of the stress overshoot increases. Sepehr *et al.* [29] explained the overshoot in the reverse direction by a tilting over of the fibers in the new flow direction, forming a new aligned fiber structure. Our results suggest that this phenomena occurs at lower deformation for the more flexible fiber suspensions and this could be attributed to less orientation of the more flexible fibers with flow direction in the first forward stress growth experiment.

The corresponding transient results for the normal stress differences are presented in Figure 6.6 (Fig. 6.6a forward, 6.6b reversed). For the unfilled LDPE, N_1 increases monotonically to reach a plateau. A very large overshoot in N_1 is observed for the LDPE reinforced with various fibers. The magnitude of the normal stress overshoot is much larger than the viscosity overshoot, and the peak is somewhat delayed. Also as flexibility increases, the magnitude of the overshoot increases in agreement with the predictions of the model of Rajabian *et al.* [30]. As mentioned previously, the presence of peaks in stress growth experiments for fiber filled polymers is attributed to fiber alignment in the flow direction [10]. Our results suggest that the orientation of the more flexible fibers with the flow direction involves more interactions with neighbouring fibers, as compared to the more rigid fibers. In reverse flow (Fig. 6.6b) the behavior of N_1 is about the same as for the forward flow for the neat LDPE. However for the fiber-filled LDPE, N_1 goes to negative values before increasing and showing a small overshoot and finally

reaching a plateau. The same behavior has been observed by Sepehr *et al.* [29] for suspensions of glass fibers in polypropylene. The strain at which negative values of the normal forces are seen decreases as fiber flexibility increased. For flexible fibers (nylon fibers) N_1 shows a negative value at the beginning of the flow reversal, but it reaches positive values very rapidly. As for rigid fibers (Vectran fibers), N_1 reaches positive values at a strain of ~ 35. The negative values are attributed to non-affine deformation or a liquid crystalline structure when the flow field is reversed. Nevertheless it is difficult to explain the difference between the behavior of the flexible and the rigid fibers.

6.3.4 Large Amplitude Oscillatory Shearing experiments

6.3.4.1 Stress-Strain Loops

The shear stress as a function of strain for LDPE and LDPE filled by Vectran and nylon fibers in the concentrated regime are depicted in Figure 6.7 at a frequency of 0.005 Hz and a maximum deformation of 3. For the neat LDPE the Lissajous curves (Fig. 6.7a) are perfectly overlapping ellipses up to the 15^{th} cycle. This shows that the matrix is thermally stable. However, in the case of LDPE filled by Vectran fibers and nylon fibers the stress amplitude decreases with time as shown by the arrow in Figures 6.7b and c, although the stress response retains an elliptical shape. The stress drop with the number of cycles is attributed to fiber orientation [11]. The same behavior was predicted by the theory of Harlen and Koch [13] and also by the simulations of Ferec *et al.* [11] based on the Folgar-Tucker-Lipscomb (FTL) model. Hereafter we compare further the effect of fiber flexibility on the LAOS results. Figure 6.8 compares the shear stress as a function

of strain for the neat LDPE and various LDPE suspensions for the 2nd cycle of oscillation. It is observed that as the flexibility increases, the stress amplitude increases, which is in agreement with our previous observations. Also as the flexibility increases the fundamental shift angle decreases (Fig. 6.9). The fundamental angle is defined as lag between the stress and deformation signals [16]:

$$\delta_1 = \delta_\sigma(f) - \delta_{\gamma_R} \tag{6-9}$$

Figure 6.9 compares the fundamental shift angle δ_1 of the neat LDPE and for fiber-filled LDPE. As the strain increases the fundamental shift angle of LDPE and the composites increases, and all of them tend towards a somehow Newtonian behavior, similarly as observed by Ferec *et al.* [11] for polypropylene containing glass fibers. But in contrast to the findings of Ferec *et al.* [11] adding fibers decreases the fundamental shift angle and also the fundamental shift angle decreases as fiber flexibility increases. The difference may be due to the average distance between fibers in these two investigations. Here nL^2D is 4.5 which is more than the critical value of $nL^2D = 4$ introduced by Flory [34]; hence, our suspensions are in the concentrated regime where the number of contacts between fibers are very high. In Ferec *et al.* [11] $nL^2D = 2.9$, which is classified as in the semi-concentrated regime [35].

The viscous dissipated energy per cycle and per unit volume (E_σ) as a function of strain has been determined from the Lissajous figures. Ferec *et al.* [11] derived the expression for the energy dissipated per unit volume for one cycle of oscillation:

$$E_\sigma = \frac{1}{2}\int_0^{T_{OSC}} \eta(a_4,t)\dot{\gamma}(t):\dot{\gamma}(t)dt = \frac{1}{2}\langle\eta(a_4)\rangle\int_0^{T_{OSC}} 2\omega^2\gamma_R^2\cos^2(\omega t)dt \qquad (6\text{-}10)$$
$$= 4\pi^2 f^2\gamma_R^2\langle\eta(a_4)\rangle\left[\frac{1}{2f}\right] = 2\pi^2\langle\eta(a_4)\rangle f\gamma_R^2$$

where $\langle\eta(a_4)\rangle$ is the viscosity of the suspension for a pre-averaged fiber orientation during a period of oscillation, T_{OSC}, and γ_R is the maximum deformation applied. Figure 6.10 presents the energy dissipated per unit volume in the 2nd cycle versus strain amplitude at a frequency of 0.005 Hz. It is observed that by adding fibers the energy lost is increased and this increase is more pronounced as fiber flexibility increases. The exponent for the neat LDPE is 1.93 (close to 2) and in agreement with Equation 6-9, but adding fibers causes the exponent to decrease to ~1.82, independent of fiber type for the second cycle.

As previously shown in Figure 6.7, the area of the Lissajous curves decreases with time for the fiber-filled LDPE. We have normalized the energy dissipated in different LAOS cycles from the 2nd to the 15th cycle by the energy dissipated during the 2nd cycle. The results are depicted in Figure 6.11 for suspensions in the semi-dilute regime ($\phi_f = 0.01$) and the concentrated regime ($\phi_f = 0.05$). It is observed that in the semi-dilute regime the dissipated energy does not change significantly with time, but in the concentrated regime it decreases considerably due to a loss of mechanical contacts occur between fibers. Hence, the reduction of the dissipated energy with time could be explained by fiber orientation under LAOS and a reduction of contacts between fibers. The much lower energy reduction in the semi-dilute regime is supporting this idea. It is also

observed that as fiber flexibility increases, the percentage of reduction of the dissipated energy is less as compared to more rigid fibers such as Vectran. This is an additional indication of a more intensive orientation for rigid fibers with the flow direction, as compared to the more flexible fibers, and to a more extensive contact reduction. These results are in agreement with our previous findings in stress growth experiments.

Ewoldt *et al.* [17] introduced a set of elastic moduli to characterize the nonlinear behavior of materials under LAOS:

$$G'_M \equiv \left.\frac{d\sigma}{d\gamma}\right|_{\gamma=0} \tag{6-11}$$

$$G'_L \equiv \left.\frac{\sigma}{\gamma}\right|_{\gamma=\pm\gamma_0} \tag{6-12}$$

where G'_M is the minimum-strain modulus or tangent modulus at $\gamma = 0$ and G'_L is the large-strain modulus or secant modulus evaluated at the maximum imposed strain. In the case that stress-strain Lissajous curves are completely elliptical, and this is the case in our experiments, $G'_M = G'_L = G'(\omega)$ [17].

The values of G'_M and G'_L were calculated from Equations (6-10) and (6-11) for various LAOS cycles for the neat LDPE and fiber-filled LDPE and were normalized by G' in the 2nd cycle of LAOS, and are presented in Figure 6.12. Results from both equations are nearly the same, due to the regular elliptical shape of stress-strain curve (Fig. 6.8). For the neat LDPE the variation of G' with time is not considerable, while for LDPE-VEC this value decreases considerably. Also for LDPE reinforced by flexible fibers, the reduction is not as important. It means that in the case of the flexible fibers,

the elasticity of the composites does not change extensively with time, as compared to the composites reinforced with rigid fibers. This could be again an indication of a reduction of fiber contacts due to the LAOS flow.

6.3.4.2 Normal force-strain loops

Figure 6.13 presents the normal stress-strain loops for the neat LDPE at a frequency of 0.005 Hz and a maximum strain of 3. The LDPE matrix (Fig. 6.13a) exhibits an almost symmetrical shape loop due to its response at twice the applied frequency. The area of the normal stress-strain loop is close to zero (due to the symmetry with the ordinate axis) indicating a pure elastic response. Moreover, the normal stress difference depicts a non zero and positive offset like Lodge [36] rubber-like liquids [11]. Figures 6.13b and 6.13c report the normal stress-strain loop for LDPE filled with Vectran and nylon fibers, respectively, for the same conditions as for the neat LDPE. By adding fibers an asymmetry in the loops is observed and the normal stress also shows negative values. A behavior similar to that of the Vectran filled-LDPE has been observed by Ferec *et al.* [11] for glass fiber-reinforced polypropylene. They attributed the asymmetrical shape of the loops to a partially pre-oriented fiber structure, owing to the procedure of sample preparation by compression molding (the same procedure was used in this work). The authors confirmed this hypothesis by pre-shearing the sample in the clockwise and counter-clockwise directions before performing the LAOS tests. Pre-shearing, causing fiber orientation in the flow direction, resulted in a completely asymmetrical shape of the normal stress-strain loops, while the shape of the shear stress-strain loops remained

elliptic. This test confirmed the role of fiber orientation in the asymmetry of the normal stress-strain loops [11]. The normal stress amplitude decrease seen in Figure 6.13b is most probably due once again to fiber orientation effects. Moreover, because the normal stress-strain loops are not symmetrical, the dissipated energy is not zero anymore. Consequently, the non-symmetrical fiber structure induces a "normal" dissipative energy. Negative values for the normal stress differences are found when the flow is reversed. It is consistent with our results in stress growth experiments, which showed negative values of the normal stress difference in flow reversal. The asymmetry in the normal stress-strain loops are less for the nylon-filled LDPE, as depicted in Figure 6.13c. This again can somehow be attributed to less fiber orientation in the case of the flexible fibers.

The FFT performed during cycles 2 to 15 are presented in Figure 6.14. The results show that the normal stress signal for LDPE oscillates at two times the applied frequency for strain (i.e. $2 \times 0.005 = 0.01$ Hz). Also a small peak is observable at a frequency of 0.005 Hz. For LDPE filled with Vectran, however, the first and the second harmonics are the predominant frequency responses, justifying the dissymmetry in the shape of the normal stress-strain loops. The appearance of the first harmonic is attributed to time-dependent memory effects induced by the orientation of the fibers [11] (the material response during the first half-cycle is different than the one in the second half-cycle). The FFT results for LDPE filled with nylon fibers show that the first and the second harmonics appear again in the frequency response, but the magnitude of the first harmonic is much smaller than observed for the Vectran fiber suspensions. This explains the less

asymmetry of the normal stress-strain loops for LDPE reinforced with nylon as compared to Vectran-filled LDPE. These results are again indicative of less fiber orientation for the more flexible fibers as compared to the rigid ones.

6.4 Conclusions

The rheological behavior of suspensions in molten LDPE using fibers with different flexibilities has been investigated in steady and transient shear, SAOS and LAOS flows using a parallel disk geometry. Based on the definition of the effective stiffness, which characterizes the relative importance of fiber stiffness to hydrodynamic forces acting on the fibers, fibers with different Young modulus values were selected to study the effect of fiber flexibility on the rheological behavior of suspensions.

Both viscosity and first normal stress difference increased with larger fiber flexibility, and the increases were more pronounced in the concentrated regime. The increase of the rheological properties has been attributed to additional fiber-fiber interactions for more flexible fibers.

Stress growth experiments were carried out in the forward and reverse directions. Viscosity and normal stress overshoots were observed for fiber-reinforced composites and attributed to fiber orientation under flow. Both the overshoot magnitude and width augmented with increasing fiber flexibility. A delayed viscosity overshoot was observed each time the flow direction was reversed, and this was explained by fiber tumbling. For flexible fibers the reverse overshoot occurred at lower deformations. This was attributed to less fiber orientation in the flow direction during the forward flow experiments.

Large normal stress overshoots were also observed for these suspensions. In addition, when the flow was reversed the primary normal stress differences took initially negative values before depicting a small positive overshoot and decreasing to a steady-state value. The width of the negative undershoots decreased as fiber flexibility increased.

SAOS tests revealed that the behavior of the complex viscosity and the storage modulus of the fiber suspensions was typical of homogeneous polymer melts. The elasticity of the matrix was not changed by the presence of the fibers if they were well pre-sheared. The pre-shearing of the samples caused a larger reduction of the dynamic properties of rigid fibers as compared to flexible ones. This was attributed again to less orientation of the flexible fibers during pre-shearing.

Finally, the behavior of the LDPE suspensions was investigated using LAOS experiments. The stress amplitude of the composites decreased with time, and this behaviour was attributed to fiber orientation and a loss of mechanical contacts between fibers. By increasing the deformation amplitude, the fundamental shift angle increased and a somehow Newtonian behavior was observed, but the fundamental shift angle was lower for the composites as compared to that of the neat matrix. The calculated viscous dissipation energy was seen to increase with fiber flexibility. It also decreased with time and the reduction was more pronounced for the more rigid fibers. The reduction of the dissipated energy was attributed to a reduction of fiber contacts, and this was confirmed by a much lower reduction of the dissipated energy in the case of semi-dilute suspensions, in which contacts between fibers are not important. It was also shown that

flexible fibers undergo a less significant reduction of fiber contacts during LAOS as compared to rigid ones.

6.5 Acknowledgements

The authors would like to acknowledge financial support from the Natural Sciences and Engineering Research Council of Canada (NSERC-CIAM program). We also wish to thank Dr. Thomas Griebel (from SwissFlock Inc.) for providing the nylon fibers, and Dr. Takashi Takayama (from Kuraray Co., Ltd.) for the Vectran® and PVA (Kuralon®) fibers.

6.6 References

1. L. H. Switzer III, L.H. and D.J. Klingenberg, *J. Rheol.*, **47 (3),** 759 (2003).

2. O. L. Forgacs, and S. G., Mason, *J. Colloid Interface Sci.,* **14,** 457 (1959).

3. M. Keshtkar, M.C. Heuzey, and P.J. Carreau, *J. Rheol.,* **53 (3),** (2009).

4. A. T. Mutel, and M. R. Kamal, *Polym. Compos.,* **7,** 283 (1986).

5. J. P. Greene, and J. P. Wilkes, *Polym. Engi. Sci.*, **35** 1670 (1995).

6. T. Kitano, T. Kataoka, and Y. Nagatsuka, *Rheol. Acta,* **23(4)**, 408 (1984)

7. C. Mobuchon, P. J. Carreau, M. C. Heuzey, M. Sepehr, and G. Ausias, *Polym. Compos.,* **26(3)**, 247 (2005)

8. H. M. Laun, *Colloid Polym. Sci.,* **262**, 257 (1984)

9. M. A. Zirnsak, D. U. Hur, and D. V. Boger, *J. Non-Newtonian Fluid Mech.,* **54**, 153 (1994)

10. M. Sepehr, P. J. Carreau, M. Moan, and G. Ausias, *J. Rheol.,* **48(5)**, 1023 (2004)

11. J. Férec, M. C. Heuzey, G. Ausias, and P. J. Carreau, *J. Non-Newtonian Fluid Mech.,* **151 (1-3),** 89 (2008).

12. J. K. Kim, and J. H. Song, *J. Rheol.*, **41,** 1061 (1997).

13. O. G. Harlen, and D. L. Koch, *J. Non-Newtonian Fluid Mech.,* **73,** 81 (1997).

14. J. M. Dealy, and K. F., Wissbrun, *Melt Rheology and Its Role in Plastics Processing: Theory and Applications,* Van Nostrand Reinhold, New York (1990).

15. M. Wilhelm, *Macromol. Mater. Eng.*, **287**, 83 (2002).

16. A. J. Giacomin, and J. M. Dealy, *Large-amplitude oscillatory shear* in Techniques in Rheological Measurement, edited by A. A. Collyer, Elsevier Applied Science, London, Chap. 4 (1993).

17. R. H. Edwoldt, A. E., Hosoi and G. H. McKinley, *J. Rheol.,* **53(3)** 1427(2009).

18. J. W. S. Hearle, *High performance fibers*. Woodhead Publishing (2001).

19. L. Huang and S. Wang, *J. Appl. Polym.Sci.*, **78**, 237 (2000).

20. J. D. Menczel, G. L. Collins, and K. Saw, *J. Therm. Anal.,* **49**, 201 (1997).

21. M. Chaouche, and D. L. Koch, *J. Rheol.*, **45 (2)**, 369 (2001).

22. C. L. Tucker III, and S. G. Advani, *Flow and rheology of polymer composites manufacturing,* (Edited by S.G. Advani), Elsevier Science, New York, 147-202 (1994).

23. M. A. Bibbo, M. A., *Rheology of semi-concentrated fiber suspensions* Ph.D.Thesis, Massachusett Institute of Technology, (1987)

24. P. J. Carreau, D. De Kee, and R.P. Chhabara, *Rheology of polymeric systems*, Hanser/Gardner, New York (1997).

25. J. A. Yosick, J. A. Giacomin, W. E. Stewart and F. Ding, *Rheol. Acta,* **37,** 365 (1998).

26. M. Djalili-Moghaddam, and S. Toll, *Rheol. Acta,* **45,** 315 (2006).

27. R. M. Soszynski, and R. J. Kerekes, *Nord. Pulp Pap. Res. J.,* **3,** 172 (1988).

28. R. M. Soszynski, and R. J. Kerekes, *Nord. Pulp Pap. Res. J.*, **3**, 180 (1988).

29. M. Sepehr, G. Ausias, and P. J. Carreau, *J. Non-Newtonian Fluid Mech.,* **123 (1)**, 19 (2004).

30. M. Rajabian, C. Dubois, and M. Grmela, *Rheol. Acta,* **44**, 521 (2005).

31. K. Hyun, S. H. Kim, K. H. Ahn and S. J. Lee, *J. Non-Newtonian Fluid Mech.,* **107**, 51 (2002).

32. G. Ausias, J. F. Agassant, M. Vincent, P.G. Lafleur, P. A. Lavoie and P. J. Carreau, *J. Rheol.,* **36(4),** 525 (1992).

33. S. A. Hashemi, A. Ait-Kadi and P. J. Carreau, *J. Polym. Eng.,* **23(4),** 281 (2003).

34. M. Doi, and S. F. Edwards, *J. Chem. Soc., Faraday Trans.,* **74(2),** 560 (1978).

35. M. P. Petrich, D. L. Koch, and C. Cohen, *J. Non-Newtonian Fluid Mech.,* **95(2-3),** 101 (2000)

36. A. S. Lodge, *Elastic Liquids* Academic Press, London - New York, (1964).

Table 6.1 : Characteristics and nomenclature of the fibers and suspensions used in this study

Suspensions nomenclature	**Fiber type**	**Young's Modulus (GPa) [T=150 °C]**	**Diameter (μm)**	**Aspect Ratio**	**Critical Stress (Pa)**	$t_s(h)$
LDPE-NYL	Nylon	~0.3	14	70	37	144
LDPE-PVA	PVA	~7.2-9.0	14	70	900-1100	73
LDPE-VEC	Polyarylate (Vectran®)	~38.0	18	70	4500	43

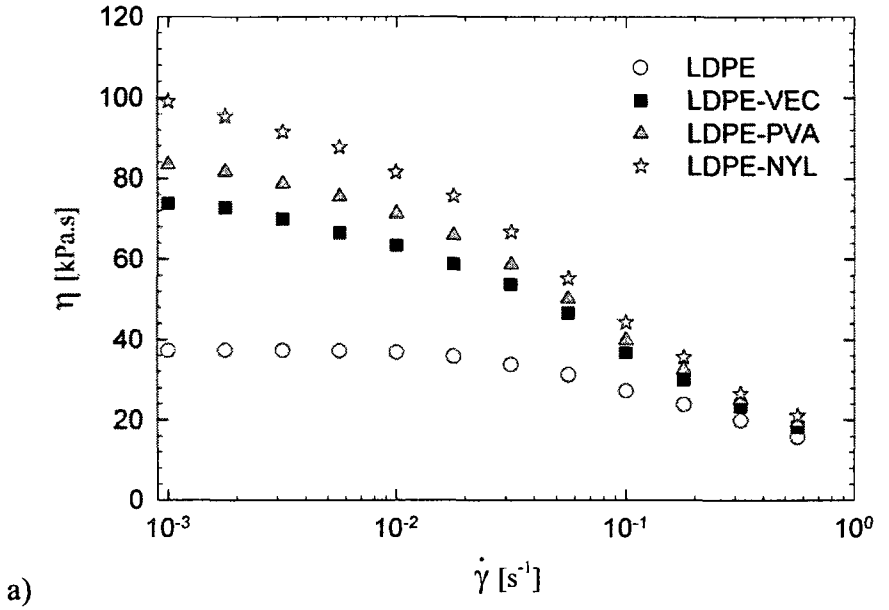

a)

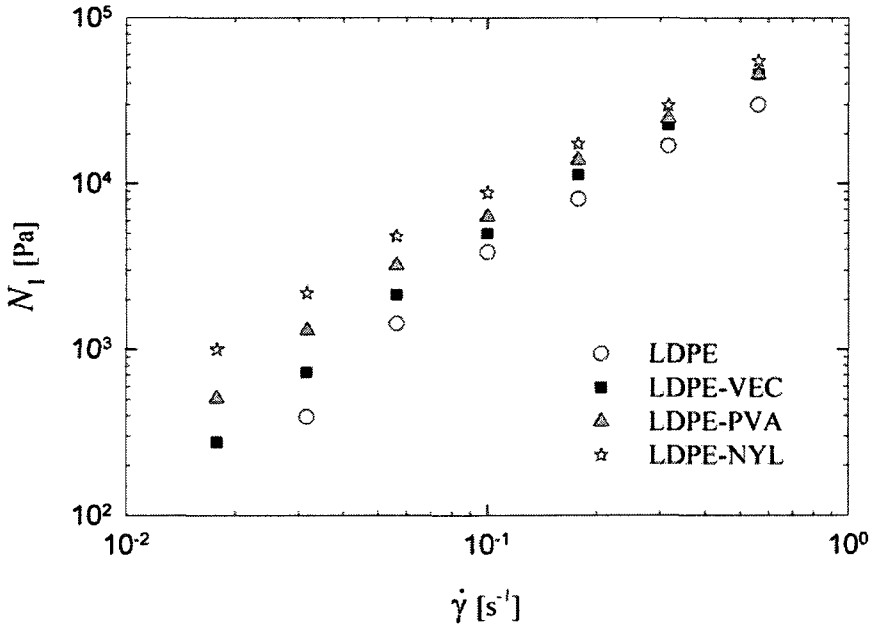

b)

Figure 6.1 : Steady state rheological properties of LDPE and fiber filled LDPE ($\phi_f = 0.05$) : a) η, b) N_1

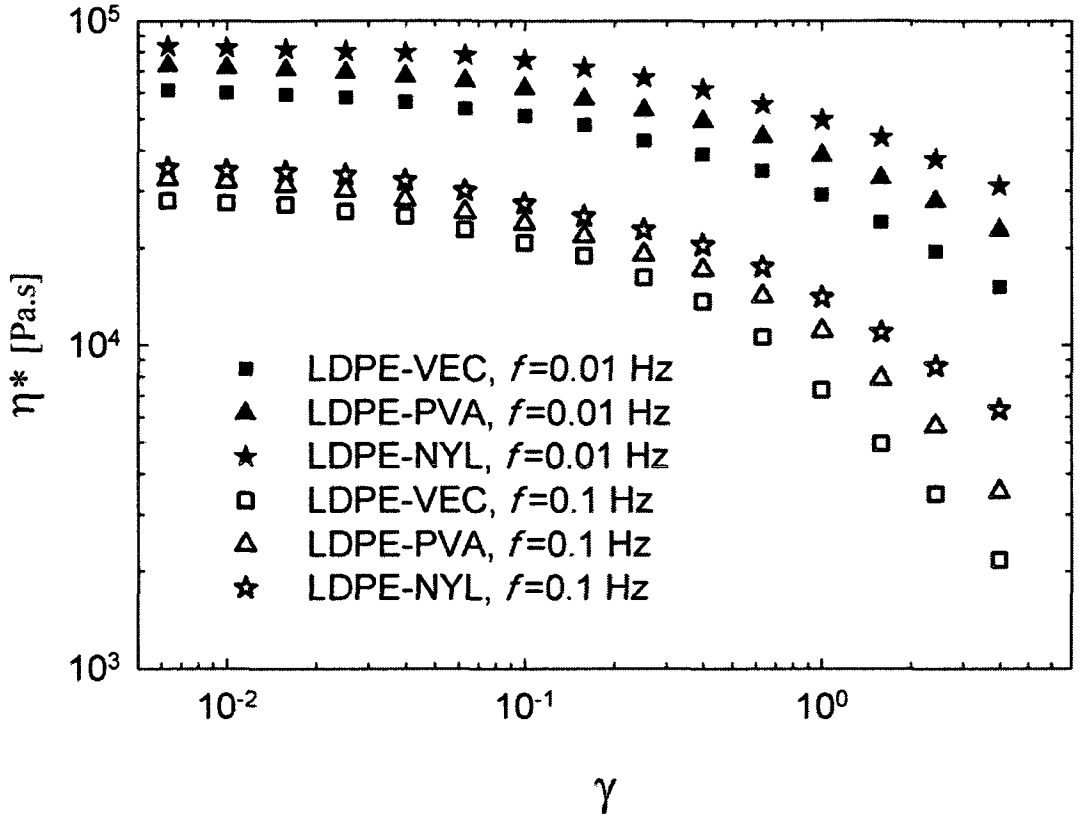

Figure 6.2 : η^* as a function of γ for suspensions in the concentrated regime, ϕ_f=0.05.

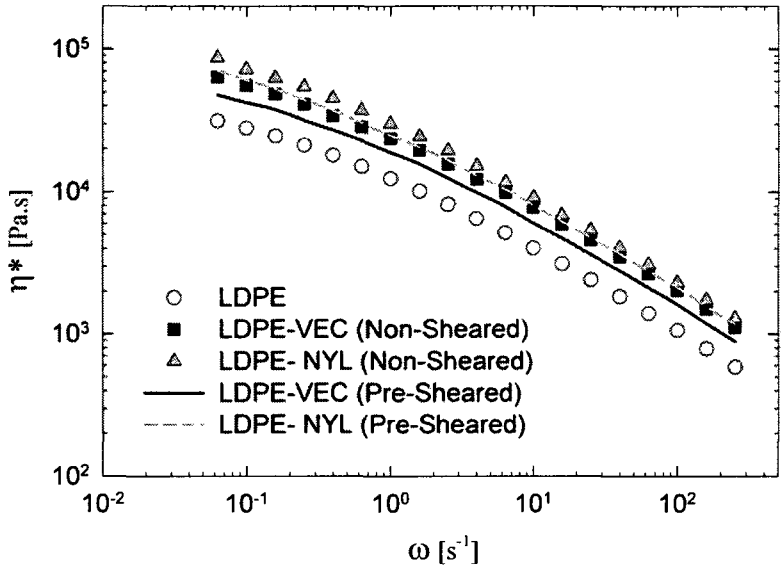

a)

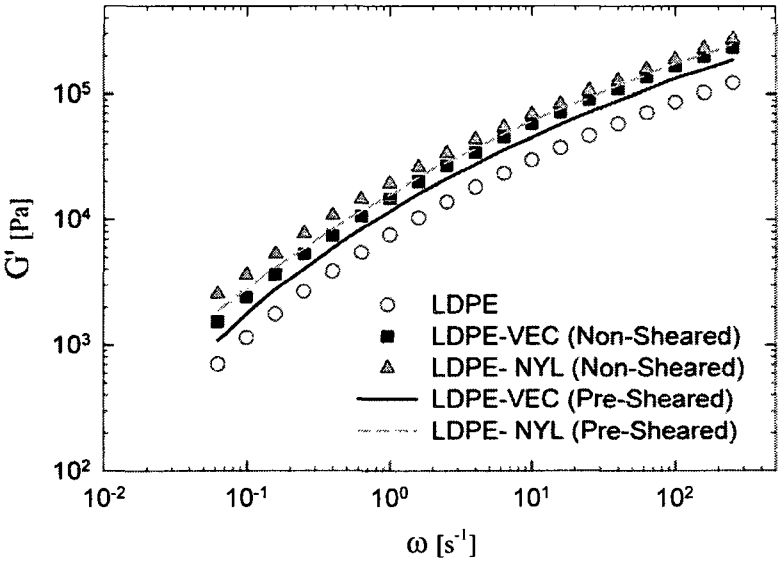

b)

Figure 6.3 : Linear viscoelastic properties of LDPE and reinforced LDPE ($\phi_f = 0.05$) suspensions a) η*, b) G'

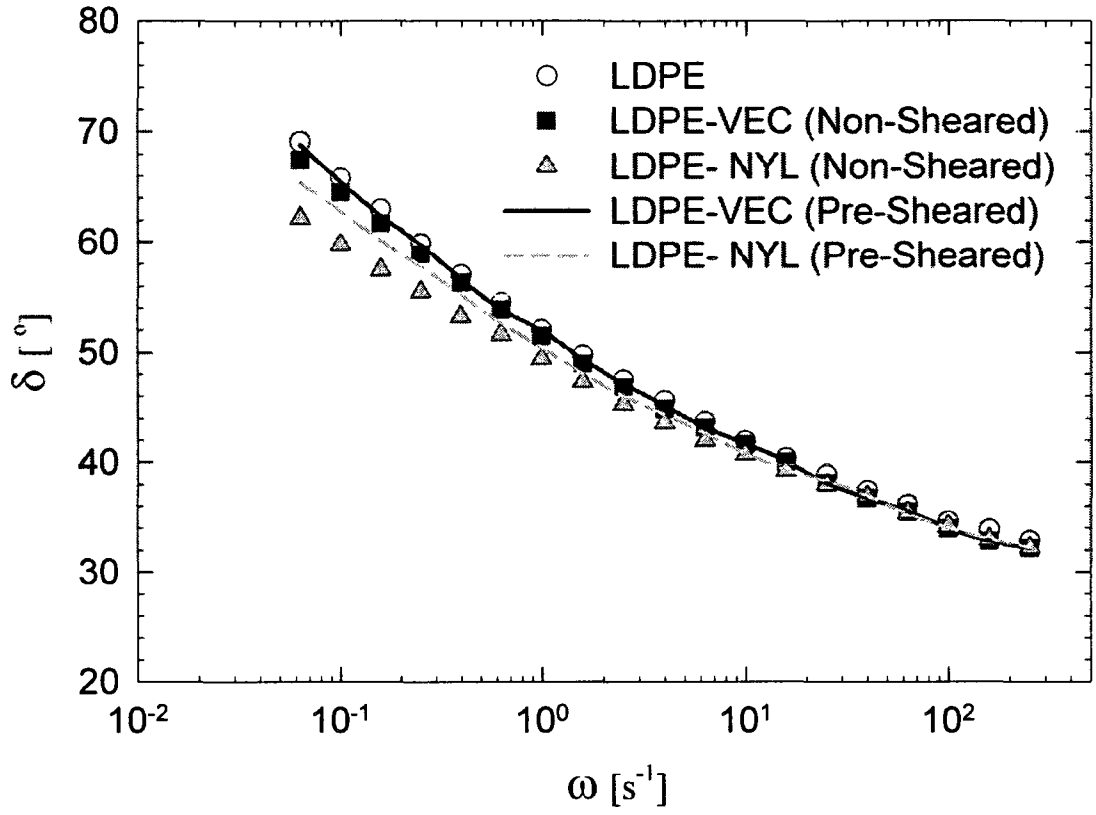

Figure 6.4 : Out of phase angle for neat LDPE and reinforced LDPE ($\phi_f = 0.05$)

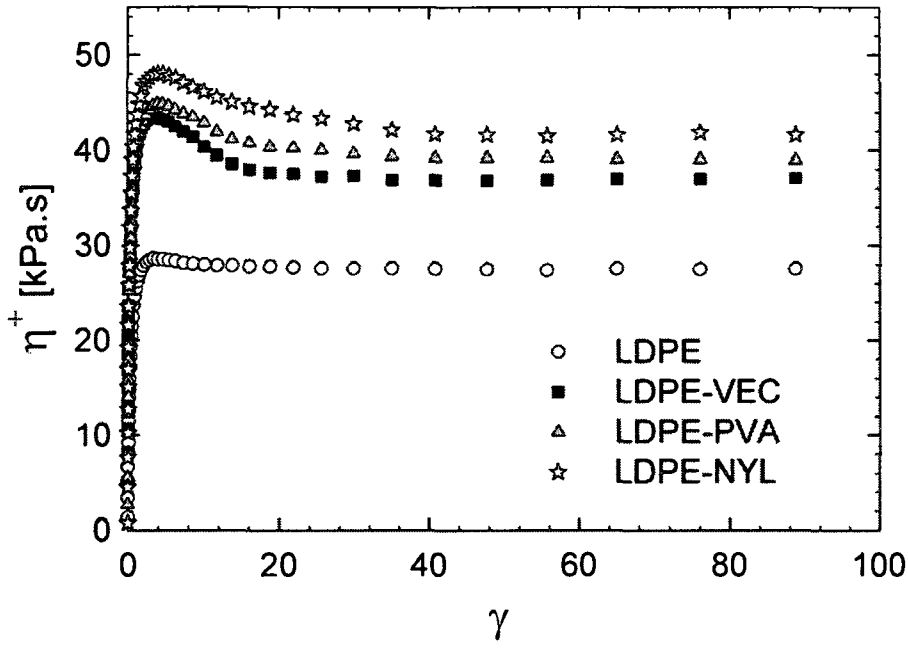

a)

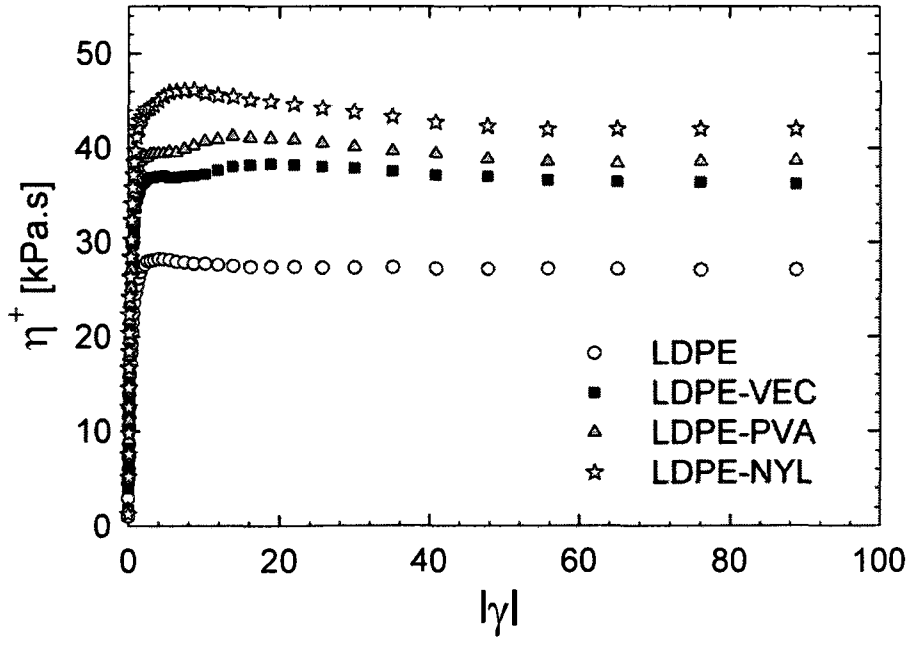

b)

Figure 6.5 : η^+ of neat LDPE and reinforced LDPE ($\phi_f = 0.05$) for experiments carried out at $\dot{\gamma} = 0.1 s^{-1}$ a) forward flow b) reverse flow

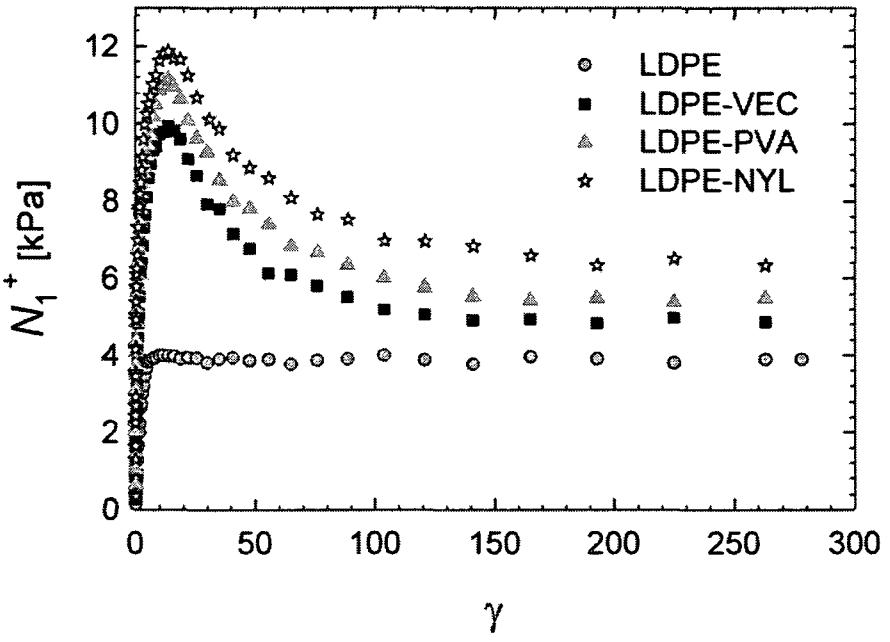

a)

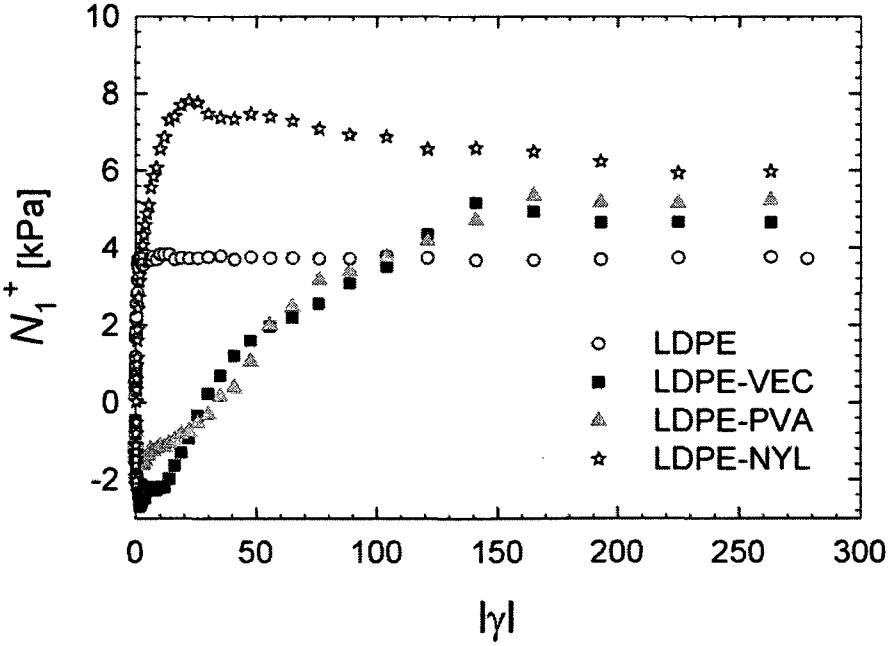

b)

Figure 6.6 : N_1^+ of neat LDPE and reinforced LDPE ($\phi_f = 0.05$) for experiments carried out at $\dot{\gamma} = 0.1 s^{-1}$ a) forward flow b) reverse flow

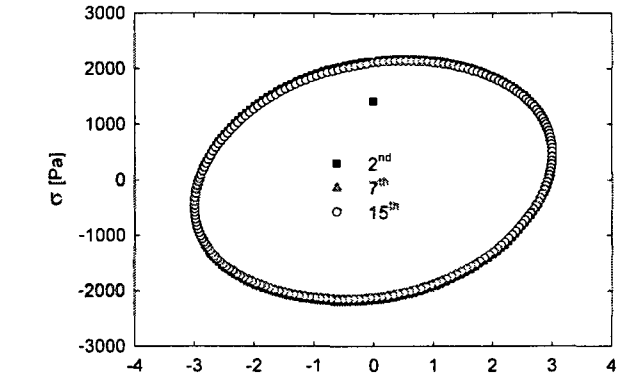

a)

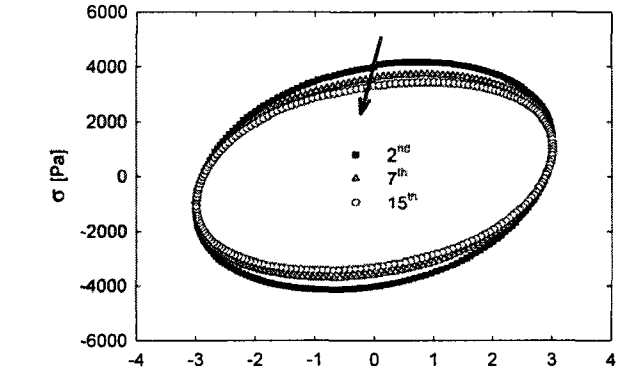

b)

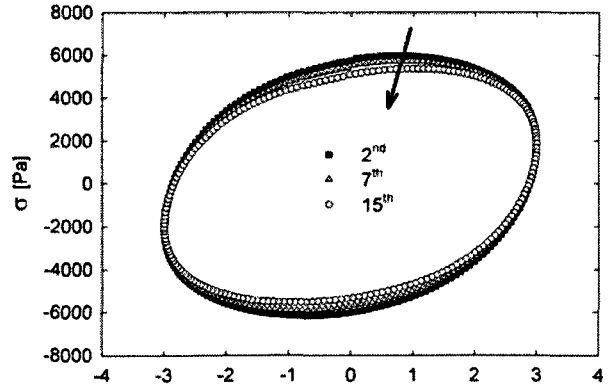

c)

Figure 6.7 : Shear stress versus strain after 3 different LAOS cycles, where $\gamma_R = 3$ and $f = 0.005$ Hz for a) LDPE, b) LDPE-VEC ($\phi_f = 0.05$) c) LDPE-NYL ($\phi_f = 0.05$).

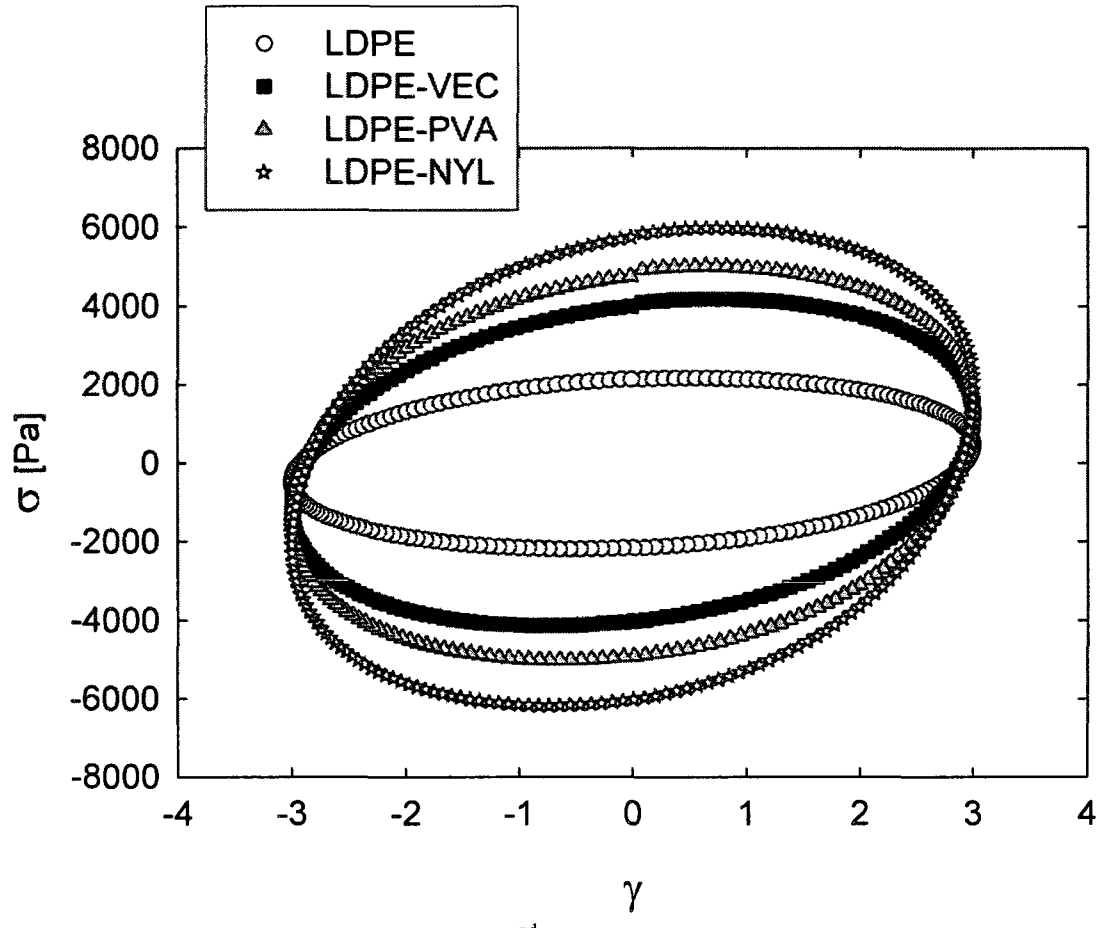

Figure 6.8 : Shear stress versus strain in 2nd LAOS cycle, where $\gamma_a = 3$ and $f = 0.005$ Hz for LDPE and reinforced LDPE ($\phi_f = 0.05$).

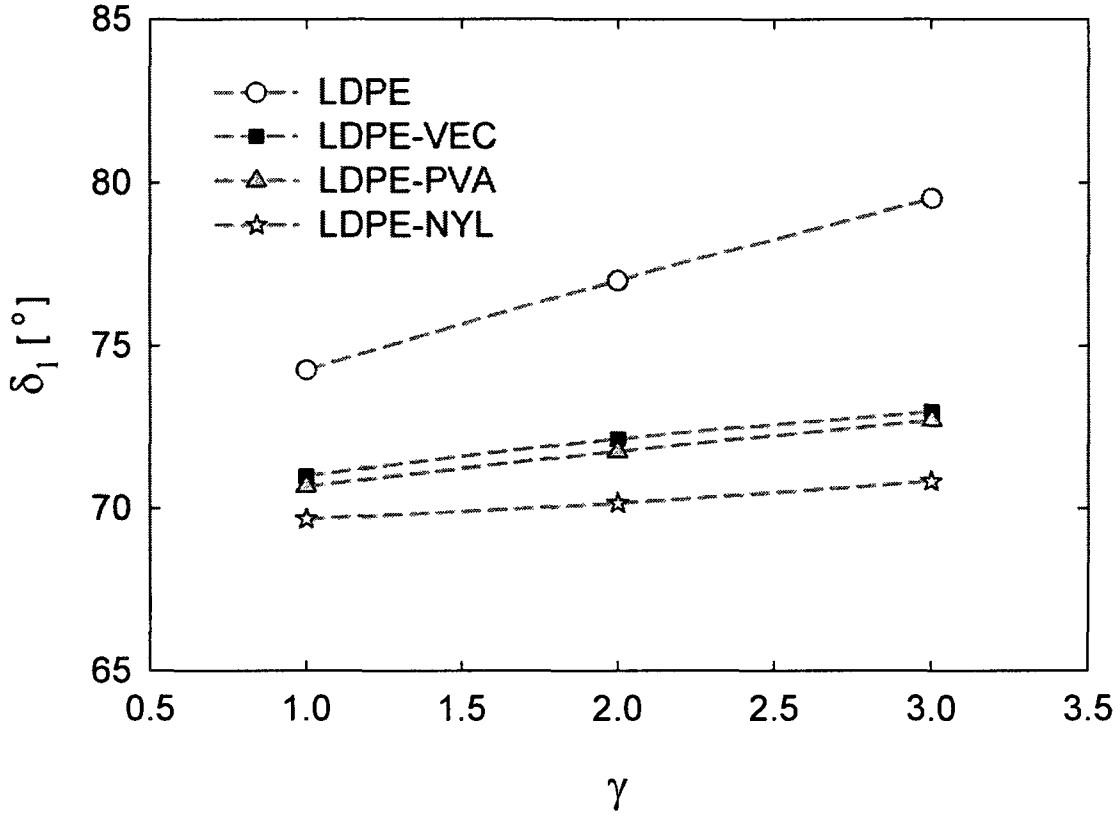

Figure 6.9 : Fundamental shift angle as a function of strain for LDPE and reinforced LDPE ($\phi_f = 0.05$).

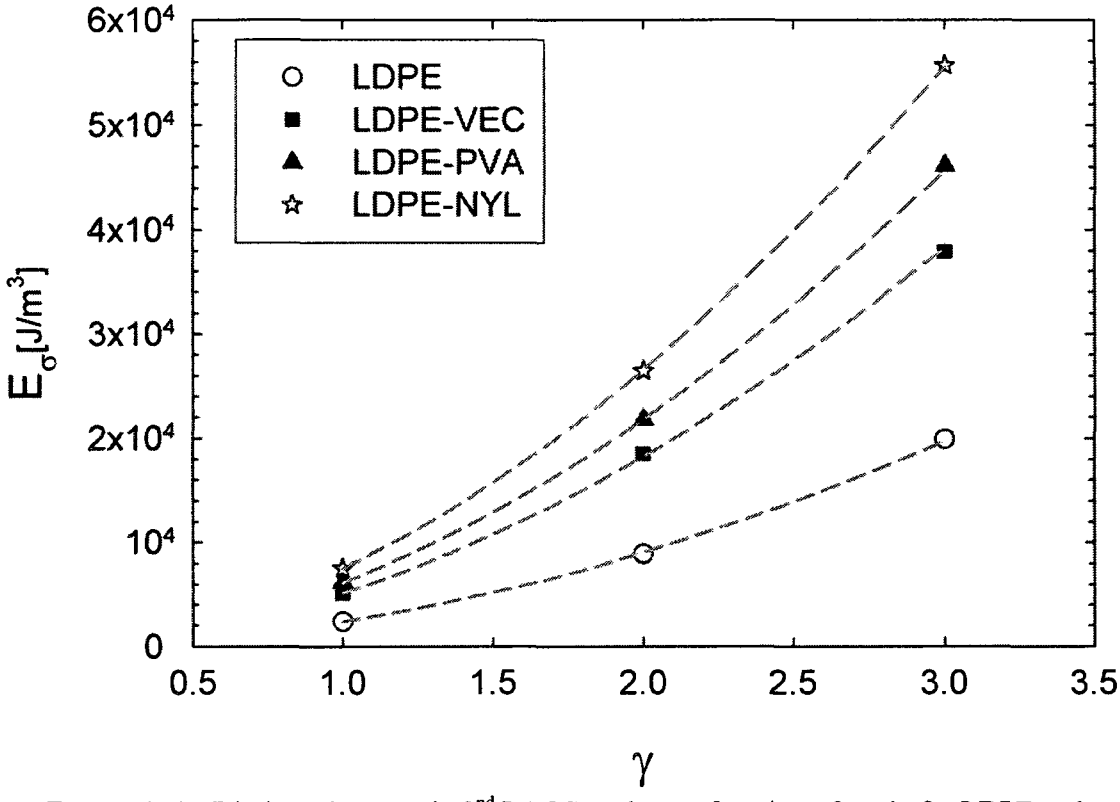

Figure 6.10 : Dissipated energy in 2nd LAOS cycle as a function of strain for LDPE and reinforced LDPE ($\phi_f = 0.05$).

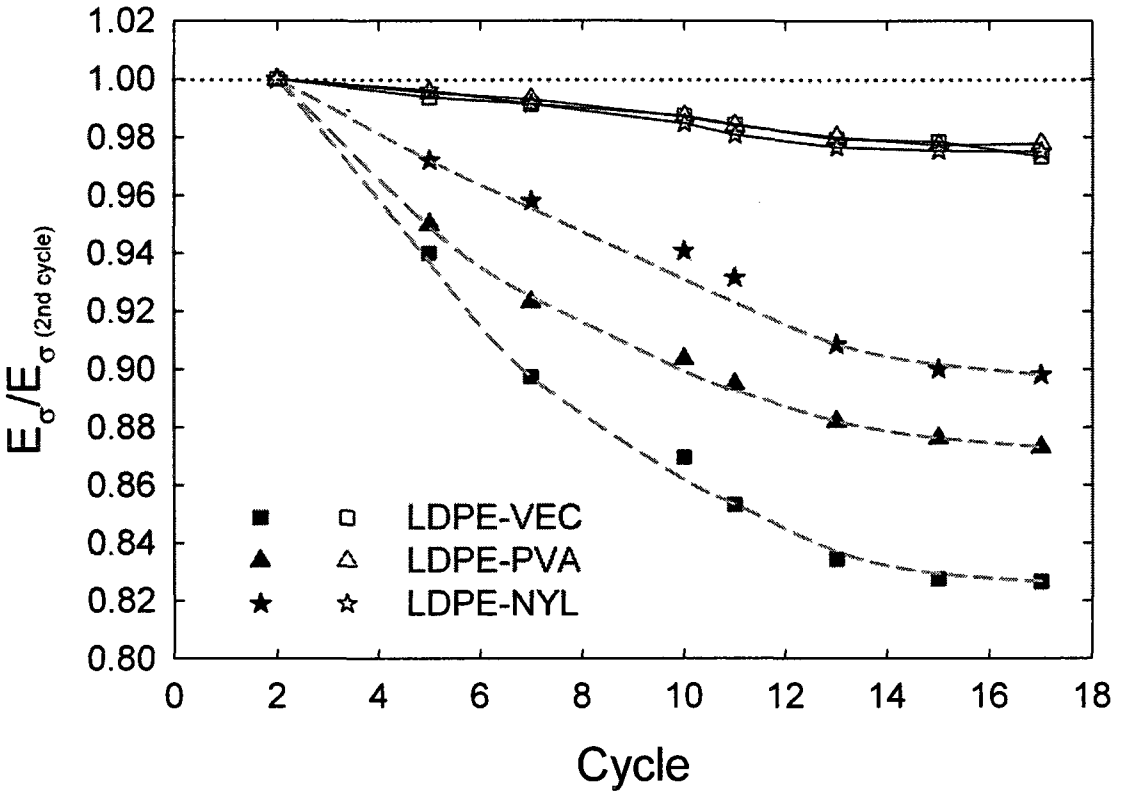

Figure 6.11 : Dissipated energy in LAOS cycles normalized by dissipated energy in 2nd cycle for LDPE and reinforced LDPE in semi-dilute regime ($\phi_f = 0.01$, open symbols) and concentrated regime ($\phi_f = 0.05$, filled symbols).

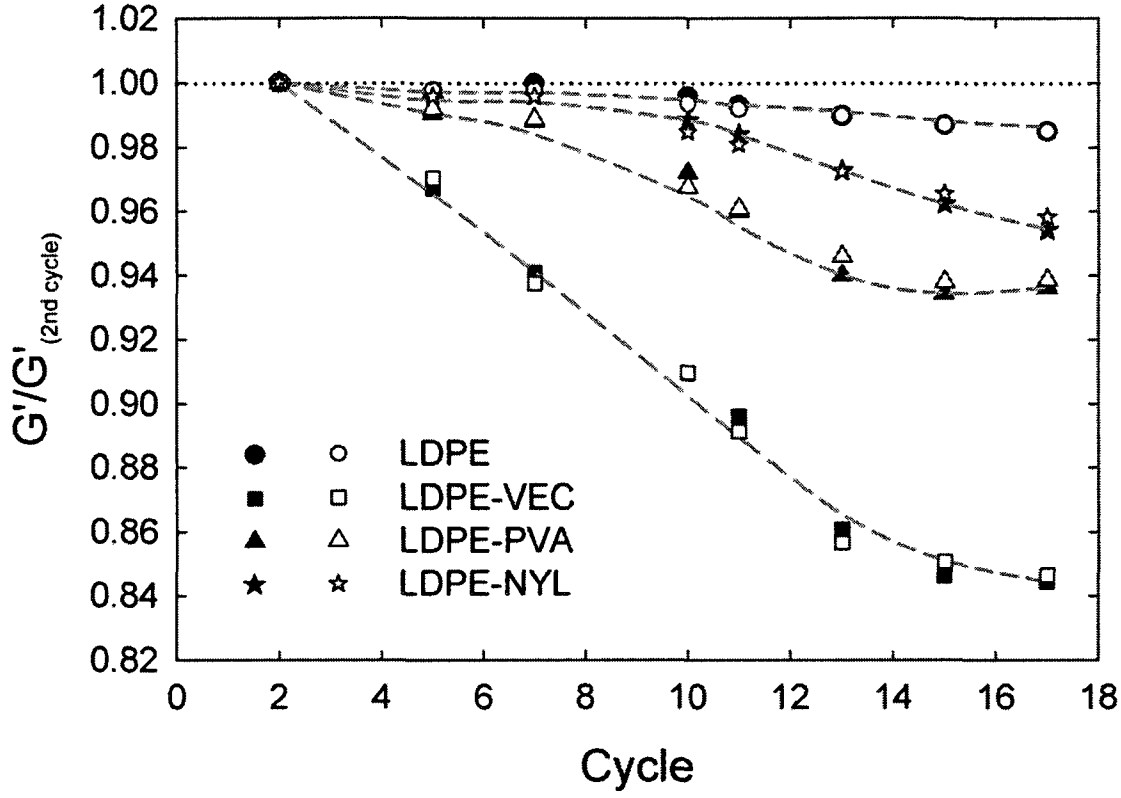

Figure 6.12 : Storage modulus calculated by Equation (6-10) and (6-11) for various LAOS cycles and normalized by the storage modulus in 2nd cycle for LDPE and reinforced LDPE in the concentrated regime ($\phi_f = 0.05$): G'_M (filled symbols), G'_L (open symbols)

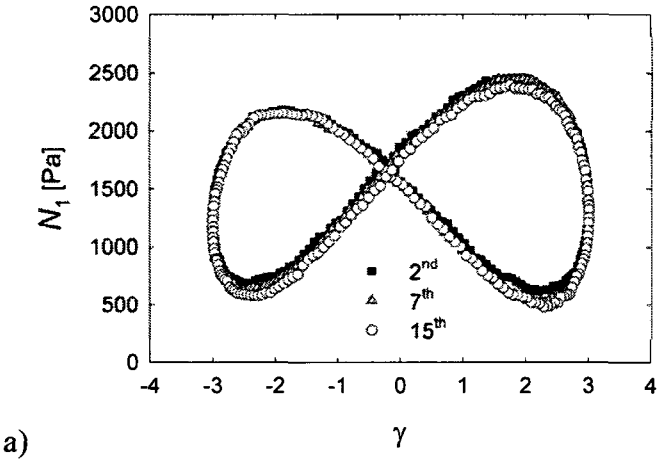

a)

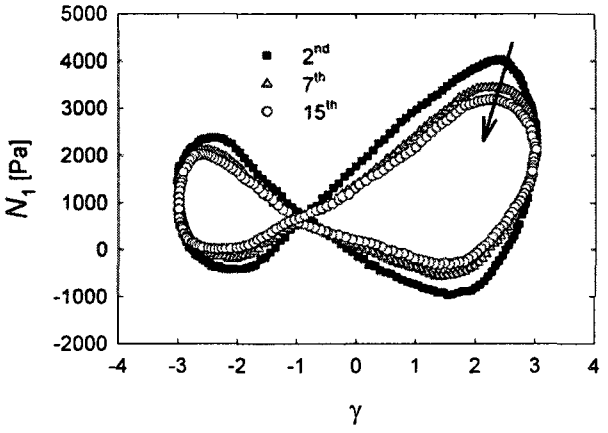

b)

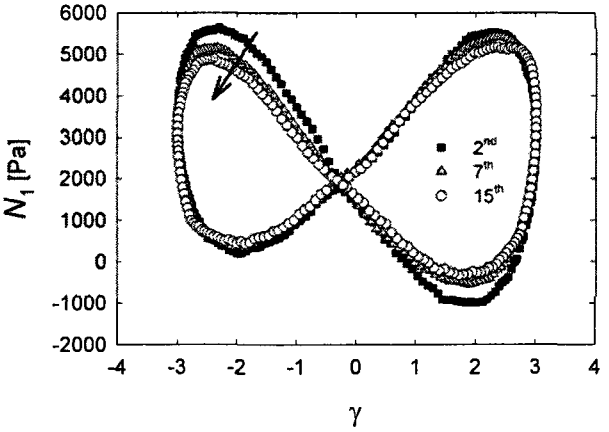

c)

Figure 6.13 : Primary normal stress versus strain after 3 different LAOS cycles, where $\gamma_A = 3$ and $f = 0.005$ Hz for a) LDPE, b) LDPE-VEC ($\phi_f = 0.05$) c) LDPE-NYL ($\phi_f = 0.05$).

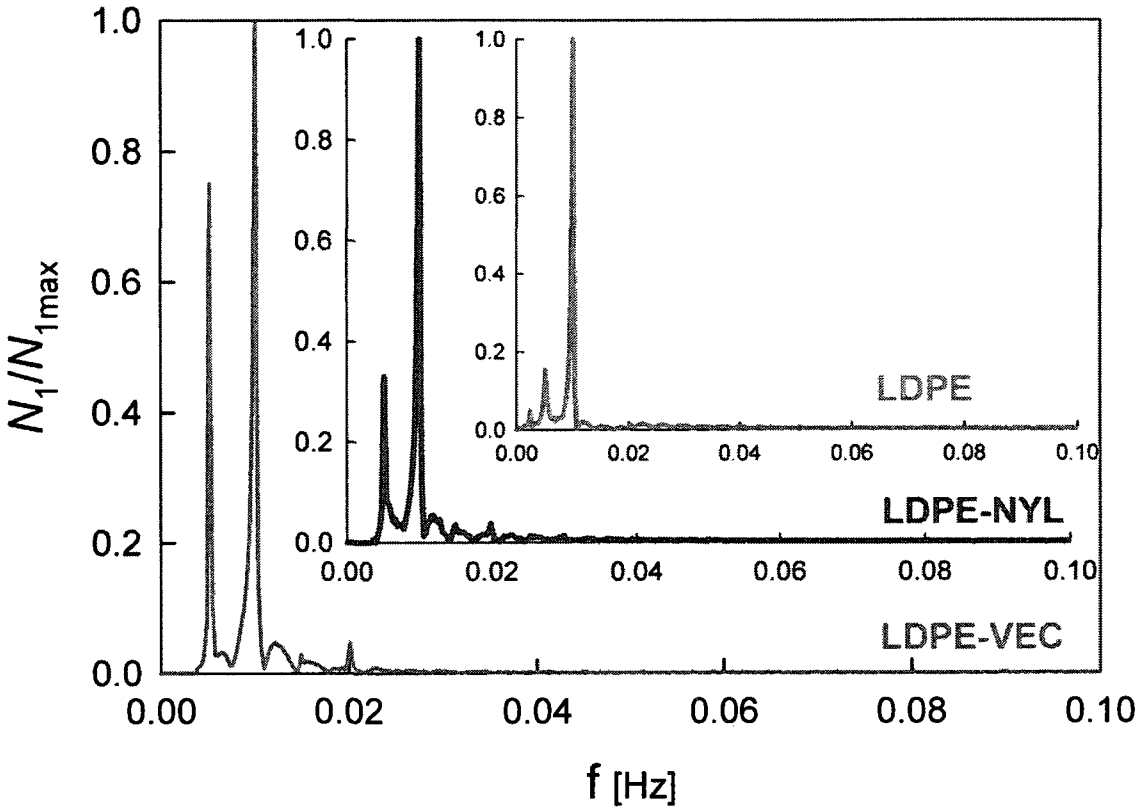

Figure 6.14 : FFT analysis of the LDPE and reinforced LDPE ($\phi_f = 0.05$) primary normal stress difference responses at $\gamma_R = 3$ and $f = 0.005$ Hz.

CHAPTER 7 - General Discussion

In most of the researches presented the abundant literature about fiber suspensions, fibers are considered as rigid bodies. But as fiber stiffness decreases or aspect ratio increases, the fibers can easily be bent and are no longer act like rigid rods anymore. The main objective in this project was to elucidate the effect of fiber flexibility on the rheological behavior and microstructure of fiber suspensions.

In most forming processes, materials are subjected to a combination of shear and elongational flows. The shear tests performed in this study represent a wide range of flows, i.e. transient, steady-state, simple shear, and oscillatory at small and large amplitude of deformation.

To better assess the effects of the presence of the fiber, first a Newtonian matrix was used, a high viscosity silicone oil. This high viscosity silicone oil was selected because flexibility effects are more pronounced when hydrodynamic forces on the fibers are considerable. After elucidating the effect of fiber flexibility in this model Newtonian matrix, the study was extended to a polymeric matrix.

Three fiber types were selected for this study; nylon ($E_Y = 2GPa$), PVA ($E_Y = 26GPa$) and Vectran ($E_Y = 78GPa$). The fibers had different aspect ratios. Different fiber concentrations representative of the semi - dilute and semi-concentrated regimes, were prepared and investigated. The study of several parameters was conducted to ensure the reliability of the measurement methods. In this chapter, the discussion lies mainly on the parameters influencing the reliability of the experiments.

7.1 Wall Effects

One of the issues that were considered for preparing the samples with a high aspect ratio was to ensure that the chosen concentration would not lead to experimental problems such as samples coming out of the rheometer parallel plate flow geometry. Different fiber concentrations were tested in the concentrated regime to find the suitable content that would give reproducible results. Gap size effects were also investigated.

In general it is reported for a suspension of solid particle in a liquid phase that wall effects are influenced by the solid content, particle size, temperature of the suspension, flow dimension, dependence of viscosity on the concentration of the dispersed phase, wall roughness, flow rate, etc. (Barnes, 1995 ; Soltani *et al.*, 1998). Gavze, et al. (1997) showed that wall effects decrease when the particle shape becomes ellipsoidal. In this work we tried to find the concentration at which reproducible data couold be obtained and with minimum wall effects. The effect of gap size on steady state and transient behavior are presented in Figures (7.1) and (7.2) in steady state and transient experiments, respectively, for suspensions prepared with Vectran fibers (the most rigid fibers) and a high aspect ratio ($r = 140$) at the optimized concentration ($nL^2D = 2.9$). It is observed that for gaps less than one fiber length the properties highly depend on the gap size, but for the optimized concentration used in our experiments, and with gaps larger than the fiber length, the results were independent of gap size and within the experimental error.

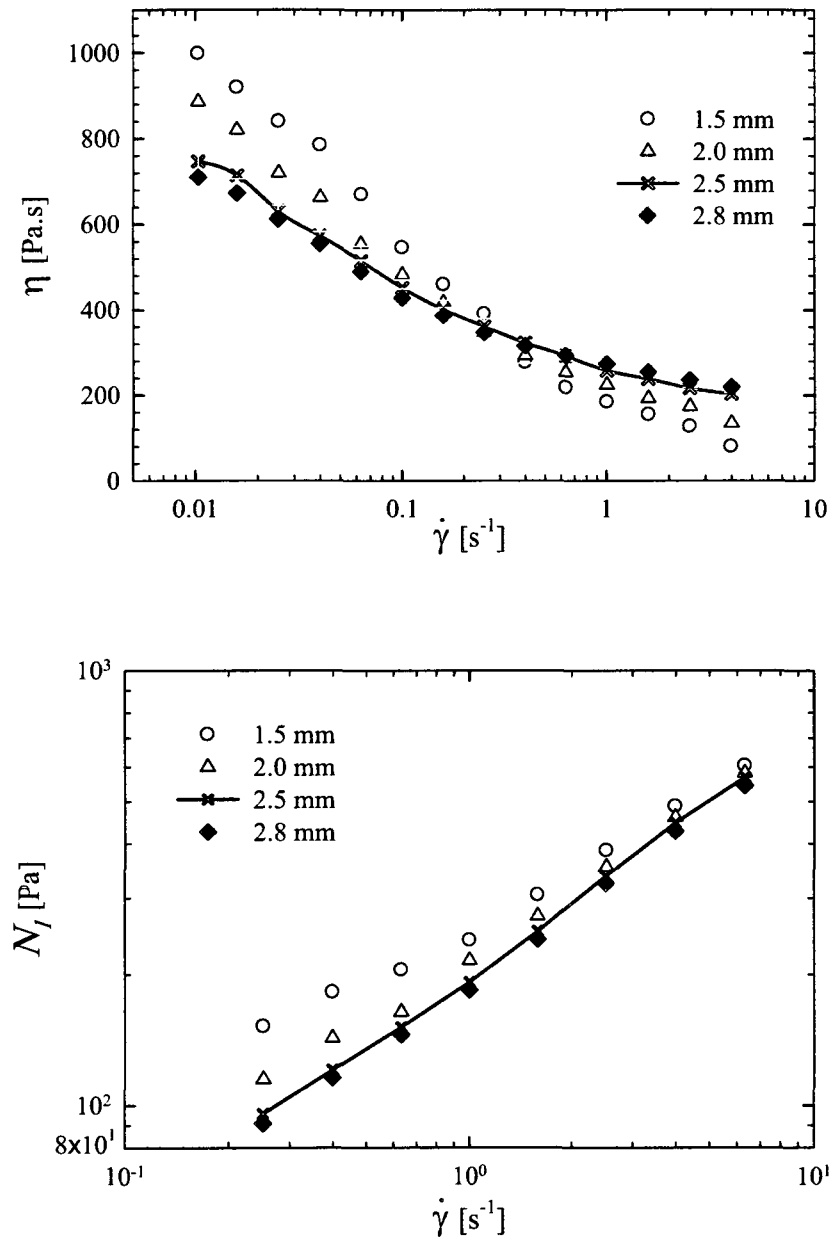

Figure 7.1 : The effect of the parallel plate geometry gap height on steady state properties of VM-140C (a) η and (b) N_1. The various symbols relate to measurements performed at the different gap heights.

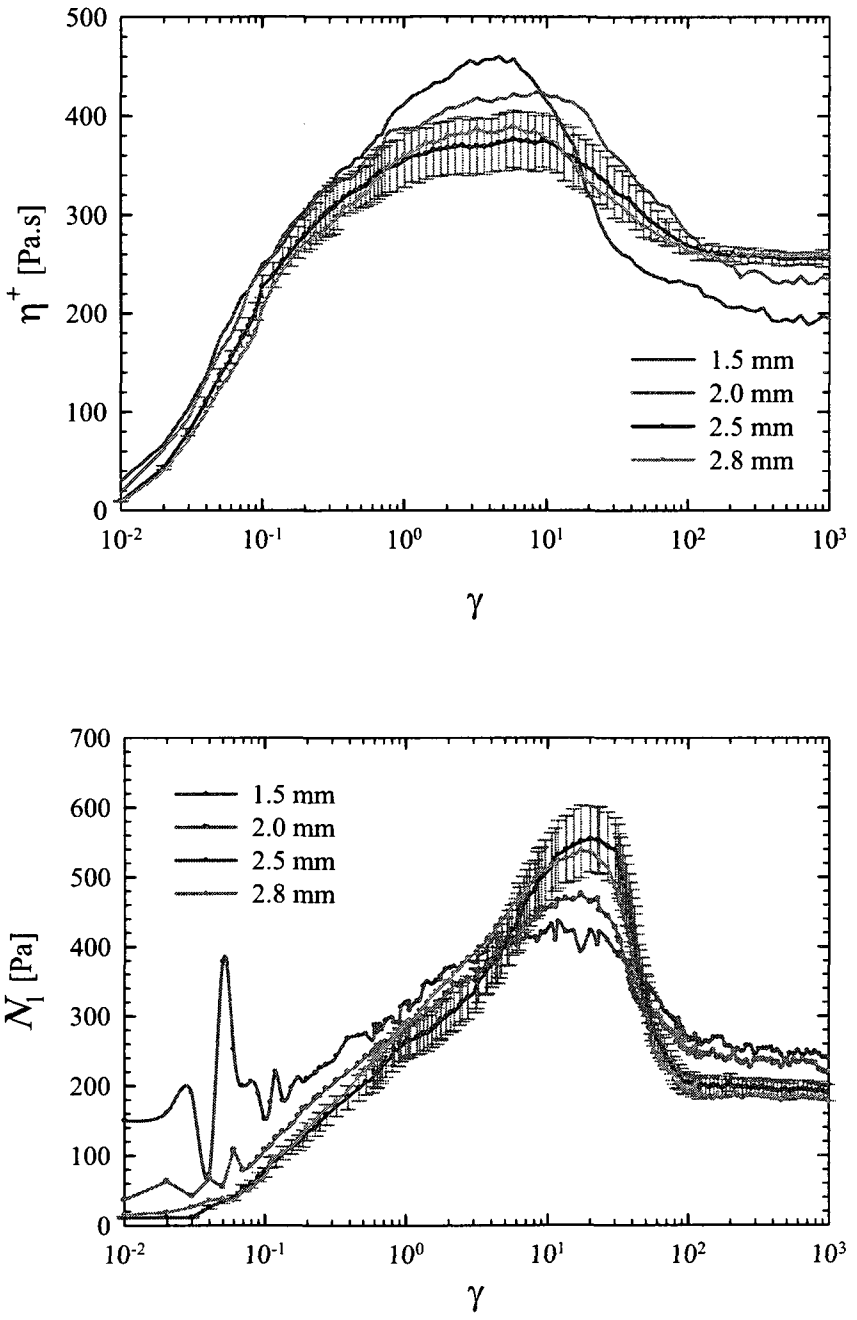

Figure 7.2 : The effect of the parallel plate geometry gap height on the stress growth behavior of VM-140C in startup of flow experiments at $\dot{\gamma} = 1\ s^{-1}$. (a) η^+ vs. strain and (b) N_1^+ vs. strain. The various symbols relate to measurements performed at the different gap heights. The error bars show experiments error at gap height= 2.5 mm

7.2 Fibers Wettability and Adhesion

Chaouche and Koch (2001) discussed that adhesive forces could be responsible for network formation. Since fibers made of different materials were used in this work, caution must be taken in order to account for the difference in physicochemical properties of these fibers that may affect the rheological properties. One of these properties is the the adhesive force, where in the concentrated regime contacts between fibers become predominant and the difference between fiber roughness and friction coefficients may influence the rheological results (Petrich and Koch 1998). These effects may be reduced if a good wetting of the fibers by the suspending medium is ensured. The degree of wetting is described by the contact angle, the angle at which the liquid-vapor interface meets the solid-liquid interface. If the wetting is favorable the contact angle is low, and the fluid spreads to cover a large area of the surface. On the other hand if the wetting is unfavorable, the fluid forms a compact droplet on the surface. A contact angle of 90° or greater generally characterizes a surface as non-wettable, and one less than 90° as wettable (Neumann and Good, 1979). The contact angle between silicone oil and various films prepared using nylon, PVA and Vectran was measured using a goniometer (Model 100-00 of Ramé-Hart, Netcong, NJ, USA). The measured contact angles between the polymer films and the silicone oil were 26 ± 2°, 19 ± 2° and 29 ± 2° for nylon, PVA and Vectran, respectively. These results suggest that all fibers used in this study were wetted well by the silicone oil and at the liquid-solid surface interface the adhesive forces between the liquid and the fibers were similar. These results also suggest that the effects of fiber surface properties were not predominant. But in an ideal

set of experiment it would be better if these effects could be considered. However because of the complexity of the required experiments to determine adhesive forces, this investigation was not performed and surface tension results were used to support to our assertion that these effects were negligible.

7.3 Fibers Equilibrium Shape

Switzer and Klingenberg (2003), who used particle level simulations, showed that relatively small deviations in the shape from a perfectly straight form can result in large increases of the viscosity of suspensions. However it is very challenging to systematically explore the effect of fiber shape on suspension structure experimentally. But the idea in this research was to show that as fiber stiffness decreased, the probability for the presence of curved shape fibers increased. The non-straight shape might favor the formation of large scale structures and result in suspensions with higher viscosities. However, after breaking these structures the viscosity rapidly decreased and resulted in a severe shear-thinning behavior. Looking at the initial fiber shape could help to figure out the importance of the shape under flow. The initial shapes of nylon and Vectran fiber with a high aspect ratio are shown in Figure (7.3). As seen in this figure, the nylon fibers have curved shapes while the Vectran fibers are straight. Nylon fibers were heated at 70 °C which is more than nylon T_g (50 °C), and some fibers became straight and while some others collapsed and this test did not result in useful information.

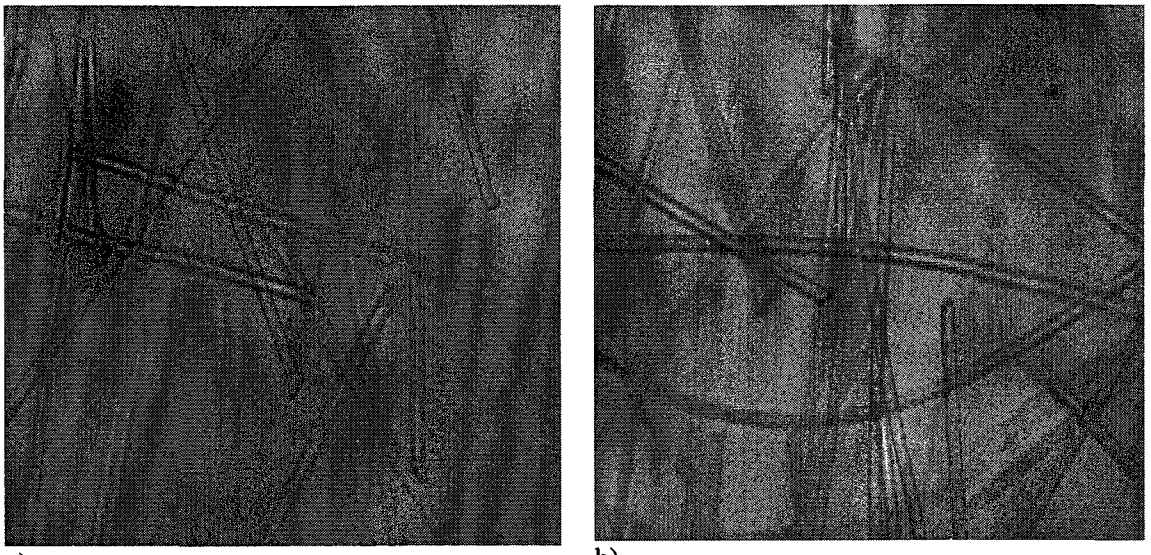

a) b)

Figure 7.3 : snapshot of initial orientation of fibers between parallel plates: a) Vectran fibers ; b) Nylon fibers in silicone oil

7.4 Rheological Properties in Transient Flow

A parallel plate flow geometry was used to obtain transient shear viscosities and transient normal stress differences. The torque, T, and normal force, F, can be measured as functions of the shear rate at the rim, $\dot{\gamma}_R$ using a force rebalance transducer. These raw data were used to calculate the viscosity and first normal stress difference assuming that the second normal stress difference was negligible (Weissenberg's hypothesis) [Carreau *et al.* (1997)]:

$$\eta(\dot{\gamma}_R) = \frac{T}{2\pi R^3 \dot{\gamma}_R}\left(3 + \frac{d\ln T}{d\ln \dot{\gamma}_R}\right) \tag{7-1}$$

$$N_1 = -(\sigma_{11} - \sigma_{22}) = \frac{2F}{\pi R^2}\left(1 + \frac{1}{2}\frac{d\ln F}{d\ln \dot{\gamma}_R}\right) \tag{7-2}$$

Equations 7-1 and 7-2 are standard viscometric equations for steady flow. Yet, similar equations apply in transient experiments. Here, the torque, normal force, shear viscosity and first normal stress difference depend not just on the edge shear rate, but also on strain. The consequence is that to obtain rigorous results for material properties, the derivatives in (7-1) and (7-2) must be taken at fixed strains for different shear rates. This correction was verified to see how it could influence the results. The numerical calculation of the derivative term is more accurate if $\Delta\dot{\gamma}$ (the step between two different shear rates applied) is small:

$$\frac{d\ln T}{d\ln \dot{\gamma}} = \lim_{\Delta\ln\dot{\gamma}\to 0}\frac{\ln T\big|_{\dot{\gamma}} - \ln T\big|_{\dot{\gamma}+\Delta\dot{\gamma}}}{\Delta\ln\dot{\gamma}} \tag{7-3}$$

Hence transient tests were performed at shear rates of 0.9, 1 and 1.1 s^{-1} to calculate the transient rheological behavior at a shear rate of 1 s^{-1}. Using the torque and normal force data, the derivative terms in Equations (7-1) and (7-2) were calculated at fixed strains. It was found that applying the new calculated derivative terms did not significantly changed the results obtained previously without this correction. The maximum difference was 2.3 % for the transient viscosity and 2.5 % for the normal stress differences, and these are within the experimental error.

CHAPTER 8 - Conclusions

This thesis entitled "Rheological study and rheo-microscopy of semi-flexible fiber suspensions" had the main objective to improve the comprehension of the rheological behavior of fiber suspensions by elucidating the effect of fiber flexibility in relation with fiber orientation, fiber-fiber and fiber-macromolecule interactions.

First of all the effective stiffness was chosen as a criterion for flexibility. The effective stiffness is the ratio of the stress required to bend a fiber to the viscous stress. With the use of the effective stiffness, fiber stiffness and aspect ratio were identified as important parameters for the effect of fiber flexibility. In the first part of this work, the effect of flexibility parameters (stiffness, aspect ratio) as well as the role of interactions in the semi-dilute and semi-concentrated regimes of fiber suspensions was investigated. The result of this study can be summarized as follows:

- Both viscosity and first normal stress differences increase with larger flexibility, and the increases are more pronounced in the semi-concentrated regime. The enhancement of the rheological properties is attributed to additional fiber-fiber interactions when using more flexible fibers. The results are also more pronounced when fiber aspect ratio increases.
- As the fiber aspect ratio increases or the fiber stiffness decreases, the critical stress needed for fiber bending decreases and the probability of finding curved fiber shapes increases. Even if the hydrodynamic forces are not sufficient to bend

the fibers, an initial non-straight fiber shape will influence the rheological behavior considerably.

- At a given fiber concentration, nL^2D, the shear-thinning effect becomes more pronounced as the fiber aspect ratio and flexibility increase: high shear rate or stress induces the break-up of the flocculated structure that exists at lower shear rates.
- In stress growth experiments, the orientation of flexible fibers with the flow direction is less important than for rigid fibers. This was confirmed by earlier tumbling of the flexible fibers in flow reversal in terms of strain.

In the second phase of this work, rheo-microscopy was used to evaluate the evolution of the fiber orientation state under shear flow, and the results obtained can be summarized as follows:

- The larger rheological properties of the flexible fibers were attributed to their slightly curved shape as opposed to the straight shape of the rigid fibers.
- Rheo-microscopy of the various suspensions showed that fibers orient in the flow direction and that the fiber orientation increased with shear rate and the amount of strain applied.
- The orientation of rigid fibers in the flow direction is more important than for flexible fibers, especially at low shear rates.

- The rate of evolution of the orientation state under shear flow is higher for rigid fibers and this could explain the fact that transient viscosity of flexible fibers reaches steady state at larger strain as compared to rigid fiber suspensions.

In conjunction with this experimental study, a GENERIC model (General Equation for Non-equilibrium Reversible-Irreversible Coupling) has been used to predict the rheological behavior of semi-flexible fiber suspensions as well as their microstructure. The model takes into account fiber-fiber interactions and also the semi-flexible nature of the fibers. Considering the fact that a Newtonian matrix was used in this investigation, the number of adjustable phenomenological parameters in Rajabian et al. (2005) model was reduced from 8 to 3. These parameters consist of a flexibility parameter, a mobility parameter and an interaction parameter. By fitting the model to stress growth data, the ability of model to predict the evolution of the orientation state of semi-flexible fibers was examined. The main findings were:

- As the fiber flexibility increased the parameter related to the excluded volume of the fibers, B_{ff}, showed a lower value, hence indicating more inter-fiber interactions. In addition, by decreasing the fiber stiffness the mobility parameter was smaller, due to the curved shape of the fiber.
- The GENERIC model can qualitatively describe the transient rheological behavior of fiber suspensions in a Newtonian fluid.
- The fiber orientation as predicted by the model was confronted with the rheo-microscopy results. Again, the model predicts qualitatively well fiber orientation for fibers of various flexibilities.

Finally, the last point tackled in this work was concerned with the effect of fiber flexibility on the rheological behavior of fiber suspensions in a viscoelastic matrix (molten LDPE) under simple shear flow, and small and large amplitude oscillatory shear flow (SAOS and LAOS, respectively). In a process such as push-pull injection, knowledge of LAOS behavior may be of great interest. Thus, the main focus of this investigation was to study the effect of fiber flexibility on large amplitude oscillatory behavior of a fiber filled polymer. The results of this investigation are summarized as follows:

- The SAOS tests revealed that the behavior of the complex viscosity and the storage modulus of the fiber suspensions was typical of homogeneous polymer melts.
- The stress amplitude of the composites in LAOS decreased with time, and this behavior was attributed to fiber orientation.
- The calculated viscous dissipation energy was seen to increase with fiber flexibility. It also decreased with time and the reduction was more pronounced in the case of the more rigid fibers. The reduction of the dissipated energy was attributed to a reduction of fiber contacts, and this was confirmed by a much lower reduction in the case of semi-dilute suspensions, in which contacts between fibers are not important. Hence, flexible fibers undergo less fiber contact reduction during LAOS as compared to rigid fibers.

Recommendations for future research

Numerous experimental research themes may be investigated to gain a better understanding of fiber suspensions. Are listed here three areas of research for experimental work, including flow visualization, determining individual fiber properties, and interactions.

As discussed previously, at low shear rate large scale structures may be formed. An experimental technique to visualize large scale structures would be very interesting. Also it would be interesting to measure the stress to break these structures. In addition it would be useful to visualize the suspension structure in the radial direction of parallel plate flow geometry, and obtain information about the heterogeneity which may be associated with the difference in shear rate in the radial direction.

The simulations of Switzer and Klingenberg (2003) have suggested that the fiber shape may have important effects on the suspension microstructure. The visualization results of the present study showed that the fiber shape changes with fiber properties. It would be helpful to find a systematic procedure to investigate the role of fiber equilibrium shape on the rheological properties and the microstructure of suspensions. The fiber shape is difficult to characterize, and is usually described in terms of "curl" and "kink" in the pulp and paper industry (Switzer and Klingenberg, 2003). The curl is related to the ratio of the end-to-end distance of a fiber to the nominal length of the fiber, while the kink is a measure of the number of abrupt direction changes along a fiber length (Page *et al.*, 1985).

Simulations and experiments have shown that fiber interactions are important in determining fibers dynamics as well as the rheological properties. It would be useful to gain a better understanding of individual fiber-fiber interactions. This may include a visual investigation of two fibers in contact in order to determine the effect of surface properties and interactions on relative fiber motion. Experimental techniques for measuring friction forces for individual fiber contacts are also needed to improve our understanding about interactions.

For the LAOS experiments, the use of rotational rheometry restricted the study to moderate deformations; it would be interesting to use a rheometer with sliding parallel plates (Giacomin *et al.* 1989) for further study at higher deformations. However deformation in this type of rheometers is limited by rheometer length and end effects. Also rheo-microscopy would help again to understand the relation between LAOS and suspension structure. The study would be even more effective if visualization experiments in the velocity gradient direction could be conducted at the same time.

References

Advani, S.G.; & Tucker, C.L. (1987). The use of tensors to describe and predict fiber orientation in shorti fber composites. *J. Rheol.,* 31, 751.

Advani, S.G.; & Tucker, C.L. (1990). Closure approximations for threedimensional orientation structure tensors. *J. Rheol.,* 34(3), 367-386.

Arlov, A. P., Forgacs, O. L., and Mason, S. G. (1958). Particle motions in sheared suspensions 4. General behavior of wood pulp fibers. *Sven. Papperstidn.* ***61***, 61.

Ausias, G. ; Agassant, J. F. ; Vincent, M. ; Lafleur, P. G. ; Lavoie, P. A. ; Carreau, P. J. ; (1992). Rheology of short glass fiber reinforced polypropylene. *J. Rheol.*, 36 (4), 525-542.

Barbosa, S. E.; Ercoli, D. R. ; Bibbo, M. A. ; & Kenny, J. M. (1994). Rheology of short fiber composites: A systematic approach. *Composite Structures,* 27(1-2), 83-91.

Batchelor, G. K. (1971). The stress generated in a non-dilute suspension of elongated particles by pure straining motion. *J. Fluid Mech.,* 46, 813.

Bay, R. S.; & Tucker III, C. L. (1992). Stereological measurement and error estimates for three-dimensional fibre orientation. *Polym. Eng. Sci.,* 32 (4), 240–253.

Bibbo, M. A., (1987) *Rheology of semi-concentrated fiber suspensions* Ph.D.Thesis, Massachusett Institute of Technology.

Bibbo, M. A.; Dinh, S. M.; & Armstrong, R. C. (1985). Shear Flow Properties of Semi-concentrated Fiber Suspensions. *J. Rheol.,* 29(6), 905-929.

Bird, R. B.; Armstrong, R. C.; & Hassager, O. (1987). *Dynamics of polymeric liquids. Volume 1, Fluid mechanics* (2nd ed.). New York; Toronto: Wiley.

Brenner, H. (1974). Rheology of a dilute suspension of axisymmetric Brownian particles. *Int. J. Multiphase Flow*, 1, 195–341.

Bretherton, F. P. (1962). The motion of rigid particles in a shear flow at low Reynolds number. *J. Fluid Mech.* 14, 284–304.

Burgers, J. M., (1938).. On the motion of small particles of elongated form suspended in a viscous liquid, *Second Report on Viscosity and Plasticity*, 16 (4), 113–184, Kon. Ned. Akad. Wet., Verhand, (Erste Sectie), North-Holland, Amsterdam

Carter, L.F. (1967) *A study of the rheology of suspensions of rod-shaped particles in a Navier–Stokes liquid.* Ph.D. Thesis. University of Michigan: Ann Arbor, MI.

Chan, Y., White, J. L., & Oyanagi, Y. (1978). A Fundamental Study of the Rheological Properties of Glass-Fiber-Reinforced Polyethylene and Polystyrene Melts. *J. Rheol.,* 22(5), 507-524.

Chaouche, M. and D.L. Koch, (2001). Rheology of non-Brownian rigid fiber suspensions with adhesive contacts. *Journal of Rheology,* 45 (2), 369-382.

Chung, D. H., & Kwon, T. H. (2002). Invariant-based optimal fitting closure approximation for the numerical prediction of flow-induced fiber orientation. *Journal of Rheology,* 46(1), 169-194.

Cintra J.S.; & Tucker, C. (1995). Orthotropic closure approxomations for flowinduced fiber orientation. *J. Rheol.,* 39, 1095-1122.

Cox, R. G., (1971) The motion of long slender bodies in a viscous fluid Part 2. Shear flow. *J. Fluid Mech.,* 45, 625–657.

Crowson, R. J.; Folkes, M. J.; & Bright, P. F. (1980). Rheology of short glass fiber reinforced thermoplastics and its application to injection molding I. Fiber motion and viscosity measurement. *Polym. Eng. Sci.,* 20(14), 925-933.

Crowson, R. J.; & Folkes, M. J. (1980). Rheology of short glass fiber-reinforced thermoplastics and its application to injection molding II. The effect of material parameters. *Polym. Eng. Sci.,* 20(14), 934-940.

Czarnecki, L.; & White, J. L. (1980). Shear flow rheological properties, fiber damage, and mastication characteristics of aramid-, glass-, and cellulose-fiber-reinforced polystyrene melts. *J. Appl. Polym. Sci.,* 25(6), 1217-1244.

Dealy, J. M.; and K. F., Wissbrun (1990). *Melt Rheology and Its Role in Plastics Processing: Theory and Applications.* (Van Nostrand Reinhold, New York)

Dinh, S. M.; & Armstrong, R. C. (1984). A Rheological Equation of State for Semi-concentrated Fiber Suspensions. *J. Rheol.,* 28(3), 207-227.

Djalili-Moghaddam, M.; & Toll, S. (2005). A model for short-range interactions in fibre suspensions. *J. Non-Newtonian Fluid Mech.,* 132(1-3), 73-83.

Doi, M.; Edwards, S. F. (1978). Dynamics of rod-like macromolecules in concentrated solution. Part 1. *J. Chem. Soc., Faraday Trans.,* 74 (2), 560.

Doi, M.; Kuzuu, N. Y. (1980). Non-linear elasticity of rodlike macromolecules in condensed state. *J. Polym. Sci., Part B.: Polym. Phys.,* 18 (3), 409.

Eberle, A. P. R.; Baird, D. G. & Wapperom, P. (2008). Rheology of non_Newtonian fluids containing glass fibers:A review of experimental literature. *Ind. Chem. Eng. Res.,* 47 (10), 3470-3488.

Edwards, B.J.; Dressler, M.; Grmela, M. & Ait-Kadi, A. (2003). Rheological models with microstructural constrains. *Rheol. Acta.,* 42, 64.

Endo, H.; & Nagasawa, M. (1970). Normal Stress and Shear Stress in a Viscoelastic Liquid under Oscillatory Shear Flow. *J. Polym. Sci.*, A28, 371-81.

Ericsson, K. A., Toll, S., & Manson, J. A. E. (1997). Sliding plate rheometry of planar oriented concentrated fiber suspension. *Rheol. Acta,* 36(4), 397-405.

Fan, Z.; & Advani,S., (2005). Characterization of orientation state of carbon nano-tubes in shear flow. *Polym.,* 46, 5232-5240.

Férec. J., Ausias, G., Heuzey, M.C., & P. J. Carreau, (2009). modeling fiber interactions in semi-concentrated fiber suspensions. *J. Rheol.,* 53(1), 49-72.

Férec. J., (2008). *Etude et modelisation du comportement rheologique de suspensions de fibres regides en regime non- dilue.* Ph.D. Thesis, Ecole Polytechnique, Montreal, Canada.

Férec. J., Heuzey,M.C., G. Ausias, and P.J. Carreau, (2008). Rheological behavior of fiber-filled polymers under large amplitude oscillatory shear flow. *Journal of Non-Newtonian Fluid Mechanics*, 151 (1-3), 89-100.

Flory, P. J. (1956) Phase equilibria in solutions of rod-like particles. *Proc. R. Soc. London,* A234, 73.

Folgar, F. P., & Tucker, C. L. (1984). Orientation behavior of fibers in concentrated suspensions. *J. Reinf. Plast. Comp.,* 3(2), 98-119.

Forgacs, O. L.; and Mason, S. G. (1959). Particle motions in sheared suspensions IX. Spin and deformation of threadlike particles. *J. Colloid Interface Sci.,* 14, 457.

Ganani, E., & Powell, R. L. (1985). Suspensions of Rodlike Particles: Literature Review and Data Correlations. *J. Comp. Mat.,* 19(3), 194-215.

Ghosh, T. (1993). *Rheological modeling of complex polymeric fluids.* Ph.D. Thesis, Ecole Polytechnique, Montreal, Canada.

Ghosh, T., Grmela, M., & Carreau, P. J. (1995). Rheology of Short-Fiber Filled Thermoplastics. *Polym. Comp.,* 16(2), 144-153.

Goto, S., Nagazono, H., & Kato, H. (1986a). The flow behavior of fiber suspensions in Newtonian fluids and polymer solutions. I Mechanical properties. *Rheol. Acta, 25(*2), 119-129.

Goto, S., Nagazono, H., & Kato, H. (1986b). The flow behavior of fiber suspensions in Newtonian fluids and polymer solutions. II Capillary flow. *Rheol. Acta,* 25(3), 246-256.

Greene, J. P.; & J.P. Wilkes; (1995). Steady state and dynamic properties of concentrated fiber filled thermoplastics. *Polym. Engi. Sci.,* 35, 1670-1681.

Grmela, M. (1986). Bracket formulation of diffusion-convection equations. *Physica D: Nonlinear Phenomena,* 21(2-3), 179-212.

Grmela, M., & Carreau, P. J. (1987). Conformation tensor rheological models. *J. Non-Newt. Fluid Mech.,* 23, 271-294.

Guo, R., Azaiez, J., & Bellehumeur, C. (2005). Rheology of Fiber Filled Polymer Melts: Role of Fiber-Fiber Interactions and Polymer-Fiber Coupling. *Polym. Eng. Sci.,* 385-399.

Harlen, O. G., and D. L. Koch; (1997). Orientation drift of a fiber suspended in a dilute polymer solution during oscillatory shear flow. *J. Non-Newtonian Fluid Mech.,* 73, 81-93

Huq, A. M. A., & Azaiez, J. (2005). Effects of length distribution on the steady shear viscosity of semiconcentrated polymer-fiber suspensions. *Polym. Eng. Sci.,* 45(10), 1357-1368.

Jeffery, G. B. (1922). The motion of ellipsoidal particles immersed in a viscous fluid. *Proceedings of the Royal Society of London Serie A,* 102, 161-179.

Joung, C. G., Phan-Thien, N., & Fan, X. J. (2001). Direct simulation of flexible fibers. *J. of Non-Newtonian Fluid Mech.,* 99(1), 1-36.

Kim, J. K., and J. H. Song, (1997) Rheological properties and fiber orientation of short fiber-reinforced plastics. *J. Rheol.,* 41, 1061-1085.

Kitano, T., Kataoka, T., Nishimura, T., & Sakai, T. (1980). Relative viscosities of polymer melts filled with inorganic fillers. *Rheol. Acta,* 19(6), 764-769.

Kitano, T., & Kataoka, T. (1981a). The rheology of suspensions of vinylon fibers in polymer liquids. I. Suspensions in silicone oil. *Rheol. Acta,* 20(4), 390-402.

Kitano, T., & Kataoka, T. (1981b). The rheology of suspensions of vinylon fibers in polymer liquids. II. Suspensions in polymer solutions. *Rheol. Acta, 20*(4), 403-415.

Kitano, T., Kataoka, T., & Nagatsuka, Y. (1984). Shear flow rheological properties of vinylon- and glass-fiber reinforced polyethylene melts. *Rheol. Acta,* 23(1), 20-30.

Khokhlov A. R, Semenov. A. (1985). On the theory of liquidcrystalline ordering of polymer chains with limited flexibility. *J Stat Phys.,* 38, 161

Kotsilkova, R. (1992). Dynamic Rheological Properties Of Glass Fiber Suspensions., *Theoretical and Applied Rheology,* edited by Moldenaers, P., Keunings, R., *Proc. XIth Int. Congr. On Rheology*, Brussels, Belgium, 856-858

Laun, H. M. (1984). Orientation effects and rheology of short glass fiber-reinforced thermoplastics. *Colloid Polym. Sci.,* 262(4), 257-269.

Laun, H. M., (1986). Prediction of elastic strains of polymer melts in shear and elongation. *J. Rheol.,* 30 (3), 459-501.

Lipscomb, G. G., Denn, M. M., Hur, D. U., & Boger, D. V. (1988). The Flow of Fiber Suspensions in Complex Geometries. *J. Non-Newtonian Fluid Mech.,* 26(3), 297-325.

Lodge, A.S. (1964). *Elastic Liquids.* Academic Press, London - New York.

Mason, S. G.; Manley, R. St. J.; (1957). Particle motions in sheared suspensions: orientations and interactions of rigid rods., *Proc. R. Soc. London*, A238: 117–131.

Milliken, W. J., Gottlieb, M., Graham, A. L., Mondy, L. A., & Powell, R. L. (1989). The viscosity-volume fraction relation for suspensions of rod-like particles by fallingball rheometry. *J. Fluid Mech.,* 202(1), 217-232.

Mobuchon, C., Carreau, P. J., Heuzey, M.-C., Sepehr, M., & G., Ausias, (2005). Shear and extensional properties of short glass fiber reinforced polypropylene. *Polym. Compos.,* 26 (3), 247-264.

Möginger, B. & Eyerer, P., (1991). Determination of the weighting function g(βi, r, vf) for fibre orientation analysis of short fibre reinforced composites. *Composites,* 22 (5), 394–399.

Mondy, L. A., Morrison, T. G., Graham, A. L., & Powell, R. L. (1990). Measurements of the viscosities of suspensions of oriented rods using falling ball rheometry. *Int. J. Multiphase Flow,* 16(4), 651-662.

Mutel, A. T., & Kamal, M. R. (1984). The effect of glass fibers on the rheological behavior of polypropylene melts between rotating parallel plates. *Polym. Compos.,* 5(1), 29-35.

Mutel, A. T., & Kamal, M. R. (1986). Characterization of the rheological behavior of fiber-filled polypropylene melts under steady and oscillatory shear using cone and-plate and rotational parallel plate rheometry. *Polym. Compos.,* 7(5), 283-294.

Mutel, A. T., & Kamal, M. R. (1987). Measurement of fiber orientation distributions in simple flows of fiber reinforced melts. *Society of Plastics Engineers,* Los Angeles, *CA, USA* (pp. 732-737) *Soc of Plastics Engineers,* Brookfield Center, CT, USA.

Mutel, A.T., (1989). *Rheological behavior and fiber orientation in simple flows of glass fiber filled polypropylene melts.* Ph.D., McGill University, Canada, 1989.

Nawab, M. A.; Mason, S. G.; (1958). The viscosity of dilute suspensions of threalike particles. *J. of Non-Newtonian Fluid Mech.,* 62, 1248-1253.

Nicodemo, L., & Nicolais, L. (1974). Viscosity of concentrated fiber suspensions. *Chem. Eng. J.,* 8(2), 155-156.

Onsager, L. (1949). The effects of shape on the interaction of colloidal particles. *Annuals of the New York Academy of Sciences*, 51, 627-659.

Page, D.H., R.S. Seth, B.D. Jordan, & M.C. Barbe, (1985). *Curls, crimps, kinks and microcompression in pulp fibers – their origin, measurement and significance.* In V. Punton., *Papermaking raw materials*, Transactions of the Eighteen Fundamental Research Symposium Held at Oxford, Pages 183-227. Mechanical Engineering Publications Limited.

Petrich, M.P., D.L. Koch, & C. Cohen, (2000). Experimental determination of the stress-microstructure relationship in semi-concentrated fiber suspensions. *J. Non-Newtonian Fluid Mech.,* 95 (2-3), 101-133.

Petrie, C. J. S. (1999). The rheology of fibre suspensions. *J. Non-Newtonian Fluid Mech.,* 87(2-3), 369-402.

Philippoff, W. (1966). Vibrational measurements with large amplitudes. *Trans. Soc. Rheol.,* 10, 317–334.

Rajabian, M., Dubois, C., and Grmela, M. (2005). *Suspensions of semiflexible fibers in polymeric fluids: Rheology and Thermodynamics., Rheologica Acta* ***44****,* 521-535.

Rajabian, M., Dubois, C., M. Grmela, & P.J. Carreau, (2008) Effect of polymer-fiber interactions on rheology and flow behavior of semi-flexible fibers in polymeric liquids. *Rheol. Acta,* 47, 701-717.

Ramazani, A., Ait-Kadi, A., & Grmela, M. (2001). Rheology of fiber suspensions in viscoelastic media: Experiments and model predictions. *J. Rheol.,* 45(4), 945-962.

Ross, R. F., and Klingenberg, D. J.; (1997). Dynamic simulation of flexible fibers composed of linked rigid bodies. *J. Chem. Phys.,* 106 (7), 2949.

Shaqfeh, E. S. G., & Fredrickson, G. H. (1990). The Hydrodynamic Stress in a Suspension of Rods. *Physics of Fluids A-Fluid Dynamics,* 2(1), 7-24.

Schmid, C. F., Switzer, L. H., and Klingenberg, D. J.; (2000). Simulations of fiber flocculation: effects of fiber properties and interfiber friction. *J. Rheol.,* 44 (4), 781-809.

Sepehr, M., Carreau, P. J., Moan, M., & Ausias, G. (2004a). Rheological properties of short fiber model suspensions. *J. Rheol.,* 48(5), 1023-1048.

Sepehr, M., Ausias, G., & Carreau, P. J. (2004b). Rheological properties of short fiber filled polypropylene in transient shear flow. *J. Non-Newtonian Fluid Mech.,* 123 (1), 19-32.

Soszynski, R.M., & Kerekes, R. J. (1988a). Elastic interlocking of nylon fibers suspended in liquid. Part 1. Nature of cohesion among fibers. *Nord. Pulp Pap. Res. J.,* 3,172-179.

Soszynski, R.M., & Kerekes, R. J. (1988a). Elastic interlocking of nylon fibers suspended in liquid. Part 2. Process of interlocking. *Nord. Pulp Pap. Res. J.,* 3, 180-184.

Souloumiac, B., Vincent, M. (1998). Steady shear viscosity of short fiber suspensions in thermoplastics. *Rheol. Acta,* 37, 289-298.

Sundararajakumar, R. R. & Koch, D. L. (1997). Structure and properties of sheared fiber suspensions with mechanical contacts. *J. Non-Newtonian Fluid Mech.,* 73 (3), 205-239.

Switzer III, L. H., & Klingenberg, D. J. (2003). Rheology of sheared flexible fiber suspensions via fiber-level simulation. *J. Rheol.* 47(3), 759-778.

Tee, T. T.; & Dealy, J. M., (1975). Nonlinear viscoelasticity of polymer melts. *Trans. Soc. Rheol.* 19, 595–615.

Thomasset, J., Carreau, P. J., Sanschagrin, B., & Ausias, G. (2005). Rheological properties of long glass fiber filled polypropylene. *J. Non-Newtonian Fluid Mech.,* 125(1), 25-34.

Trevlyan, B. J.; Mason, S. G.; (1951). Particle motions in sheared suspensions I. Rotations. *J. Colloid Sci.* 6, 354–367.

Tucker III, C.L. and S.G. Advani, (1994) *Flow and rheology of polymer composites manufacturing.* (Edited by S.G. Advani) 147-202, Elsevier Science, New York.

Verleye, V., Couniot, A., & Dupret, F. (1994). Numerical prediction of fiber orientation in complex injection molded parts. *ASME Winter Annual Meeting* (Vol. 49, pp. 265-279.

VerWeyst, B. E. (1998). *Numerical simulations of flow-induced fiber orientation in three dimensional geometries.* Ph.D. thesis, University of Illinois at Urbana-Champaign, Urbana, IL.

Wang, G.; Yu, W.; & Zhou, C.; (2006). Optimization of the rod chain model to simulate the motions of a long flexible fiber in simple shear flows. *Europ. J. Mech., B/Fluids,* 25 (3), 337-347.

Wetzel, E. D., & Tucker, C. L. (1999). Area tensors for modeling microstructure during laminar liquid-liquid mixing. *Int. J. Multiphase Flow,* 25, 35.

Wetzel, E. D. (1999). *Modeling flow-induced microstructure of inhomogeneous liquidliquid mixtures.* Ph.D. Thesis, University of Illinois at Urbana-Champaign, United States - IL.

Wilhelm, M.; (2002). Fourier-transform rheology. *Macromol. Mater. Eng.* 287, 83–105.

Yamamoto, S., & Matsuoka, T. (1993). Method for dynamic simulation of rigid and flexible fibers in a flow field. *J. Chem. Phys.* 98(1), 644.

Yamamoto, S., and Matsuoka, T. (1996). Dynamic simulation of microstructure and rheology of fiber suspensions. *Polym Eng Sci* 36 (19), 2396-2403.

Zhu, Y. T., Blumenthal, W. R. & Lowe, T. C., (1997). Determination of non-symmetric 3-D fibre- orientation distribution and average fibre length in short-fibre composites. *J. Compos. Mater.,* 31 (13), 1287–1301.

Zirnsak, M. A., Hur, D. U., & Boger, D. V. (1994). Normal stresses in fibre suspensions. *J. Non-Newtonian Fluid Mech.,* 54, 153-193.

Appendix A
Characterization of orientation state of fibers in shear flow

As described in Section (2-7) of this thesis, one can use the components of the orientation tensor in two or three dimensions to draw an ellipse or ellipsoid to describe the orientation state graphically. In this section the orientation state of the fibers is presented in the form of ellipses.

Various fibers (polyarylate (Vectran®), vinylon (PVA) and nylon fibers with different Young modulus were used in this investigation. The aspect ratio of all fibers is around 70 and they are dispersed in a high viscosity silicone oil, polydimethylsiloxane (Clearco Products) with a density of 0.974 g/cm^3 and a nominal viscosity of 103 ± 2 Pa.s at 20 °C.

Visualization experiments were performed to characterize the fiber orientation. To this end, the Paar Physica UDS 200 rheometer with parallel plate geometry (diameter = 50 mm) was used. The lower metal plate was replaced by a glass plate and the temperature in the room was controlled at 20 °C by an air conditioner. The visualization was carried out using a continuously-focusable InfiniVar® microscope placed under the lower plate of the rheometer. The microscope was coupled to a color CCD camera (Lumenera) and the data acquired using the software StreamPix III® (NorPix). All the measurements were performed at the same light intensity, and the maximum depth of observation above the lower plate was measured to be 60 μm. The visualization window illuminate an area of (2393 μm × 1914 μm) in the radial position r/R = (21-23)/25. The experimental setup is illustrated in Figure A1.

Fresh samples were loaded in the shearing cell and the gap was adjusted to 2 mm. Samples were deformed at various shear rates ($\dot{\gamma}|_{r=23}$ = 0.1, 0.5, 1, 2 and 4 s^{-1}) until steady state, and sequences of images were collected at a rate of 4 images per second. A typical micrograph obtained from the visualization experiments is shown in Figure A2a and A2b for Vectran (most rigid) and nylon (most flexible) fibers respectively.

A-1 Effect of shear rate

The component of the orientation tensor in the flow direction, $a_{\theta\theta}$ and the angle of average orientation state of fibers with flow direction are presented in Figure A3 at different shear rates ($\dot{\gamma}|_{r=23}$ = 0.1, 0.5, 1, 2 and 4 s^{-1}) as a function of shear rate. It has been determined for the dimensionless radial position r/R = (21 to 23)/25. For all suspensions, $a_{\theta\theta}$ is seen to increase with shear rate towards a maximum value (of $\approx$ 0.8), while the average angle with flow direction decreases. The results are indicative of a shear flow-induced fiber orientation. At low shear rates the orientation with the flow direction is more important for the most rigid fibers, indicating that the latter are more easily oriented by than flexible fibers. The representation of the suspension orientation state at different shear rates as ellipses are depicted in figure A4.

A-2 Time evolution of orientation state of fibers

Figure A5 shows the time evolution of the second-order orientation tensor component $a_{\theta\theta}$ and the average angle of the fibers with the flow direction at $\dot{\gamma}$ = 1 s^{-1} for Vectran

(rigid) and nylon (semi-flexible) fiber suspensions. For both suspensions, the experimental orientation tensor component was evaluated at strains of 0, 4, 12, 20, 60 and 100. Strain 0 relates to the initial fiber orientation of the suspensions at rest before the application of the shear. We note from Figure A5a that $a_{\theta\theta}$ increases with shear. This shows that the fibers, with an initial random orientation in the $r\theta$ plane reorient to align with the flow direction (θ), as shown in Figure A5b. The rate of increase of $a_{\theta\theta}$ is also higher for the more rigid fibers. The representation of the evolution of the second order orientation tensor at different shear rates as ellipses is depicted in Figure A6. Solid lines represent the orientation of Vectran fibers, and dashed lines depict the orientation of nylon fibers. It is shown that the initial state of orientation for both suspensions is the same, but by applying deformation, flexible fibers remain more distributed in other directions, as compared to rigid fibers that tend to be aligned more with the flow direction.

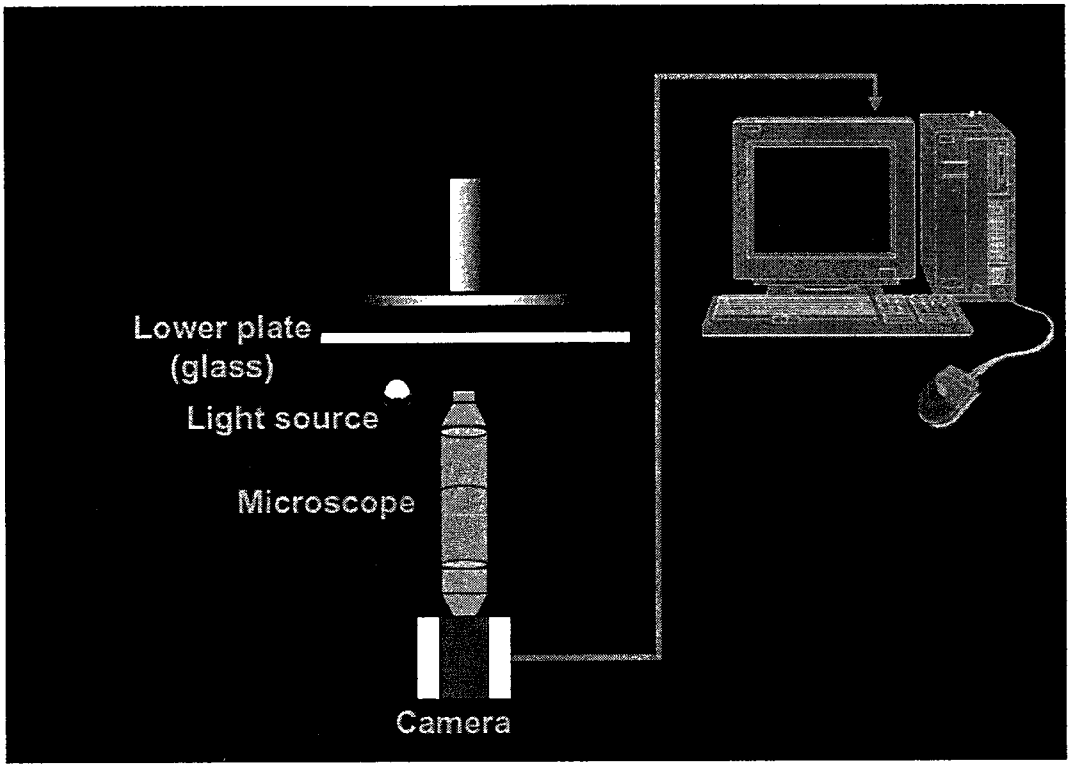

Figure A1. Experimental setup

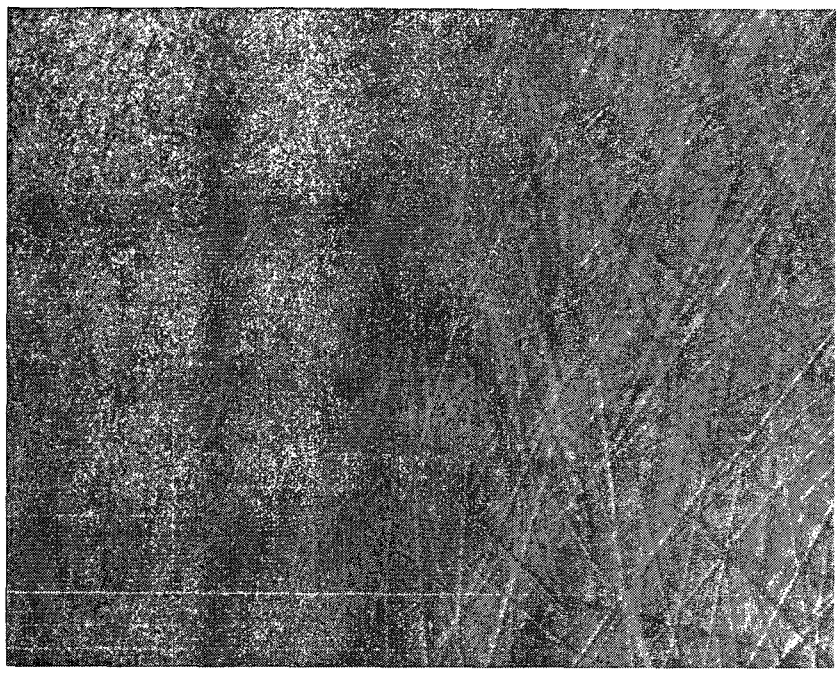

a)

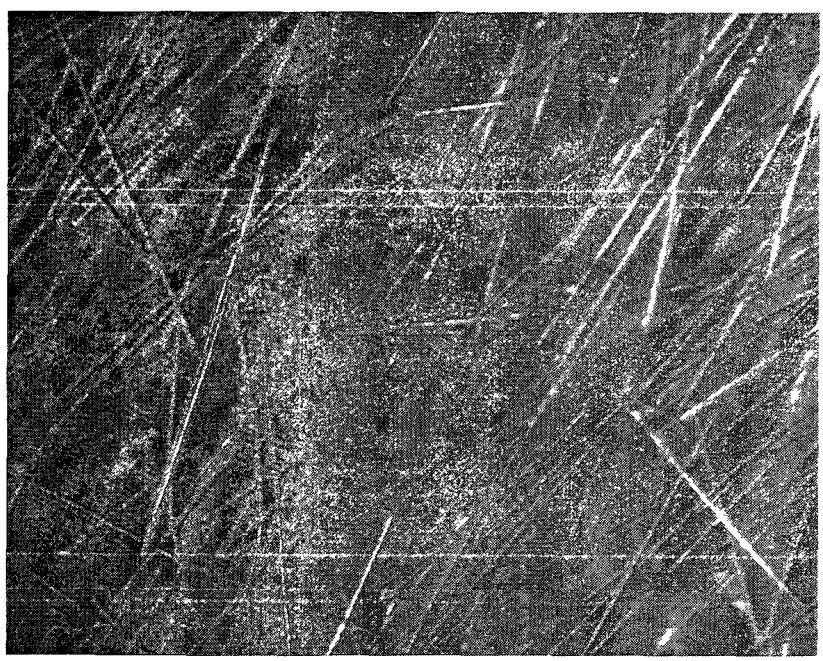

b)

Figure A2. Micrograph of a fiber suspension in visualization experiments: a) Vectran fibers, b) Nylon fibers suspended in silicone oil.

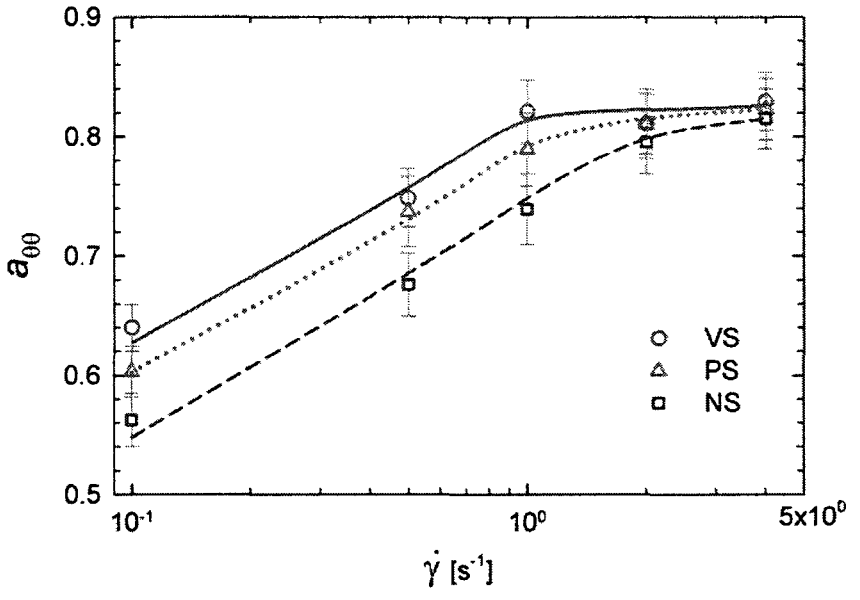

a)

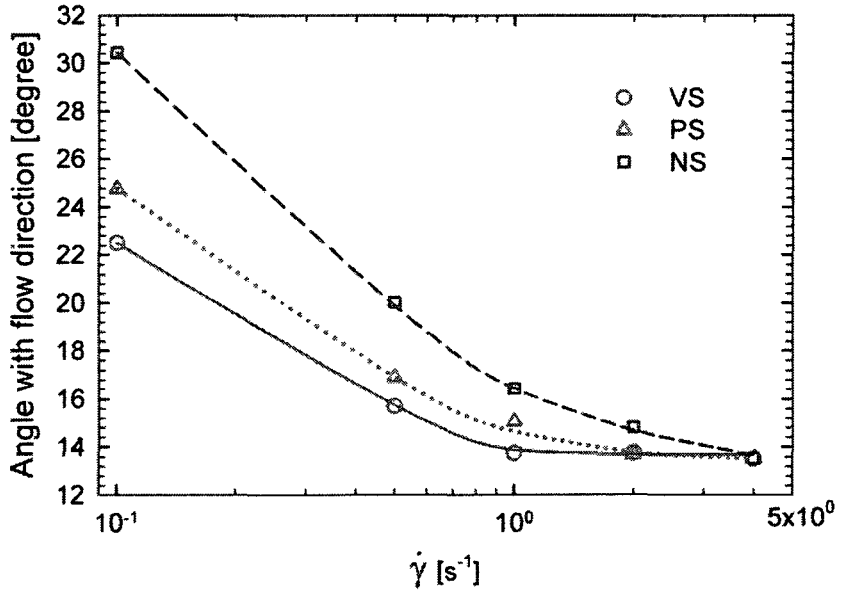

b)

Figure A3. a) Steady state fiber orientation in the flow direction $a_{\theta\theta}$ determined experimentally ; ϕf=0.03, b) Average angle of fibers with flow direction

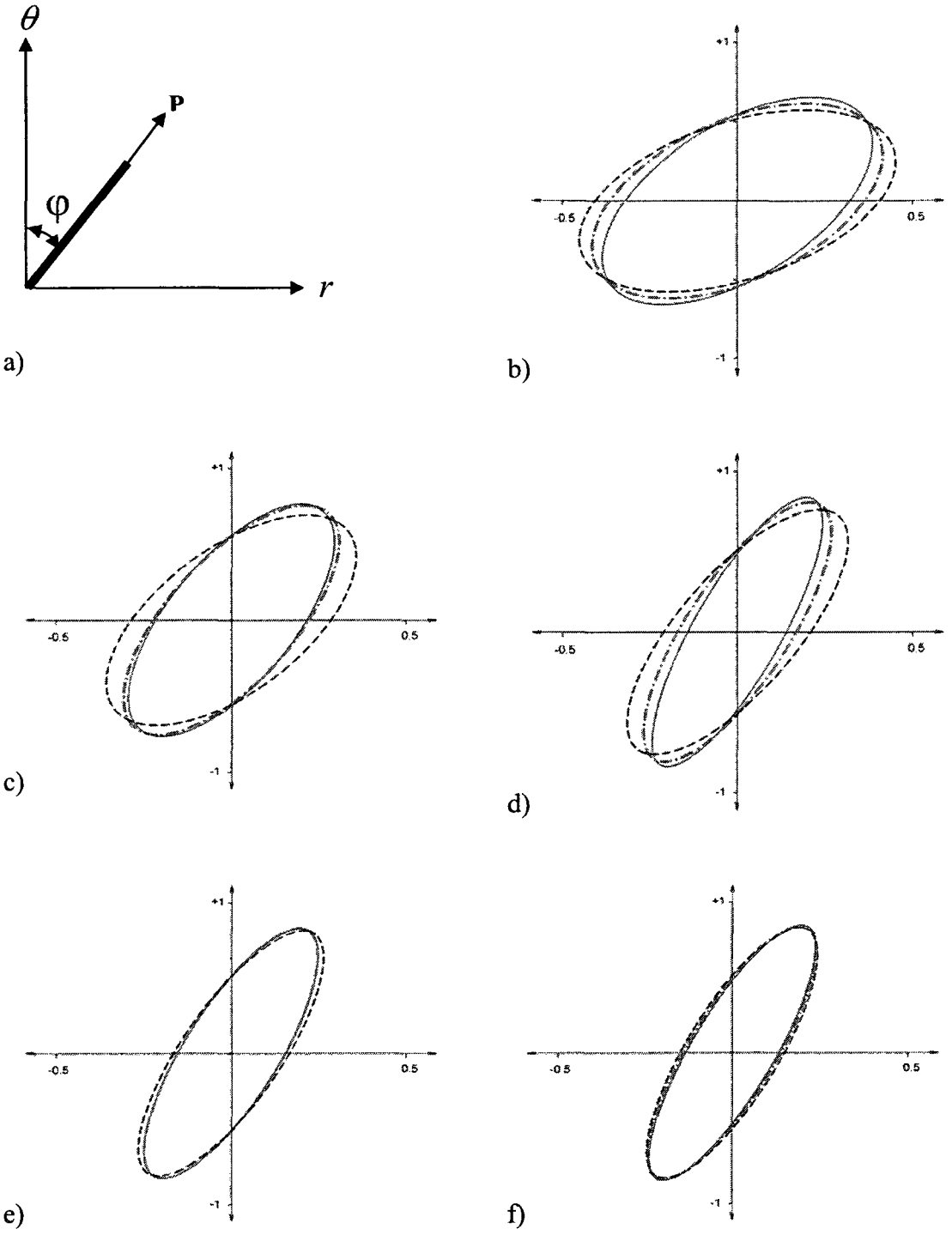

Figure A4. Illustration of second order orientation tensor and use of an ellipse a) flow direction, b) $\dot{\gamma} = 0.1s^{-1}$, c) $\dot{\gamma} = 0.5s^{-1}$, d) $\dot{\gamma} = 1s^{-1}$, e) $\dot{\gamma} = 2s^{-1}$, f) $\dot{\gamma} = 4s^{-1}$ (Vectran: solid line, PVA: dash-dot, Nylon: dash lines)

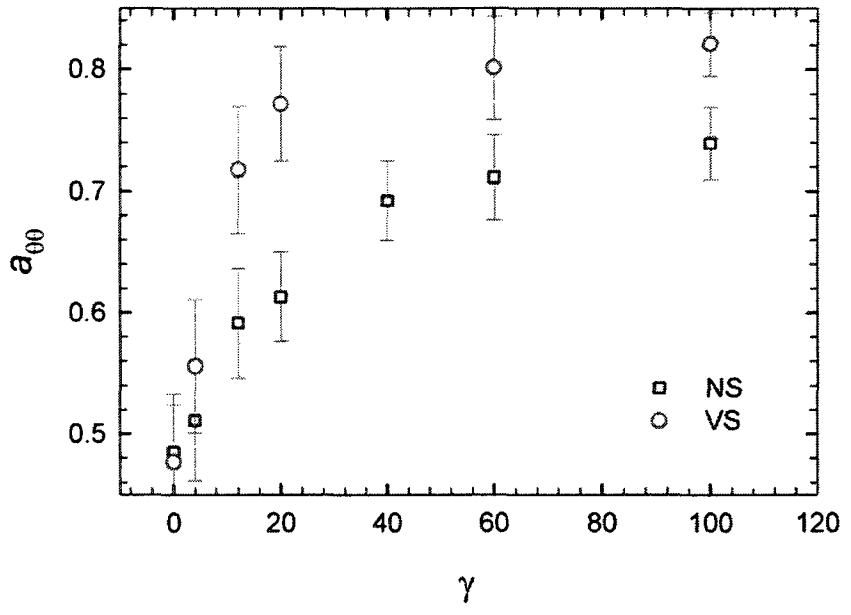

a)

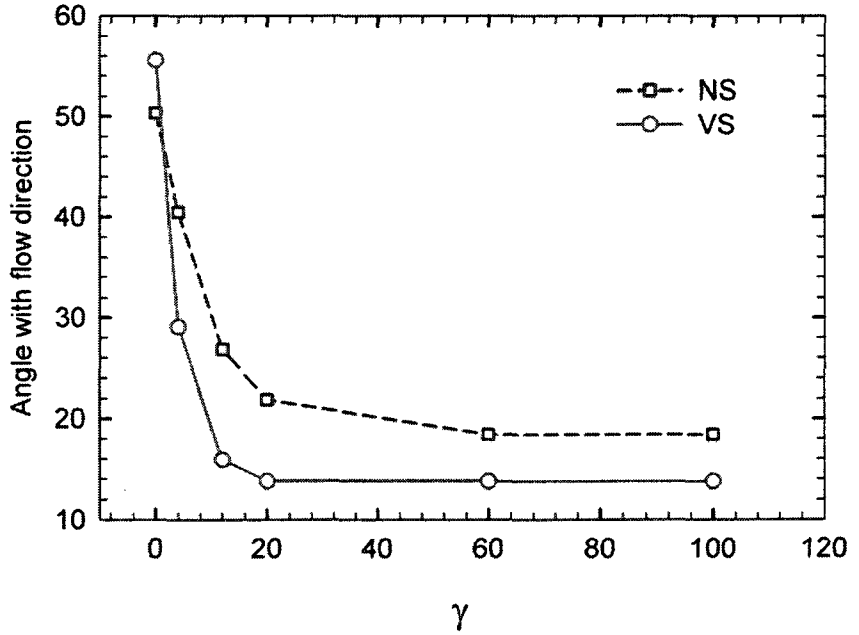

b)

Figure A5. Fiber orientation represented through the a) $a_{\theta\theta}$, b) angle with flow direction in stress growth at $\dot{\gamma} = 1\ s^{-1}$.

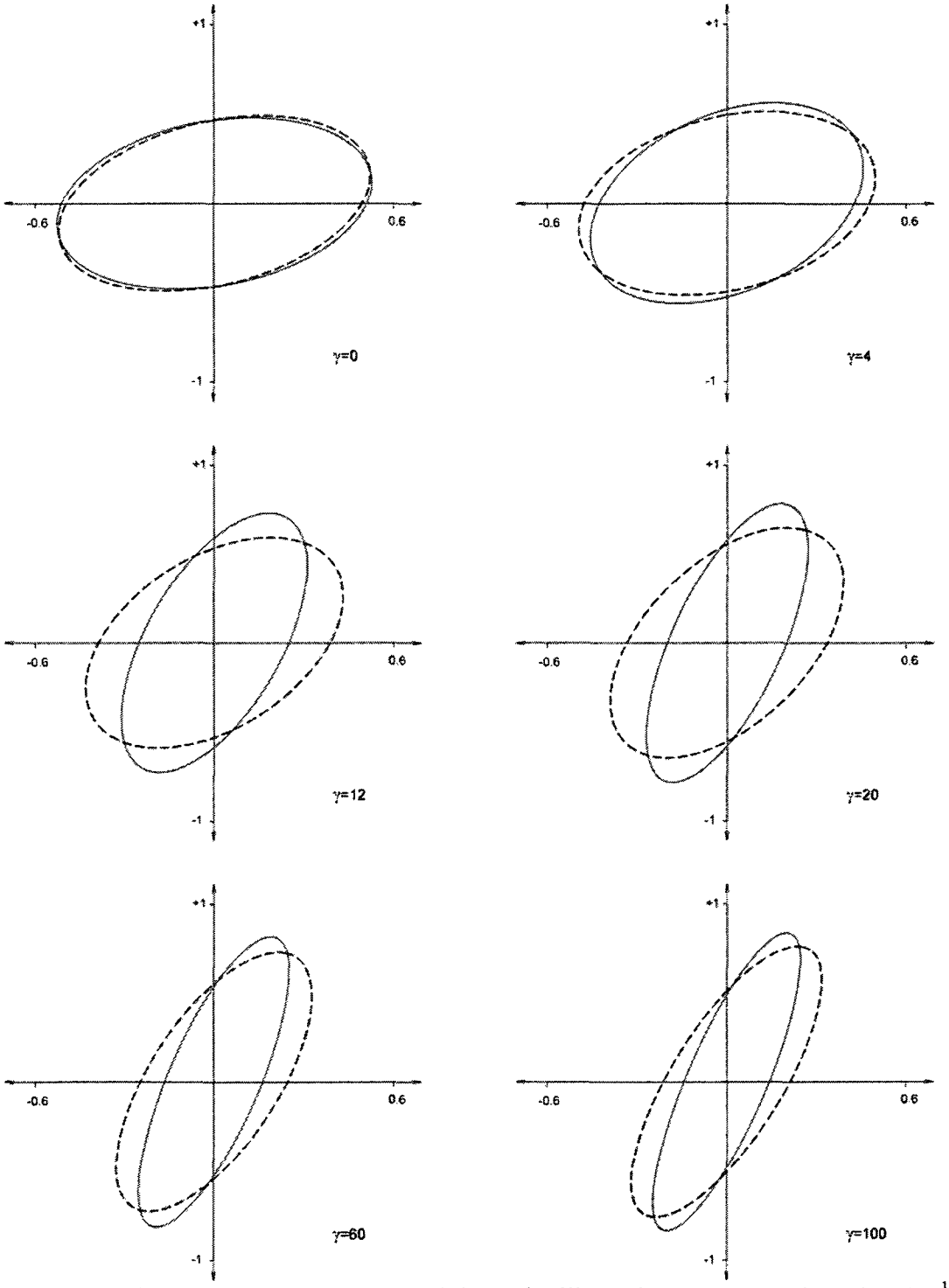

Figure A6. Fiber orientation represented through ellipses in stress growth at $\dot{\gamma} = 1\ s^{-1}$.